In presenting the dissertation as a partial fulfillment of the requirements for an advanced degree from the Georgia Institute of Technology, I agree that the Library of the Institute shall make it available for inspection and circulation in accordance with its regulations governing materials of this type. I agree that permission to copy from, or to publish from, this dissertation may be granted by the professor under whose direction it was written, or, in his absence, by the Dean of the Graduate Division when such copying or publication is solely for scholarly purposes and does not involve potential financial gain. It is understood that any copying from, or publication of, this dissertation which involves potential financial gain will not be allowed without written permission.

_____

7/25/68

CONFLUENT BOUNDARY LAYER FLOW DEVELOPMENT WITH ARBITRARY PRESSURE DISTRIBUTION

A THESIS

Presented to

The Faculty of the Division of Graduate

Studies and Research

by

Suresh H. Goradia

In Partial Fulfillment

of the Requirements for the Degree

Doctor of Philosophy

in the School of Mechanical Engineering

Georgia Institute of Technology

August 1971

CONFLUENT BOUNDARY LAYER FLOW DEVELOPMENT WITH

ARBITRARY PRESSURE DISTRIBUTION

Approved:

Chairman, Dr. G. T. Colwell

Dr. P. V. Desai

Dr. L. H. Bangert

Dr. J. H. Hubbart

Dr. W. Wulff

Dr. J. C. Wu

Date approved by Chairman August 16, 1971

DEDICATION

In return for her constant patience, tolerance, and understanding, this dissertation is dedicated to my wife, Shobha Goradia.

ACKNOWLEDGMENTS

Several persons and organizations have contributed toward the completion of the research presented in this thesis document. In particular, Dr. G. T. Colwell, author's adviser, has been of continuing assistance throughout this investigation. Dr. Colwell's guidance, cooperation and encouragment have been most significant factors in bringing this program to completion. Appreciation is extended to the members of the reading committee for their liberal contribution of time and energy to the careful critique of the manuscript. The suggestions and advice of Dr. P. V. Desai during the initial phase of this program and his continuing encouragements during the course of this research is gratefully appreciated. The author is thankful and appreciative to Dr. W. Wulff for his valuable suggestions and recommendations in regard to the various numerical methods for the solution of various sets of differential equations encountered in this study. The author is thankful to Professor J. H. Hubbart for his valuable discussion of the problem of this research during the initial stages. The time and effort of Dr. L. Bangert in reading this thesis is appreciated.

Concerning completion of the experimental phase of this research, gratitude is extended to Mr. Ted Dansby, Manager of Advanced Technology Department, and Dr. B. H. Little, Jr., Associate Director of Aerospace Sciences of Lockheed-Georgia. Both of the above individuals made necessary arrangements for making available the experimental wall jet facility at Lockheed-Georgia Company, for use by the author for the

experimental part of this research. The author is indebted to the personnel of the machine shop of the School of Mechanical Engineering at Georgia Tech for helping him make components needed to modify the experimental facility at Lockheed. The author is thankful to Dr. S. P. Kezios, Director of School of Mechanical Engineering, for his permission to construct these components. The author is indebted to Mr. R. F. Tanner at Lockheed-Georgia Company who helped from time to time in overcoming instrumentation and tunnel problems encountered during testing.

The Lockheed-Georgia Company is due much credit for this research because of its support of the author and because it supplied computer and wind tunnel facilities. The author especially appreciates the advice, support, patience and encouragement of Mr. Ted Dansby, Manager of the Advanced Technology Department, Mr. J. A. Braden, Research and Development Engineer, and Mr. D. M. Ryle, Jr., Division Manager of the Advanced Flight Sciences Division, all of Lockheed-Georgia Company.

TABLE OF CONTENTS

LIST OF TABLES

LIST OF FIGURES

LIST OF SYMBOLS

c	chord of airfoil, inches
C_p	pressure coefficient
$C_{P(0)}$	pressure coefficient at station 0 in Figure (1)
$f(\eta_1)$	similarity function for jet layer velocity profiles in the initial region of Figure (1)
$f(\eta_2)$	similarity function for wake layer velocity profiles in the initial region of Figure (1)
$f(\eta_3)$	similarity function for jet layer velocity profiles in the main region I of Figure (1)
$f(\eta_4)$	similarity function for wake layer velocity profiles in the main region I of Figure (1)
$f(\eta_5)$	similarity function for jet layer velocity profiles in the main region II of Figure (1)
H_1	wall layer form factor in the initial region = $\frac{\delta_1^*}{\theta_1}$
H_5	wall layer form factor in the main region I = $\frac{\delta_5^*}{\theta_5}$
H_7	form factor in the ordinary turbulent boundary layer region = $\frac{\delta_7^*}{\theta_7}$
$\tilde{H}_1$	$\frac{\delta^{**}\ \text{wall layer}}{\theta_1}$
$\tilde{H}_5$	$\frac{\delta^{**}\ \text{wall layer}}{\theta_5}$

H_7 $\quad \dfrac{\delta^{**}}{\theta_7}$

$\bar{h}$ heat transfer coefficient (BTU/Hr-ft^2)

h slot height (inch)

K_1 value of η_2 at $y = \delta_4$

K_2 value of η_4 at $y = \delta_4$

n exponent in the wall layer velocity profile assumption

P wall static pressure ($\frac{lb_f}{ft^2}$)

P_∞ free stream static pressure ($\frac{lb_f}{ft^2}$)

P_r wall static pressure at station 0 ($\frac{lb_f}{ft^2}$)

P_r Prandtl number

$\bar{q}$ velocity vector

q_t turbulent heat transfer at any point in the viscous layer = $\rho C_p \overline{v't'}$ ($\frac{BTU}{hr}$)

q_w heat transfer at wall ($\frac{BTU}{hr}$)

R_1 $\quad \dfrac{U_{e(x)}}{U_{c(x)}}$

R_0 $\quad \dfrac{U_{e(o)}}{U_{c(o)}}$

t	temperature at any distance y above wall in the viscous layer (°R)
t_w	wall temperature (°R)
t_∞	free stream temperature (°R)
u	velocity at any point y in the viscous layer $(\frac{ft}{sec})$
$U_{c(x)}$	velocity in the core in initial region $(\frac{ft}{sec})$
$U_{e(x)}$	velocity at the edge of viscous layer $(\frac{ft}{sec})$
$U_{e(0)}$	velocity at the edge of viscous layer at station 0 $(\frac{ft}{sec})$
$U_{c(0)}$	velocity in the core in the initial region at station 0 $(\frac{ft}{sec})$
u^*	friction velocity = $\sqrt{\frac{\tau_w}{\rho}}$ $(\frac{ft}{sec})$
U_w	velocity at the junction of jet and wake layer $(\frac{ft}{sec})$
U_{m_1}	velocity at the edge of wall layer in main region $(\frac{ft}{sec})$
U_∞	free stream velocity $(\frac{ft}{sec})$
v	y component of velocity in the viscous layer $(\frac{ft}{sec})$
x, y	rectangular coordinates
y_{1c}	distance y above wall in the wake layer in the initial region where $f(\eta_{2c}) = 0.5$ (inch)

y_{2c} distance y above wall in the wake layer in the main region where $f(\eta_2) = 0.5$ (inch)

δ_1 wall layer thickness in initial region (inch)

δ_2 distance y above wall at the junction of potential core and jet layer in initial region (inch)

δ_3 distance y above wall at the junction of jet and wake layers (inch)

δ_4 distance y above wall where the flow can be considered an inviscid (inch)

δ_5 wall layer thickness in the main region between stations 1 and 3 of Figure 1 (inch)

δ_6 edge of viscous layer in the main region II (inch)

δ_7 edge of viscous layer in the ordinary turbulent boundary layer region of Figure (1) (inch)

δ_e outer edge of viscous layer where $\frac{u}{U_e} = 0.995$ (inch)

δ_1^* wall layer displacement thickness in the initial region $= \int_0^{\delta_1} (1 - \frac{u}{U_c})\, dy$ (inch)

δ_5^* wall layer displacement thickness in main region (inch) $= \int_0^{\delta_5} (1 - \frac{u}{U_m})\, dy$

δ_7^* displacement thickness in the ordinary turbulent boundary layer region $= \int_0^{\delta_7} (1 - \frac{u}{U_e})\, dy$ (inch)

δ_1^{**} wall-layer dissipation energy thickness in the initial region (inch) $= \int_0^{\delta_1} \frac{u}{U_c} \{1 - (\frac{u}{U_c})^2\}\, dy$

δ_5^{**} wall-layer dissipation energy thickness in the main region (inch) $= \int_0^{\delta_5} \frac{u}{U_m}\left\{1-\left(\frac{u}{U_m}\right)^2\right\} dy$

δ_7^{**} dissipation energy thickness in the ordinary turbulent boundary layer region (inch) $= \int_0^{\delta_7} \frac{u}{U_e}\left\{1-\left(\frac{u}{U_e}\right)^2\right\} dy$

δ_F flap angle

η_1 similarity parameter for jet layer in the initial region

η_2 similarity parameter for wake layer in the initial region

η_3 similarity parameter for jet layer in the main region I

η_4 similarity parameter for wake layer in main region I

η_5 similarity parameter for jet layer in the main region II

θ_1 wall layer momentum thickness in initial region (inch) $= \int_0^{\delta_1} \frac{u}{U_c}\left(1-\frac{u}{U_c}\right) dy$

θ_5 wall layer momentum thickness in the main region (inch) $= \int_0^{\delta_5} \frac{u}{U_m}\left(1-\frac{u}{U_m}\right) dy$

θ_7 momentum thickness in the ordinary turbulent boundary layer region (inch) $= \int_0^{\delta_7} \frac{u}{U_e}\left(1-\frac{u}{U_e}\right) dy$

α angle of attack (degrees)

ϵ	eddy viscosity for momentum transfer $(\frac{ft^2}{sec})$
ϵ_H	eddy diffussivity for heat transfer $(\frac{ft^2}{sec})$
μ	molecular dynamic viscosity $(\frac{lb_m}{ft\text{-}sec})$
ν	molecular kinematic viscosity $(\frac{ft^2}{sec}) = \frac{\mu}{\rho}$
C_f	$\frac{\tau_w}{1/2 \rho U_\infty^2}$
ρ	density $(\frac{lb_m}{ft^3})$
τ	shear stress at any point y in the viscous layer $(\frac{lb_m}{ft^2})$
τ_w	wall shear stress

Subscripts:

∞	free stream value
e	edge of the viscous layer where the flow can be considered inviscid
$( )$	functional dependence of the quantity in the bracket

SUMMARY

A combined analytical and experimental investigation has been performed in order to study and evaluate the development of viscous flow when two air streams with different initial velocities and having initial boundary layers mix with each other over a solid surface in the presence of an arbitrary externally impressed pressure distribution. The above turbulent mixing phenomena, which is also known as wall jet flow, is defined in this document as confluent boundary layer flow. A central objective of the work was to investigate the important physical parameters and develop a method for calculation of confluent boundary layer viscous flow over the upper surfaces of multiple airfoils.

A mathematical model for the confluent boundary layer flow was developed from preliminary experimental data. The flow model is divided into an initial region, main regions, and an ordinary turbulent boundary layer region. Furthermore each region is sub-divided into various layers such as. wall layer, jet layer and wake layer, according to the characteristic of velocity profiles in the different layers. Integral equations are derived for each region mentioned above and for the various layers in the specific region. The equations in each region are ordinary, non-linear, and non-homogeneous differential equations; the number of these equations to be solved simultaneously for a particular region depends on the region of flow. Parameters, such as wall shear, shear at the edge of wall and jet layers, wall layer dissipation integral, etc., appear in the above equations. Functional representation of these parameters in

terms of dependent variables, arranged in non-dimensional groups, is accomplished with the help of the principle of local dynamic similarity. Similarity functions for the various regions of flow were obtained from experimental data taken during the present investigation. These similarity expressions have also been checked against data published by others and the agreement is very satisfactory.

Velocity profiles and pressure distributions were measured under conditions which are encountered in unblown or blown boundary layer controlled multiple airfoils. A technique was developed for computing wall shear and shear distribution from the experimental data with the aid of digital computers.

Comparison is made of computed values with experimental data of the present investigation as well as with previously published confluent boundary layers airfoil surface data. Reasonable agreement is obtained between measured and calculated viscous flow quantities. Calculations of the displacement thickness for confluent boundary layers indicate that confluent boundary layers are very thick compared to ordinary boundary layers. The results explain the large amount of viscous correction necessary for C_L in the case of a multiple airfoil as compared to the single component airfoil.

CHAPTER I

INTRODUCTION

Discussion of Applications

The study of the behavior of confluent boundary layers is of practical interest because of their application in film cooling and in boundary layer control devices of various types of aircraft. Until recently, however, the design and analysis of blown or unblown high lift systems for aircraft remained an outstanding example of "cut and try" empirically oriented processes. The aircraft in question may be of the more conventional type or STOL (short take-off and landing) and VTOL (vertical take-off and landing) types in which recent interest has been indicated by the military and the airlines in the United States. Design methods for high lift systems of the above mentioned aircraft have been based mostly on correlation in terms of geometrical parameters, of lift, drag, and pitching moment type of experimental data. This method of design which utilizes wind tunnel testing has proved to be expensive and is also associated with high risk.

A basic requirement of high lift systems for any type of aircraft is a high value of lift coefficient on the wing surface at low free-stream dynamic head. This requires the presence of very large adverse pressure gradients on the upper surface of the wing. Low kinetic energy fluid particles in the viscous layer near the wing surface do not have enough kinetic energy to surmount the "pressure hill" of such high adverse

pressure distribution and thus the fluid separation occurs from the wing surface causing sizable increase in drag and loss in lift. One of the commonly used schemes to suppress separation on the wing surface is to blow tangentially either cold or hot air (which is available from the power plant at some stage of compression or from engine exhaust) at one or more places on the upper surface of wing. The other most common way to suppress separation for unblown high lift systems is to cause mixing of air with a certain velocity through a slot with the free-stream air. This occurs with slatted and single or double slotted flap high lift systems. In the second case the observed velocity ratio $\frac{U_{c(o)}}{U_{e(o)}}$ varies from 0.9 to approximately 1.3.

Background

The behavior during mixing of two parallel streams over a wall has been investigated in detail experimentally by prominent investigators such as Bradshaw and Gee [5], Kruka and Eskinazi [3], Myers, Schauer and Eustis [2], Neale [54], Kacker and Whitelaw [4], Escudier and Whitelaw [7], and Nicoll and Whitelaw [8]. Some of the investigators concentrated their efforts on very high values of the velocity ratio $\frac{U_{c(o)}}{U_{e(o)}}$, some confined their attention to flow without pressure gradient, some did not consider the initial region where the core flow exists and some confined their attention to slot exit velocity corresponding to Mach numbers near unity when flow can not be analyzed according to incompressible assumptions. The reason for concentration by the individual investigators on higher velocity ratios and on flow without pressure gradient is quite understandable since in these cases the velocity profile beyond the

initial region is composed of two layers only. This type of flow can then be analyzed approximately by methods of similarity.

Brief Description of Proposed Work

The present study is concerned with the detailed behavior of the viscous flow shown in Figure (1), its mean properties and the relation between various boundary layer physical parameters for, a two-dimensional, incompressible wall jet flow in a moving stream and in the presence of pressure gradients of practical interest. The study, both analytical and experimental, is concentrated in the range of slot exit velocity ratio $1 \leq \frac{U_{c(o)}}{U_{e(o)}} \leq 1.5$. The above range of velocity ratios is encountered in the case of confluent boundary layer flow on the upper surfaces of multiple airfoils in which case the wake layer shown in Figure (1) exists quite far downstream of slot exit. This is illustrated schematically in Figure (1A) which shows the presence of various types of boundary layers encountered in the case of multiple airfoil solution.

The work described in this thesis is intended to formulate a prediction method which may be used to calculate downstream development of the viscous flow when a flow through a slot, with initial boundary layers, mixes with a parallel stream, also having an initial boundary layer in the presence of arbitrary pressure distribution. The sequence of steps taken under this study for the accomplishment of the stated purpose can be summarized as follows:

1) Measurements were made of velocity profiles and pressure distribution for various values of velocity ratios $\frac{U_{c(o)}}{U_{e(o)}}$. A physical model formulated from the experimental data is shown in Figure (1).

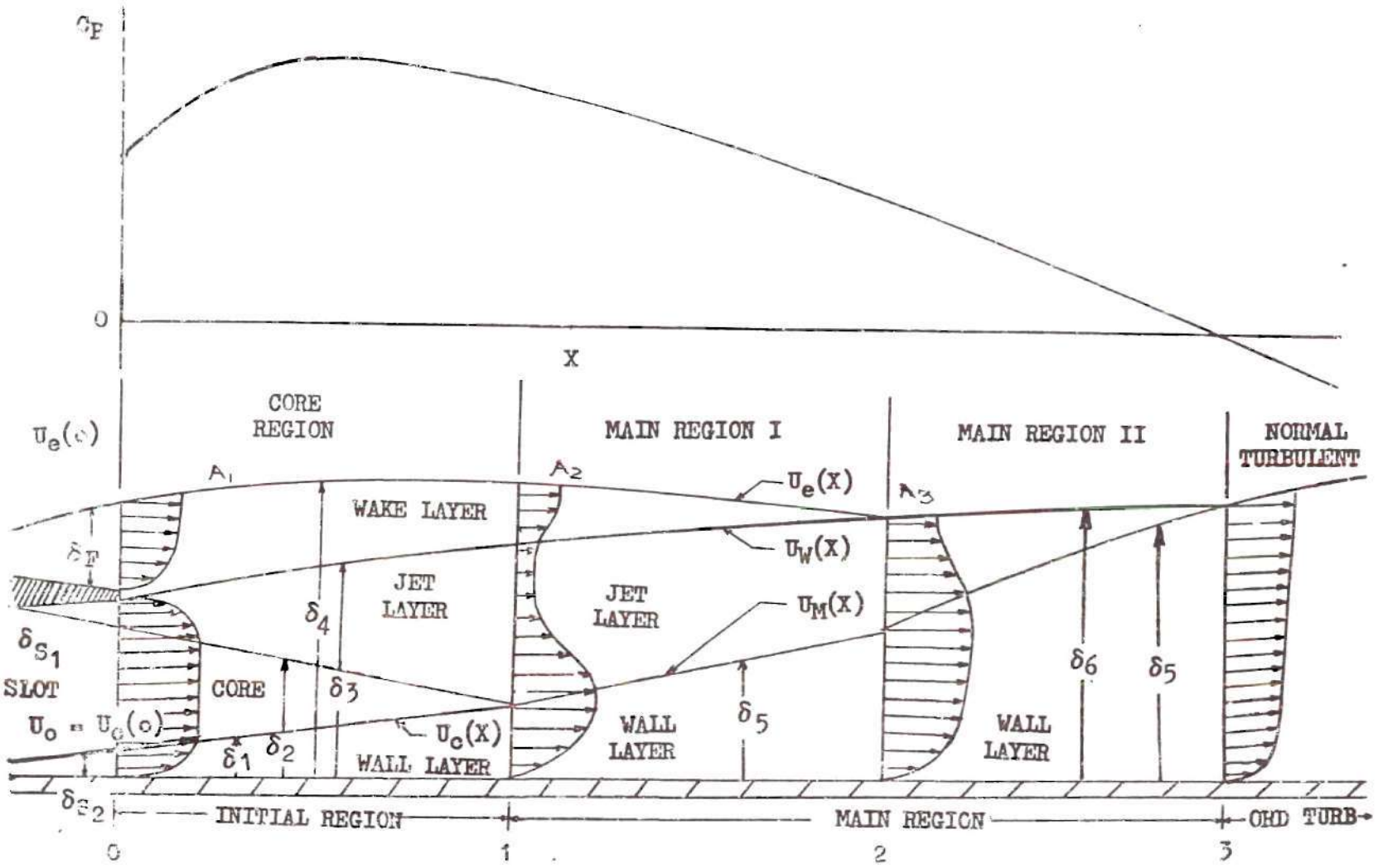

Figure 1. Physical Model for Confluent Boundary Layer Flow

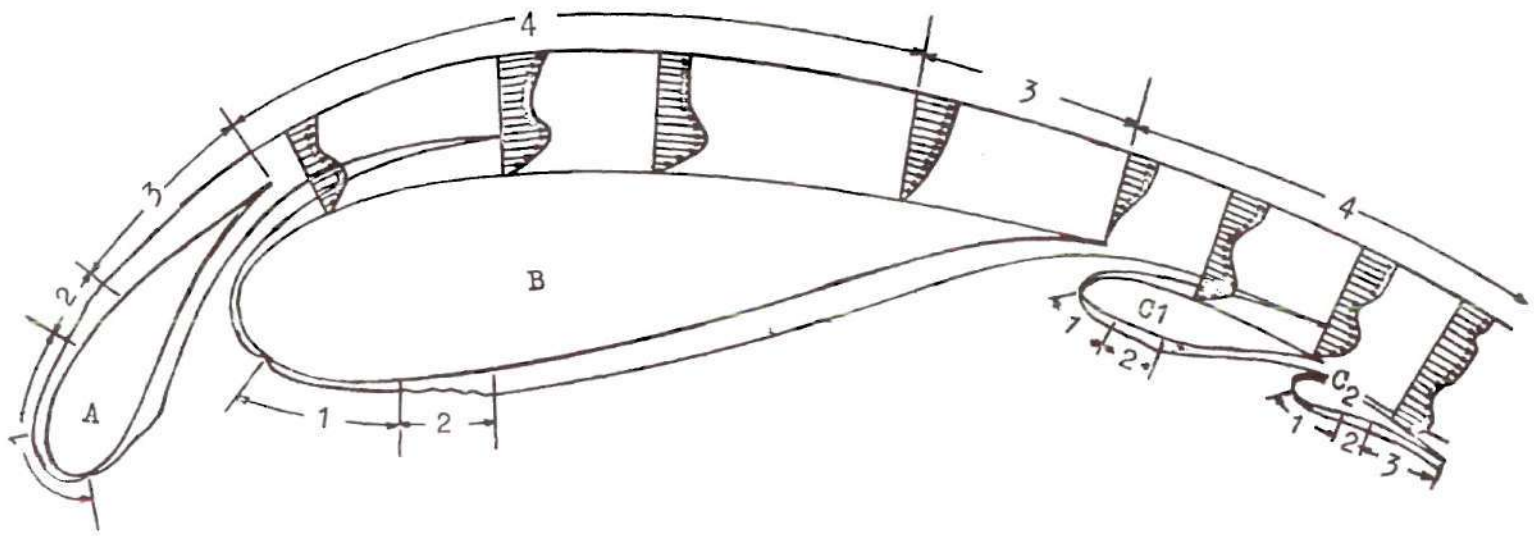

A LEADING EDGE SLAT

B MAIN COMPONENT

C1, C2 } DOUBLE SLOTTED FLAP

1 = LAMINAR B.L.

2 = TRANSITION REGION

3 = ORDINARY TURBULENT B.L.

4 = CONFLUENT BOUNDARY LAYER

Figure 1A. Boundary Layer Development on Multi-Components Airfoil

2) Derivations were made of the various relevant and pertinent integral equations with applicable boundary conditions for various layers and in various regions shown in Figure (1).

3) A number of parameters such as wall shear, shear stress at the edges of the various layers, wall-layer dissipation integral, etc. which appear in the equations derived under 2) above were computed. In order to reduce the number of unknowns in a particular region of Figure (1) to the number of equations derived for that region, the non-dimensional wall shear and shear at the edges of various layers were related to the dependent variables from considerations of local dynamic similarity laws. Auxiliary equations are derived for the above parameters as a function of one or several dependent variables.

4) The integral equations derived in 2) with the auxiliary equations for parameters are then reduced to a form suitable for numerical solution by the modified single step Euler method. The above equations were programmed for a Univac 1106 computer at the Lockheed-Georgia Company.

5) Experimental data obtained in the present study as well as confluent boundary layer data on the flap of an NACA 4418 airfoil and RAE airfoil are compared with the output of the computer program mentioned in Step 4) above. In addition, correlation of calculated viscous pressures and lift coefficients on multiple-airfoils is made with experimental measurements to further justify the validity of the theoretical method for the confluent boundary layer presented in this thesis.

The above steps along with previously published wall jet work is discussed in detail in the following sections.

CHAPTER II

RELATED INVESTIGATIONS

Glauert [1] used a similarity solution approach for the solution of the wall-jet problem in a still medium. Based on physical reasoning in this simple type of flow, he was the first to postulate that the entire flow field of the wall-jet cannot conform to one overall similarity solution. He divided the flow into a wall layer and a jet layer on either side of maximum velocity and treated the two regions separately. Myers, Schaurer and Eustis [2] conducted an analytical and experimental study of the wall-jet with no external stream. They treated the flow in both initial regions and main regions by integral methods. The velocity profile was divided into a wall layer and a jet layer. The velocity profile in the wall layer was assumed to be of the 1/7th power law type and the velocity profiles in the outer layer were assumed to be similar having the same similarity function as for a free jet. The wall shearing stress was measured by a hot film technique and the results were generalized as a function of Reynold's number and slot height. Kruka and Eskinazi [3] have studied experimentally and analytically wall-jet flow with an external stream at a large distance from slot exit. The ratios of injection to free stream velocity considered by these authors were greater than 2.5 and only the zero pressure gradient case was considered. The flow was again divided into inner and outer layers and similar velocity profiles were found to exist in both layers. Experimentally

the friction factor was found to be proportional to the inner Reynold's number raised to a power and consequently not constant with X. Thus

$$C_f = K_1 \left[\frac{U_m \delta_i}{\nu}\right]^{K_2}$$

Where K1 and K2 are constants but depend on the initial velocity ratio at the slot exit. Good agreement was found between calculated shear stress distribution across the viscous layer and that experimentally determined from Preston probe and hot wire anemometer measurements. Kacker and Whitelaw [4] investigated wall-jet flow experimentally for zero pressure gradient and in the range of velocity ratios of 0.75 to 2.74. Measurements were made of mean velocity profiles and turbulent shear distribution across the viscous layer. It was found that the shear work integral decreases exponentially for flows with velocity maxima and that the point of zero shear was closer to the wall than that of zero velocity gradient. The characteristic of the shear distribution profile measured by these authors is similar to the one calculated numerically under the present investigation. The authors obtained the value of skin friction coefficient at a distance greater than 50 slot heights from the slot exit by the use of a Clauser chart in which the constant shear lines are plotted from the equation,

$$U^+ = \frac{1}{K} \ln(y^+) + C$$

where

$$U^+ = \frac{u}{\sqrt{\tau_w/\rho}} \quad ; \quad y^+ = \frac{y\sqrt{\tau_w/\rho}}{\nu}$$

and K and C are constants.

Bradshaw and Gee [5] conducted experiments on wall-jets in still air on flat and curved surfaces and beneath an external stream. The behavior of wall-jets was discussed on the basis of experimental results and they concluded that assumptions of layer independence are not valid and as a result a satisfactory calculation method was not immediately practicable. They measured the wall shear for the case of no external stream and without any pressure gradient and formulated an expression for it as a function of Reynolds number based on peak velocity at the edge of wall layer and wall layer thickness. Thus

$$\frac{\tau_w}{\frac{1}{2}\rho U_m^2} = 0.0315\left(\frac{U_m \delta_s}{\nu}\right)^{-.182}$$

where

δ_s = Wall layer thickness

They found that Reynolds shear stress was not zero at the velocity maximum thus invalidating the simple assumptions of layer independence made by other workers.

G. L. Harris [6] conducted analytical work on the turbulent wall-jet in a moving stream with arbitrary pressure gradient. His mathematical model consisted of a wall layer and a jet layer only and furthermore, it was assumed in his analysis that slot velocity and slot height are very large compared to the free stream value at the exit of the slot. In that case the momentum deficit of the upstream boundary layer at the slot lip is not large and thus he could justify no interference of external stream boundary layer on the flow development down-

stream. He also did not consider the initial region and assumed that initial conditions for the main region are available from experimental data.

Escudier and Whitelaw [7] reported results, on boundary layers with adverse pressure gradients, of injecting secondary flow normal to the main stream through a strip of porous material placed across the test plate flush with its surface. The authors reached the conclusion that pressure gradient has relatively little influence on effectiveness up to the condition of separation. Their conclusion seems to be in agreement with results reported by Hartnett, Birkebak and Eckert [12] and Seban and Back [13].

Nicoll and Whitelaw [8] investigated the wall-jet in the range of slot to free stream velocity from 0.46 to 2.26 with helium as a tracer gas. The authors proposed a prediction technique which gives good correlation with experimental data when the upstream boundary layer is small and at a distance greater than 10 slot heights downstream of slot exit.

R. J. Kind [9] published a paper entitled, "A Calculation Method for Circulation Control by Tangential Blowing Around a Bluff Trailing Edge". He included curvature effects in his two-dimensional analysis but calculations in the initial region were not considered. The method was restricted to the two layers, i.e., wall layer and jet layer only and initial conditions for the main region (see Figure (1)) were assumed as given.

I. S. Gastshore and B. G. Newman [10] conducted an analysis of the turbulent wall-jet with an arbitrary pressure gradient. Their velocity

profile assumption was of a 'simple wall-jet type' instead of a more realistic velocity profile having a distinct minimum point. The expression for wall shear was arrived at from measurement in self-preserving wall jets in a moving stream. This expression for wall shear was then assumed to be valid for the wall shear stress beneath a wall jet in any pressure gradient. The authors neglected calculations in the initial region.

Recently, Bangert [11] developed a method in which a four or five parameter profile is assumed depending on the presence or absence of a velocity minimum. Momentum and kinetic energy integrals are written for various parts of the layer and empiricism enters as dissipation integrals are correlated with profile parameters, in this case using several constant turbulent Reynolds numbers to define eddy viscosities in the various parts of the layer.

CHAPTER III

THEORETICAL STUDY

In this section a brief description of the flow model derived from the preliminary experimental data is first given. This is then followed by a brief derivation, in summary form, of the various sets of pertinent differential equations for the initial region, the main region, and the ordinary turbulent boundary layer region. At approximate points in the derivations of the pertinent equations, mention is made of the governing equations, applicable boundary conditions and various assumptions.

A detailed derivation of equations in main region I is given in the Appendix. The reason for presenting a detailed derivation of the equations in main region I only, is that it is typical for the other regions as shown in Figure (1).

Description of Flow Model

Figure (1) shows a sketch of a physical model which was derived from preliminary experimental data. This model is used as a basis for derivation of the differential equations necessary for the solution of the various physical quantities involved.

As seen in Figure (1), the flap is represented by a flat plate thus ignoring curvature effects, but the viscous region is assumed to be subjected to an arbitrary external pressure distribution. The boundary layer emerging from the slot is assumed to have a constant-

velocity core, as indicated in Figure (1) at station 0. This boundary layer mixes with the second boundary layer developed up to the trailing edge of the fore-component. It is assumed that the required initial conditions, for example δ_F, slot exit velocity $U_{c(o)}$, velocity at the trailing edge, $U_{e(o)}$, δs_1 and δs_2 are known.

The region between stations 0 and 1 is defined as the Initial Region. The region between stations 1 and 2 is defined as the Main Region I and between stations 2 and 3 as Main Region II. The region downstream of station 3 and up to the point of separation, is similar to the ordinary turbulent boundary layer flow.

A typical velocity profile in the Initial Region between stations 0 and 1 is as shown at station 0. The layer from $y = 0$ to $y = \delta_1$, is called the wall layer. If the velocity in this layer is non-dimensionalized with respect to U_c and distance y is non-dimensionalized with respect to δ_1, this non-dimensional velocity plot looks similar to the ordinary boundary layer velocity profile. From $y = \delta_1$ to $y = \delta_2$, the velocity is constant and this layer is called the "potential core." Due to differences in the velocities at the slot exit and the fore-component trailing-edge, and also due to finite trailing-edge thickness as well as trailing-edge boundary layer, there is a depression in the velocity at $y = \delta_3$. The layer from $y = \delta_2$ to $y = \delta_3$ is defined as the jet layer because "similar velocity profiles" are obtained when the velocity and distances for the points in this layer are non-dimensionalized in a way analogous to that for free-jet flow. The layer from $y = \delta_3$ to $y = \delta_4$ is defined as the wake layer for this same reason.

The Initial Region terminates at stion 1 which forms the starting point for calculations for the Main Region. A typical velocity profile in the Main Region between stations 1 and 2 is shown in Figure (1) at station 1. The velocity $U_{m(x)}$ at the edge of wall layer ($y = \delta_5$) must be determined from a viscous solution in contrast to $U_{c(x)}$ which is determined from potential flow. The wake layer from $y = \delta_3$ to $y = \delta_4$ is shown to terminate at station 2. Actually, this wake layer may terminate in either the Initial Region between stations 0 and 1 or in the Main Region I between station 1 and 2 depending upon the initial conditions at station 0 and the pressure distribution. The Main Region II is distinguished from Main Region I in that Main Region II does not have wake layer.

At station 3, the jet layer terminates and the viscous flow becomes qualitatively similar to ordinary turbulent boundary layer flow. The initial conditions at station 3, necessary for the solution of pertinent quantities downstream, are obtained from solution of the equations in the Main Region up to station 3.

Derivation of Equations in Initial Region

Referring to Figure (1), there are seven dependent variables which are to be calculated as a function of the independent variable X for the given initial conditions at the slot exit and the external impressed pressure distribution. These variables to be calculated are (i) wall layer momentum thickness, $\theta_{1(x)}$, (ii) wall layer form factor, $H_{1(x)}$, (iii) velocity in the core, $U_{c(x)}$, (iv) edge of core and jet layer, $\delta_{2(x)}$, (v) edge of jet layer and wake layer, $\delta_{3(x)}$, (vi) velocity at

the edge of jet and wake layer, $U_{w(x)}$, and (vii) external edge of wake layer, $\delta_{4(x)}$. However, the calculation of the velocity, $U_{c(x)}$, in the core is straightforward.

Relation Between $U_{c(x)}$ and $C_{p(x)}$

In order to derive an equation for $U_{c(x)}$ in terms of $U_{c(o)}$, $C_{p(o)}$, $C_{p(x)}$ and $U_{e(o)}$, the following assumptions are made:

$\frac{\partial p}{\partial y} = 0$ i.e., static pressure remains constant in the y direction,

$\rho \neq \rho(p)$ i.e., density is not a function of pressure (specifically, ρ_o and ρ_e are based on suitable mean temperatures which are functions of wall temperature, temperature of slot stream at exit and free stream temperature).

The Bernoulli equation, $\int \frac{dp}{\rho} + \frac{q^2}{2} = \text{constant}$, is assumed to be valid in the core as well as at the external edge of viscous layer.

When use is made of the above assumptions the following equations can be derived:

$$\{R_{1(x)}\}^2 = \left(\frac{U_{e(x)}}{U_{c(x)}}\right)^2 = \frac{\rho_o}{\rho_e}\left[1 - \frac{\{1-(\frac{\rho_e}{\rho_o})R_o^2\}}{\{1+\frac{\rho_\infty U_\infty^2}{\rho_o U_o^2}(C_{p_o}-C_{p(x)})\}}\right] \qquad (1)$$

$$\frac{U_{c(x)}^2}{U_{c(o)}^2} = \frac{1-(\frac{\rho_e}{\rho_o})R_o^2}{1-(\frac{\rho_e}{\rho_o})R_1^2} \qquad (2)$$

Thus, $U_{c(x)}$ can be computer by equation (2) with the aid of equation (1). Therefore in the Initial Region six variables remain unknown, namely, $\delta_{1(x)}$ $H_{1(x)}$, $\delta_{2(x)}$, $\delta_{3(x)}$, $U_{w(x)}$ and $\delta_{4(x)}$. Six equations are required for the solution of the six variables in the

Initial Region.

Wall Layer, Initial Region

Velocity profiles in the wall layer are assumed to be of one parameter family rather than of the similar velocity profile type. Under the assumption of a one parameter family, one is able to account for the effects of pressure gradient on viscous flow for the wall layer. It is not possible to take into account the effect of pressure gradient if the wall-layer velocity profiles are assumed to be similar. Use of a one parameter family for the wall layer velocity profile, however, makes it necessary to use two dependent variables. These variables are chosen as the wall layer momentum thickness, $\theta_{1(x)}$ and the wall layer form factor, $H_{1(x)}$. Thus, two equations are needed to solve for these two variables. The following approach is taken to derive the desired equations.

Continuity Equation -

$$\frac{\partial u}{\partial x} + \frac{\partial v}{\partial y} = 0 \tag{3}$$

X - Momentum Equation -

$$u\frac{\partial u}{\partial x} + v\frac{\partial u}{\partial y} = -\frac{1}{\rho}\frac{dP}{dx} + \frac{1}{\rho}\frac{\partial \tau}{\partial y} \tag{4}$$

Y - Momentum Equation with the usual boundary layer assumptions for attached flow.

$$\frac{\partial P}{\partial y} = 0 \tag{5}$$

Following Truckenbrodt, (p. 574, ref. 15), we assume that wall layer velocity profiles form a one parameter family of curves and can be represented as,

$$\frac{u}{U_c} = \left(\frac{y}{\delta_1}\right)^{1/n} \tag{6}$$

where n is dependent on the previous upstream history and is primarily a function of pressure gradient.

By making use of Equation (6) in the definitions for ϑ_1, δ_1^*, δ_1^{**}, etc. the following relations can be derived:

$$\frac{\theta_1}{\delta_1} = \frac{n}{(n+2)(n+1)} \; ; \; \frac{\delta_1^*}{\delta_1} = \frac{1}{(n+1)} \; ; \; H_1 = \frac{(n+2)}{n} \tag{7}$$

$$\frac{\delta_1^{**}}{\delta_1} = \frac{2n}{(n+1)(n+3)} \; ; \; \frac{\theta_1}{\delta_1} = \frac{(H_1-1)}{H_1(H_1+1)} \; ; \; \tilde{H} = \frac{2(n+2)}{(n+3)} = \frac{4H_1}{3H_1-1}$$

The Euler equation, valid at the external edge $A_1A_2A_3$ in Figure (1), can be written as:

$$\frac{dP}{dx} = -\rho_e U_{e(x)} \frac{dU_e}{dx} \tag{8}$$

By making use of Equation (5), we can write,

$$\frac{dP}{dx} = -\rho_0 U_{(c)(x)} \frac{dU_c}{dx} \tag{9}$$

From the continuity Equation (3), we have,

$$v = -\int_0^y \frac{\partial u}{\partial y}\, dy \tag{10}$$

Boundary conditions applicable to the wall layer under consideration are:

$$\text{at} \quad y=0 \;:\; u=0,\; v=0,\; \tau = \tau_w \tag{11}$$

$$\text{at} \quad y=\delta_1 \;:\; u=U_c,\; \tau = \tau_{(\delta_1)},\; -\frac{1}{\rho_0}\frac{dP}{dx} = U_c \frac{dU_c}{dx}$$

Integrating Equations (4) from y = 0 to y = δ_1 and making use of Equations (5) through (11), the following momentum integral equation for wall layer in the Initial Region is derived:

$$\frac{d\theta_1}{dx} + \frac{\theta_1}{U_c}\frac{dU_c}{dx}(H_1 + 2) = \frac{\tau_w}{\rho_0 U_c^2}\left(1 - \frac{\tau_{(\delta_1)}}{\tau_w}\right) \tag{12}$$

A second equation is derived by first multiplying Equation (4), by u and then integrating from y = 0 to y = δ_1. Use is also made of Equations (5) through (10) to obtain the following equation:

$$\frac{dH_1}{dx} = \frac{H_1}{\theta_1}(3H_1-1)\frac{\tau_w}{\rho_0 U_c^2} + \frac{(H_1-1)(3H_1-1)}{2\theta_1}\frac{\tau_w}{\rho_0 U_c^2}\frac{\tau_{(\delta_1)}}{\tau_w} \qquad (13)$$

$$- H_1(3H_1-1)(H_1-1)\left(\frac{1}{U_c}\frac{dU_c}{dx}\right) - \frac{(3H_1-1)}{2\theta_1}\int_0^{\delta_1}\frac{\tau}{\rho_0 U_c^2}\frac{\partial}{\partial y}\left(\frac{u}{U_c}\right)dy$$

The above equation is the dissipation energy integral equation or the form factor equation for the wall layer in the initial region.

Jet-Layer, Initial Region

In order to be able to reduce the Prandtl viscous flow equation, e.g. equations (4) which are partial differential equations, into ordinary differential equations which are amenable to solution by numerical methods, it is necessary to observe either similarity of velocity profiles or a one parameter family of velocity profiles. For the complex flow of Figure (1), it would be hopeless to find such velocity profiles for the entire viscous layer extending from the wall to the external edge of the viscous flow. In such circumstances, one would try to divide the flow into various layers and attempt to find parameters such that velocity profiles in each individual layer are similar or can be represented by a one parameter family. From the experimental velocity data, it is found that velocity profiles in the jet layer in the initial region are similar for various pressure distributions as well as for different ratios of slot exit to free stream velocities if the similarity parameters and similarity functions are defined in the following manner:

$$\eta_1 = \frac{\delta_3 - y}{\delta_3 - \delta_2} \quad , \quad f(\eta_1) = \frac{U_c - u}{U_c - U_w} \tag{14}$$

where

u = velocity in $\delta_2 - \delta_3$ layer at any distance y above wall

$U_w = U_w(x)$ = velocity at $y = \delta_3$

U_c = velocity in the core

It will be shown in Chapter V that experimental data for different pressure distributions, different X locations and for various conditions at slot exit, fall nicely along a single curve when similarity parameters are chosen as indicated in equation (14). The least square polynomial expression for $f(\eta_1)$ is given by the following expression:

$$f(\eta_1) = 0.992 + 0.487(\eta_1) - 6.105(\eta_1)^2 + 6.796(\eta_1)^3 - 2.166(\eta_1)^4 \tag{14A}$$

Boundary conditions for the jet layer $\delta_2 - \delta_3$ are as follows:

$$\begin{aligned} &\text{at} \quad y = \delta_2 \quad : \quad \eta_1 = 1 \;, \quad f(\eta_1) = 0 \;, \quad \tau = \tau_{(\delta_2)} \\ &\text{at} \quad y = \delta_3 \quad : \quad \eta_1 = 0 \;, \quad f(\eta_1) = 1 \;, \quad \tau = \tau_{(\delta_3)} \end{aligned} \tag{15}$$

Integrating equation (4) from $y = \delta_2$ to $y = \delta_3$, making use of equation (14) and boundary conditions (15) and also equations (12) and (13) leads to the following momentum integral equation for the jet layer, $\delta_2 - \delta_3$, in the initial region:

$$\left\{\int_0^1 (1-f(\eta_1))\,d\eta_1\right\}\left[\frac{d}{dx}\left\{(\delta_3-\delta_2)\,U_c\,(U_c-U_w)\right\}\right] - \left\{\int_0^1 f(\eta_1)\,d\eta_1\right\}\left[\frac{d}{dx}\left\{(\delta_3-\delta_2)(U_c-U_w)^2\right\}\right]$$
$$+\left\{\int_0^1 f^2(\eta_1)\,d\eta_1\right\}\left[\frac{d}{dx}\left\{(\delta_3-\delta_2)(U_c-U_w)^2\right\}\right] + U_c\left(\frac{dU_w}{dx}\right)(\delta_3-\delta_2) \qquad (16)$$
$$-(U_c-U_w)(\delta_3-\delta_2)\left(\frac{dU_w}{dx}\right)\int_0^1 f(\eta_1)\,d\eta_1 + U_c(U_c-U_w)\frac{d\delta_2}{dx}$$
$$-(U_c-U_w)\,U_c\,H_1\left\{\frac{\tau_w}{\rho_0 U_c^2}\left(1-\frac{\tau_{(\delta_1)}}{\tau_w}\right) - \frac{\theta_1}{U_c}\frac{dU_c}{dx}(H_1+2)\right\}$$
$$-(U_c-U_w)\,U_c\left\{H_1(3H_1-1)\frac{\tau_w}{\rho_0 U_c^2} + \frac{(H_1-1)(3H_1-1)}{2}\left(\frac{\tau_w}{\rho_0 U_c^2}\right)\left(\frac{\tau_{(\delta_1)}}{\tau_w}\right)\right.$$
$$\left. - H_1(3H-1)(H_1-1)\left(\frac{1}{U_c}\frac{dU_c}{dx}\right)\theta_1 - \frac{(3H_1-1)^2}{2}\int_0^{\delta_1}\frac{\tau}{\rho_0 U_c^2}\frac{\partial}{\partial y}\left(\frac{u}{U_c}\right)dy\right\}$$
$$-(U_c-U_w)\,H_1\,\theta_1\frac{dU_c}{dx} + (U_c-U_w)\,\delta_2\frac{dU_c}{dx} - U_c\frac{dU_c}{dx}(\delta_3-\delta_2)$$
$$= \frac{\tau_w}{\rho_0}\left\{\frac{\tau_{(\delta_3)}}{\tau_w} - \frac{\tau_{(\delta_2)}}{\tau_w}\right\}$$

In analogy with free jet flow, the rate of growth of the boundaries of the jet layer $\delta_2 - \delta_3$ can be expressed as:

$$\frac{d(\delta_3-\delta_2)}{dx} = C_1\frac{(U_c-U_w)}{(U_c+U_w)} \qquad (17)$$

where

C_1 = constant determined experimentally (≈ 0.4).

It should be noted that in equation (17), U_w is an unknown function of x. $U_{c(x)}$ is determined from equation (2) when the pressure distribution is specified and velocities $U_{c(o)}$ and $U_{e(o)}$ are known.

Wake-Layer, Initial Region

As in the case of the jet layer it would be necessary to find similarity parameters in order to get ordinary differential equation with the appropriate boundary conditions. Experimental velocity profiles in the wake layer in the initial region for different x locations and slot exit condition and also for different pressure distributions fall on a single curve when the similarity parameter and function are chosen as follows:

$$\eta_2 = \frac{y - \delta_3}{y_{1c} - \delta_3} \quad ; \qquad f(\eta_2) = \frac{U_e - u}{U_e - U_w} \tag{18}$$

where, (see Figure (1))

δ_3 = distance above surface at the common boundary of jet and wake layers

u = velocity at any distance y above wall in the wake layer

U_e = velocity at $y = \delta_4$ where the flow can be considered inviscid

y_{1_c} = distance y where $u = \frac{U_e + U_w}{2}$

A discussion of the similarity for velocity profiles in the wake layer of initial region will be given in Chapter V. With the use of experimental data the following least square polynomial is obtained for

wake layer in initial region,

$$f(\eta_2) = 1.032 - 0.416(\eta_2) - 0.145(\eta_2)^2 + 0.12(\eta_2)^3 - 0.015(\eta_2)^4 \qquad (19)$$

The boundary conditions for the wake layer δ_3 - δ_4 are as follows:

$$\text{at } y = \delta_3 : \eta_2 = 0 , f(\eta_2) = 1 , \tau = \tau_w \qquad (20)$$

$$\text{at } y = y_{1c} : \eta_2 = 1 , f(\eta_2) = 0.5 , u = \frac{U_e + U_w}{2}$$

$$\text{at } y = \delta_4 : f(\eta_2) = 0 , u = U_e , \tau = 0 ; \eta_2 = K_1$$

$$\text{where } K_1 = \eta_2 \big|_{y=\delta_4}$$

Integrating equation (4) from $y = \delta_3$ to $y = \delta_4$ and making use of equations (10), (12), (13), and (18) and also boundary conditions given by (20), the following equation is obtained:

$$
\begin{aligned}
&- \left\{ \int_0^{K_1} f(\eta_2)\, d\eta_2 \right\} \left[\frac{d}{dx} \left\{ (y_{1c} - \delta_3)(U_e)(U_e - U_w) \right\} \right] \qquad (21)\\
&+ \left\{ \int_0^{K_1} f^2(\eta_2)\, d\eta_2 \right\} \left[\frac{d}{dx} \left\{ (y_c - \delta_3)(U_e - U_w)^2 \right\} \right] - \frac{d\delta_3}{dx} U_w (U_e - U_w)\\
&- \left\{ \int_0^{K_1} f(\eta_2)\, d\eta_2 \right\} \left[\frac{dU_e}{dx} (U_e - U_w)(y_{1c} - \delta_3) \right] + (U_e - U_w) U_c H_1 (3H_1 - 1) \frac{\tau_w}{\rho_0 U_c^2}\\
&+ \frac{(U_e - U_w)}{2} U_c (H_1 - 1)(3H_1 - 1) \frac{\tau_w}{\rho_0 U_c^2} \frac{\tau_{(\delta_1)}}{\tau_w} - (U_e - U_w)\theta_1 H_1 (3H_1 - 1)(H_1 - 1) \frac{dU_c}{dx}\\
&- \frac{U_e - U_w}{2} U_c (3H_1 - 1)^2 \int_0^{\delta_1} \frac{\tau}{\rho_0 U_c^2} \frac{\partial}{\partial y} \left(\frac{u}{U_c} \right) dy + (U_e - U_w) U_c H_1 \frac{\tau_w}{\rho_0 U_c^2}\\
&- (U_e - U_w) U_c H_1 \frac{\tau_w}{\rho_0 U_c^2} \frac{\tau_{\delta_1}}{\tau_w} - 2(U_e - U_w) H_1 \theta_1 \frac{dU_c}{dx} - (U_e - U_w) H_1^2 \theta_1 \frac{dU_c}{dx}\\
&+ (U_e - U_w)\theta_1 H_1 \frac{dU_c}{dx} - (U_e - U_w)\delta_2 \frac{dU_c}{dx} - (U_e - U_w)(\delta_3 - \delta_2) \frac{dU_c}{dx}\\
&- (U_e - U_w) \frac{d\delta_3}{dx} (U_c - U_w) + (U_e - U_w) \left\{ \int_0^1 f(\eta_1)\, d\eta_1 \right\} \frac{d}{dx} \left\{ (\delta_3 - \delta_2)(U_c - U_w) \right\}\\
&= - \frac{\tau}{\rho_e} \frac{\tau_{(\delta_3)}}{\tau_w}
\end{aligned}
$$

The above equation is the momentum integral equation for the wake layer in the Initial Region.

The rate of growth of the wake layer $\delta_3 - \delta_4$ is expressed in an analogous manner to the jet layer $\delta_2 - \delta_3$ as follows:

$$
\frac{d(y_{1c} - \delta_3)}{dx} = C_2 \frac{(U_e - U_w)}{(U_e + U_w)} \qquad (22)
$$

where

C_2 = constant determined empirically (≈ 0.18)

The six unknown dependant variables in the initial region, namely, (i) $\delta_{1(x)}$, (ii) $H_{1(x)}$, (iii) $\theta_{2(x)}$, (iv) $\delta_{3(x)}$, (v) $U_{w(x)}$, and (vi) $\delta_{4(x)}$ are calculated by numerical methods discussed in a later section. This problem becomes initial value problem and thus requires initial conditions. These initial conditions are to be specified at the exit of slot. Those shown in Figure (1) are (1) boundary layer thickness on the upper surface of the main component at the trailing edge, (2) momentum thickness on the upper surface of the main component at the trailing edge, (3) boundary layer thickness δ_{s_1}, on the under surface of the main component at the trailing edge, (4) momentum thickness on the under surface at the trailing edge, θ_{s_1} (5) velocity at the trailing edge, $U_{e(o)}$, (6) slot velocity at the exit, $U_{c(o)}$, (7) boundary layer momentum thickness on the flap upper surface at slot exit, θ_{s_2} and (8) boundary layer thickness on the flap upper surface at slot exit, δ_{s_2}. A starting value of U_w is obtained by making a momentum balance at the trailing edge of the fore-component. Boundary layer thickness both on the upper and lower surface at the trailing edge are assumed to remain unchanged for the momentum balance.

Derivation of Equations in Main Region I

Solution of the equations derived in the previous section for the Initial region will yield values of H_1, θ_1, $\delta_1 (= \delta_2)$, δ_3, δ_4 and U_w at station 1 in Figure (1). These values then become the initial conditions for the solution of equations for the Main region I. Referring to Figure (1), Main Region I is defined as extending between

stations 1 and 2. Main Region I is distinguished from the Main Region II by the presence of a wake layer in Main Region I.

The velocity $U_{c(x)}$ at the edge of the wall layer in the Initial region was obtained with the use of the Bernoulli equation and the condition of constancy of pressure in the y direction. This was possible because of the existance of a potential core in the Initial region. In the Main Region, however, the velocity $U_{m(x)}$ at the edge of the wall layer has to be determined from a viscous solution which involves simultaneously solving the equations developed in this section.

In the Main Region I, there are six dependable variables to be solved, namely, (i) wall layer momentum thickness, θ_5, (ii) wall layer form factors, H_5, (iii) velocity U_m at the edge of wall layer, (iv) velocity U_w at the juncture of the jet layer and the wake layer, i.e., at $y = \delta_{3(x)}$, (v) locus of velocity $U_{w(x)}$, i.e., line $y = \delta_{3(x)}$ and (vi) external edge of the wake layer where the flow can be considered inviscid, i.e., the line $y = \delta_{4(x)}$. Thus six equations are needed to determine the above six variables. As mentioned previously, a detailed derivation of these six equations will be given in the Appendix. However, assumptions and boundary conditions and a brief derivation of the equations will be given in the following pages so as to maintain continuity.

Wall Layer, Main Region I

Wall layer velocity profiles in this region also will be assumed as a one parameter family rather than similar. Under this assumption, the effects of streamwise pressure gradient on the flow are taken into account and at the same time the boundary layer type partial differential

equations, such as equations (3) and (4) are transformed to ordinary differential equations which are more amenable to a solution. Thus. assume the wall layer velocity profile of the following form

$$\frac{u}{U_m} = \left(\frac{y}{\delta_5}\right)^{\frac{1}{n_2}} \tag{23}$$

where $n_2 = n_{2(x)}$ = Function of pressure gradient.

Making use of equation (23) in the definitions for δ_5^*, θ_5, H_5, $\tilde{H}_5$, and δ_5^{**} the following relations can be derived:

$$\frac{u}{U_m} = \left(\frac{y}{\delta_5}\right)^{\frac{1}{n_2}} \; ; \quad \frac{\theta_5}{\delta_5} = \frac{H_5 - 1}{H_5(H_5+1)} = \frac{n_2}{(n_2+1)(n_2+2)} \tag{24}$$

$$\tilde{H}_5 = \frac{4H_5}{3H_5 - 1} \; , \qquad n_2 = \frac{2}{H_5 - 1} \; ; \quad \frac{n_2}{n_2+1} = \frac{2}{H_5+1}$$

$$\delta_5 \frac{n_2}{n_2+1} = 2\theta_5 \frac{H_6}{H_5 - 1} \; ; \quad \delta_5^{**} = \frac{\delta_5}{n_2+1} \; ; \quad H_5 = \frac{n_2+2}{n_2}$$

Boundary conditions for the wall layer are:

$$\text{at } y=0 : \; u=0, \; v=0, \; \tau = \tau_w \tag{25}$$

$$\text{at } y=\delta_5 : \; u = U_m, \; \tau = \tau_{(\delta 5)}$$

The Euler equation, valid at the external edge of the viscous layer,

is:

$$-\frac{1}{\rho}\frac{dP}{dx} = U_e\frac{dU_e}{dx} \tag{26}$$

Integrating equation (4) with respect to y from y = 0 to y = δ_5, and making use of equations (16) and (26), and (24) and boundary conditions (25) one obtains the following momentum integral for the wall layer in the Main Region between stations 1 and 2:

$$\frac{d\theta_5}{dx} - 2\frac{\theta_5}{H_5-1}\frac{1}{U_m}\frac{dU_m}{dx} + \frac{U_e}{U_m^2}\frac{dU_e}{dx}\frac{\theta_5 H_5(H_5+1)}{H_5-1} = \frac{\tau_w}{\rho U_m^2}\left\{1 - \frac{\tau_{(\delta_5)}}{\tau_w}\right\} \tag{27}$$

Multiplying both sides of equation (4) by u, integrate from y = 0 to y = δ_5 and making use of equations (10), (24), (26) and boundary conditions (25) one obtains the following equation:

$$\frac{dH_5}{dx} = \frac{H_5}{\theta_5}(3H_5-1)\frac{\tau_w}{\rho U_m^2} + \frac{H_5-1}{2\theta_5}(3H_5-1)\left(\frac{\tau_w}{\rho U_m^2}\right)\left(\frac{\tau_{(\delta_5)}}{\tau_w}\right) - \frac{U_e}{U_m^2}\frac{dU_e}{dx}(H_5)(3H_5-1)(H_5-1) - \frac{(3H_5-1)^2}{2\theta_5}\int_0^{\delta_5}\frac{\tau}{\rho U_m^2}\frac{\partial}{\partial y}\left(\frac{u}{U_m}\right)dy \tag{28}$$

Equation (28) is the form factor equation for the wall layer in the Main Region between stations 1 and 2.

Jet Layer, Main Region I

As indicated previously for the jet-layer in the Initial Region, similar velocity profiles were obtained with certain chosen parameters. It is also necessary to observe in Main Region I if experimental data indicate similarity of velocity profiles in order to obtain the momentum integral equation for this layer. Figure (10) shows a similarity plot of experimental data for various pressure distributions and slot exit conditions for different X locations in the Main Region. In this case experimental data also falls nicely on a single curve showing that similarity is obtained with the use of the following similarity parameter and function:

$$\eta_3 = \frac{\delta_3 - y}{\delta_3 - \delta_5} \quad ; \quad f(\eta_3) = \frac{U_m - U_w}{U_m + U_w} \qquad (29)$$

A fourth order least square polynomial fit for the Main Region is given by,

$$f(\eta_3) = 1.002 - 0.164(\eta_3) - 1.967(\eta_3)^2 + 1.338(\eta_3)^3 - 0.209(\eta_3)^4 \qquad (29A)$$

Applicable boundary conditions for this layer are:

$$\text{At} \quad y = \delta_5 \; : \; u = U_m, \quad \eta_3 = 1, \quad f(\eta_3) = 0, \quad \tau = \tau_w \qquad (30)$$

$$\text{At} \quad y = \delta_3 \; : \; u = U_w, \quad \eta_3 = 0, \quad f(\eta_3) = 1, \quad \tau = \tau_{(\delta_3)}$$

Integrating equation (4) with respect to y from $y = \delta_5$ to $y = \delta_3$, making use of equations (24), (10), (26), (27) and (28) and also boundary conditions (30), one obtains the following momentum integral equation for the jet layer in the Main Region between stations 1 and 2:

$$\left\{\int_0^1 (1 - f(\eta_3))\, d\eta_3\right\}\left[\frac{d}{dx}\left\{U_m(U_m - U_w)(\delta_3 - \delta_5)\right\}\right] \tag{31}$$

$$-\left\{\int_0^1 f(\eta_3)\, d\eta_3\right\}\left[\frac{d}{dx}\left\{(U_m - U_w)^2(\delta_3 - \delta_5)\right\}\right]$$

$$+\left\{\int_0^1 f^2(\eta_3)\, d\eta_3\right\}\left[\frac{d}{dx}\left\{(U_m - U_w)^2(\delta_3 - \delta_5)\right\}\right] + U_m(\delta_3 - \delta_5)\left(\frac{dU_w}{dx}\right)$$

$$-\left(\frac{dU_w}{dx}\right)(\delta_3 - \delta_5)(U_m - U_w)\int_0^1 f(\eta_3)\, d\eta_3 + 2(U_m - U_w)\theta_5\,\frac{H_5(H_5+1)}{(H_5+1)^2}\left(\frac{dU_m}{dx}\right)$$

$$-4U_m(U_m - U_w)\frac{H_5^2}{(H_5-1)^2}\left(\frac{\tau_w}{\rho U_m^2}\right) - U_m(U_m - U_w)\frac{\tau_w}{\rho U_m^2}\,\frac{\tau_{(\delta_5)}}{\tau_w}\,\frac{5H_5 - 1}{H_5 - 1}$$

$$+2(U_m - U_w)\frac{H_5}{(H_5-1)^2}(2H_5^2 - 5H_5 + 1)\,\theta_3\,\frac{U_e}{U_m}\,\frac{dU_e}{dx}$$

$$+U_m(U_m - U_w)\frac{(3H_5 - 1)^2}{(H_5-1)^2}\int_0^{\delta_5}\frac{\tau}{\rho U_m^2}\,\frac{\partial}{\partial y}\left(\frac{u}{U_m}\right)dy$$

$$-U_e\frac{dU_e}{dx}(\delta_3 - \delta_5) = \frac{\tau_w}{\rho}\,\frac{\tau_{(\delta_3)}}{\tau_w} - \frac{\tau_w}{\rho}\,\frac{\tau_{(\delta_5)}}{\tau_w}$$

The rate of growth of the jet layer $\delta_5 - \delta_3$ between stations 1 and 2 can be expressed as follows:

$$\frac{d}{dx}(\delta_3 - \delta_5) = C_3\frac{(U_m - U_w)}{(U_m + U_w)} \tag{32}$$

where C_3 is an empirical constant (≈ 0.17).

It should be noted that U_m and U_w in equation (32) are both unknown functions of the independent variable X.

Wake Layer, Main Region I

The velocity profiles in the wake layer of Main Region I are also found to be "similar." Experimental data for the velocity profiles in the wake layer of Main Region I shows that the velocity profile become similar if the following similarity parameter and similarity function is used,

$$\eta_4 = \frac{y - \delta_3}{y_{2c} - \delta_3} \quad \text{and} \quad f(\eta_4) = \frac{U_e - U_w}{U_e + U_w} \tag{33}$$

where,

u = velocity at any point y above wall in the wake layer

U_e = velocity at $y = \delta_4$ where the flow is considered inviscid

y_{2c} = distance y above surface where $u = \frac{U_e + U_w}{2}$

A least square fourth order fit through the experimental points is given by,

$$f(\eta_4) = 1.0195 - 0.45(\eta_4) - 0.2029(\eta_4)^2 + 0.1543(\eta_4)^3 - 0.024(\eta_4)^4 \tag{33A}$$

Applicable boundary conditions for the wake-layer in Main Region I are:

At $y = \delta_3$: $\eta_4 = 0$, $f(\eta_4) = 1$, $\tau = \tau_{(\delta_4)}$, $u = U_w$ (35)

At $y = y_{2c}$: $\eta_4 = 1$, $f(\eta_4) = 0.5$, $u = \frac{U_e + U_w}{2}$

and At $y = \delta_4$: $f(\eta_4) = 0$, $u = U_e$, $\tau = 0$, $\eta_4 = K_2 = \text{constant}$

By making use of the above boundary conditions and following the procedure previously described, the following momentum integral equation for the wake layer in the Main Region between station 2 and 3 can be derived:

$$
\begin{aligned}
&- \left\{ \int_0^{K_2} f(\eta_4)\, d\eta_4 \right\} \left[\frac{d}{dx} \left\{ U_e (U_e - U_w)(y_{2c} - \delta_3) \right\} \right] \qquad (36)\\
&+ \left\{ \int_0^{K_2} f^2(\eta_4)\, d\eta_4 \right\} \left[\frac{d}{dx} \left\{ (U_e - U_w)^2 (y_{2c} - \delta_3) \right\} \right]\\
&- \left\{ \int_0^{K_2} f(\eta_4)\, d\eta_4 \right\} \left[\left(\frac{dU_e}{dx} \right) (U_e - U_w)(y_{2c} - \delta_3) \right]\\
&- (U_e - U_w)(U_m) \frac{d}{dx} (\delta_3 - \delta_2) - (U_e - U_w)(\delta_3 - \delta_5) \frac{dU_m}{dx}\\
&+ \left\{ \int_0^{1} f(\eta_3)\, d\eta_3 \right\} \left[(U_e - U_w) \frac{d}{dx} \left\{ (U_m - U_w)(\delta_3 - \delta_5) \right\} \right]\\
&- 2(U_e - U_w)\, \theta_5 \frac{H_5 (H_5 + 1)}{(H_5 - 1)^2} \frac{dU_m}{dx} + 4 U_m (U_e - U_w) \frac{\tau_w}{\rho U_m^2} \frac{H_5^2}{(H_5 - 1)^2}\\
&+ U_m (U_e - U_w) \left(\frac{5H_5 - 1}{H_5 - 1} \right) \frac{\tau_w}{\rho U_m^2} \frac{\tau_{(\delta_5)}}{\tau_w}\\
&- 2(U_e - U_w) \frac{U_e}{U_m} \frac{dU_e}{dx}\, \theta_5 \frac{H_5}{(H_5 - 1)^2} (2H_5^2 - 5H_5 + 1)\\
&- U_m (U_e - U_w) \frac{(3H_5 - 1)^2}{(H_5 - 1)^2} \int_0^{\delta_5} \frac{\tau}{\rho U_m^2} \frac{\partial}{\partial y} \left(\frac{u}{U_m} \right) dy\\
&= - \frac{\tau_{(\delta_3)}}{\rho}
\end{aligned}
$$

The growth of wake layer $\delta_3 - \delta_4$ is expressed by the following equation:

$$\frac{d}{dx}(y_{2c} - \delta_3) = C_4 \frac{(U_e - U_w)}{(U_e + U_w)} \tag{37}$$

where C_4 is the empirical constant (≈ 0.185).

It should be noted that U_w, which appears in equation (37), is an unknown function of the independent variable X. The velocity U_e, however, is known once the externally impressed pressure is specified.

The solution for the six unknowns is to be found as a function of the independent variable X at discrete points in Main Region I. These unknowns are (1) wall layer momentum thickness, θ_5, (2) wall layer form factor, H_5, (3) velocity at the junction of the wall layer and the jet layer, $U_{m(x)}$, (4) velocity at the junction of the jet and the wake layer, $U_{w(x)}$, (5) outer edge of the jet layer, $\delta_{3(x)}$, and (6) outer edge of the wake layer $\delta_{4(x)}$. These six unknowns are evaluated by simultaneous solution of the six differential equations (27), (28), (31), (32), (36) and (37).

The initial conditions required for the above equations are the values calculated at station 1 by solution of the equations in the Initial Region. The initial conditions at station 1 are, (1) wall layer momentum thickness, θ_5, (2) wall layer form factor, H_5, (3) velocity at the edge of wall layer, U_c, (4) outer edge of jet layer, δ_3, (5) velocity at the junction of wake layer and jet layer, U_w,

and (6) outer edge of wake layer, δ_4.

Derivation of Equations in Main Region II

Main Region II differs from Main Region I in that the former does not have a wake layer. Main Region II is shown in Figure (1) between stations 2 and 3. Thus the region between stations 2 and 3 consists of a wall layer and a jet layer.

Solution of the equations derived in the previous section for Main Region I will yield values of (i) wall layer momentum thickness, θ_5, (ii) wall layer form factor, H_5, (iii) velocity $U_{m(x)}$ at the junction of the wall and the jet layers, and (iv) jet layer thickness $\delta_4 - \delta_5$. These values then become the initial condition required in the solution of the equations in the Main Region II.

There are four dependent variables to be determined in Main Region 2. These are, (i) wall layer form factor, $H_{5(x)}$, (ii) wall layer momentum thickness $\theta_{5(x)}$, (iii) velocity $U_{m(x)}$ at the junction of wall layer and jet layer and (iv) jet layer thickness. Thus four equations are needed for the solution of these quantities. Brief derivation of the needed four equations along with pertinent assumptions and boundary conditions will be given in subsequent paragraphs.

Wall-Layer, Main Region II

In this region velocity profiles in the wall-layer are also assumed to be of the one parameter family type. With the assumption of one parameter family of velocity profiles for the wall layer, effects of external pressure gradient on the wall layer are taken into account.

This is not possible when the wall layer profiles are assumed to be similar. Due to the nature of turbulent flow, separation prediction or prediction of $C_{L_{MAX}}$ for two component airfoils has to be based on some semi-empirical criteria. It is known from measurements that effects of pressure gradients, in particular adverse pressure gradients, are felt much more in the viscous flow near the wall than in the flow far from the wall. Under these circumstances it would be desirable to introduce proper assumptions into derivations of equations for the wall layer such that effects of pressure gradients on it will be taken into account. It is for these reasons that the assumptions of the one parameter family of velocity profiles are introduced into the theory rather than those of similar wall layer velocity profiles.

The two wall layer equations for the Main Region II, momentum integral equation and form factor or energy integral equation, are essentially the same as those for the wall layer Main Region I. These are repeated here, however, for the sake of continuity.

Wall-Layer Momentum Integral equation, Stations 2 - 3.

$$\frac{d\theta_5}{dx} = 2\frac{\theta_5}{H_5-1}\frac{1}{U_m}\frac{dU_m}{dx} - \theta_5 H_5 \frac{H_5+1}{H_5-1}\frac{U_e}{U_m^2}\frac{dU_e}{dx} \qquad (38)$$

$$+\frac{\tau_w}{\rho U_m^2} - \frac{\tau_{(s_5)}}{\tau_w}\frac{\tau_w}{\rho U_m^2},$$

Wall-Layer Form Factor Equation, Stations 2 - 3.

$$\frac{dH_5}{dx} = \frac{H_5}{\theta_5}(3H_5-1)\frac{\tau_w}{\rho U_m^2} + \frac{H_5-1}{2\theta_5}(3H_5-1)\frac{\tau_w}{\rho U_m^2}\frac{\tau_{(\delta_5)}}{\tau_w} \qquad (39)$$

$$- \frac{U_e}{U_m^2}\frac{dU_e}{dx} H_5(H_5-1)(3H_5-1) - \frac{(3H_5-1)^2}{2\theta_5}\int_0^{\delta_5}\frac{\tau}{\rho U_m^2}\frac{\partial}{\partial y}\left(\frac{u}{U_m}\right)dy .$$

Jet Layer, Main Region II

Experimental data for velocity profiles in the jet layer in Main Region II indicate that velocity profiles for this layer become similar with the following definitions of similarity parameter and function:

$$\eta_5 = \frac{\delta_6 - y}{\delta_6 - \delta_5} \quad ; \quad f(\eta_5) = \frac{U_m - u}{U_m - U_e} . \qquad (39A)$$

With the above definitions, the measured data fall within allowable scatter as for Main Region I. For this reason the same least square curve fit for the jet-layer similarity function is used for Main Region II and for Main Region I. Thus for the jet layer in Main Region II,

$$f(\eta_5) = 1.002 - 0.164(\eta_5) - 1.967(\eta_5)^2 + 1.338(\eta_5)^3 - 0.209(\eta_5)^4 . \qquad (29A)$$

Applicable boundary conditions for this layer are:

$$\text{At } y=\delta_5: \quad u=U_m,\ \eta_5=1,\ f(\eta_5)=0,\ \tau=\tau_{(\delta_5)} \tag{39B}$$

$$\text{At } y=\delta_6: \quad u=U_e,\ \eta_5=0,\ f(\eta_5)=1,\ \tau=0$$

Integrating equation (4) with respect to y from $y=\delta_5$ to $y=\delta_6$, making use of equations (24), (10), (38), (39) and (26) and also the boundary conditions (39B), one obtains the following momentum integral equation for the jet layer in Main Region II.

$$\begin{aligned}
&\left\{\int_0^1 (1-f(\eta_5))\,d\eta_5\right\}\left[\frac{d}{dx}\left\{U_m(U_m-U_e)(\delta_6-\delta_5)\right\}\right] \\
&-\left\{\int_0^1 f(\eta_5)\,d\eta_5\right\}\left[\frac{d}{dx}\left\{(U_m-U_e)^2(\delta_6-\delta_5)\right\}\right] \\
&+\left\{\int_0^1 f^2(\eta_5)\,d\eta_5\right\}\left[\frac{d}{dx}\left\{(U_m-U_e)^2(\delta_6-\delta_5)\right\}\right] \\
&+\left\{\int_0^1 (1-f(\eta_5))\,d\eta_5\right\}\left[(U_m-U_e)(\delta_6-\delta_5)\right\}\Big] \qquad \frac{dU_e}{dx}\Big] \\
&-4U_m(U_m-U_e)\frac{\tau_w}{\rho U_m^2}\frac{H_5^2}{(H_5-1)^2}-U_m(U_m-U_e)\frac{\tau_w}{\rho U_m^2}\frac{\tau_{(\delta_5)}}{\tau_w}\frac{5H_5-1}{H_5-1} \\
&+2(U_m-U_e)\frac{U_e}{U_m}\frac{dU_e}{dx}\theta_5\frac{H_5}{(H_5-1)^2}(2H_5^2-5H_5+1) \\
&+U_m(U_m-U_e)\frac{(3H_5-1)^2}{(H_5-1)^2}\int_0^{\delta_5}\frac{\tau}{\rho U_m^2}\frac{\partial}{\partial y}\left(\frac{u}{U_m}\right)dy \\
&+2(U_m-U_e)\theta_5\frac{H_5(H_5+1)}{(H_5-1)^2}\frac{dU_m}{dx}=-\frac{\tau_w}{\rho}\frac{\tau_{(\delta_5)}}{\tau_w}
\end{aligned} \tag{40}$$

The growth rate equation for jet layer in Main Region II is given as:

$$\frac{d}{dx}(\delta_6 - \delta_5) = C_5 \left(\frac{U_m - U_e}{U_m + U_e}\right) \tag{41}$$

where C_5 is an empirical constant (≈ 0.17).

In the above equation U_m is an unknown function of X. External edge velocity, U_e, is known, however, when pressure distribution is specified.

Thus equations (38), (39), (40) and (41) are to be used in obtaining four dependent variables $\delta_{5(x)}$, $H_{5(x)}$, $U_{m(x)}$, and $\delta_{6(x)}$ in the Main Region II. It should be noted that wall-layer thickness δ_5 is known from calculation of δ_5 and H_5 by using equations (24).

Derivation of Equations in Ordinary Turbulent Boundary Layer Region

The viscous layer downstream of station 3 in Figure (1) behaves like an ordinary turbulent boundary layer. In this region the velocity profiles for the entire viscous layer from the wall to the edge of the boundary layer are assumed to be a one parameter family. With the one parameter velocity profile assumption, two dependent variables must be found as a function of the independent variable X. Thus two equations and two initial conditions are required for these calculations. These two quantities are momentum thickness, δ_7, and form factor, H_7, which is a strong function of pressure gradient.

With initial conditions θ_5 and H_5 known at station 3 for solution of the equations in Main Region II, calculation of boundary layer thickness, momentum thickness, form factor, etc., can be carried out using the momentum integral equation and the form factor equations. Derivation of equations for the ordinary turbulent boundary layer region are much more straightforward than for the other regions considered. This is true because of the more simple boundary conditions and form of the velocity profiles.

Applicable boundary conditions in this region are:

$$\text{At} \quad y=0 : \quad u=0 \, , \, v=0 \, , \quad \tau = \tau_w \tag{42}$$

and

$$\text{At} \quad y=\delta_7 : \quad u = U_e \, , \quad \tau = 0$$

Using the above boundary conditions, the following equations are derived for the ordinary turbulent boundary layer regions. Thus the momentum integral equation in the ordinary turbulent boundary layer region can be derived as:

$$\frac{d\theta_7}{dx} = \frac{\tau_w}{\rho U_e^2} - \frac{\theta_7}{U_e}\frac{dU_e}{dx}(H_7 + 2) \, . \tag{43}$$

Theoretical form factor equation in the ordinary turbulent boundary layer region is given as follows:

$$\frac{dH_7}{dx} = H_7(3H_7-1)\frac{1}{\theta_7}\left(\frac{\tau_w}{\rho U_e^2}\right) - \frac{1}{U_e}\frac{dU_e}{dx} H_7(H_7-1)(3H_7-1) \quad (44)$$

$$- (3H_7-1)\frac{1}{2\theta_7}\int_0^{\delta_7} \frac{\tau}{\rho U_e^2}\frac{\partial}{\partial y}\left(\frac{u}{U_e}\right)dy \ .$$

The above equation is derived with the assumption of one parameter family of power law velocity profile. The major portion of ordinary turbulent boundary layer velocity profile, as measured experimentally, can be represented by power law. However, velocity profile near the wall and at large distance away from the wall deviate somewhat from power law assumption. For this reason, the better correlation for the computer values of δ^* and θ with experiments is obtained when the above equation is slightly modified as follows:

$$\frac{dH_7}{dx} = H_7(3H_7-1)\frac{1}{\theta_7}\left(\frac{\tau_w}{\rho U_e^2}\right) - \frac{1}{U_e}\frac{dU_e}{dx} H_7(H_7-1.1)(3H_7-1.1)$$

$$- (3H_7-1.1)^2\frac{1}{2\theta_7}\int_0^{\delta_7} \frac{\tau}{\rho U_e^2}\frac{\partial}{\partial y}\left(\frac{u}{U_e}\right)dy \ . \quad (45)$$

Computed values of momentum thickness, form factor and displacement thickness, by the use of equations (43) and (45), are shown in Figures (48A) and (48B). Experimental data for the ordinary turbulent boundary layer development on single piece airfoils are also plotted

in these figures. This shows reasonable correlation with the experimental data. Detailed discussion of the correlation is given in Chapter V.

Numerical Solution

The sets of relevant differential equations derived for various regions of Figure (1) are summarized in the previous sections. Because of the complexity of these differential equations, it would be hopeless to make an attempt at obtaining analytical closed form solutions to these equations. In this case one attempts to solve these differential equations by known numerical methods with the aid of a digital computer.

In order to solve these sets of differential equations by numerical methods, they must be reduced to a certain form. The procedure will be demonstrated for the six equations in Main Region I. The same procedures have been carried out for equations in the other regions of Figure (1).

General Statement of Problem. Let $f_1(x, y_1, y_2 - - - y_m)$, $f_2(x, y_1, y_2 - - - y_m)$ and $f_m(x, y_1, y_2 - - - y_m)$ be given functions of m + 1 variables x, y_1, y_2 - - - y_m and α_1, α_2 - - - - , α_m be given constants. The problem is to find m functions $y_1(x)$, $y_2(x)$ - - - $y_{m(x)}$ defined in a neighborhood of some specified point x = a such that

$$y'_{1(x)} = f_1(x, y_{1(x)}, y_{2(x)} \cdots y_{(m-1)(x)}, y_{m(x)}) \quad (46)$$

$$y'_{2(x)} = f_2(x, y_{1(x)}, y_{2(x)} \cdots y_{(m-1)(x)}, y_{m(x)})$$

$$\vdots$$

$$y'_{m(x)} = f_m(x, y_{1(x)}, y_{2(x)} \cdots y_{(m-1)(x)}, y_{m(x)})$$

where $\left(' = \frac{d}{dx} \right)$.

Also let $y_{1(a)} = \alpha_1$, $y_{2(a)} = \alpha_2 \ldots$ and $y_{m(a)} = \alpha_m$ be initial values of the dependent variables at $x = a$.

Use the following vector notation:

$$\bar{y} = \begin{bmatrix} y_1 \\ \vdots \\ y_m \end{bmatrix}, \quad \bar{y}_a = \begin{bmatrix} \alpha_1 \\ \vdots \\ \alpha_m \end{bmatrix}; \quad \overline{f(x, \bar{y})} = \begin{bmatrix} f_1(x, \bar{y}) \\ \vdots \\ f_m(x, \bar{y}) \end{bmatrix} . \quad (47)$$

Using the above vector notation, equations (46) and (47) can be written in short form as follows,

$$\bar{y}' = \overline{f(x, \bar{y})} \quad ; \quad \bar{y}_{(a)} = \bar{y}_a \quad (48)$$

The problem represented by equation (48) is called an Initial value problem. Various single-step or multi-step methods are available

for the solution of Initial value problem. The most commonly used methods are the single-step Euler method, the single-step modified Euler method, the multi-step predictor corrector method, the Runga-Kutta method and a few others. Choice of a method depends upon the particular problem and is governed by desired accuracy, time of computation, core size available in the particular computer, etc.

Numerical Form for Equations in Main Region I (Stations 1 and 2)

In Main Region I, there are six independent variables, namely, (i) non-dimensional velocity at the junction of wake layer and jet layer, $\left.\frac{U_w}{U_e}\right|_{(x)}$, (ii) wake layer thickness, $(\delta_4 - \delta_3)_{(x)}$, (iii) non-dimensional velocity at the junction of jet layer and wall-layer, $\left.\frac{U_m}{U_e}\right|_{(x)}$, (iv) jet layer thickness, $(\delta_3 - \delta_5)_{(x)}$, (v) wall-layer momentum thickness, $\theta_{5(x)}$, and (vi) wall-layer form factor, $H_{5(x)}$. In order to solve for these unknowns numerically, six equations (36), (37), (31), (32), (28) and (27) must be expressed in the form of equation (46). That is to say that the terms containing first derivatives, e.g., $\frac{d}{dx}\left(\frac{U_w}{U_e}\right)$, $\frac{d}{dx}\left(\frac{U_m}{U_e}\right)$ in each of the above mentioned equations have to be on the left hand side of the equations for calculating that particular unknown variable and the rest of the terms have to be on the right hand side. Each term in equations (36), (31), etc. are individually operated on and algebraically simplified. Also, the following notation is used.

x_1 = x location where all above six variables are known

h = step size

x_2 = x location where above six variables are to be calculated from known values at x_1

$= x_1 + h$

$U_{EM} = (U_{e(x_1)} + U_{e(x_2)})/2.0$

BJ = Jet layer thickness = $(\delta_3 - \delta_5)$

BW = Wake layer thickness = $(y_{2_c} - \delta_3)$

$$SM1 = \int_0^{\eta_{42}} f(\eta_4)\, d\eta_4$$

$$SM2 = \int_0^{\eta_{42}} f^2(\eta_4)\, d\eta_4$$

$$SM3 = \int_{\eta_{31}}^{1} f(\eta_3)\, d\eta_3$$

$$SM4 = \int_{\eta_{31}}^{1} (1 - f(\eta_3))\, d\eta_3$$

$$SM5 = \int_0^1 f^2(\eta_3)\, d\eta_3$$

$$UW = \frac{U_w}{U_e}$$

$$UM = \frac{U_m}{U_e}$$

Using the above notation, the following difference equation for $\left(\frac{U_w}{U_e}\right)_{(x)}$ is obtained from the theoretical differential equation:

$$\left[\frac{d}{dx}\left(\frac{U_W}{U_e}\right)\right] = \tag{50}$$

$$\left[\frac{1.0}{\{(SM1)(BW)-2(SM2)(BW)(1-U_W)-(SM3)(1-U_W)(BI)\}}\right]$$

$$\cdot\left[\{(SM1)(1-U_W)\frac{d}{dx}(BW)\}-\{(SM2)(1-U_W)^2\frac{d}{dx}(BW)\}\right.$$

$$-\{3(SM1)(1-U_W)(BW)\frac{1}{U_{EM}}\frac{dU_e}{dx}\}+\{(1-U_W)(U_M)\frac{d}{dx}(BI)\}$$

$$+\{(BI)(1-U_W)\frac{d}{dx}(U_M)\}-\{(SM3)(1-U_W)(BI)\frac{d}{dx}(U_M)\}$$

$$-\{(SM3)(1-U_W)(U_M-U_W)\frac{d}{dx}(BI)\}+\{2(1-U_W)\theta_5 H_5$$

$$\cdot\frac{(H_5+1)}{(H_5-1)^2}\frac{d}{dx}(U_M)\}-\{4(U_M)(1-U_W)\frac{(H_5)^2}{(H_5-1)^2}\left(\frac{\tau_w}{\rho U_m^2}\right)\}$$

$$-\{(U_M)(1-U_W)\left(\frac{3H_5-1}{H_5-1}\right)\left(\frac{\tau_{(55)}}{\rho U_m^2}\right)\}+\{2(1-U_W)\left(\frac{1}{U_M}\right)$$

$$\cdot\left(\frac{1}{U_{EM}}\right)\frac{dU_e}{dx}(\theta_5)\frac{(H_5)}{(H_5-1)^2}(2H_5^2-5H_5+1)\}+\{(U_M)$$

$$\cdot(1-U_W)\frac{(2H_5-1)^2}{(H_5-1)^2}\cdot\int_0^{55}\frac{\tau}{\rho U_m^2}\frac{\partial}{\partial y}\left(\frac{u}{U_m}\right)dy\}-\{\left(\frac{\tau_{(55)}}{\tau_w}\right)$$

$$\cdot\left(\frac{\tau_w}{\rho U_m^2}\right)(U_M^2)\left(\frac{U_e^2}{U_{EM}^2}\right)\}-\{(SM2)(1-U_W)^2(BW)$$

$$\cdot\left(\frac{2}{U_{EM}}\right)\frac{dU_e}{dx}\}+\{(BI)(1-U_W)\left(\frac{dU_e}{dx}\right)(U_M)\left(\frac{1}{U_{EM}}\right)\}$$

$$-\{(SM2)\left(\frac{1}{U_{EM}}\right)(1-U_W)(BI)(U_M-U_W)\frac{dU_e}{dx}\}$$

$$\left.+\{2\left(\frac{1}{U_{EM}}\right)(1-U_W)(\theta_5)(H_5)\frac{(H_5+1)}{(H_5-1)^2}(U_M)\frac{dU_e}{dx}\}\right].$$

This equation allows computation of $(UW)_{(x2)}$ from $(UW)_{(x1)}$. In Figure (1), the initial region ends and Main Region I begins at station 1. Quantities $\frac{dU_m}{d_x}$, $\frac{d(BJ)}{d_x}$, UM, BW, BJ, etc. appearing on the right hand side of the equation are obtained from solution of the equations in the Initial Region. The term $\frac{dU_e}{d_x}$ is obtained from the external specified pressure distribution using the Euler equation.

The growth equation for the wake layer in Main Region I in difference form is written as

$$\frac{d}{dx}(BW) = \frac{1 - UW}{1 + UW} \tag{51}$$

UW appearing in equation (51) is obtained at station 1 from computation in the Initial Region. Thus $BW_{(x2)}$ is calculated from equation (51) since $BW_{(x1)}$ is known.

After operation on each term of equation (31), followed by algebraic simplification and rearrangement, yields the following difference equation in terms of the notation of equation (49).

$$\left[\frac{d}{dx}(UM)\right] = \tag{52}$$

$$\left[1.0\Big/\{2(BI)(UM)(SM4) - (SM4)(BI)(UW) - 2(SM3)\right.$$

$$.(BI)(UM-UW) + 2(SM5)(BI)(UM-UW) + 2(\theta_5)$$

$$\left..(H_5)\frac{(H_5+1)^2}{(H_5-1)^2}(UM-UW)\}\right].\left[-\{(SM4)(UM-UW)\right.$$

$$.(UM)\frac{d}{dx}(BI)\} + \{(SM4)(BI)(UM)\frac{d}{dx}(UW)\} + \{(SM3)$$

$$.(UM-UW)^2\frac{d}{dx}(BI)\} - \{2(SM3)(BI)(UM-UW)\frac{d}{dx}(UW)\}$$

$$- \{(SM5)(UM-UW)\frac{d}{dx}(BI)\} + \{2(SM5)(BI)(UM-UW)$$

$$.\frac{d}{dx}(UW)\} - \{(UM)(BI)\frac{d}{dx}(UW)\} + \{(SM3)(BI)(UM-UW)$$

$$.\frac{d}{dx}(UW)\} + \{4(UM)(UM-UW)\frac{(H_5)^2}{(H_5-1)^2}\left(\frac{\tau_w}{\rho U_m^2}\right)\} +$$

$$\{(UM)(UM-UW)\frac{(5H_5-1)}{(H_5-1)}\left(\frac{\tau_{(55)}}{\tau_w}\right)\left(\frac{\tau_w}{\rho U_m^2}\right)\} - \{\frac{2(H_5)}{(H_5-1)^2}$$

$$.(2H_5^2-5H_5+1)(\theta_5)(UM-UW)\left(\frac{1}{UM}\right)\left(\frac{1}{UEM}\right)\frac{dUe}{dx}\} - \{(UM)$$

$$.(UM-UW)\frac{(3H_5-1)^2}{(H_5-1)^2}\int_0^{\delta_5}\frac{\tau}{\rho U_m^2}\frac{\partial}{\partial y}\left(\frac{u}{U_m}\right)dy\} + \{(BI)\left(\frac{1}{UEM}\right)$$

$$.\frac{dUe}{dx}\} + \{\left(\frac{\tau_{(53)}}{\tau_w}\right)\left(\frac{\tau_w}{\rho U_m^2}\right)(UM^2)\} - \{\left(\frac{\tau_{(55)}}{\rho U_m^2}\right)(UM^2)\} -$$

$$\{(SM4)(UM)(UM-UW)(BI)\left(\frac{2}{UEM}\right)\frac{dUe}{dx}\} + \{(SM3)(UM-UW)^2(BI)$$

$$.\left(\frac{2}{UEM}\right)\frac{dUe}{dx}\} - \{(UM)(BI)(UW)\left(\frac{1}{UEM}\right)\frac{dUe}{dx}\} - \{(SM5)$$

$$.(UM-UW)^2(BI)\left(\frac{2}{UEm}\right)\frac{dUe}{dx}\} + \{(SM3)(BI)(UM-UW)\left(\frac{1}{UEM}\right)$$

$$\left..(UW)\frac{dUe}{dx}\} - \{\left(\frac{2}{UEM}\right)(UM-UW)\theta_5\frac{(H_5^2+H_5)}{(H_5-1)^2}(UM)\frac{dUe}{dx}\}\right].$$

UM is thus obtained from equation (52) for the first iteration, at a location one step size away from station 1, and is calculated by knowing values obtained from Initial Region calculations up to station 1.

The difference equation for the growth rate for the jet layer is given by

$$\frac{d}{dx}(BJ) = \left(\frac{UM - UW}{UM + UW}\right) \quad . \tag{53}$$

The difference equation for momentum thickness in the wall layer of Main Region I is written as

$$\frac{d\theta_s}{dx} = 2\frac{(\theta_s)}{(H_s-1)}\left(\frac{1}{UM}\right)\frac{d}{dx}(UM) + 2\frac{(\theta_s)}{(H_s-1)}\left(\frac{1}{Ue}\right)\left(\frac{dUe}{dx}\right) \tag{54}$$

$$-\left(\frac{1}{UEM}\right)\left(\frac{1}{UM^2}\right)\left(\frac{dUe}{dx}\right)(\theta_s)\frac{(H_s)(H_s+1)}{(H_s-1)} + \frac{\tau_w - \tau_{(ss)}}{\rho Um^2} \quad .$$

In order to compute the form factor for the wall layer in Main Region I, the difference equation for wall layer energy thickness is first written as

$$\frac{d\delta_5^{**}}{dx} = -3(\theta_5)\tilde{H}_5\left(\frac{1}{UM}\right)\frac{d}{dx}(UM) + 2(\theta_5)\frac{(\tilde{H}_5)}{(2-\tilde{H}_5)}\left(\frac{1}{UM}\right)\frac{d}{dx}(UM) \quad (55)$$

$$-2(\theta_5)\frac{\tilde{H}_5}{(2-\tilde{H}_5)}\left(\frac{1}{UM^2}\right)\cdot\frac{1}{Ue}\frac{dUe}{dx} + 2\int_0^{\delta_5}\frac{\tau}{\rho U_m^2}\frac{\partial}{\partial y}\left(\frac{u}{U_m}\right)dy$$

$$-2\frac{\tau(\delta_5)}{\rho U_m^2} - 3(\theta_5)\tilde{H}_5\frac{1}{Ue}\frac{dUe}{dx} + 2(\theta_5)\frac{\tilde{H}_5}{(2-\tilde{H}_5)}\left(\frac{1}{Ue}\right)\frac{dUe}{dx}$$

Quantities on the right hand side of the above equation are available, at station 1 in Figure 1, from the Initial Region solution. Thus δ_5^{**} at a location step size, h, downstream of station 1 is calculated from equation (55). From δ_5^{**}, $\tilde{H}_5$ is calculated using

$$\tilde{H}_5 = \frac{\delta_5^{**}}{\theta_5} \quad (56)$$

The wall layer form factor H_5 is calculated using the functional relationship of $\tilde{H}_5$ vs H_5 obtained from experimental correlation for the confluent boundary layer flow. This will be discussed in Chapter V.

Using these procedures, values of UW, UM, BJ, BW, θ_5 and H_5 are obtained at a distance one step-size, h, downstream from station 1 in Figure (1). These values correspond to the first iteration. For the second iteration, for computation of UW, UM - - - θ_5 and H_5, the mean values of the quantities appearing on the right hand side of equations (49) through (56) are used, i.e., for UW, UM. etc.

$$UW_{2\text{nd iteration}} = (UW_{\text{station 1}} + UW_{\text{1st iteration}})/2.0 \quad .$$

This process is continued until sufficient convergence is obtained.

The method outlined is called single-step modified Euler method. It has been shown in Reference (53) that the order of the modified Euler method is equal to 2. In other words for the modified Euler method

$$\left| \text{Truncation error} \right| \propto h^3$$

where h = step size.

This sequence of steps is carried out for downstream points in the Main Region I up to and including station 2.

List of Parameters

In the previous sections, the resulting sets of equations for various regions shown in Figure (1) were derived. The simultaneous solution of these coupled equations in a particular region for a given pressure distribution yields the solution for such dependent variables as $\theta_{(x)}$, $U_{w(x)}$, jet layer thickness, $U_{m(x)}$, etc. These sets of equations, however, include terms containing such parameters as wall shear τ_w, shear at the juncture of wall and jet layer $\tau_{(\delta_2)}$, shear stress at the junction of jet layer and wake layer $\tau_{(\delta_3)}$, similarity function for jet and wake layers, etc. These parameters have to be expressed as a function of the dependent variables in order to be able to solve the sets of differential equations.

Laws of local dynamic similarity make it possible to establish functional dependence of the parameters $\tau_{(\delta s)}$, τ_w and others by proper combinations of the dependent variables expressed in non-dimensional form. For example, the local wall shear for the wall layer in Figure (1) can be expressed as,

$$\frac{\tau_w}{\rho U_m^2} = F\left(\frac{U_m \theta_s}{\nu}, H_s\right)$$

Local Wall Shear

Local Wall-Layer Momentum Thickness Reynolds Number

Local Wall Layer Form Factor

Actual functional relations for these needed parameters have to be determined, however, from experimental measurements for the particular flow to be investigated.

Functional dependence and functional relationship of these parameters are discussed in detail in Chapter V of Results & Discussions. The following are, however, the specific items and parameters encountered in the sets of differential equations derived in the previous sections:

1) Wall shear, $\frac{\tau_w}{\rho U_m^2}$

2) Shear at the edge of wall-layer, $\frac{\tau_{(\delta s)}}{\rho U_m^2}$

3) Shear at the junction of wake layer and jet layer, $\frac{\tau_{(\delta 3)}}{\tau_w}$

4) Wall-layer shear integral, $\int_0^{\delta s} \frac{\tau}{\rho U_m^2} \frac{\partial}{\partial y}\left(\frac{u}{U_m}\right) dy$

5) Integrals for the similarity function for jet layers in Initial and Main Regions, $\int_0^1 f(\eta_1)\, d\eta_1$, $\int_0^1 f(\eta_2)\, d\eta_2$, $\int_0^1 f(\eta_3)\, d\eta_3$ and $\int_0^1 f(\eta_3)\, d\eta_3$

6) Integrals for the similarity function for wake layers in Initial and Main Region, typical ones being, $\int_0^{K_1} f(\eta_2)\,d\eta_2$, $\int_0^{K_1} f^2(\eta_2)\,d\eta_2$, $\int_0^{K_2} f(\eta_4)\,d\eta_4$ and $\int_0^{K_2} f^2(\eta_4)\,d\eta_4$

7) One parameter family representation for wall layer velocity profiles in Initial Region, Main Region and ordinary turbulent boundary layer region.

CHAPTER IV

EXPERIMENTAL WORK

In order to facilitate understanding of turbulent confluent boundary layer flow for the purpose of developing an analytical model and also to check the validity of theoretical predictions, an experimental facility at the Lockheed-Georgia plant was used to obtain the desired experimental data. The existing facility at Lockheed was designed and built for high Mach number and constant pressure wall jet flow was modified to obtain low speed flow (i.e., maximum slot exit Mach number = 0.35 and maximum free stream Mach number of 0.2 to 0.25) as well as to obtain the desired pressure distribution in the flow direction. The necessary components were designed and built at Georgia Tech with the permission of the Director of the School of Mechanical Engineering. This included a deflecting solid boundary for producing the desired pressure distribution, water tube manometer and connections for measuring wall static pressure on the solid boundary, and velocity probes to measure total pressure profiles in the viscous flow region.

Description of Experimental Facility

A sketch of the wall-jet facility with the preceeding modifications is shown in Figure (2). Air is available at a pressure of 350 psia from large storage tanks connected in parallel. This air is throttled by means of a valve (13) to the pressure which is determined

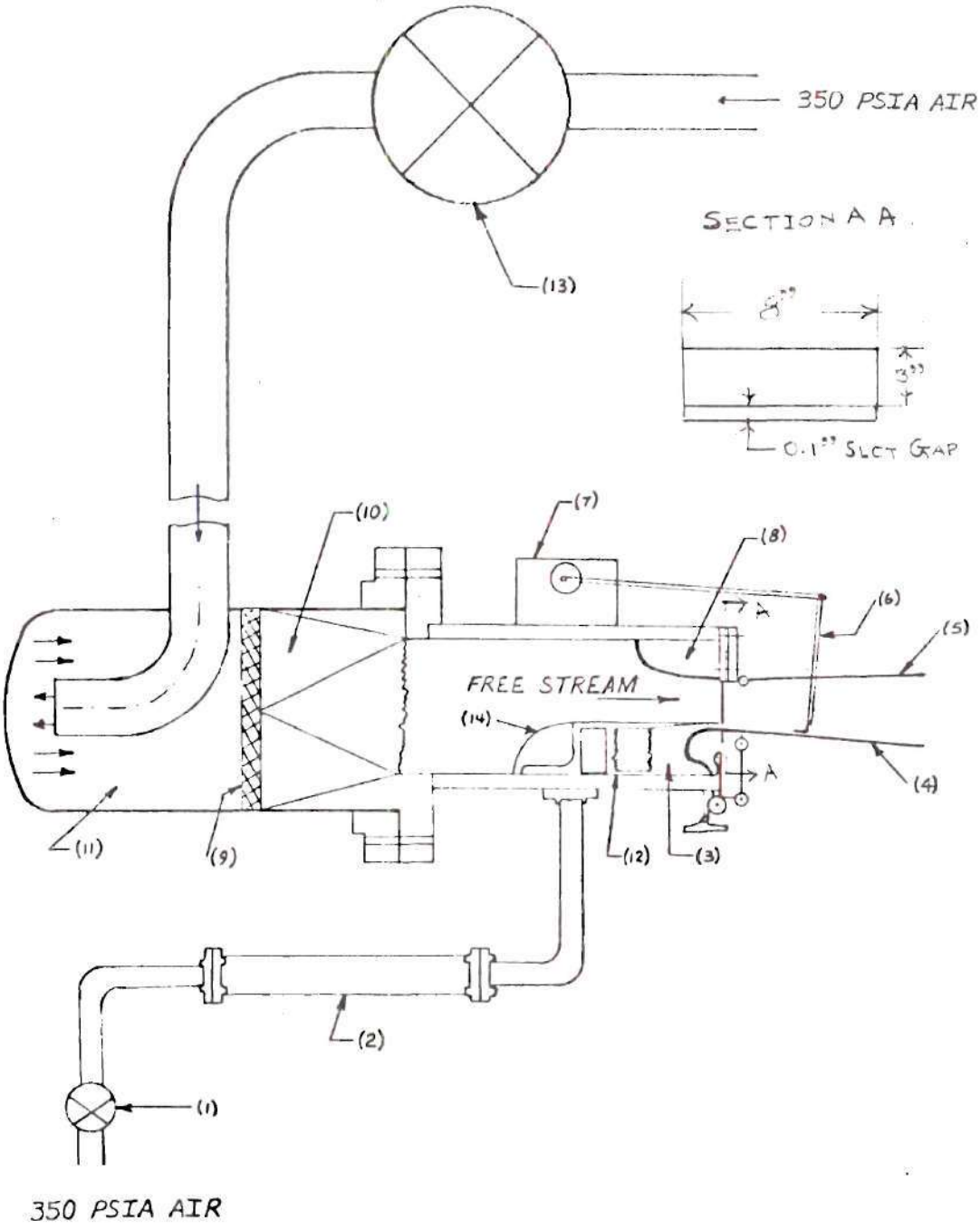

Figure 2. Schematics of Experimental Facility

by the free stream Mach number at station (A) and the static pressure at the exit plant (A). The air then flows through the free stream air plenum (11) which is used to prevent surges in the free stream flow. It then passes through honey comb rings (9) and flow straighteners (10) which smooth free stream flow. The free stream flow is then accelerated by means of nozzle block (8) and plant (14) to the desired Mach number at the exit plane (A).

Air for the slot flow is also obtained from storage tanks at 350 psia. Valve (1) throttles this air to the pressure which is determined by the static pressure at the exit plane (A) and the slot flow exit Mach number at station (A). It then passes through the slot flow plenum (3) which prevents surges in the slot air. Wire screen (12) smoothes the flow which then emerges at the slot exit at section (A) to develop the turbulent confluent wall jet flow downstream.

Desired pressure distribution in the axial direction is obtained by deflecting the flap (4) and the solid boundary (5) by certain amounts. Wall pressure taps, both on the flap and solid boundary, were spaced 1/2 inch apart. The pressure taps are connected to two separate water manometers for measuring the static pressure distribution. A velocity probe is used to measure total pressure in the viscous region. This probe is inserted in the probe holder (6) which is connected to a gear box and electric motor (7) by which the probe's vertical motion is controlled within an accuracy of .001 inch. The gear box can be moved horizontally to locate the probe at a desired axial distance from slot exit. The probe holder can be rotated to a desired angle such that motion of the probe is in a plane perpendicular to the local surface contour.

Summary of Conditions for Measured Data

Table 1 shows a list of conditions for which measurements were performed under the present study. Measurements were confined to the range of velocities through the slot and free stream at the slot exit where the flow can be considered incompressible. The range of slot velocities was confined to 120 ft/sec. to 307 ft/sec. and the range of external stream velocity at the exit of slot was confined to 80 ft/sec. to 250 ft/sec. Desired pressure distribution was obtained by deflecting both the flap and the hard boundary from 0° to approximately 7°. Static pressures were measured both on the flap upper surface as well as on the surface of the hard boundary. The same values of static pressure were obtained on the flap and the hard boundary at the same X locations except at approximately 140 slot heights downstream where local separation was observed for $\frac{U_{c(\infty)}}{U_{e(\infty)}} \approx 1.12$ and $\delta_F = 7°$.

Measurements of velocity profiles with a total pressure probe were performed from the exit of the slot to approximately 160 slot heights downstream. The spacing between two X locations where the velocity profiles were measured was kept small for two purposes, namely, (i) to accurately determine the beginning and end of various regions shown in Figure (1) and of more importance (ii) to determine a more precise relationship of various physical parameters by numerical methods with the aid of digital computers. These parameters appear in the theoretical equations derived in Chapter III and have been discussed under subtitle "List of Parameters".

Table 1. Designation of Experimental Runs

CASE	RUNS	$M_{e(o)}$	$M_{c(o)}$	$\frac{M_{c(o)}}{M_{e(o)}}$	δ Flap	δ Plate	Pressure Gradient
1	1-24	0.1	0.3	3.0	0	-	Zero
2	25-43	0.2	0.3	1.57	0	-	Zero
3	48-66	0.23	0.17	0.74	0	-	Zero
4	67-85	0.195	0.325	1.67	3°	3°	Mild Adverse
5	86-96	0.25	0.425	1.7	4°	4°	Mild Adverse
6	97-106	0.25	0.185	0.74	4°	4°	Medium Adverse
7	107-119	0.25	0.325	1.3	7°	7°	High Adverse
8	122-133	0.25	0.28	1.12	7°	7°	High Adverse

Data Reduction Technique

A computer program was formulated for data reduction and analysis of the experimental data taken under the present investigation. Experimentally measured values of wall static pressures on the flap, wall static pressures on the hard boundary, total pressures across the viscous layer and ambient temperature and barometric pressures at two closely spaced X locations constitute the input to the computer program for data reduction. This program then calculates and prints out the following informations:

(1) Velocity profiles at two stations,

(2) Wall shear stress between two stations,

(3) Shear stress distribution across the viscous layer between two stations,

(4) For wall-layer at both the stations, Reynolds number based on momentum thickness, displacement thickness, wall layer thickness, form factor H, ratio $\widetilde{H}$ of energy thickness δ^{**} and momentum thickness θ for the wall layer at the two stations,

(5) Turbulent dissipation for the wall layer and entire viscous layer, and wall shear calculated from expressions developed by Nash[51], Bradshaw[5], Kruka and Eskinazi[13], Clauser[32], Sigalla[37],

(6) Calculated non-dimensional velocity profiles for jet-layer and wake layer at both stations, and

(7) Various integrals at each of stations such as $\int_0^{y_1}\left\{\frac{u}{U_e}\right\}dy$, $\int_0^{y_1}\left\{\frac{u}{U_e}\right\}^2 dy$, $u_{(y_1)}\cdot\left\{\int_0^{y_1}\left(\frac{u}{U_e}\right)dy\right\}$, and $u_{(y_1)}\cdot\left\{\int_0^{y_1}\left(\frac{u}{U_e}\right)^2 dy\right\}$, where y_1 is any distance above wall in the viscous region and $u_{(y1)}$ is the velocity at distance

y_1 above the wall.

All mean velocities were calculated using the following equation:

$$P_T = P_{ST} + \tfrac{1}{2}\rho u^2 \quad . \tag{57}$$

where

P_T = pitot tube total pressure

P_{S_T} = wall static pressure.

The total pressures were measured by means of a probe with external dimensions of approximately 0.007 in. by .03 in. MacMillan's[38] correction was applied to all values of velocities computed by Equation (57) even though his correction was developed for circular pitot tube.

In order to calculate the wall shear and shear stress distribution across the viscous layer use of the following basic equations was made:

$$v = -\int_0^y \frac{\partial u}{\partial x}\, dy \tag{58}$$

$$u\frac{\partial u}{\partial x} + v\frac{\partial u}{\partial y} = -\frac{1}{\rho}\frac{dP}{dx} + \frac{1}{\rho}\frac{\partial \tau}{\partial y} \quad , \tag{59}$$

$$\frac{\partial P}{\partial y} = 0 \quad .$$

and

$$\frac{dP}{dx} = -\rho u_e \frac{du}{dx} \tag{60}$$

By integrating equation (59) from y = 0 to y = y_1 , making use of equations (58) and (60), and using Leibnitz's rule and integration by

parts, the following equation can be derived after some algebraic simplification:

$$\frac{1}{\rho}\left(\tau_{(y_1)}-\tau_w\right) = \tag{61}$$

$$U_e^2\left[\frac{d}{dx}\left\{\int_0^{y_1}\frac{u}{U_e}\left(\frac{u}{U_e}-\frac{u_{(y_1)}}{U_e}\right)dy\right\}\right]+\left[U_e\left\{\int_0^{y_1}\frac{u}{U_e}dy\right\}\right]\cdot\left[U_e\frac{d}{dx}\left\{\frac{u_{(y_1)}}{U_e}-1\right\}\right]+\left[\left\{U_e\frac{dU_e}{dx}\right\}\cdot\left\{\int_0^{y_1}\left(\frac{u}{U_e}-1\right)dy\right\}\right]+\left[\left\{2U_e\frac{dU_e}{dx}\right\}\cdot\left\{\int_0^{y_1}\frac{u}{U_e}\left(\frac{u}{U_e}-\frac{u_{(y_1)}}{U_e}\right)dy\right\}\right]+\left[U_e\left\{\int_0^{y_1}\frac{u}{U_e}dy\right\}\right]\cdot\left[\left\{\frac{u_{(y_1)}}{U_e}-1\right\}\frac{dU_e}{dx}\right]$$

In this equation the symbols have the following meaning:

y_1 = distance above wall,

U_e = velocity at the edge of viscous layer,

$\tau_{(y1)}$ = shear stress at $y = y_1$ and

τ_w = wall shear stress

The right hand side of equation (61) was programmed to compute $\left(\tau_{(y_1)}-\tau_w\right)$ at various distances, y_1, from the wall. Shear stress was assumed to be zero at very large distances from the wall in order to obtain wall shear. The same equation and the same numerical procedure was used to compute shear distribution, wall shear and turbulent dissipation for the initial region, main regions and the ordinary turbulent boundary layer region for the conditions listed in Table 1.

CHAPTER V

RESULTS AND DISCUSSION

The previous chapter described the experimental facility, type and manner of experimental measurements and data reduction procedure. From the output of this data reduction computer program various physical parameters for the confluent boundary layer flow are studied. The relationship among various physical parameters which appeared in theoretical equations are derived. Establishment of these relations between physical parameters is of vital importance in the solution of this type of viscous flow on airfoil surfaces by the simultaneous solutions of sets of differential equations derived in the theoretical section.

Presentation of Typical Measured Experimental Data

Figures (4), (6) and (8) show the pressure distribution which was imposed on the viscous flow for case numbers 8, 7, and 4, respectively shown in Table 1. Here the pressure is plotted as pressure coefficient vs X measured from slot exit in inches. These pressure distributions were obtained by deflecting the flap and hard boundary as shown in Figure (2). The favorable pressure distribution from slot exit to approximately 1/2 inch downstream was due to the curvature effect near the knee of the flap. As seen in Figure (4) the pressure becomes constant near the rear end of the flap where incipient separation was observed.

Figures (3), (5) and (7) show plots of velocity profiles for cases 8, 7 and 6, respectively shown in Table 1. These experimental data for

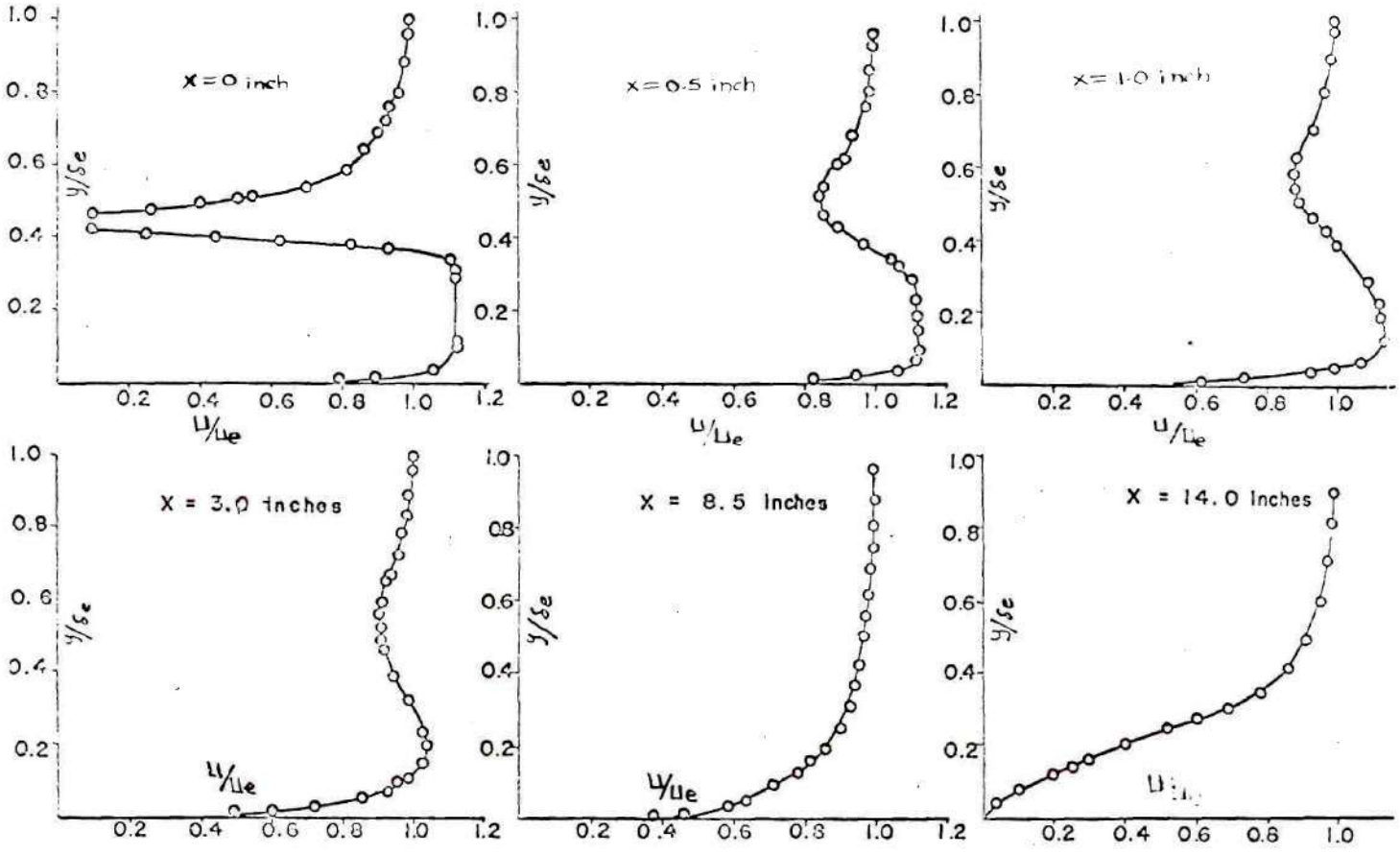

Figure 3. Velocity Profiles for Initial Velocity Ratio of 1.12

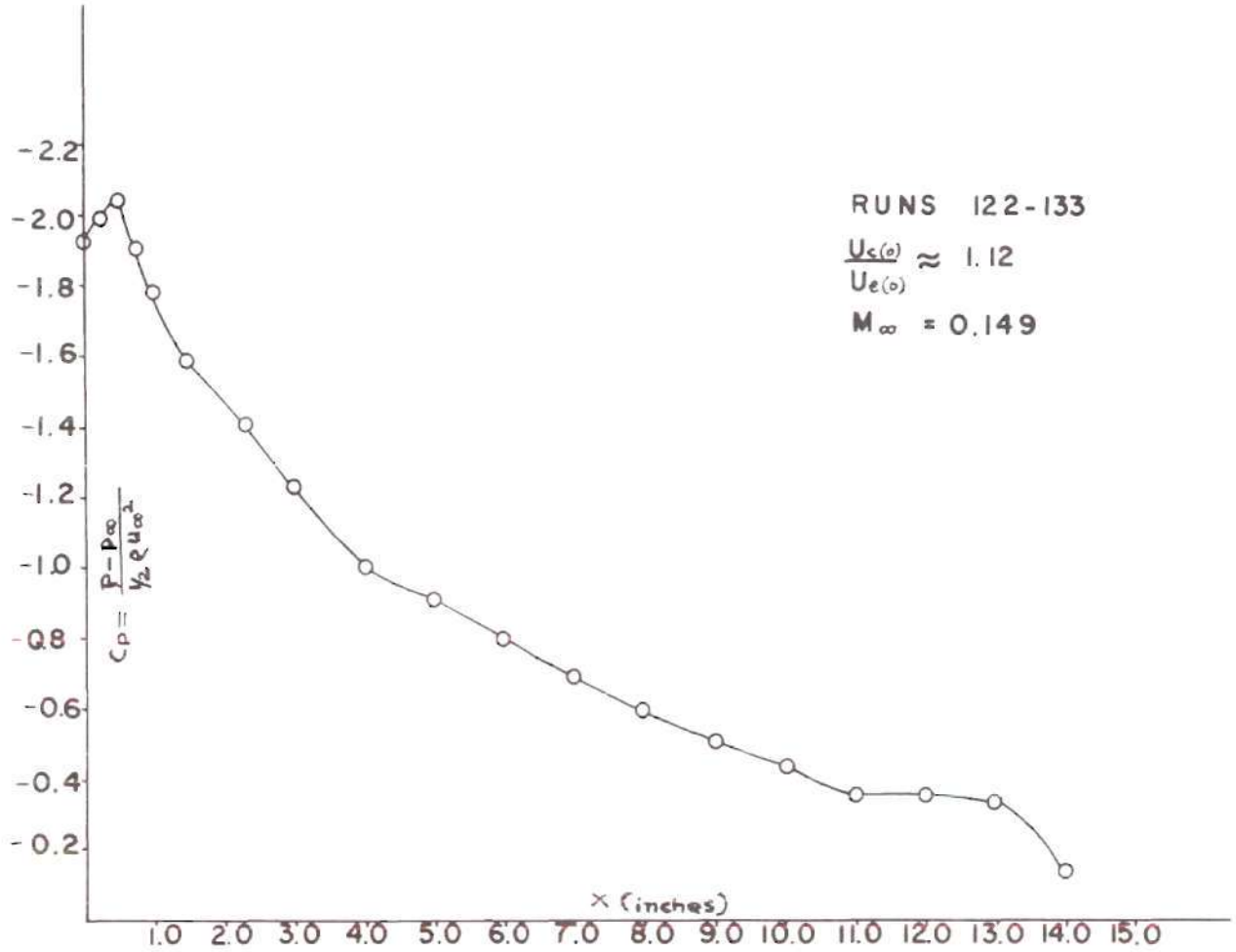

Figure 4. Pressure Distribution for Initial Velocity Ratio of 1.12

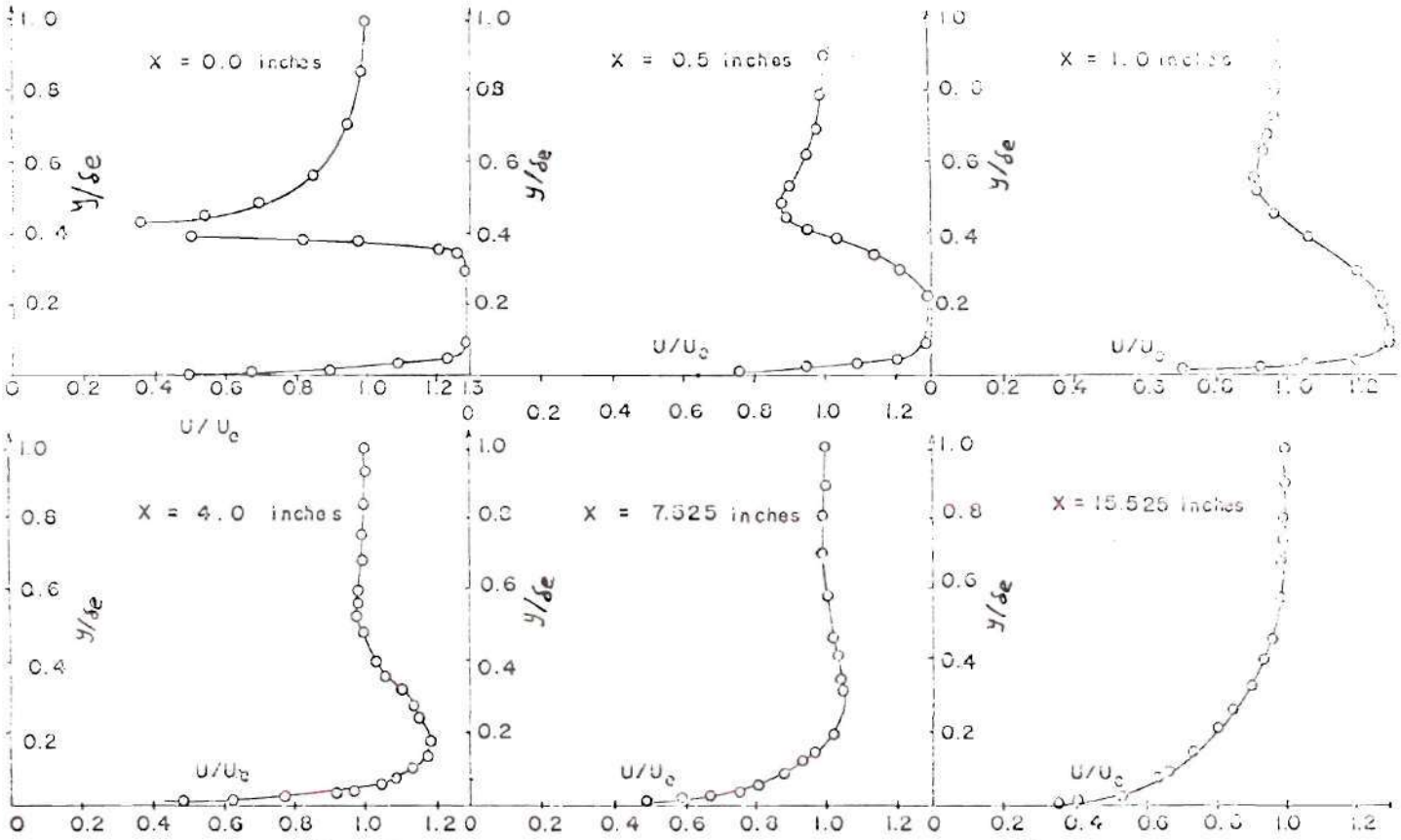

Figure 5. Velocity Profiles for Initial Velocity Ratio of 1.29

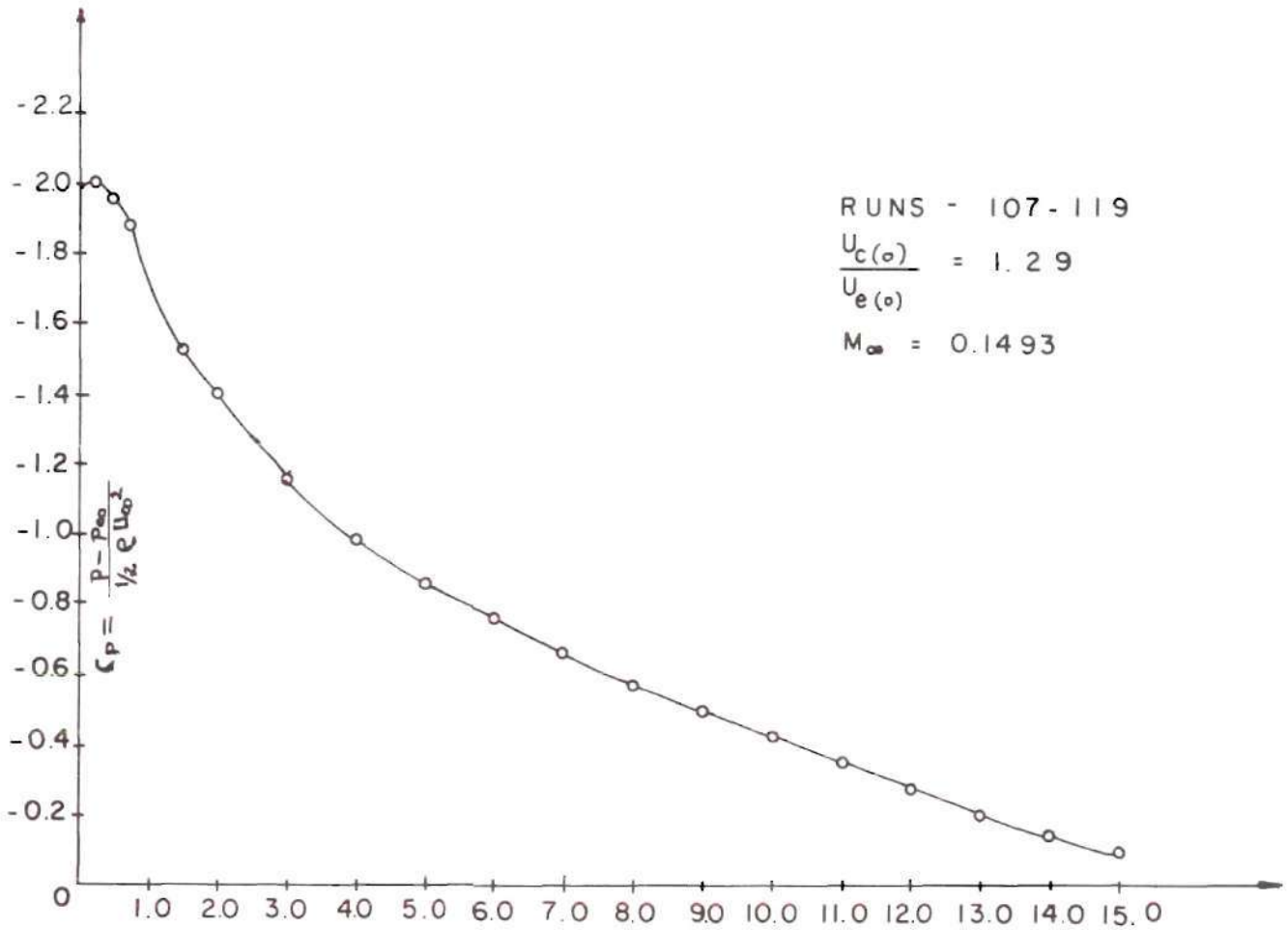

Figure 6. Pressure Distribution for Initial Velocity Ratio of 1.29

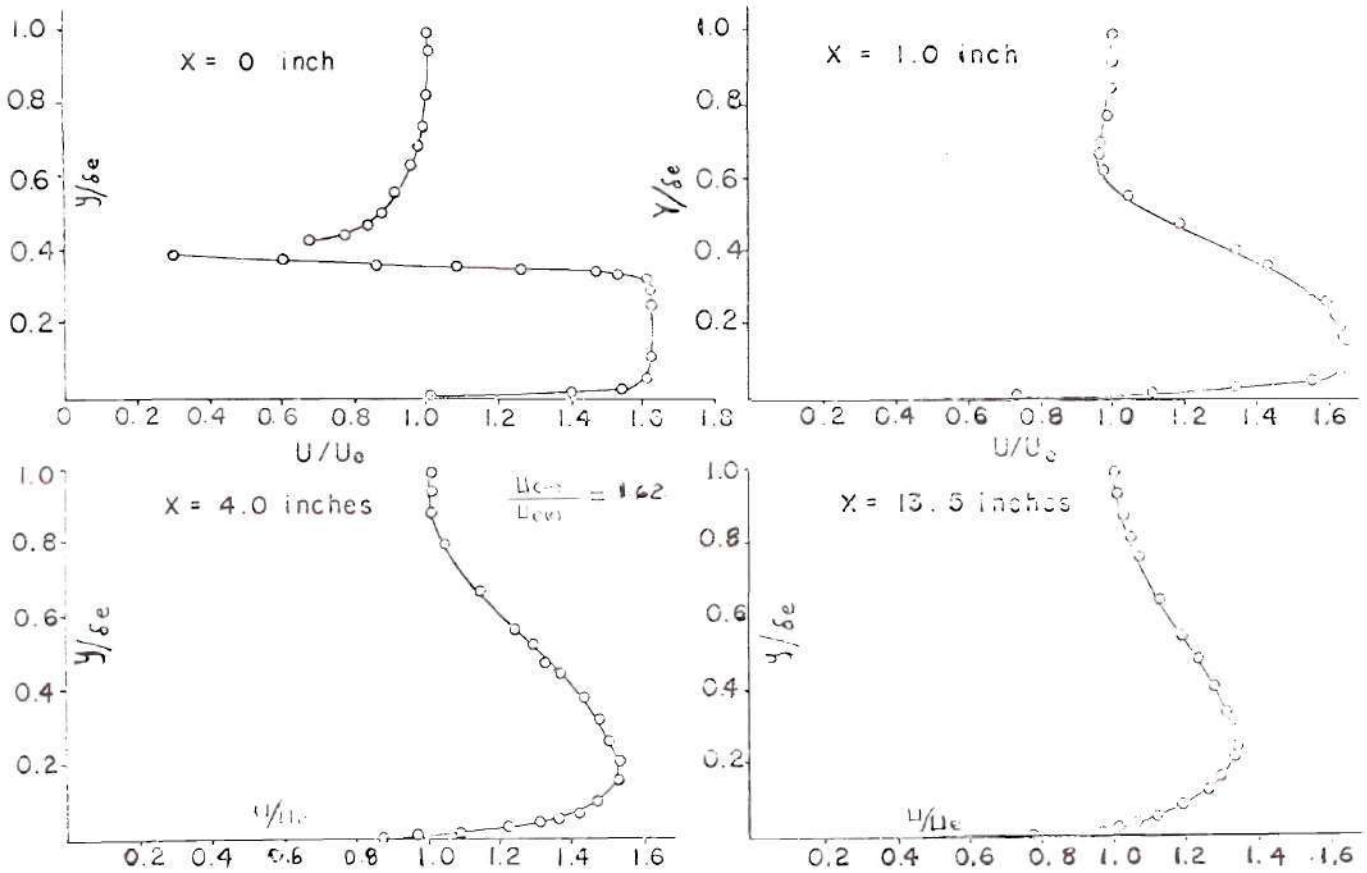

Figure 7. Velocity Profiles for Initial Velocity Ratio of 1.62

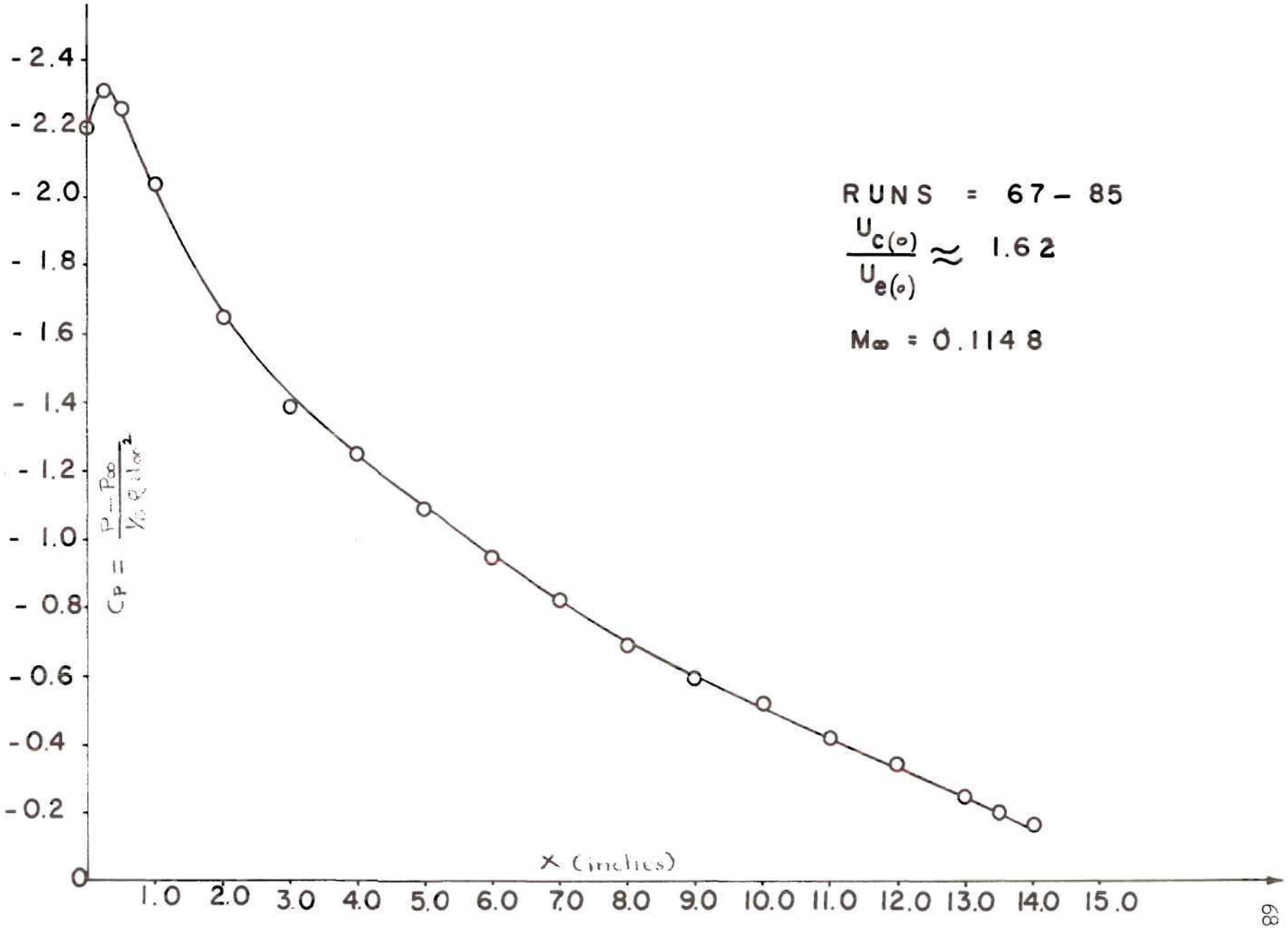

Figure 8. Pressure Distribution for Initial Velocity Ratio of 1.62

the velocity profiles at various distances downstream of the slot exit are in agreement with the mathematical model of the viscous flow shown in Figure (1). The length of the initial region for different velocity ratios and different flow conditions and pressure distributions is between 1 and 2 inches which is approximately 10 to 20 slot heights. The conditions at the end of the initial region such as well layer momentum thickness, wall layer form factor, jet layer thickness, wake layer thickness, etc. vary with the velocity ratio $\frac{U_{c(o)}}{U_{e(o)}}$ at slot exit and pressure distribution. The distance, downstream of slot exit up to which the minimum velocity point is observed, increases as the initial velocity ratio $\frac{U_{c(o)}}{U_{e(o)}}$ approaches a value of one. At lower values of initial velocity ratio $\frac{U_{c(o)}}{U_{e(o)}}$ of 1.12 and 1.29 the velocity profile becomes that of an ordinary turbulent boundary layer, as shown in Figures (3) and (5), respectively. Incipient separation occurs for $\frac{U_{c(o)}}{U_{e(o)}} = 1.12$ as seen from the velocity profile in Figure (3). The existence of incipient separation was also verified by observation of the movements of tufts which were attached to the flap surface. At higher values of initial velocity ratio a wall jet type velocity profile still exists at the end of the flap as seen in Figure (7).

Similarity Function for Jet Layer Velocity Profiles in Initial and Main Region

Figures (9) and (10) show non-dimensional plots of the jet layer velocity profiles in the initial and main regions, respectively. Experimental points shown in these figures are for various conditions at the slot exit as well as for different pressure distributions and

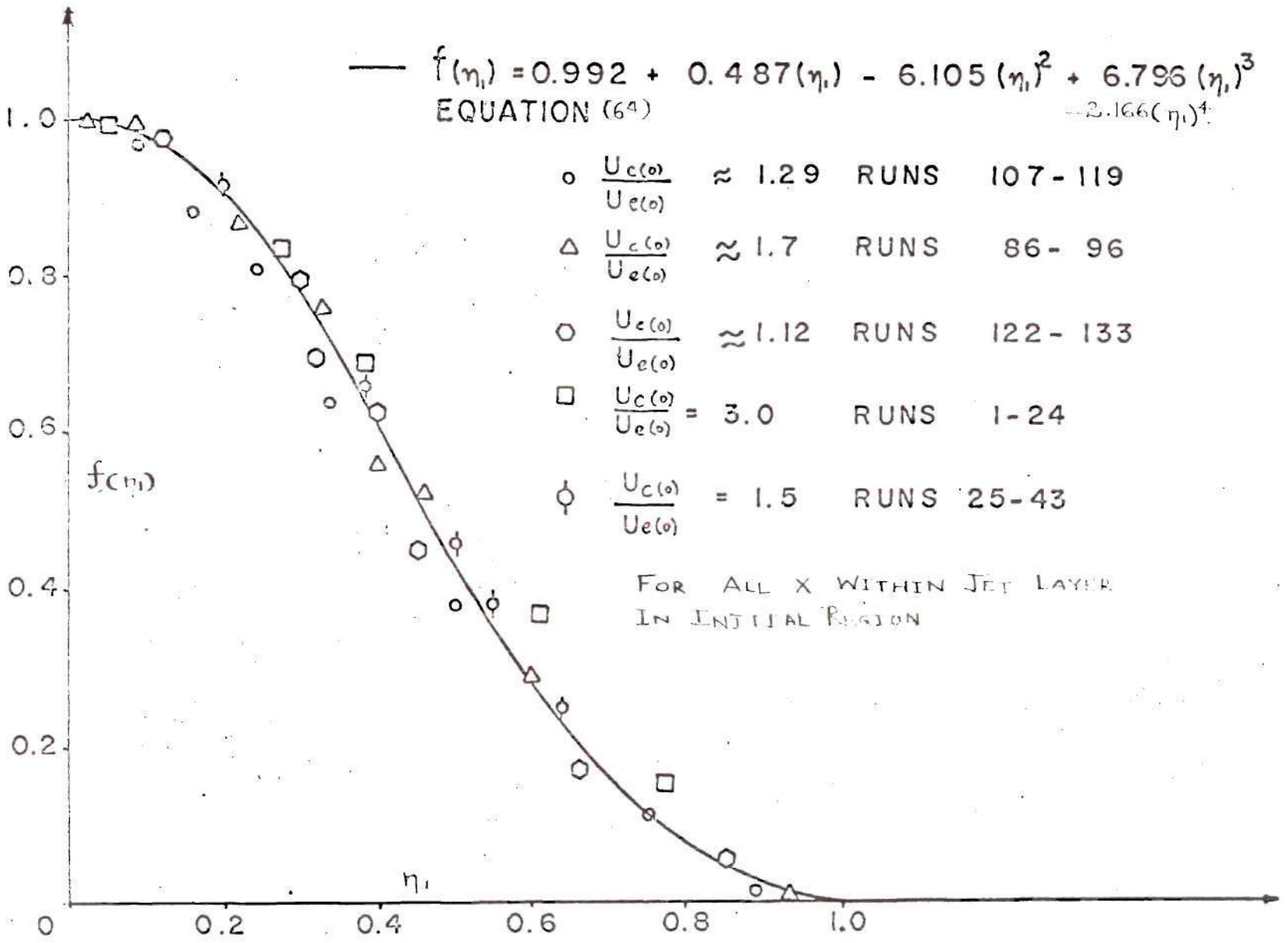

Figure 9. Similarity for Jet Layer Velocity Profiles in the Initial Region

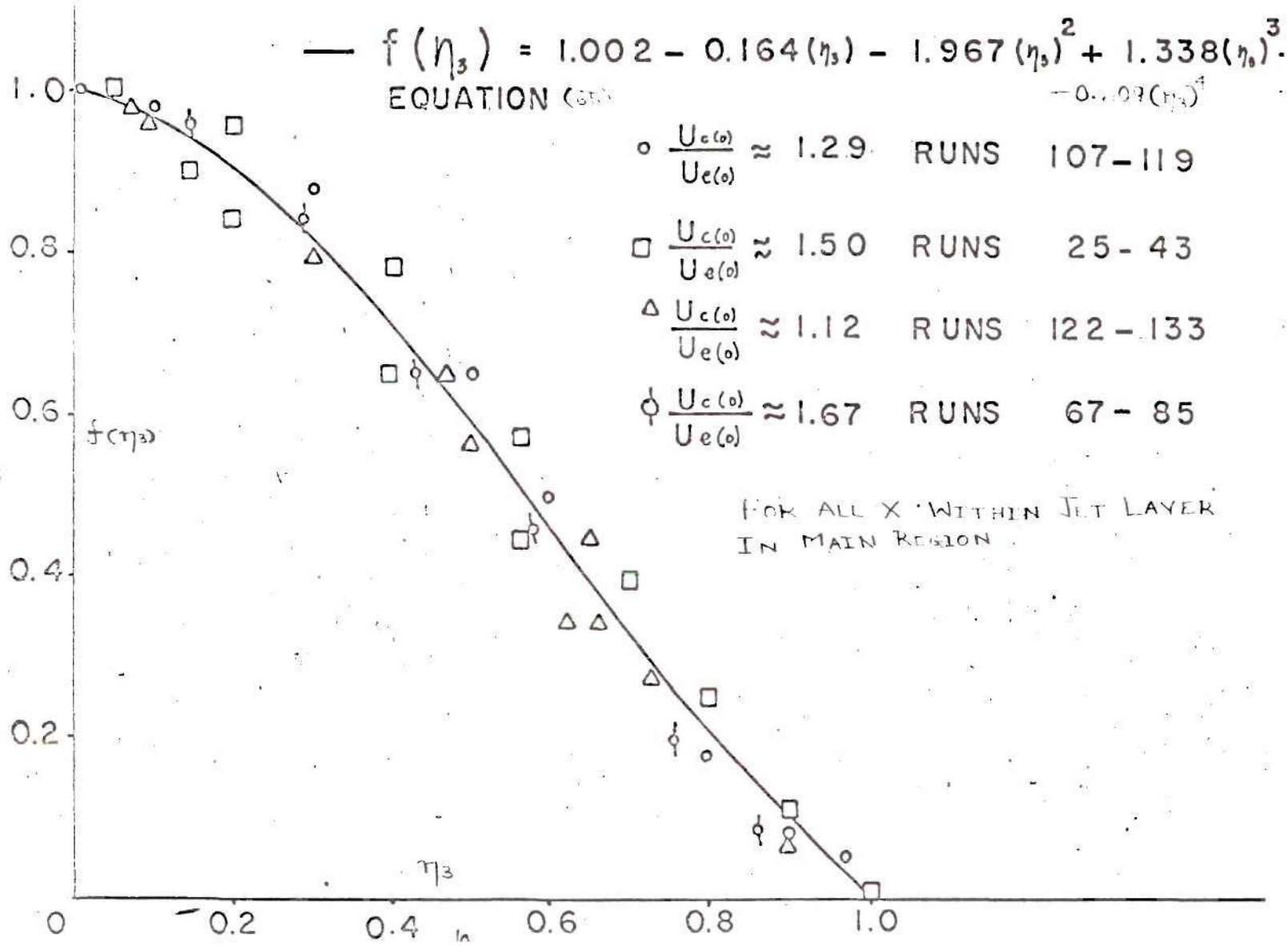

Figure 10. Similarity for Jet Layer Velocity Profiles in the Main Region

different X locations. The similarity parameter and similarity function for jet layer velocity profile in the initial region are defined as,

$$\eta_1 = \frac{\delta_3 - y}{\delta_3 - \delta_2} \quad ; \quad f(\eta_1) = \frac{U_c - u}{U_c - U_w} \quad . \tag{62}$$

In an analogous way the similarity parameter and similarity function for the jet layer in the main region in Figure (10) are defined as,

$$\eta_3 = \frac{\delta_3 - y}{\delta_3 - \delta_2} \quad ; \quad f(\eta_3) = \frac{U_m - u}{U_m - U_w} \quad . \tag{63}$$

It is important to notice that the experimental data for different velocity ratios at slot exit and for different pressure distributions and X locations fall very nicely on a single curve when similarity functions and parameters are chosen as above. It is this fact which facilitates the transformation of Pradtl's boundary layer partial differential equations into ordinary differential equations which are amenable to solutions by numerical methods.

The least square polynomial expression for $f(\eta_1)$ in the initial region is given by the following expression:

$$f(\eta_1) = 0.992 + 0.487(\eta_1) - 6.105(\eta_1)^2 + 6.796(\eta_1)^3 - 2.116(\eta_1)^4 \quad . \tag{64}$$

The least square polynomial function for $f(\eta_3)$ in the main region for the jet layer is

$$f(\eta_3) = 1.002 - 0.164(\eta_3) - 1.967(\eta_3)^2 + 1.338(\eta_3)^3 - 0.209(\eta_3)^4 . \tag{65}$$

Figure (11) shows plots of equations (64) and equation (65) which represent the similarity function for the jet layers in the initial and main region of the confluent boundary layer flow. In this Figure (11) are also plotted Albertson's et al (14) experimental data for free jet flow between two parallel streams. It can be concluded from this comparison that the free jet data also fall very nicely on the present similarity curve of jet layer in the initial region.

Similarity Functions for the Wake Layer In the Initial and Main Regions

The similarity variable and similarity function for velocity profiles in the wake layer of the initial region are defined as follows:

$$\eta_2 = \frac{y - \delta_3}{y_{1c} - \delta_3} \quad ; \quad f(\eta_2) = \frac{U_e - u}{U_e - U_w} \quad . \tag{66}$$

where y_{1_c} is the distance y in the wake layer where $f(\eta_2) = 0.5$.

In an analogous manner the similarity parameter and similarity function are defined for the wake layer in the main region as,

$$\eta_4 = \frac{y - \delta_3}{y_{2c} - \delta_3} \quad ; \quad f(\eta_4) = \frac{U_e - u}{U_e - U_w} \tag{67}$$

where y_{2_c} is the distance y in the wake layer in main region where $f(\eta_4) = 0.5$.

Figures (12) and (13) show non-dimensional plots of velocity profiles obtained from experimental measurements of velocities in the wake layer of the initial and main regions of Figure (1). Experimental points shown in these figures are for various conditions at the slot exit as well as for different pressure distributions, and different X

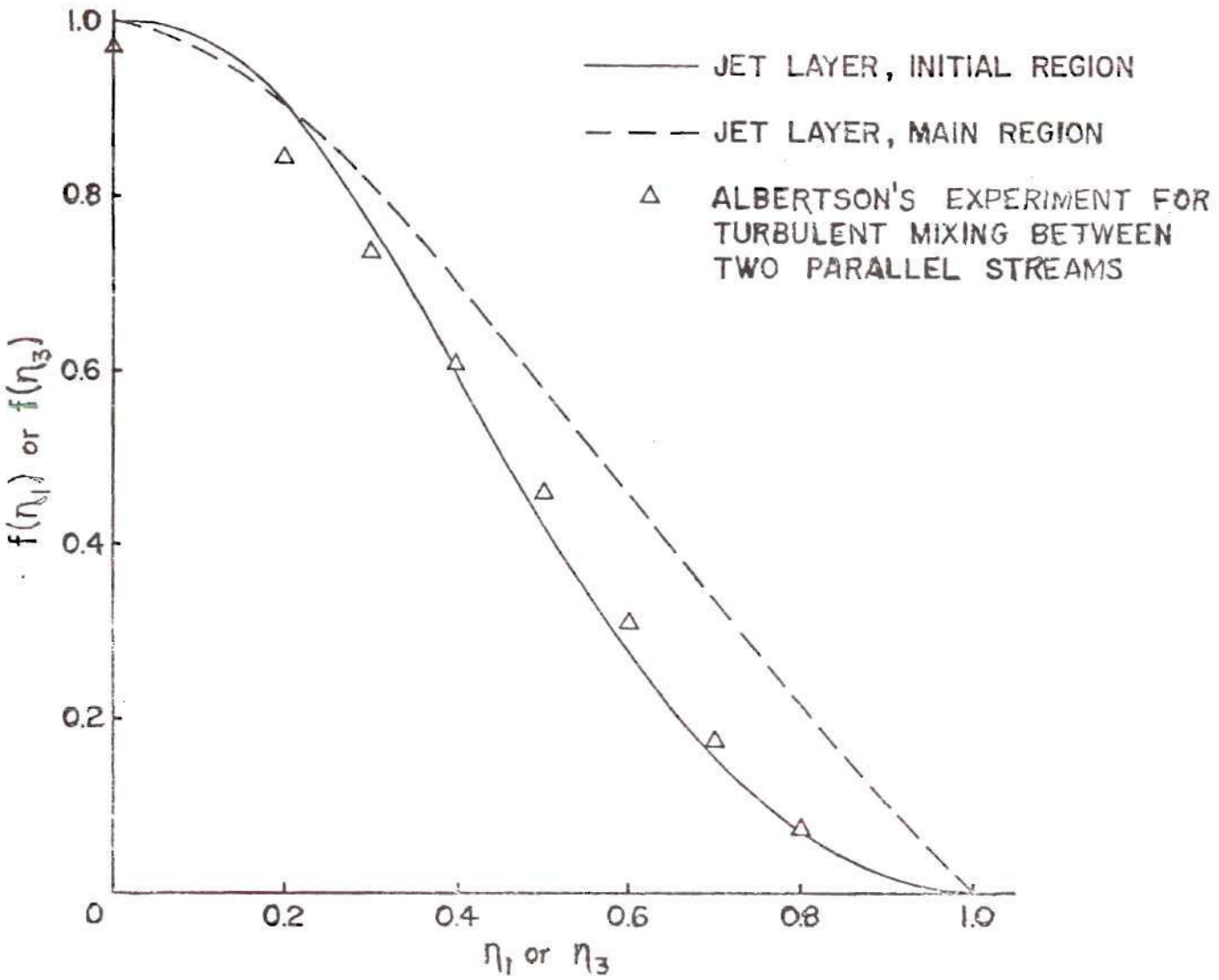

Figure 11. Comparison of the Present Similarity Function for Jet Layer in the Initial and Main Region with the Free Jet Data

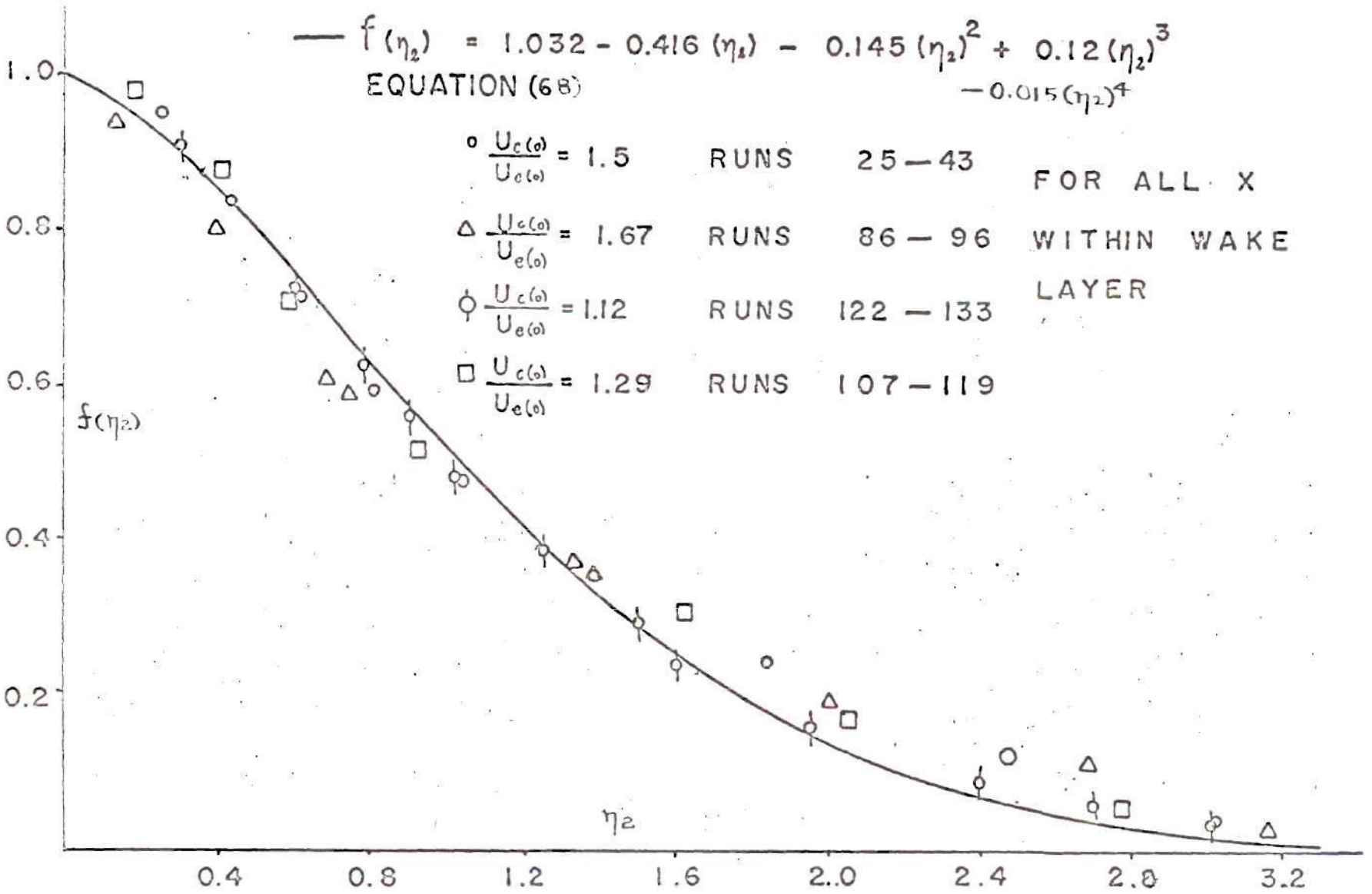

Figure 12. Similarity for Wake Layer Velocity Profiles in the Initial Region

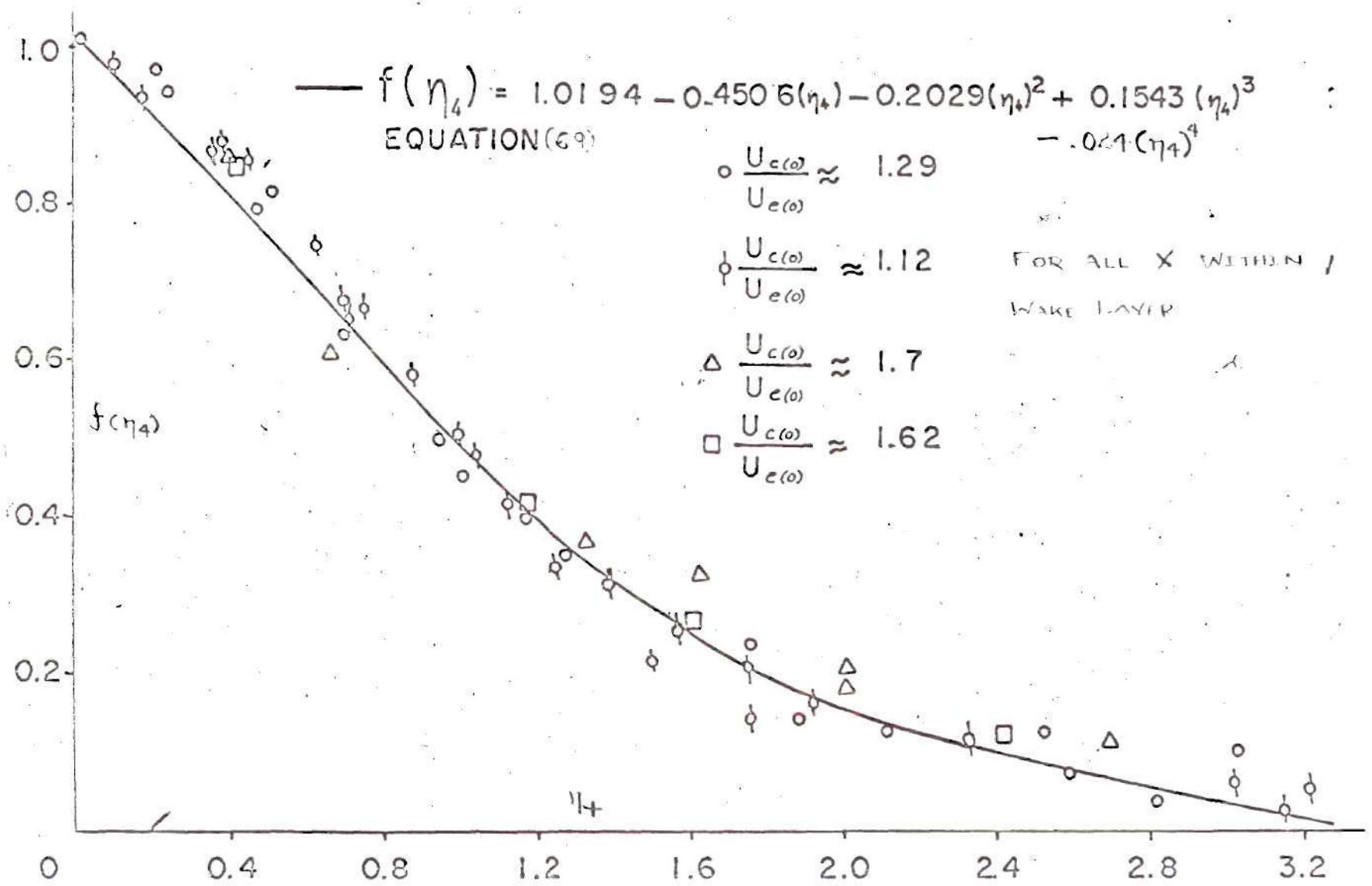

Figure 13. Similarity for Wake Layer Velocity Profiles in the Main Region

locations. It is both interesting and important to notice that with the choice and definitions of parameters and functions as given by equations (66) and (67), the experimental data for vastly different conditions fall on a single curve.

The least square curve fit for the similarity function $f(\eta_2)$ for wake layer in the initial region and for the similarity function $f(\eta_4)$ for the wake layer in the main region are given by following expressions. In the present calculation method these similarity curves are used for the purpose of obtaining area under the similarity curves and for that reason the accuracy will not be affected by the use of least square curve fits.

$$f(\eta_2) = 1.032 - 0.416(\eta_2) - 0.145(\eta_2)^2 + 0.12(\eta_2)^3 - 0.015(\eta_2)^4 \quad (68)$$

$$f(\eta_4) = 1.0194 - 0.450(\eta_4) - 0.2029(\eta_4)^2 + 0.1543(\eta_4)^3 - 0.024(\eta_4)^4 \quad (69)$$

Figure (14) shows a plot of equations (12) and (13) for comparison purposes. Also plotted in this figure is a non-dimensional representation of the velocity profiles for two-dimensional free turbulent wake flow. The Prandtl-Schlicting (15) expression for free turbulent wake flow is given by,

$$\frac{u_1}{u_{1m}} = (1 - \eta^{3/2})^2 \quad (70)$$

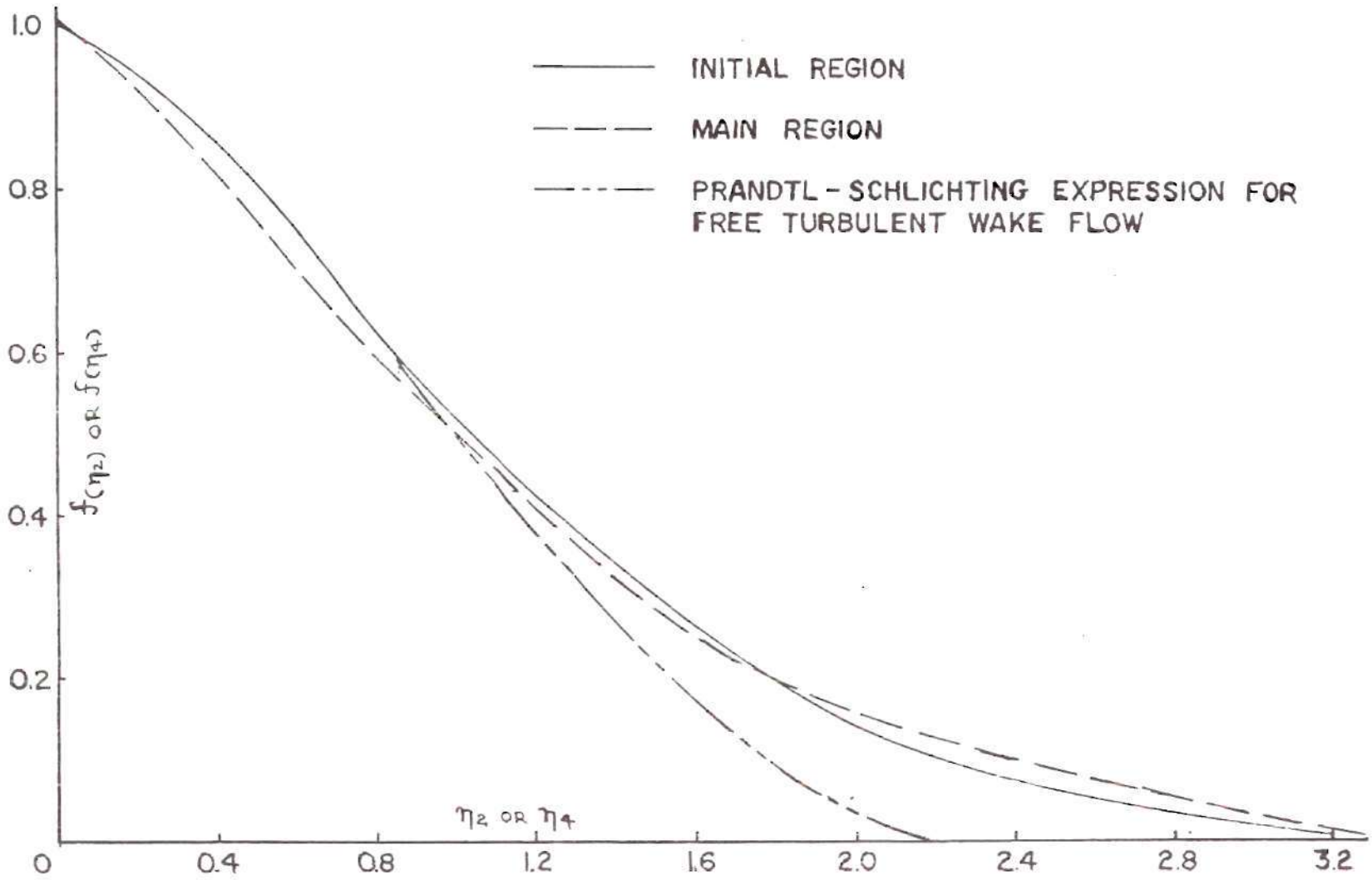

Figure 14. Comparison of the Present Similarity Function for Wake Layer in the Initial and Main Region with Prandtl-Schlichting Expression for Free Turbulent Flow

where

$$u_1 = U_\infty - u$$

$$u_{1m} = U_\infty - U_w$$

$$\eta = \frac{\text{distance from minimum velocity point}}{\text{half width of free wake}} .$$

The relation between η as used in equation (70) to the present definitions for η_2 or η_4 as used in equations (66) and (67) can be derived as,

$$\eta = 0.44(\eta_2 \text{ or } \eta_4) . \tag{71}$$

Thus non-dimensional velocity profile in the free turbulent wake can be expressed as,

$$f(\eta) = \{1 - (0.44\eta)^{3/2}\}^2 . \tag{72}$$

The above equation is plotted in Figure (14). It is apparent from this figure that the difference between the similarity curve for the wake layer in the initial and main region is slight as compared to those between the similarity curves for the jet layer in the initial and main region of Figure (11). Also seen from Figures (11) and (14) is the fact that the similarity curves for free jet and free wake flow are not significantly different from those of jet and wake layer of the confluent boundary layer. The above observation facilities derivation of an

expression for calculating the profile drag of a multi-component airfoil from the confluent boundary layer quantities evaluated (or measured experimentally) at the trailing edge of a flap.

One Parametric Family Representation for Wall Layer Velocity Profiles

It was mentioned previously in Chapter III that with the assumption of a one parameter family of wall layer velocity profiles, two advantages are obtained, namely, (i) Pradtl's partial differential equations for boundary layer flow are transformed into ordinary differential equations and, more importantly, (ii) one is able to consider the effect of pressure gradient on the wall layer physical parameters. Experimental observations on viscous flow in general indicate that variation of external pressure gradient, in particular adverse pressure gradient, causes relatively much larger changes in the velocity profiles near the wall than on the flow away from the wall. This fact emphasizes that if the separation phenomena, or perhaps $C_{L_{MAX}}$ for 2-component airfoils, is to be studied in some semi-empirical manner, this is possible with the assumption of one parameter family of wall layer profiles.

Figures (15) and (16) show plots of experimental data for relations between the quotient $\frac{\delta^{**}_{wall}}{\theta_{wall}} = \tilde{H}$ and the thickness ratio $H = \frac{\delta^{*}_{wall}}{\theta_{wall}}$ Figure (15) is for the wall layer of the initial and main regions while Figure (16) shows the corresponding relation in the region where the confluent boundary layer profile becomes that of an ordinary turbulent boundary layer. Experimental data for various conditions of slot exit velocity ratio, pressure distributions and various X locations fall on the single curves. This result indicates that all the velocity profiles for the wall layer in the initial and main region constitute a

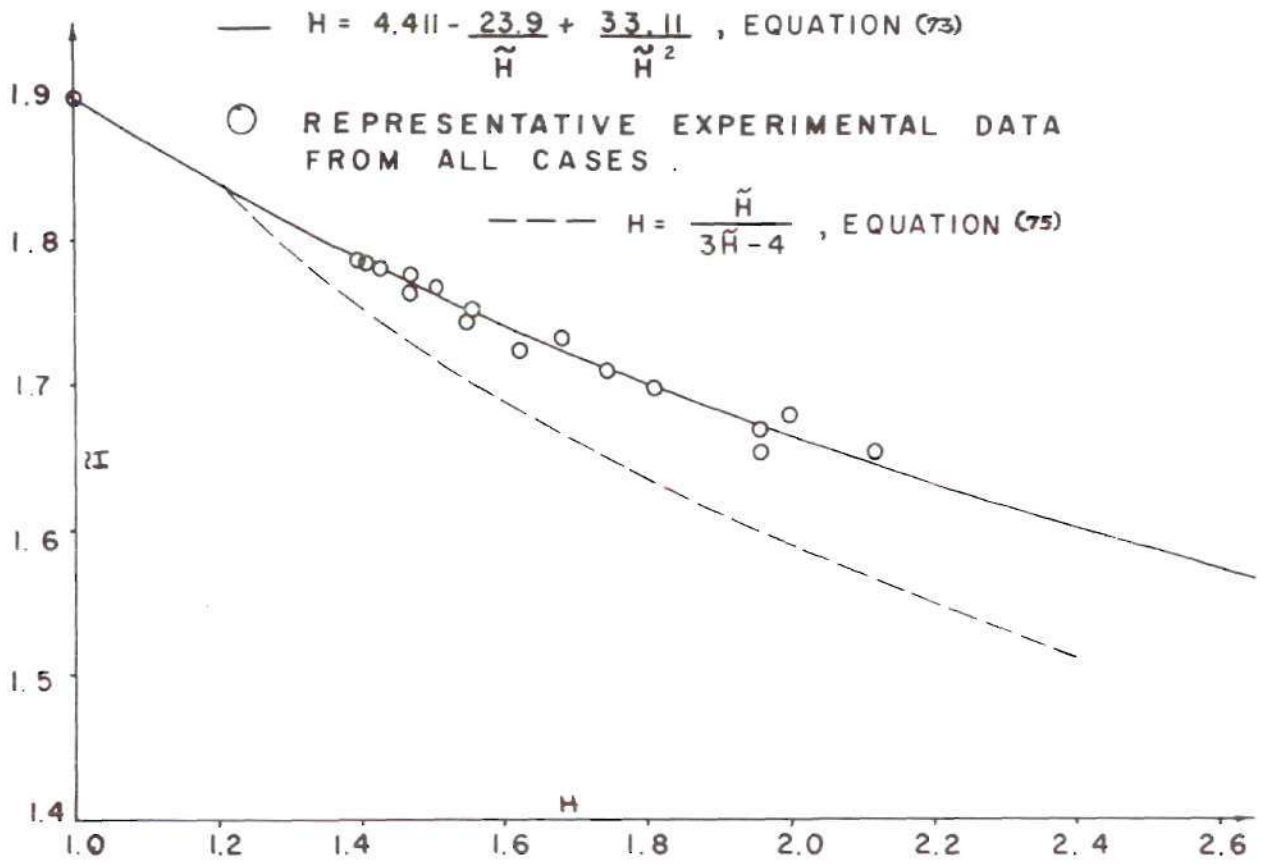

Figure 15. Relation Between H and $\tilde{H}$ for Wall-Layer in the Initial and Main Region

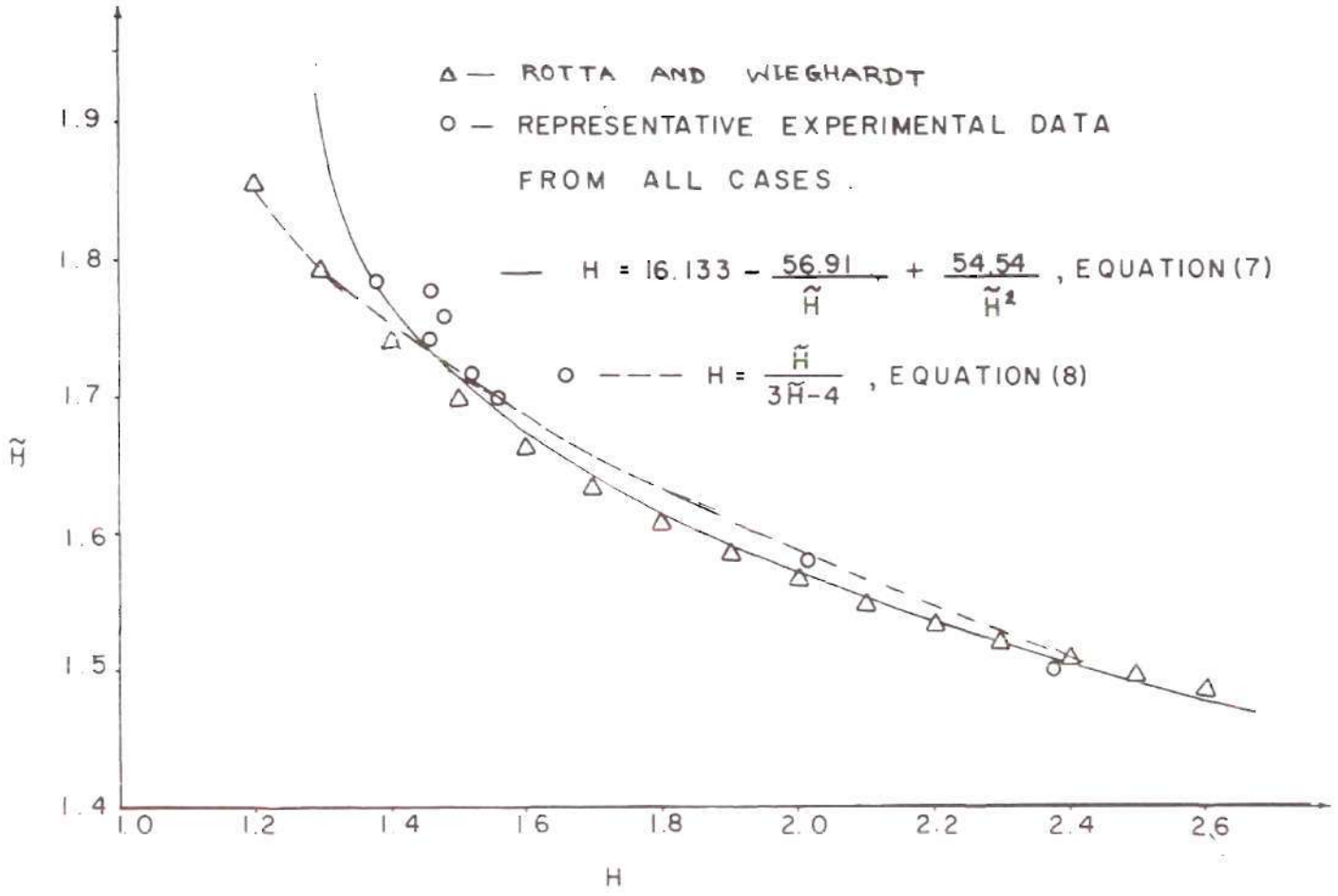

Figure 16. Relation Between H and $\tilde{H}$ for the Ordinary Turbulent Boundary Layer Region

one parameter family and the same is true for velocity profiles when the viscous flow becomes of the ordinary turbulent boundary layer type. The relationship between H and $\tilde{H}$ for the wall layer in the initial and main regions is given by,

$$H = 4.411 - \frac{23.9}{\tilde{H}} + \frac{33.11}{\tilde{H}^2} \quad . \tag{73}$$

while the relationship between H and $\tilde{H}$ when the viscous flow becomes of the ordinary turbulent boundary layer type is given by,

$$H = 16.133 - \frac{56.91}{\tilde{H}} + \frac{54.54}{\tilde{H}^2} \quad . \tag{74}$$

The expressions given by both equations (73) and (74) have been obtained from experimental data by least square fit. Figure (16) also shows the points obtained from experimental results by J. Rotta (16) for ordinary turbulent boundary layers. The theoretical relation between H and $\tilde{H}$, which can be derived with the assumption of power law velocity profiles and definitions of wall layer displacement, momentum and energy thicknesses, is given by the following equation:

$$H = \frac{\tilde{H}}{3\tilde{H} - 4} \tag{75}$$

The relation between H and $\tilde{H}$ given by equation (75) is also plotted in both Figures (15) and (16). It can be concluded from Figures (15) and (16) that the relation between H and $\tilde{H}$ as experimentally observed for confluent boundary layer in the initial and main

region differs from the theoretical relation of equation (75). In the ordinary turbulent boundary layer region, however, the present experimental data show good comparison with theoretical equation (75). In addition, Rotta's experimental data for ordinary turbulent boundary layer also agree with the present experimental data in ordinary turbulent boundary layer region.

Functional Representation of Wall-Shear Stress

The principle of local dynamic similarity asserts that local wall friction coefficient be proportional to the local value of Reynolds number based on some physical quantities associated with the local boundary layer thickness. Jet and wake layers of the confluent boundary layer being farther away from the wall than the wall layer, it is conceivable that the physical quantities associated with jet and wake layer thickness would have comparatively less effect on local skin friction. For these reasons, the appropriate Reynolds number to use is the local wall layer momentum thickness Reynolds number, $\frac{U_m \theta_s}{\nu}$.

It is also known that local wall shear is also a function of pressure gradient in the flow direction. Pressure gradients in the flow direction retard the flow near the wall to a larger extent than far away from the wall. The above fact has been observed from experimental measurements. For this reason, wall layer form factor, H, is selected as another parameter on which local value of wall shear is dependent. In addition, local wall shear is non-dimensionalized by the dynamic head based on the velocity at the edge of wall layer, i.e., ρU_m^2 . Thus wall friction can be expressed as,

$$\frac{\tau_w}{\rho U_m^2} = F\left(\frac{U_m \theta_{(wall\text{-}layer)}}{\nu}, \; H_{(wall\text{-}layer)}\right) \qquad (76)$$

Figure (17) shows a plot of $\frac{\tau_w}{1/2\ \rho U_m^2}$ vs wall layer momentum thickness Reynolds number, $\frac{U_m \theta_5}{\nu}$ or Re_θ, for various values of wall layer form factor, H. These curves have been obtained from indirect skin friction measurement described in Chapter IV. Least square fits are applied to the experimental points for various slot exit conditions, X locations in various regions of confluent boundary layer flow, and pressure gradients. Figure (17A) shows the comparison of the output of least square curve fit, equation (77), with indirect experimental shear stress coefficient points which were input to the least square fit computer program. This figure shows that experimental scatter is reduced by the least square curve fit.

Figure (17) indicates a peculiar characteristic of skin friction coefficient for confluent boundary layer flow in that it increases with wall-layer momentum thickness Reynolds number for constant value of wall layer form factor up to the point where peak velocity disappears, i.e., up to the end of main region II. Downstream of the end of main region II, i.e., in the ordinary turbulent boundary layer region, the wall friction coefficient decreases with increasing momentum thickness Reynolds number for constant value of form factor. For comparison, in the ordinary turbulent boundary layer region the points calculated from the Ludwieg-Tillman skin friction expression are shown plotted for various momentum thickness Reynolds numbers for

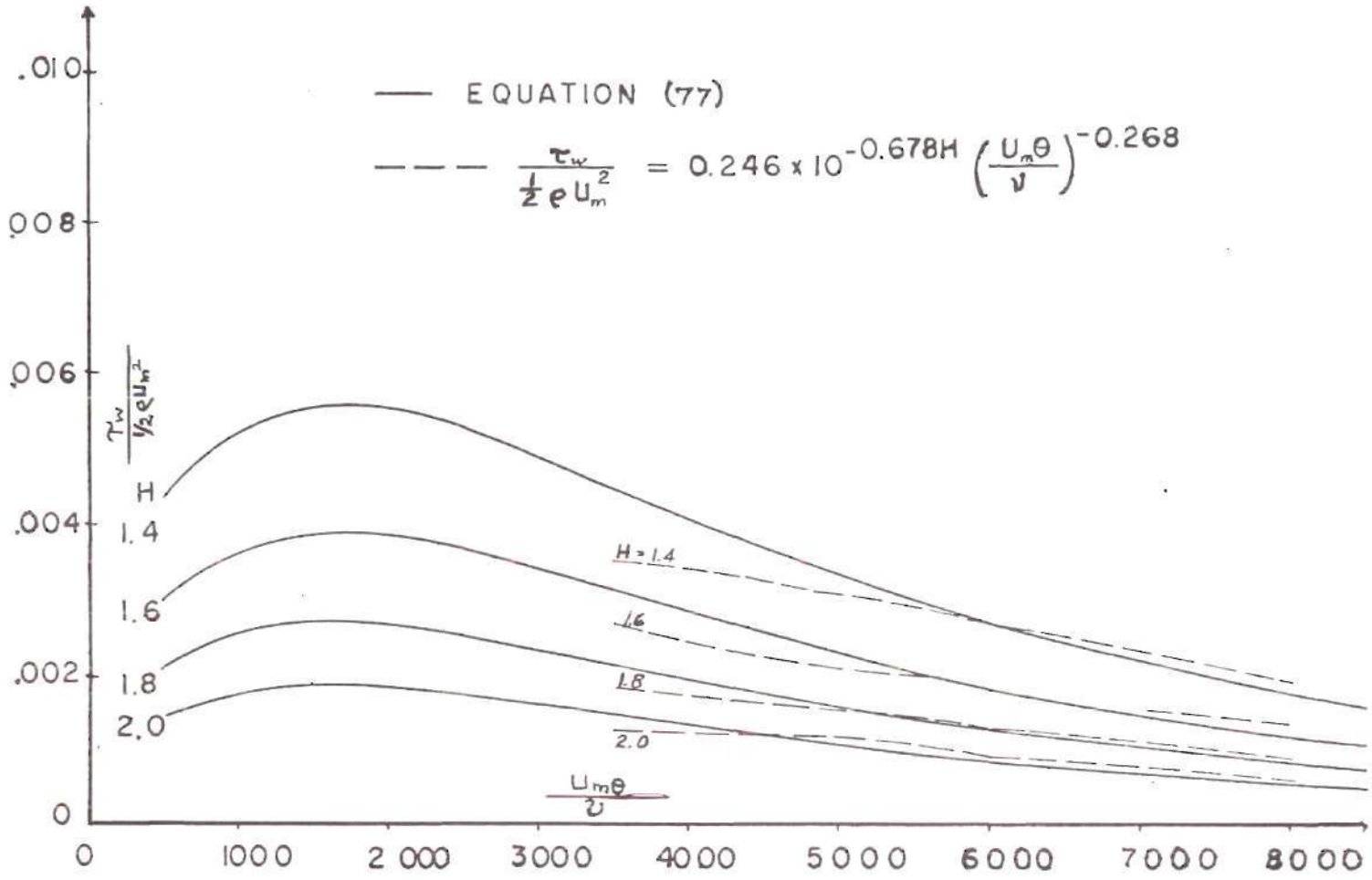

Figure 17. Parametric Relation of Wall Shear Coefficient

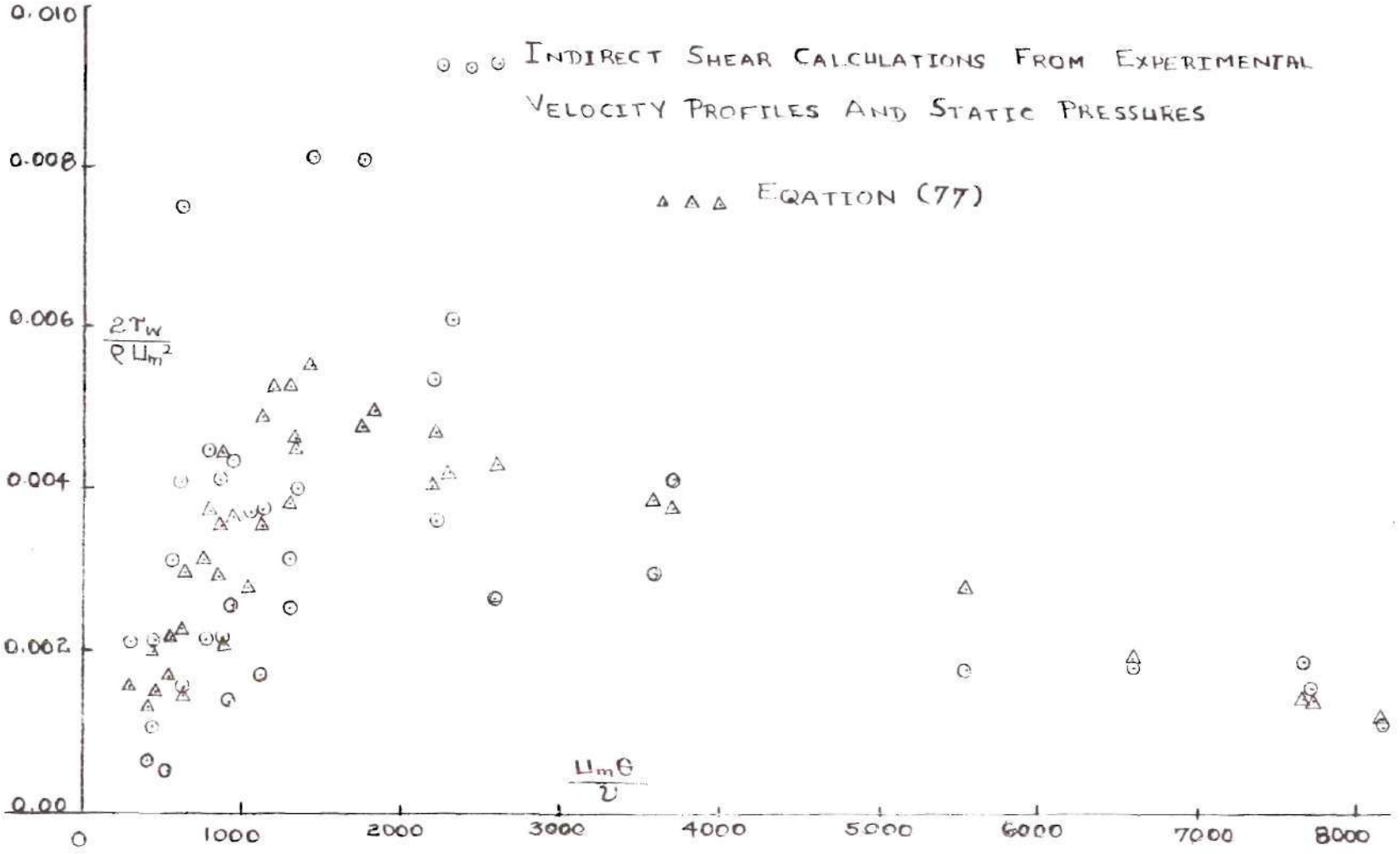

Figure 17A. Comparison of Output of Least Square Curve-Fit with Experimental Wall Shear Stress Coefficient

constant values of the form factor. It is seen from this comparison, that the present indirect calculation of wall shear from the velocity profiles is in good agreement with experimental skin friction law in the region where the wall jet profile has changed to an ordinary turbulent boundary layer profile.

The least square fit expression which was obtained from the points calculated from experimental velocity profiles and known pressure distribution is given by,

$$\frac{\tau_\omega}{\frac{1}{2}\rho U_m^2} = 1.964\ \mathrm{EXP}\left[-1.819H + 35.68\{\ln(Re\theta)\} - 1.365\{\ln(Re\theta)\}^2\right] \cdot \left[\ln(Re\theta)\right]^{-114.6} \cdot (10)^{16} \tag{77}$$

Wall-Layer Turbulent Dissipation Integral

This integral is defined as,

$$\pi = \int_0^{\delta_i} \frac{\tau}{\rho U_i^2} \frac{\partial}{\partial y}\left(\frac{u}{U_i}\right) dy \tag{78}$$

where

δ_i = wall layer thickness δ_1 in initial region

or = wall layer thickness δ_3 in main region

or = boundary layer thickness in the ordinary turbulent boundary layer region

and

U_i = core velocity U_c in initial region

or = velocity at the edge of wall layer, U_m

or = external edge velocity U_e in the ordinary turbulent boundary layer region

The integral π was encountered in the theoretical equations of Chapter III. It was mentioned previously that this integral should be expressed as a function of the dependent variables to be calculated. Application of the principle of local dynamic similarity would indicate that π can be expressed as a function of local wall layer momentum thickness Reynolds number, $\frac{U_m \theta_s}{\nu}$. The wall layer form factor H may constitute another parametric dependence for shear integral π for the effect of pressure gradient. Thus the functional dependence of shear integral can be expressed by,

$$\pi = F\left(\frac{U_i \theta_{(wall-layer)}}{\nu}, H\right) \tag{79}$$

where U_i may be core velocity U_c or velocity U_m at the edge of wall-layer or external edge velocity, U_e.

Figure (18) shows a plot of wall layer shear integral plotted as a function of local wall layer momentum thickness Reynolds number with wall layer form factor, H, as a parameter. Figure (18A) shows the comparison of the output of least square curve fit, equation (80), with indirect experimental wall layer shear integral points which were input to the least square fit computer program. This figure shows that experimental scatter is reduced by the least square curve fit. Curves in Figure (18) display similar characteristics to the wall shear, i.e., the value of π increases with local wall layer momentum thickness

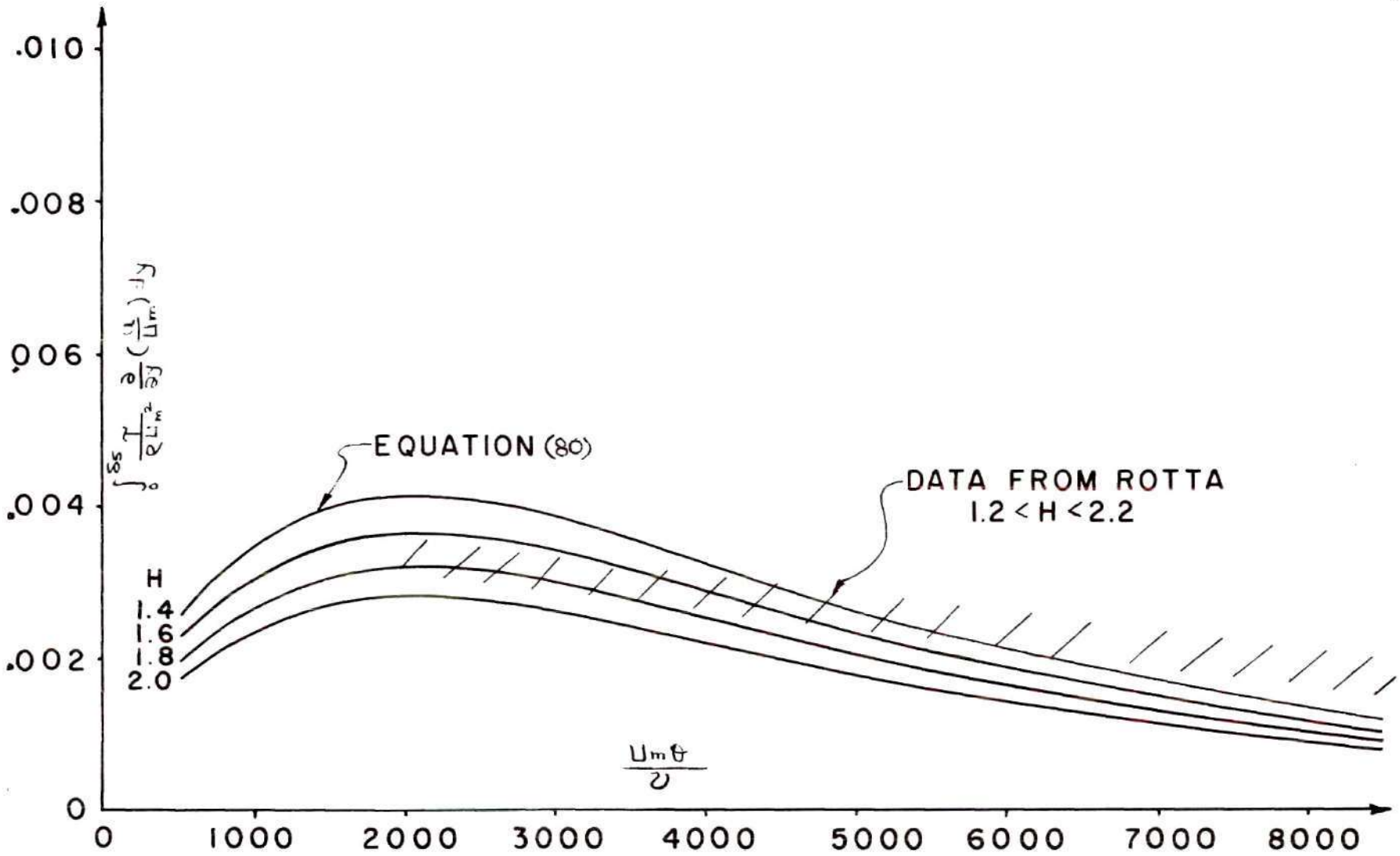

Figure 18. Parametric Relation of Wall Layer Shear Dissipation Integral

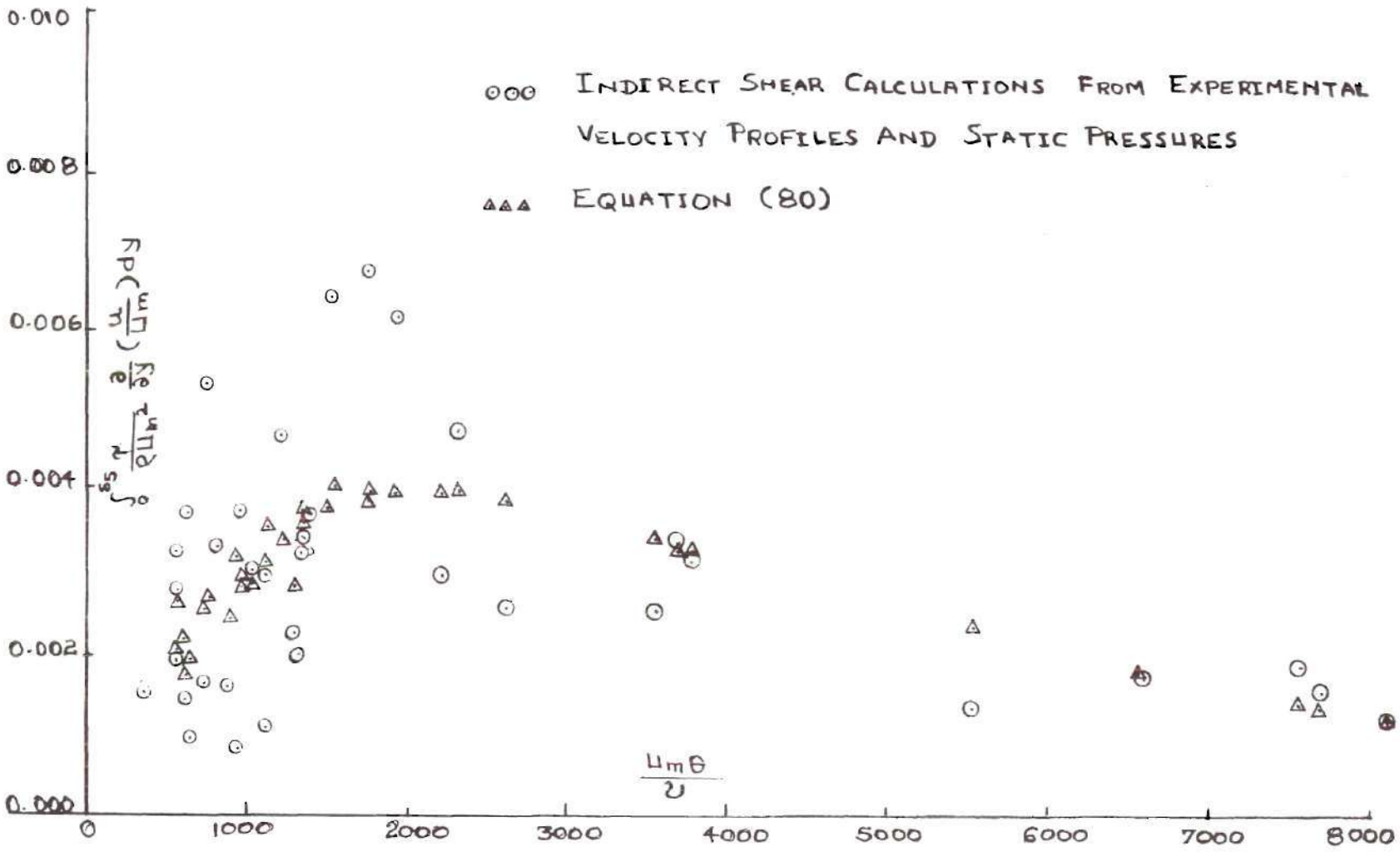

Figure 18A. Comparison of Output of Least Square Curve-Fit with Input Experimental Wall Layer Shear Integral

Reynolds number up to the end of main region II. This holds true for any initial velocity ratio at the slot exit and external pressure distribution. The magnitude of shear integral Π then decreases when the velocity profile in the viscous region is of the ordinary boundary layer type. Figure (18) also shows the experimental data of J. Rotta[16], plotted as a band, for ordinary turbulent boundary layer flow. This band includes velocity profiles having varying form factors. This comparison indicates that good agreement is obtained between indirect shear stress profile calculation in the ordinary turbulent boundary layer region of confluent boundary layer flow and the experimental measurements for the ordinary turbulent boundary layer flow.

An analytical expression obtained by least square curve fit for shear integral Π is given by,

$$\Pi = 1.616\ EXP\left[-0.636(H) + 48.55\{\ln(Re\theta)\} - 1.82\{\ln(Re\theta)\}^2\right] \cdot \left[\ln(Re\theta)\right]^{-158.7} \cdot (10)^{23} \qquad (80)$$

= wall layer turbulent dissipation integral

Shear Stress at the Edge of the Wall Layer

Figure (19) shows a plot of difference between wall shear and shear at the edge of wall layer versus wall layer momentum thickness Reynolds number. Figure (19A) shows the comparison of the output of least square curve fit, equation (81), with indirect experimental points which were input points which were input to the least square curve fit computer program. This figure shows that experimental scatter

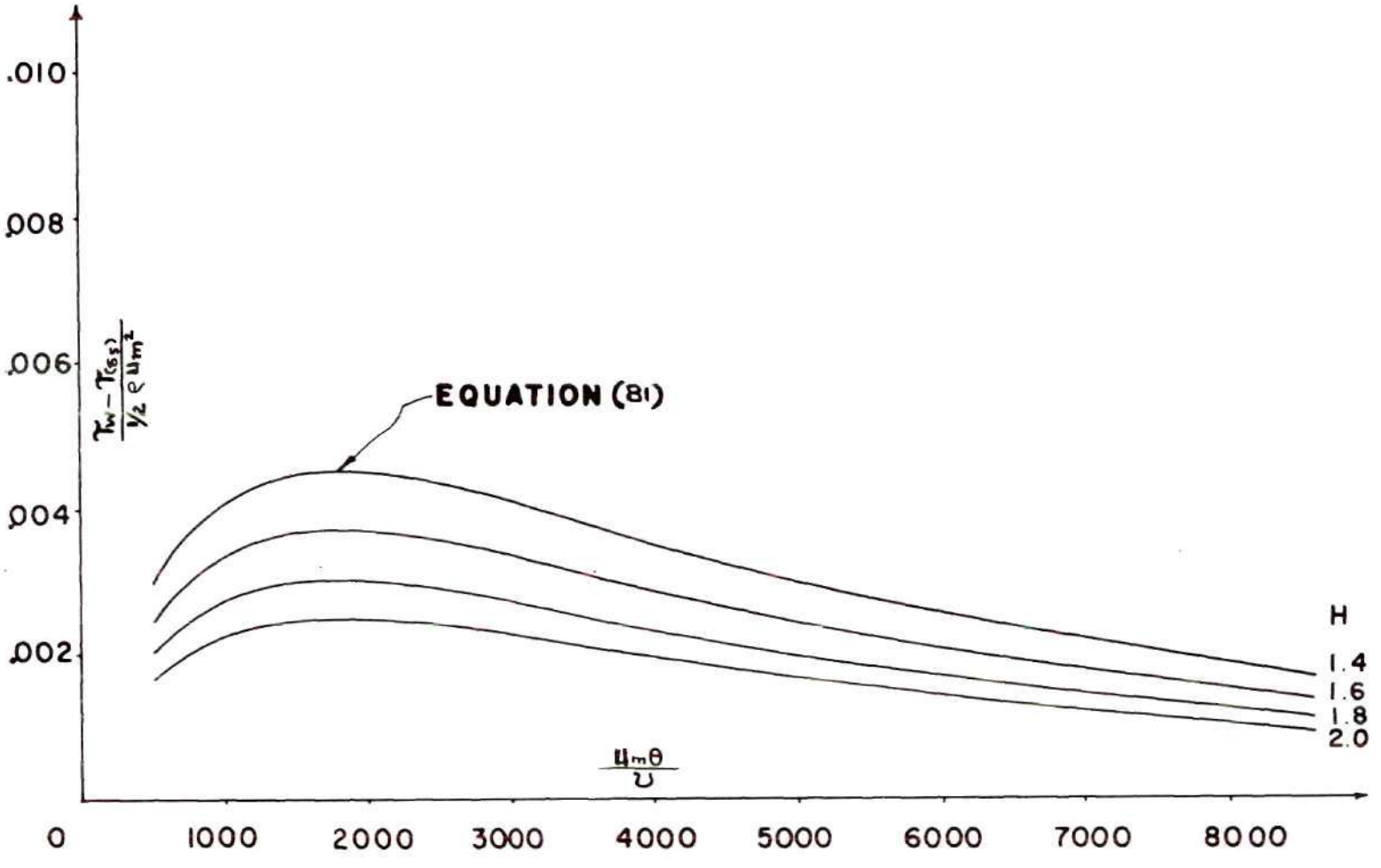

Figure 19. Parametric Relation of Shear at Edge of Wall Layer

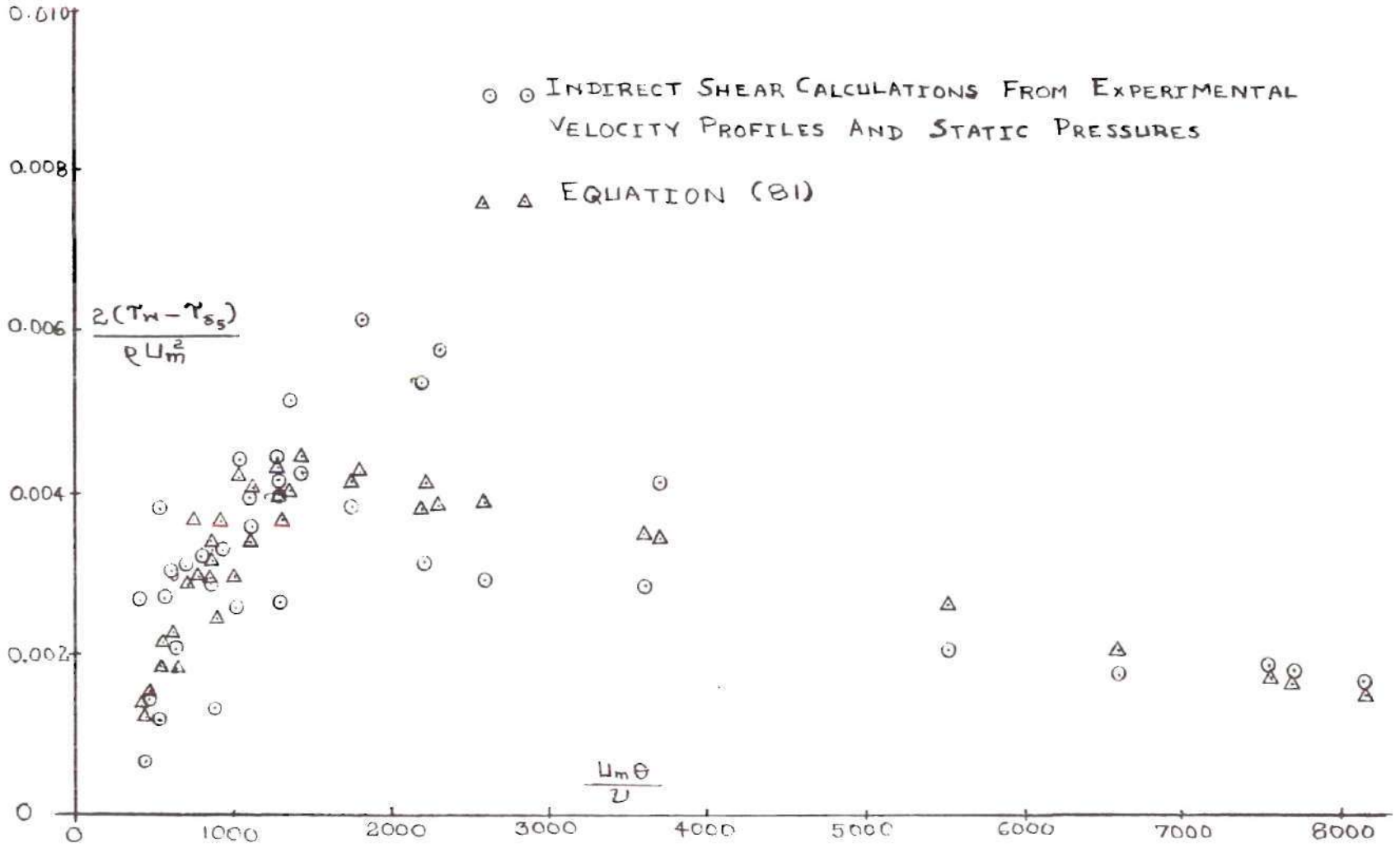

Figure 19A. Comparison of Least Square Curve-Fit Output and Input Experimental Data for Shear at Edge of Wall-Layer

is reduced by the least square curve fit. The curves in Figure (19) also illustrate that the shear at the edge of the wall layer when correlated with parameters similar to wall shear does give good correlation. Auxiliary equation for shear at the edge of wall-layer, obtained by least square fit of the points calculated from experimental velocity profiles and known external pressure distribution, is given by,

$$\frac{\tau_w - \tau_{(ss)}}{1/2\,\rho\,U_m^2} = 2.518\ \mathrm{EXP}\left[-0.918(H) + 17.21\{\ln(Re\theta)\} - 0.743\{\ln(Re\theta)\}^2\right] \cdot \left[\ln(Re\theta)\right]^{-45.79} \quad (81)$$

where

$\tau_{(ss)}$ = shear stress at the edge of wall layer

U_m = velocity at the edge of wall layer

Generalized Parametric Representation of Shear Stress at Velocity Minimum

Experimental evidence indicates that the shear stress at the point of minimum velocity of the velocity profiles shown in Figure (1) is not zero but may vary from a large positive value near the exit of the slot to a slight negative value farther away from the slot when the depression in the velocity profiles is small.

In the multi-layer Integral method solution for the viscous flow which develops, for example, on the upper surfaces of a multi-element airfoil and also on the upper surfaces of an internally or externally blown flap, pertinent coupled equations contain terms involving shear

stress at the velocity minimum. It is found from numerical solution of these equations that the contribution of the terms containing shear stress at the maximum and minimum velocities is significant near the slot exit to some distance (about 30 slot height) downstream. Moreover in the case of marching type solutions, errors encountered due to neglecting certain terms are magnified at the trailing edges of the airfoil. Hence it is very desirable to find parameters such that shear stress at velocity minima and maxima can be represented by auxiliary equations.

It was shown previously that the velocity profiles in the jet layer and also in the wake layer were found "similar" when similarity variables were chosen as indicated previously. In addition, it was also shown that plot of the functions representing similarity of the velocity profile in the jet and wake layer did resemble somewhat the one obtained for free jet flow or for the velocity profile in the cross-section of a two-dimensional wake.

From the above considerations it might be reasoned that the possibility may exist for deriving functional representation for the shear stress at the minimum velocity point from the classical Prandtl's (17) old and new shear stress hypothesis for free turbulent jet flow. Effects of wall shear and pressure gradient will then determine the functional relationship between the shear at velocity minimum and the parameters.

Consider Prandtl's (17) new shear stress hypothesis for free turbulent shear flow. According to this hypothesis, at any X location the turbulent stress is given by,

$$\tau(y) = \rho_c b_c U_c \frac{du}{dy} \tag{82}$$

where

$\tau(y)$ = shear stress at any y in viscous layer

b_c = characteristic length of viscous layer

U_c = characteristic velocity in viscous layer

K_1 = constant

For the jet layer the characteristic length is

$$b_c = \delta_3 - \delta_5 \tag{83A}$$

and the characteristic velocity is

$$U_c = U_{m(x)} - U_{w(x)} \tag{83B}$$

For the wake layer the characteristic length is

$$b_c = y_{2c} - \delta_3 \tag{84A}$$

and the characteristic velocity is

$$U_c = U_{e(x)} - U_{w(x)} \tag{84B}$$

The locus of the minimum velocity $U_{w(x)}$ is contained in both the jet and wake layers. Assuming that shear at the locus of the minimum velocity is proportional to the product of the four quantities given by equations (83A), (83B), (84A) and (84B), we can write the following functional representation after non-dimensionalizing,

$$\frac{\tau_{(y=\delta_3)}}{\tau_w} = F\left[\left(\frac{\delta_3-\delta_r}{\delta e}\right)\left(\frac{y_{1c}-\delta_3}{\delta e}\right)\left(\frac{U_{m(x)}-U_{w(x)}}{U_{e(x)}}\right)\left(\frac{U_{e(x)}-U_{w(x)}}{U_{e(x)}}\right)\right] \quad (85)$$

Figure (20) shows the functional relationship between the ratio of shear at minimum velocity to the wall shear and the product of parameters indicated in equation (85). Experimental data plotted in this figure are from present experiments for various conditions shown in Table 1. Ratios of the shear stresses were obtained from the indirect shear measurement from velocity profiles by numerical methods. The numerical computations were done on a computer. The least square polynomial expression for the ratio of shear stresses is given by the following expression:

$$\frac{\tau_{(\delta 3)}}{\tau_w} = 0.465(10)^5(X)^2 - 0.0438(10)^3(X) \quad (86)$$

where

$$X = \left[\left\{\frac{(\delta_3 - \delta_{5\ or\ \delta_r})}{\delta e}\right\}\left\{\frac{(y_{1c}-\delta_3)}{\delta e}\right\}\left\{\frac{U_{m(x)}-U_{w(x)}}{U_{e(x)}}\right\}\left\{\frac{U_{e(x)}-U_{w(x)}}{U_{e(x)}}\right\}\right]$$

δe = external edge of viscous flow where $\frac{u}{U_e} = 0.995$

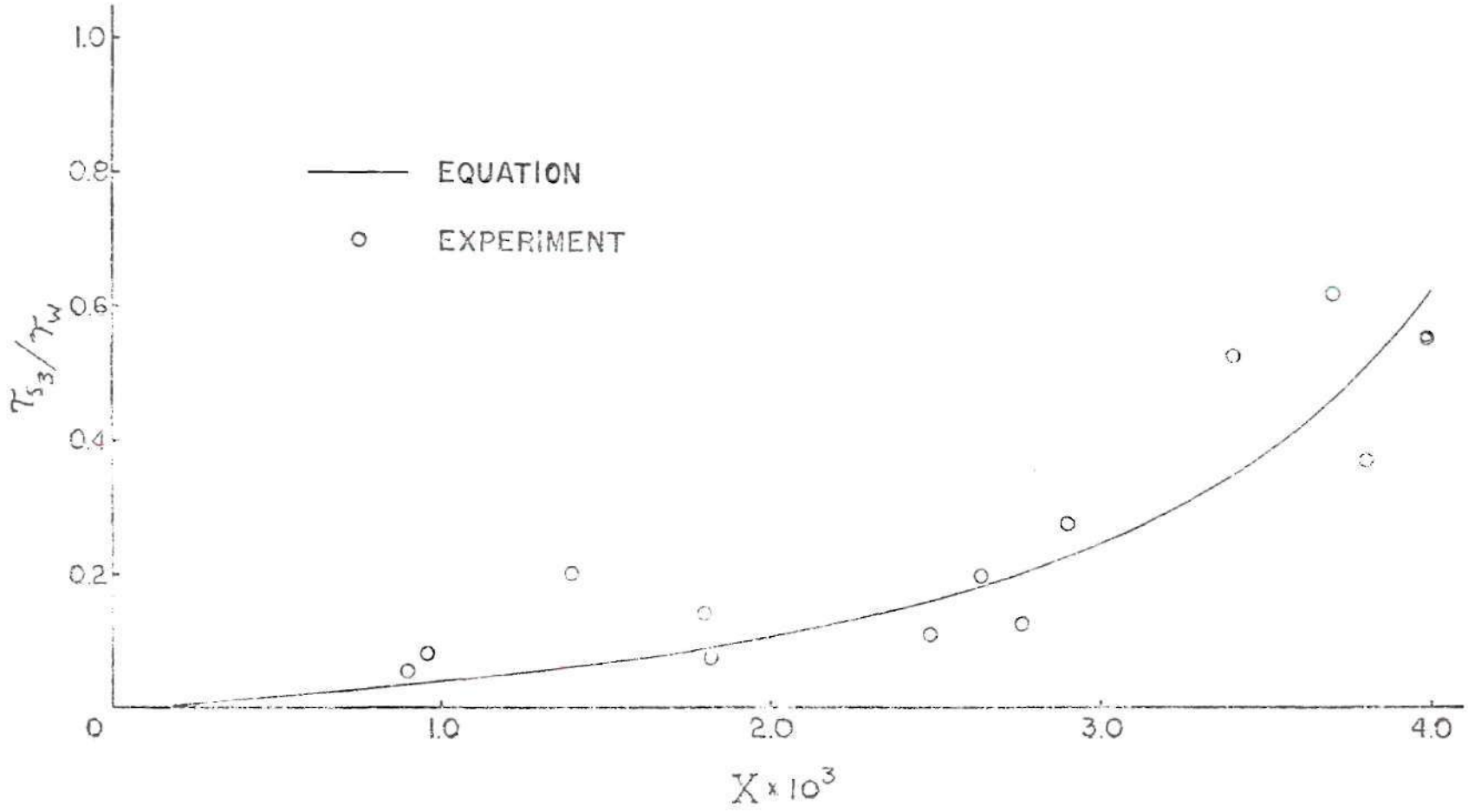

Figure 20. Parametric Relation of Shear Stress at Junction of Jet and Wake Layer

General Discussion of Other Important Wall Jet Parameters

In previous paragraphs various physical parameters were discussed and their functional relationships to the dependent variables, for example, wall layer momentum thickness, jet and wake layer thickness, velocities at the edge of wall layer $U_{m(x)}$, velocity $U_{w(x)}$ at the junction of jet and wake layers, etc. were formulated. These parameters appeared explicitly in the theoretical integral equations for the solution of quantities in various regions of the flow shown in Figure (1). Thus functional representation and relationships of these parameters to the physical flow variables is of vital importance for the confluent boundary layer flow solution. In the following paragraphs additional results of interests are discussed. For example, the knowledge of shear stress or eddy viscosity distribution discussed in the following paragraphs can be helpful in solving the confluent boundary layer problem by other approaches such as the finite difference method. Knowledge of the behavior of eddy viscosity across the viscous layer is also helpful in the study of the problem of two streams at slot exit at different temperature. In this case the temperature profile and heat transfer across the viscous layer has to be considered in addition to velocity profile. It is known that for turbulent flow, eddy diffussivity is related to eddy viscosity and local Reynolds and Prandtl number. Even an approximate variation of eddy diffussivity is helpful in the consideration of flow problems with heat transfer and temperature variation.

Shear Stress Profile

Figures (21), (22), ans (23) show plots of shear distributions in

the viscous layer from the wall to the edge of viscous region where shear stress is zero. These figures are for different initial velocity ratios at the slot exit and different pressure distributions. These curves are calculated from experimental velocity profiles and pressure distributions by numerical methods described previously. They are similar in shape and characteristics to those measured by various investigators such as Kracker and Whitelaw [4], Kruka and Eskinazi [3], and by Bradshaw and Gee [5]. The value of the shear stress changes sign in the neighborhood of the edge of the wall layer. The maximum value of the negative shear stress which is reached in the neighborhood of the wall-layer depends greatly upon whether the X location is in the initial region or main region or in the ordinary turbulent boundary layer region. The value of the negative shear stress is maximum for X locations in the initial region and progressively decreases as distance from slot exit increases. It can also be observed that the value of the shear stress in the core of the initial region remains approximately constant and near a value of zero. The value of the shear stress in the viscous layer at the junction of jet and wake layer changes in sign from negative to positive. The magnitude of this shear stress at the minimum velocity point may vary from a large positive value near slot exit to a slight negative value farther away from the slot when depression in the velocity profile is small.

Eddy Viscosity Distribution

In the case of two-dimensional. incompressible turbulent flow, we obtained the following system of differential equations for the velocity boundary layers:

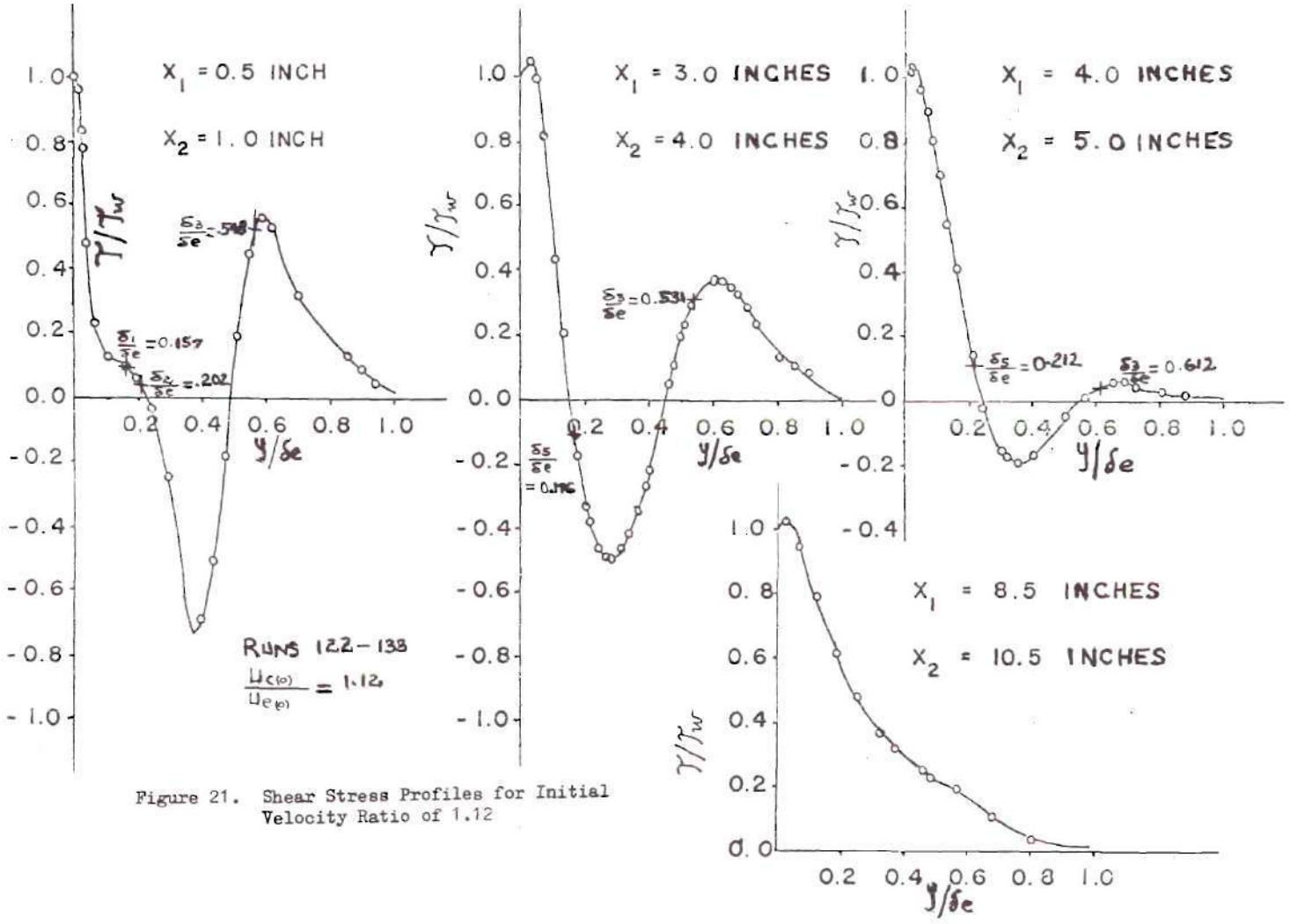

Figure 21. Shear Stress Profiles for Initial Velocity Ratio of 1.12

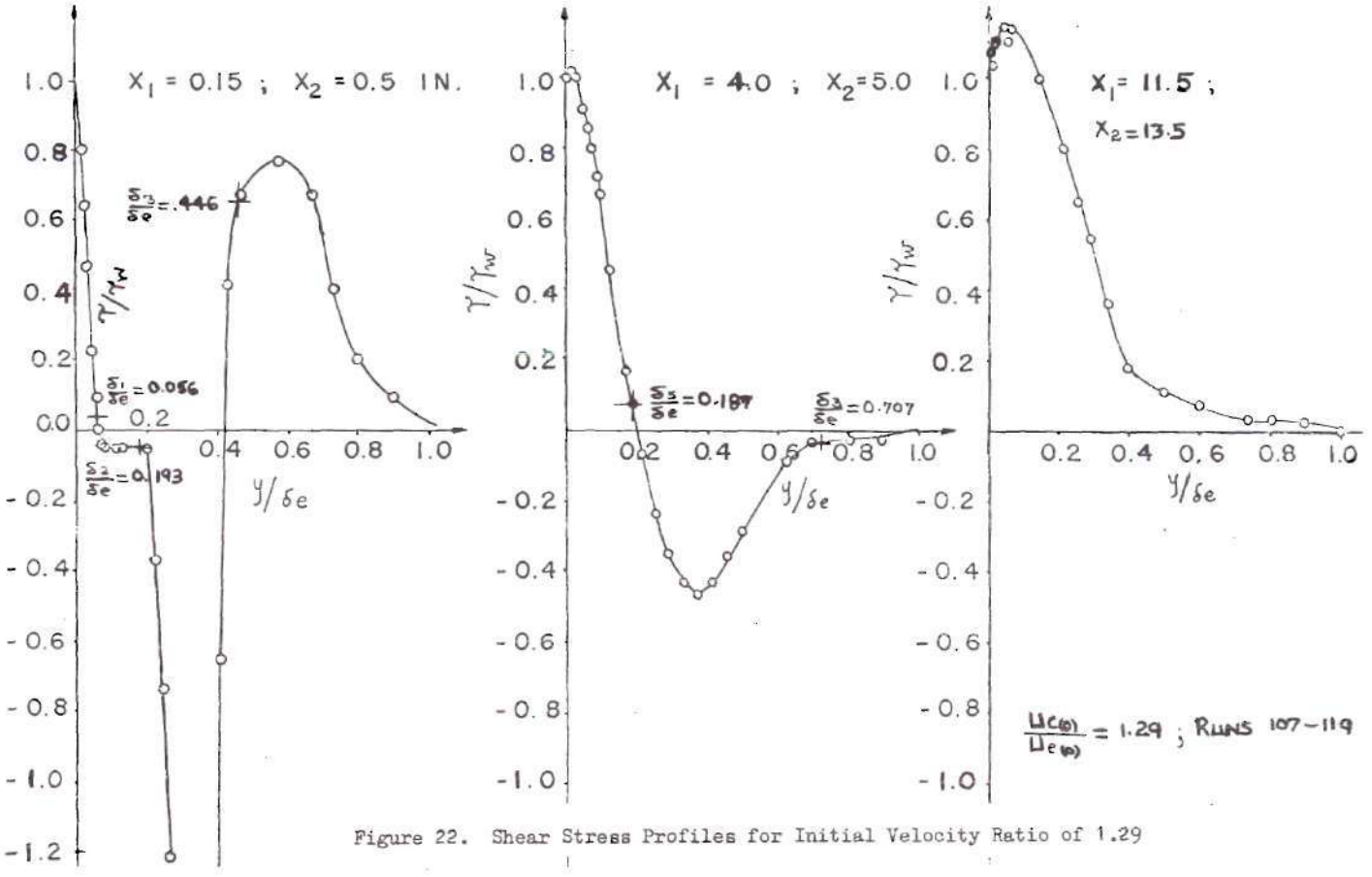

Figure 22. Shear Stress Profiles for Initial Velocity Ratio of 1.29

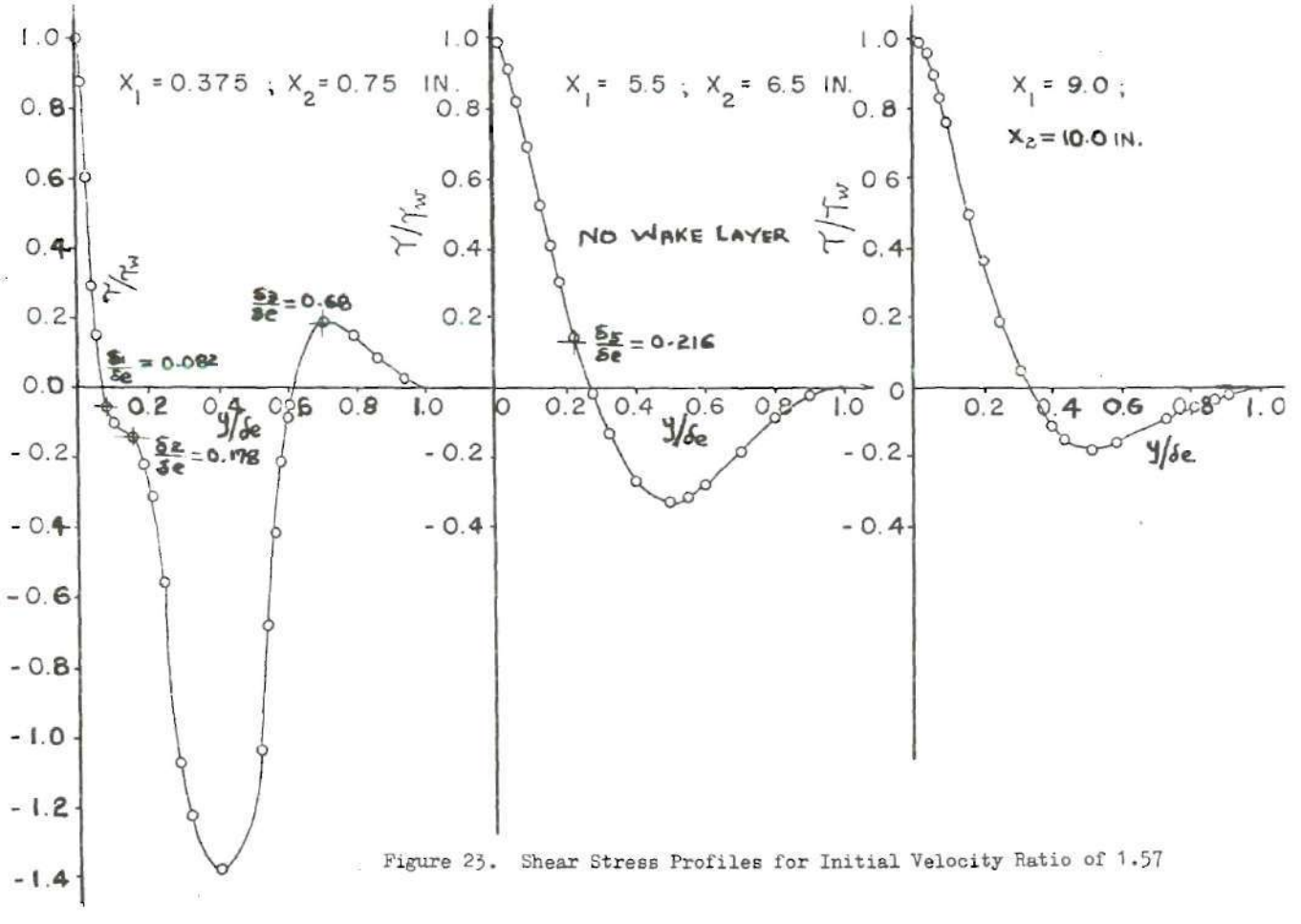

Figure 23. Shear Stress Profiles for Initial Velocity Ratio of 1.57

(87)

$$\frac{\partial \bar{u}}{\partial x} + \frac{\partial \bar{v}}{\partial y} = 0$$

$$\bar{u}\frac{\partial \bar{u}}{\partial x} + \bar{v}\frac{\partial \bar{u}}{\partial y} = -\frac{1}{\rho}\frac{d\bar{P}}{dx} + \frac{1}{\rho}\frac{\partial}{\partial y}(\bar{\tau}_{xy}) \quad .$$

In the above equation the bar above various quantities indicates time averaging. The shear stress term appearing in the above equation can be represented as the algebraic sum of the shear stress due to laminar contribution and that due to turbulent mixing. Thus,

$$\bar{\tau}_{xy} = \tau_{laminar} + \tau_{turbulent} \qquad (88)$$

$$= \rho\nu\frac{\partial \bar{u}}{\partial y} + \rho\epsilon\frac{\partial \bar{u}}{\partial y} \quad .$$

where ν is the molecular kinematic viscosity and ϵ is the eddy kinematic viscosity. This concept of representing the shear stress in turbulent flows was first due to Boussinesc [18].

According to Prandtl's mixing length theory, eddy viscosity appearing in the above equation (88) is given by,

$$\epsilon = l_1^2 \left|\frac{d\bar{u}}{dy}\right| \quad . \qquad (89)$$

where l_1 is the mixing length, the magnitude and variation of which depends on the particular type of turbulent flow and must be determined

from experimental measurements for the flow under consideration. For example, for ordinary turbulent boundary layer flow along smooth, flat plates, l_1 must vanish at the wall because the transverse motions are inhibited by its presence. Whereas, for flow along rough walls of pipes or channels the mixing length near the wall must approach a value of the same order of magnitude as the dimension of solid protusions.

According to the expression for eddy viscosity as given by equation (33), ϵ vanishes at points where $\frac{d\bar{u}}{dy}$ is zero, i.e. at points of maximum or minimum velocity. This is certainly not correct since turbulent mixing does not vanish at the maximum and minimum velocities according to experimental measurements of fluctuating turbulent velocity components. These type measurements have been performed, for example, by Reichardt [20] in channel flow, by Bradshaw [3] and by Kracker and Whitelaw [4]. This apparent discrepancy between mixing length hypothesis and experiment can be removed by assuming the following expression for eddy viscosity as suggested by Prandtl:

$$\epsilon = l_2^2 \left[\left(\frac{d\bar{u}}{dy} \right)^2 + l_3^2 \left(\frac{d^2 u}{dy^2} \right) \right]^{1/2} . \qquad (90)$$

The expression for eddy viscosity from Prandtl's new shear stress hypothesis for free jet flow is given as follows:

$$\epsilon = c_1 b_{(x)} (U m_{(x)} - U_\infty) . \qquad (91)$$

where

C_1 = constant; b = $\frac{1}{2}$ width of jet

$U_{m(x)}$ = maximum velocity at any cross-section of a jet

According to the above expression, eddy viscosity is constant at any X station and is not a function of y coordinate.

In order to formulate the expression for the eddy viscosity, Von Karman (20) assumed that the turbulent transport processes are determined by local flow conditions and that geometric similarity holds throughout the flow field. The coefficient of eddy viscosity was then derived as,

$$\epsilon = l_4^2 \frac{(d\bar{u}/dy)^2}{(d^2\bar{u}/dy^2)} \left|\frac{d\bar{u}}{dy}\right| \quad . \tag{92}$$

The above expression shows that ϵ becomes infinite at the points where $\frac{d^2\bar{u}}{dy^2} = 0$ and simultaneously $\frac{d\bar{u}}{dy} \neq 0$. This result is not very reasonable.

The above paragraphs give a brief summary of the various expressions of eddy viscosity which are formulated on the basis of mixing length hypothesis, or shear stress hypothesis or on the basis of local geometric similarity conditions in the flow field. The above expressions for eddy viscosities have been used by various investigations for formulating theory for free jets, free wakes and for predicting the growth of turbulent boundary layers on flat plates.

Eddy Viscosity Distribution for the Ordinary Turbulent Boundary Layer on a Flat Plate

It is of interest to calculate the eddy viscosity distribution across the ordinary turbulent boundary layer with zero pressure gradient. In this case the velocity profile for the entire viscous layer can be reasonably represented by a power law. For this simple turbulent boundary layer flow it is possible to derive an analytical expression for eddy viscosity distribution.

The distribution of eddy viscosity across ordinary turbulent boundary layers can be obtained with an assumed velocity profile using a momentum integral equation and a skin friction expression for the flat plate. The velocity profile for the ordinary turbulent boundary layer flow along a flat plate is normally assumed as,

$$\frac{u}{U_\infty} = \left(\frac{y}{\delta_e}\right)^{1/n} \tag{93}$$

where n can be assumed approximately constant in the absence of pressure gradient. As is well known from J. Nikuradse [21] experimental investigation for pipe flow, the value of n varies between 5 to 10 depending upon the Reynolds number.

For an incompressible boundary layer on a flat plate, the momentum equation is written as,

$$\frac{\tau_{(x,y)}}{\rho U_\infty^2} = \frac{d}{dx}\left\{\int_0^{\delta_e} \frac{u}{U_\infty}\left(1-\frac{u}{U_\infty}\right)dy\right\} + \frac{d}{dx}\left\{\int_0^{y}\left(\frac{u}{U_\infty}\right)^2 dy\right\} - \frac{u}{U_\infty}\frac{dp}{dx}\left\{\int_0^{y}\left(\frac{u}{U_\infty}\right)dy\right\} \quad . \tag{94}$$

For y = 0, the equation reduces to,

$$\frac{\tau_w}{\rho U_\infty^2} = \frac{d}{dx}\left\{\int_0^{\delta_e} \frac{u}{U_\infty}\left(1-\frac{u}{U_\infty}\right)dy\right\} \quad . \tag{95}$$

Making use of equation (93) in equations (94) and (95), the following simple expression can be obtained for the shear distribution for the flat plate ordinary turbulent boundary layer,

$$\frac{\tau_{(y)}}{\tau_w} = \left\{1 - \left(\frac{y}{\delta_e}\right)^{\frac{n+2}{n}}\right\} \tag{96}$$

where

$$\tau_{(y)} = \rho(\nu + \epsilon)\frac{dU}{dy} \quad . \tag{97}$$

Because $\frac{dU}{dy}$ at the wall as computed from equation (93) is infinite for any $n > 0$ and also because across the boundary layer $\epsilon >> \nu$, the following expression can be obtained after simplifications:

$$\frac{\tau_{(y)}}{\rho} = \frac{\epsilon}{\nu} \cdot U_\infty \cdot \left(\frac{y}{\delta_e}\right)^{1/n} \cdot \frac{\delta_e}{y} \cdot \frac{1}{\delta_e} \quad . \tag{98}$$

By making use of equations (98) and (93) in (95) we have,

$$\epsilon = \frac{\tau_w}{\rho U_\infty} \cdot \delta_e \cdot n \cdot \left[1 - \left(\frac{y}{\delta_e}\right)^{(n+2)/n}\right] \cdot \left(\frac{y}{\delta_e}\right)^{(n-1)/n} \tag{99}$$

or

$$\frac{\epsilon}{u^* \delta_e} = \frac{u^*}{U_\infty} \cdot n \cdot \left[1 - \left(\frac{y}{\delta_e}\right)^{(n+2)/2}\right] \cdot \left(\frac{y}{\delta_e}\right)^{(n-1)/n} .$$

For the power law velocity profile the exponent n in equation (93) is related to the form factor H by,

$$n = \frac{2}{H-1} \quad . \tag{100}$$

Equation (99) is obtained in terms of shape factor by use of equation (100) as,

$$\frac{\epsilon}{u^* \delta_e} = \frac{u^*}{U_\infty} \cdot \frac{2}{H-1} \cdot \left[1 - \left(\frac{y}{\delta_e}\right)^{H}\right] \cdot \left(\frac{y}{\delta_e}\right)^{(3-H)/2} . \tag{101}$$

Figure (24) shows the distribution of eddy viscosity across an ordinary turbulent boundary layer along a flat plate. Experimental data shown in this figure were obtained from measurements by Klebanoff [22] for $u^*/U_\infty = .037$ and by Townsend [23] for $u^*/U_\infty = .044$. For an average value of $u^*/U_\infty = .04$, a value for the shape factor of 1.4 is obtained from a plot of experimental data of H vs $\frac{U_\infty}{u^*}$, taken by Hama [24]. Figure (24) also shows a plot of eddy viscosity distribution calculated from equation (101). In calculating the eddy viscosity distribution by equation (101), the values of H = 1.4 and $\frac{u^*}{U_\infty} = 0.04$ were used so as to approximately correspond to the conditions at which measurements were obtained.

It can be seen from this comparison that the maximum value of the eddy diffussivity in the boundary layer is predicted fairly well by equation (101). Equation (101) predicts also the trends of the distribution of eddy viscosity quite well although there is a shift in the predicted values compared to experiments. An important reason for the shift of the predicted values lies in the assumption of power law velocity profiles implied by equation (93).

Ratio of ϵ_H/ϵ for Flat Plate Ordinary Turbulent Boundary Layer

It is desirable to obtain an expression for the average value of the ratio ϵ_H/ϵ across the flat plate turbulent boundary layer. ϵ_H is the eddy diffussivity for heat. An expression for the average value of ϵ_H/ϵ for this simple turbulent flow may be useful in making appropriate assumptions for more complicated wall jet flows.

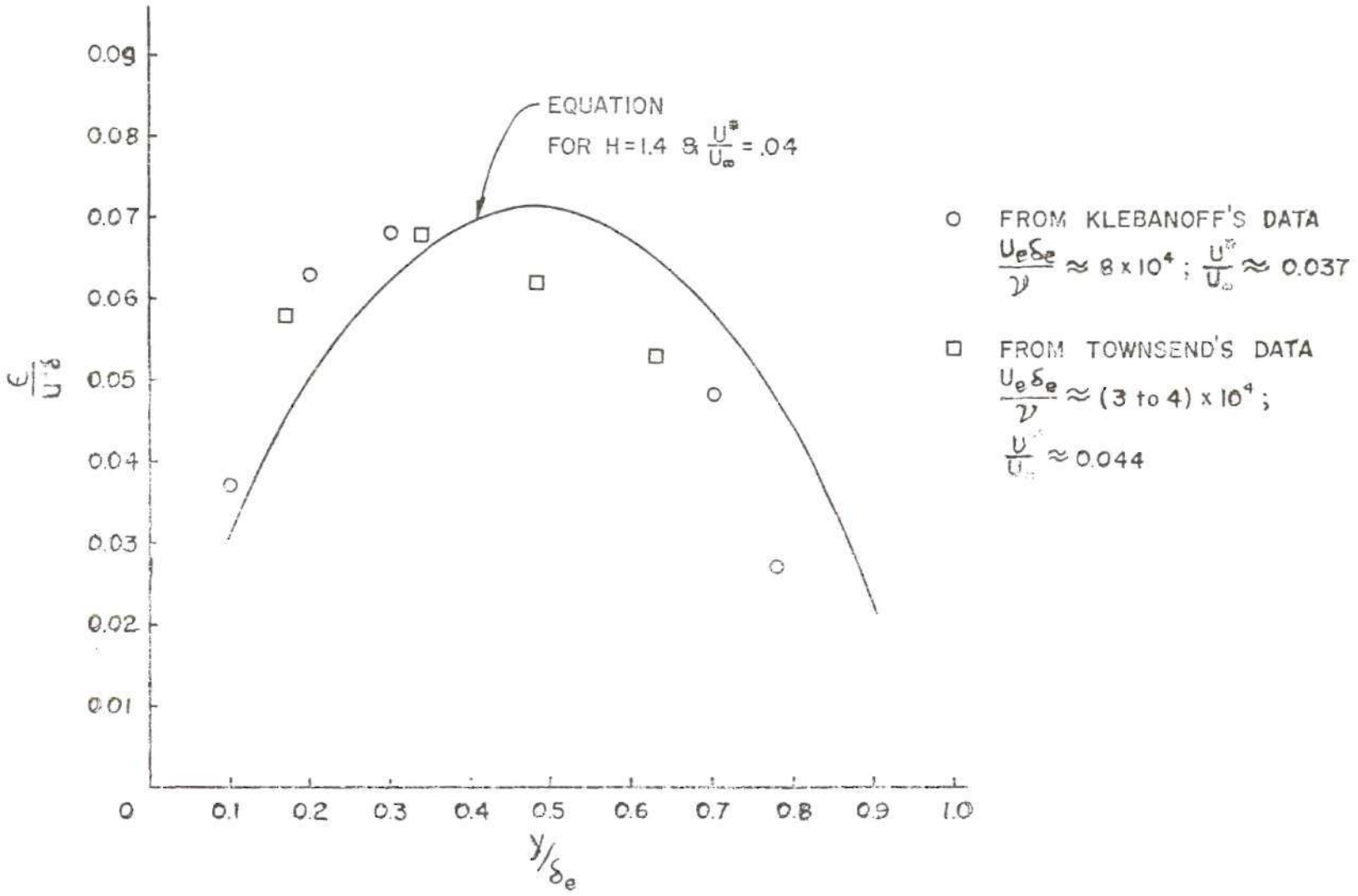

Figure 24. Comparison of Predicted and Measured Eddy Viscosity Distribution on an Ordinary Turbulent Boundary Layer with Zero Pressure Gradient

The Stanton number, St , is defined as

$$St = \frac{Nu}{Re_x Pr} = \frac{\bar{h}}{\rho U_\infty \bar{C_p}} \tag{102}$$

where

Nu = Nusselt's number = $\frac{\bar{h}x}{k}$

$Re_x = \frac{U_\infty x}{\nu}$

Pr = Prandtl number = $\frac{\mu \bar{C_p}}{k}$

$\bar{C_p}$ = constant pressure specific heat

$\bar{h}$ = heat transfer coefficient

The heat transfer at wall, q_w , is defined as,

$$q_w = \bar{h}(t - t_\infty) = St(t_w - t_\infty)\rho U_\infty \bar{C_p} \,. \tag{103}$$

For air the Prandtl number is approximately equal to 0.723. Reference (15), p. 497, shows that for turbulent boundary layer flow on a flat plate for Prandtl number near one the following expression for Nusselt's number is valid:

$$Nu = \frac{1}{2} \cdot \frac{\tau_w}{\frac{1}{2}\rho U_\infty^2} \cdot Re_x \cdot (Pr)^{1/3} \tag{104}$$

$$= \frac{u^{*2}}{U_\infty^2} \cdot Re_x \cdot (Pr)^{1/3}$$

where u^* = friction velocity.

Neglecting the molecular diffussivity for heat as small compared to eddy diffussivity for heat and also neglecting kinematic viscosity as small compared to eddy viscosity, the local heat transfer and local shear in boundary layer can be approximately written as follows:

$$\frac{q_{t(y)}}{\rho C_{\bar{p}}} = -(\alpha + \epsilon_H)\frac{\partial t}{\partial y} \approx -\epsilon_H \frac{\partial t}{\partial y} \quad . \tag{105}$$

and

$$\frac{\tau_{(y)}}{\rho} = (\nu + \epsilon)\frac{\partial u}{\partial y} \approx \epsilon \frac{\partial u}{\partial y} \quad . \tag{106}$$

The ratio, ϵ_H/ϵ , thus can be written from the above two equations as,

$$\frac{\epsilon_H}{\epsilon} = -\frac{1}{C_{\bar{p}}} \cdot \frac{q_{t(y)}}{\tau_{(y)}} \cdot \frac{\partial u/\partial y}{\partial t/\partial y} \quad . \tag{107}$$

According to Prandtl, the ratio of local heat transfer in the boundary layer to local shear stress in the boundary layer for the flat

plate remains constant. Thus we can write

$$\frac{q_{(y)}}{\tau_{(y)}} = \frac{q_w}{\tau_w} = \text{Constant across boundary-layer} \qquad (108)$$

or

$$\frac{q_{(y)}}{\tau_{(y)}} = \frac{S_t (t_w - t_\infty) \rho U_\infty C_p}{Re_x \cdot Pr \cdot u^{*2} \cdot \rho} \quad .$$

The temperature profile for the flat plate boundary layer, as evidenced from various experimental data, are similar and similarity can be expressed by a power law. Thus,

$$\frac{t_w - t_{(y)}}{t_w - t_\infty} = \left(\frac{y}{\delta_T}\right)^{1/m_1} \quad . \qquad (109)$$

where

δ_T = thermal boundary layer thickness

t_∞ = temperature at the edge of thermal boundary layer.

The expression for local temperature slope within boundary layer by the use of equation (109) is given by,

$$\frac{\partial t}{\partial y} = -\frac{1}{m_1} \cdot (t_w - t_\infty) \cdot \frac{1}{\delta_T} \left(\frac{y}{\delta_T}\right)^{(1-m_1)/m_1} \quad . \qquad (110)$$

For power law velocity profile for flat plate turbulent boundary layer the local velocity slope within the boundary layer is given by,

$$\left(\frac{u}{U_\infty}\right) = \left(\frac{y}{\delta}\right)^{1/m_2} \tag{111}$$

$$\frac{\partial u}{\partial y} = \frac{U_\infty}{m_2}\,\frac{1}{\delta}\left(\frac{y}{\delta}\right)^{(1-m_2)/m_2}$$

where

δ = velocity boundary layer thickness.

According to Rubesin [25] for turbulent boundary layers on flat plates with constant wall temperature, the ratio of thermal boundary layer thickness to hydrodynamic boundary layer thickness is given by

$$\frac{\delta_T}{\delta} = (P_r)^{-\frac{7}{12}} . \tag{112}$$

All of the above relations can be substituted in equation (107) for the ratio of ϵ_H/ϵ and after simplifications the following equation can be derived,

$$\frac{\epsilon_H}{\epsilon} = -\frac{1}{c_p}\cdot\left\{\frac{q(y)}{\tau(y)}\right\}\cdot\left\{\frac{\partial u/\partial y}{\partial t/\partial y}\right\} \tag{113}$$

$$= \frac{m_1}{m_2}(P_r)^{\left\{-\frac{2}{3}-\frac{7}{12}\cdot\frac{1}{m_1}\right\}}\cdot(y/\delta)^{\left\{\frac{1}{m_2}-\frac{1}{m_1}\right\}}$$

where

m_1 = exponent for power law temperature profile for flat plate

m_2 = exponent for power law velocity profile for flat plate turbulent boundary layer

δ = hydrodynamic boundary layer thickness.

Experimental data for temperature and velocity profile for flat plate turbulent boundary layer indicate that the exponent $m_1 (\approx 7)$ is slightly larger than $m_2 (\approx 5.6)$. If both m_1 and m_2 are assumed to be the same then the ratio ϵ_H/ϵ ceases to be function of y as indicated by equation (113). If also m_1 and m_2 are assumed equal then the ratio of eddy diffussivity for heat and eddy viscosity, ϵ_H/ϵ, becomes approximately equal to the Prandtl number raised to a power of -0.8.

Eddy Viscosity Distribution for Confluent Boundary Layer Flow

As discussed previously, it was possible to derive an analytical expression for the eddy viscosity distribution across an ordinary turbulent boundary layer on the flat plate with zero pressure gradient. This was possible because the visocity profile across most of the viscous layer can be reasonably represented by a power law velocity profile and, in addition, the pressure gradient term is absent from the momentum equation. In the case of confluent boundary layer flow with pressure gradient, i.e. the viscous flow shown in Figure (1), the shape of the velocity profile is very complex and hence the velocity profile cannot be adequately described by a simple expression for the entire viscous layer. It was for this reason that the flow field was divided into various layers, across which either similarity or a one parameter family of velocity profiles was sought.

The shear stress at any point in the viscous layer, according to Boussinesc's hypothesis, can be represented as an algebraic sum of laminar and turbulent contributions. Thus,

$$\tau = \tau_{laminar} + \tau_{turubulent} = \rho\nu\frac{du}{dy} + \rho\epsilon\frac{du}{dy}$$

or

$$\frac{\epsilon}{\nu} = \frac{\tau_w(\tau/\tau_w)}{\rho\nu\frac{du}{dy}} - 1 \qquad (114)$$

where

ϵ = eddy viscosity

ν = kinematic viscosity

τ_w = wall shear stress

τ = shear stress at a point in viscous layer.

Wall shear stress, τ_w, and shear stress distribution, $\frac{\tau}{\tau_w}$, are calculated from experimental velocity profiles and pressure distributions by the numerical methods described in the section on data reduction. Figures (25), (26) and (27) show plots of eddy viscosity distributions in the viscous layer from the wall to the edge of the viscous layer where shear stress is zero. The eddy viscosity distribution curves in these figures are for different velocity ratios and different pressure distributions. Each figure contains eddy viscosity distributions for

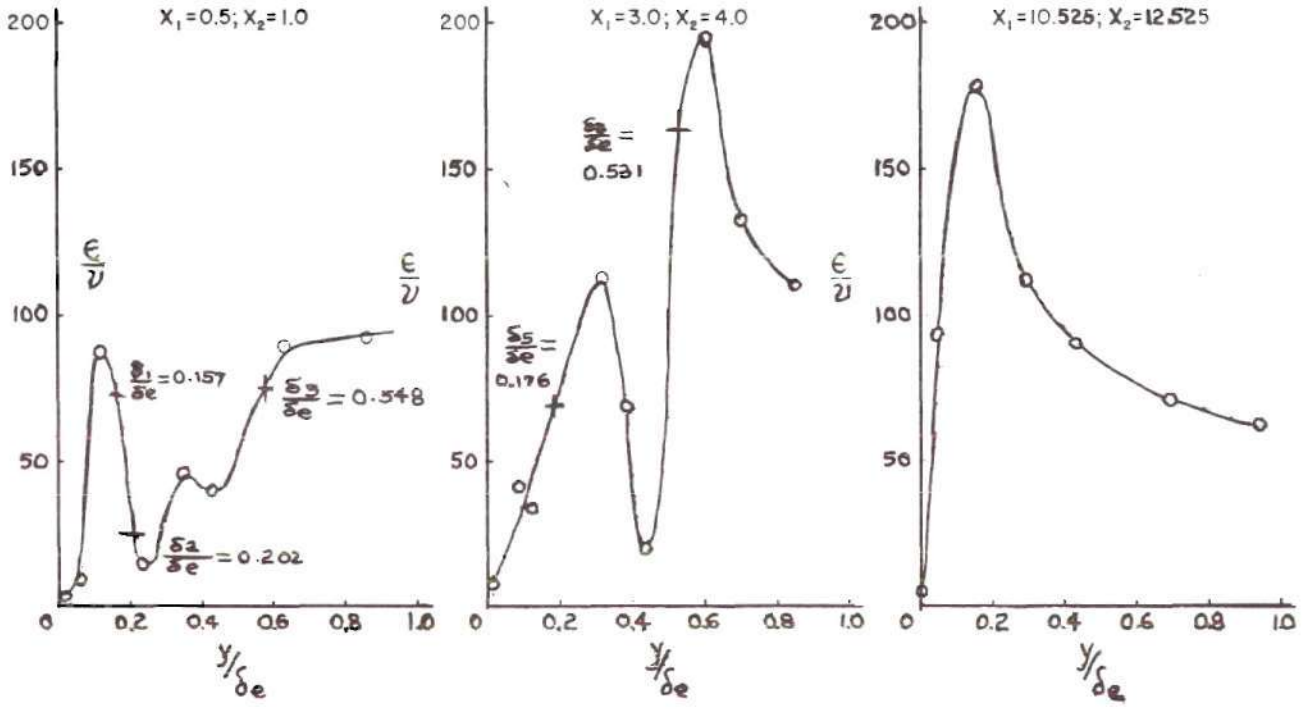

Figure 25. Eddy Viscosity Distribution for the Initial Velocity Ratio of 1.12

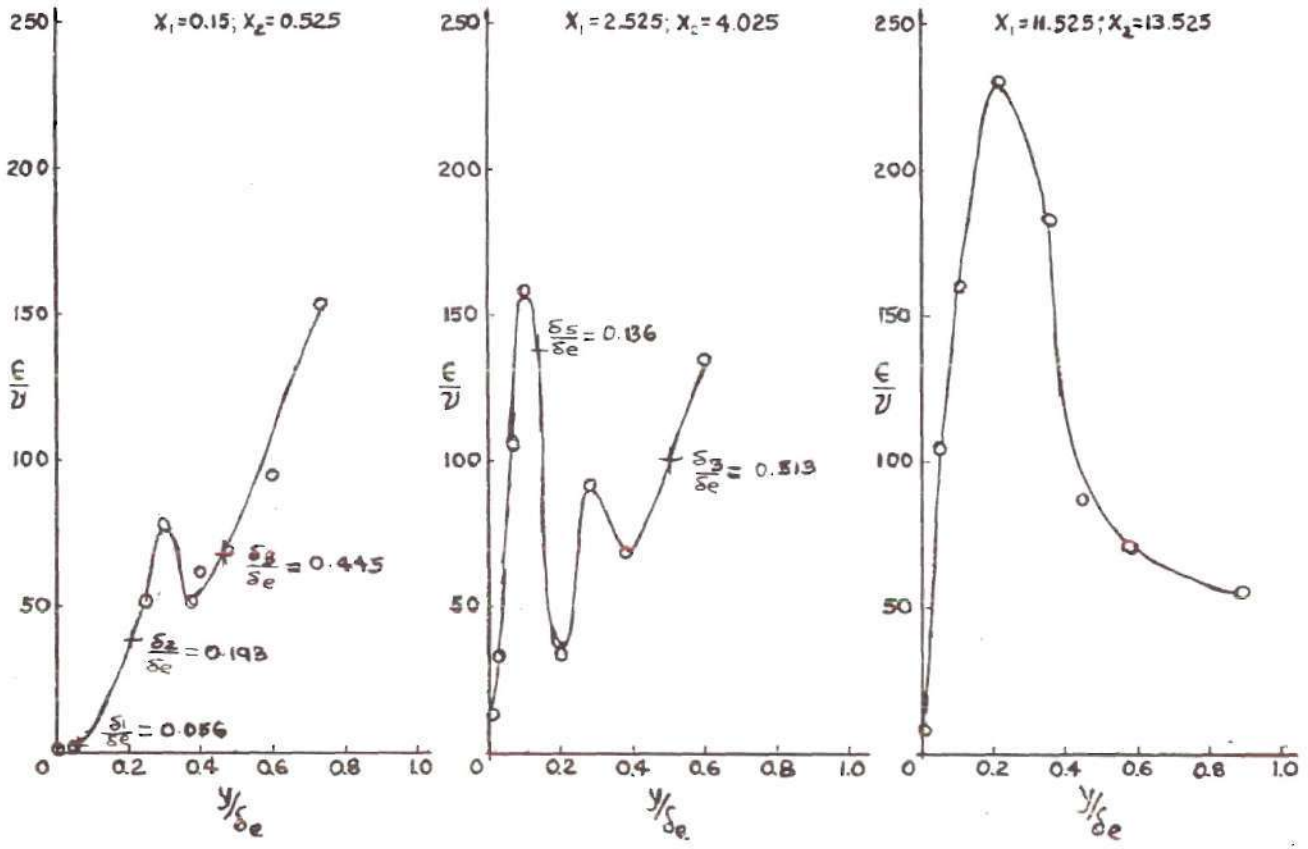

Figure 26. Eddy Viscosity Distribution for the Initial Velocity Ratio of 1.29

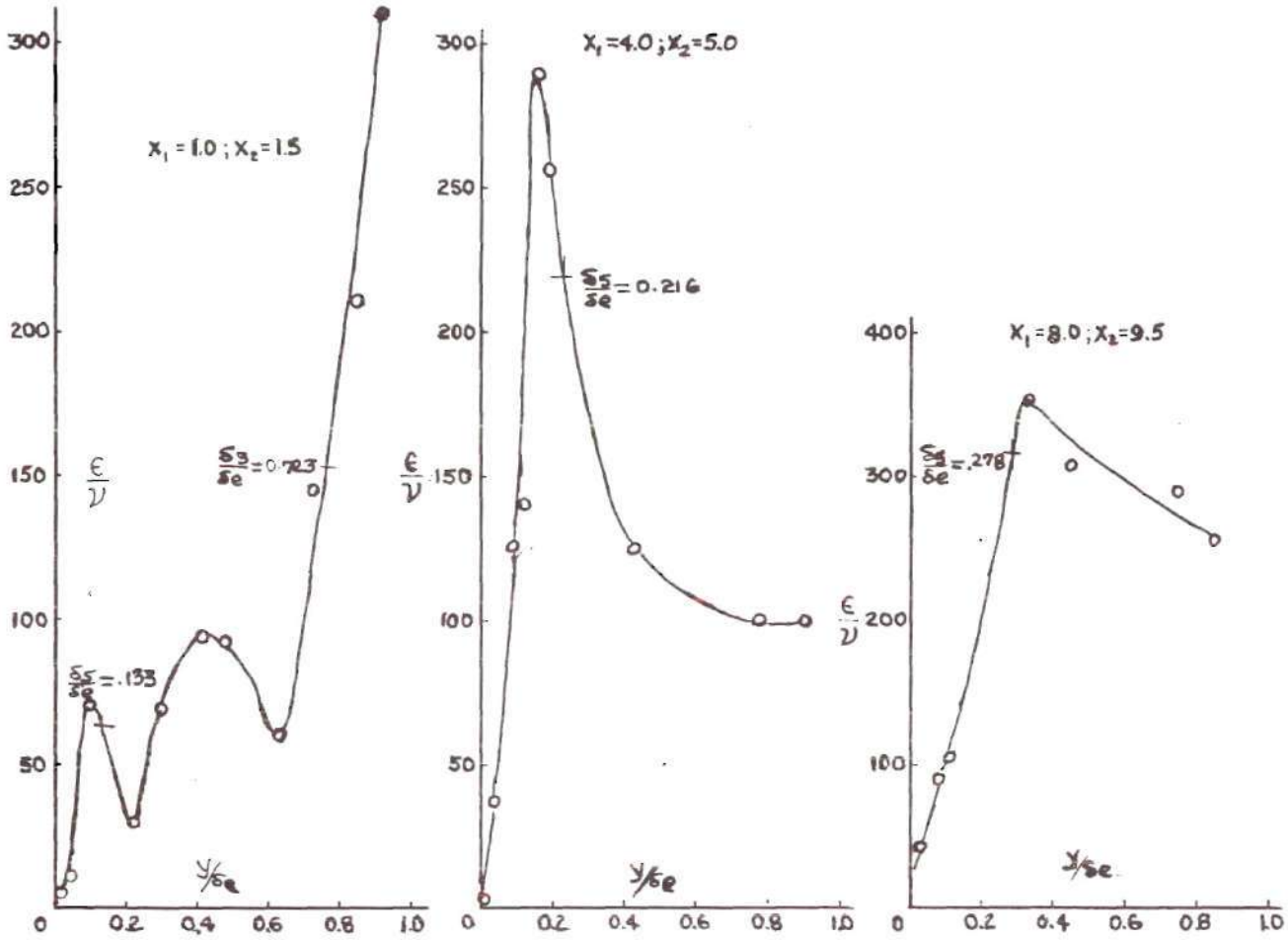

Figure 27. Eddy Viscosity Distributions for the Initial Velocity Ratio of 1.67

three different X locations. Some important observations can be made from these curves. The maximum value of the eddy viscosity ratio ϵ/ν increases as distance from the slot exit increases. The maximum value of eddy viscosity also increases as the ratio of velocities $\frac{U_{c(o)}}{U_{e(o)}}$ increases. In the ordinary turbulent boundary layer region, for example, at $X \approx 11.50$ and $X \approx 12.50$ in Figures (24) and (25), respectively, only one maximum value of ratio ϵ/ν exists. Nearer the wall, in the initial or main regions, the eddy viscosity distribution has more than one maximum or minimum and maxima and minima occur at the junction of various layers. The ratio of eddy viscosity, ϵ/ν, varies from a value of 100 to approximately 350, depending upon X location, slot exit velocity ratio, and pressure distribution. These large values of eddy viscosity ratios indicate that diffusion of mass and momentum due to turbulent fluctuations is much larger than that caused by molecular action.

Skin Friction for Wall Jet in an External Stream and Zero Pressure Gradient

For the ordinary turbulent boundary layer along a smooth flat plate experimental data obtained by Ludwig-Tillman [26], Schubauer and Klebanoff [27], Klebanoff and Diehl [28], Schultz-Grunow [29], Alan and Cutland [30] and many others are available. Attempts have been made to represent the results of the measurements made by the above investigators with reference to the "constant-stress" wall region by an expression of the form

$$\frac{u}{u^*} = A \ln \frac{u^* y}{\nu} + B \tag{115}$$

where

u^* = Friction velocity

$= (\tau_w/\rho)^{1/2}$

and A and B are constant.

In the case of an ordinary turbulent boundary layer on a flat plate various investigators recommend different values of A and B in the above equation in order to correlate their data. For example, Clauser [31] suggests values of A = 2.44 and B = 4.9. Townsend [33] remarked that many of the observed data seem to indicate a value of B nearer 7 than 4.9. Opinion, however, about the value of the constant A are less divergent. In earlier investigations a value of A = 2.5, based upon experiments by Nikuradse on pipe flow, was usually accepted. This becomes especially apparent from Rotta's [34] theory on velocity distribution close to the wall. For large values of $\frac{u^* y}{\nu}$, Rotta derived the following equation using Prandl's mixing length hypothesis in the transition region between the laminar-sublayer and completely turbulent flow:

$$\frac{u}{u^*} = A \ln \frac{u^* y}{\nu} + A\left(\ln \frac{4}{A} - 1\right) + \frac{u^* \delta_2}{\nu} \tag{116}$$

where

δ_l = thickness of laminar sublayer.

From a comparison of equations (115) and (116), the constant B can be written as,

$$B = A\left(\ln \frac{\delta}{A} - 1\right) + \frac{u^* \delta_l}{\nu} \tag{117}$$

For ordinary turbulent boundary layers without pressure gradient, Rotta assumed values of A = 2.5 and $\frac{u^* \delta_l}{\nu}$ = 6.7 on the basis of Nikuradse's [35] experiment. In that case the value of B = 5.37. On the other hand, Nikuradse himself suggested a value of $\frac{u^* \delta_l}{\nu}$ = 5 to characterize the average thickness of the laminar sublayer. This would yield, with A = 2.5, a value of B = 3.68 from equation (117). On the basis of the above discussion it is seen that in the case of ordinary turbulent boundary layer on flat plates or in pipe flow, the value of A = 2.5 but the value of B varies approximately from 3.5 to 7 depending upon the assumed thickness of the laminar sublayer.

In order to obtain values of wall shear stress for wall jet flow with an external stream but without pressure gradient, the "law of the wall" given by equation (115) can be used in conjunction with the mean measured velocity distribution in the wall layer of Figure (1). This can be done by plotting the mean velocity profiles in the wall layer on the coordinates proposed by Clauser [32]. The law of the wall equation (115) can be rearranged as follows for construction of constant shear-stress lines on the Clauser chart:

$$\frac{u}{\sqrt{\tau_w/\rho}} = A \ln\left\{\sqrt{\frac{\tau_w}{\rho U_e^2}}\ \frac{U_e y}{\nu}\right\} + B$$

$$\therefore \frac{u}{U_e} = \sqrt{\frac{\tau_w}{\rho U_e^2}} A_1 \ln\left\{\sqrt{\frac{\tau_w}{\rho U_e^2}}\ \frac{U_e y}{\nu}\right\} + \sqrt{\frac{\tau_w}{\rho U_e^2}} B_1$$

or

$$\frac{u}{U_e} = \sqrt{\frac{C_{f(e)}}{2}}\ A_1 \ln\left\{\sqrt{\frac{C_{f(e)}}{2}}\ \frac{U_e y}{\nu}\right\} + \sqrt{\frac{C_{f(e)}}{2}} B_1 \quad (118)$$

If the velocity in the wall layer is non-dimensionalized with respect to velocity U_m at the junction of wall and jet layers, rather than free stream velocity, the following equation results.

$$\frac{u}{U_m} = \sqrt{\frac{\tau_w}{\rho U_m^2}}\ A_2 \ln\left\{\sqrt{\frac{\tau_w}{\rho U_m^2}}\ \frac{U_m y}{\nu}\right\} + \sqrt{\frac{\tau_w}{\rho U_m^2}} B_2$$

or

$$\frac{u}{U_m} = \sqrt{\frac{C_f}{2}}\ A_2 \ln\left\{\sqrt{\frac{C_f}{2}}\ \frac{U_m y}{\nu}\right\} + \sqrt{\frac{C_f}{2}} B_2 \quad (119)$$

In equations (118) and (119) the following nomenclature is used:

$$C_{f(e)} = \frac{\tau_w}{1/2 \rho U_e^2} \quad ; \quad C_f = \frac{\tau_w}{1/2 \rho U_m^2} \tag{120}$$

U_m = velocity at the edge of wall layer

U_e = external edge velocity. In the case considered it is equal to freestream velocity as pressure gradient is equal to zero.

A_1 & B_1 are constants in equation (118) when velocity and wall shear stress are non-dimensionalized with respect to U_e.

A_2 & B_2 are constants in equation (119) when velocity and wall shear stress are non-dimensionalized with respect to U_m.

Kaker and Whitelaw (4) represented mean velocity profiles for the wall jet with an external stream on the Clauser chart using values of $A_1 = 2.39$ and $B_1 = 5.45$ in equation (118). These values of the constants were recommended by Patel (36). However, better representation of the mean velocity measurements under the present investigation is obtained when values of $A_1 = 2.55$ and $B_1 = 3.02$ are chosen. Figures (28) and (29) show lines of constant shear stress obtained from equation (118) with the above values of A_1 and B_1. Also plotted in the above figures are measured values of mean velocity at various distances from slot exit for two cases, namely, for $\frac{U_{c(o)}}{U_{e(o)}} = 1.58$ and $\frac{U_{c(o)}}{U_{e(o)}} = 3.2$.

In situations where free stream velocity is zero, or very small compared to the slot exit velocity, non-dimensionalizing mean velocity and shear stress with respect to U_e is of little value. Under these

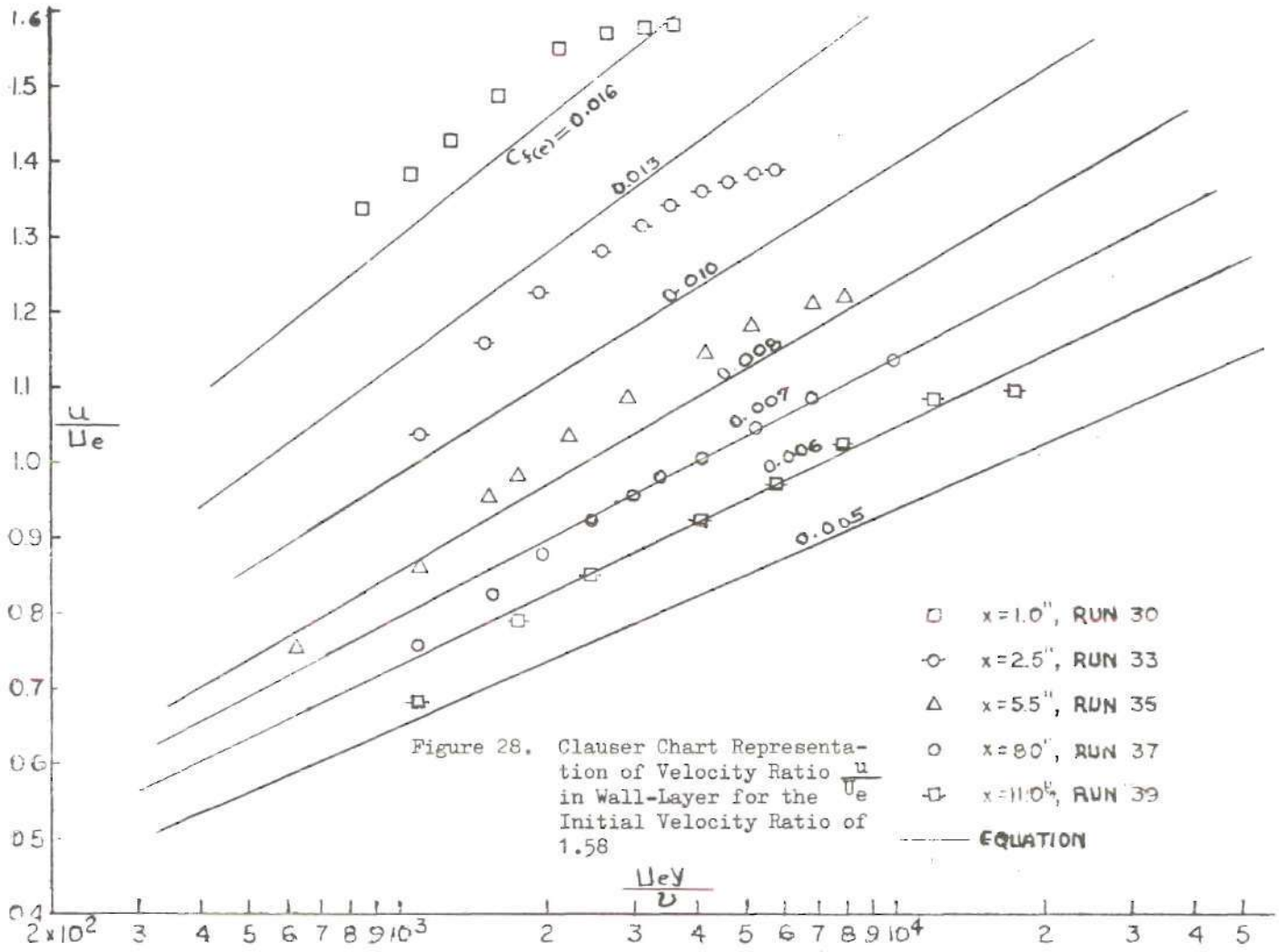

Figure 28. Clauser Chart Representation of Velocity Ratio $\frac{u}{U_e}$ in Wall-Layer for the Initial Velocity Ratio of 1.58

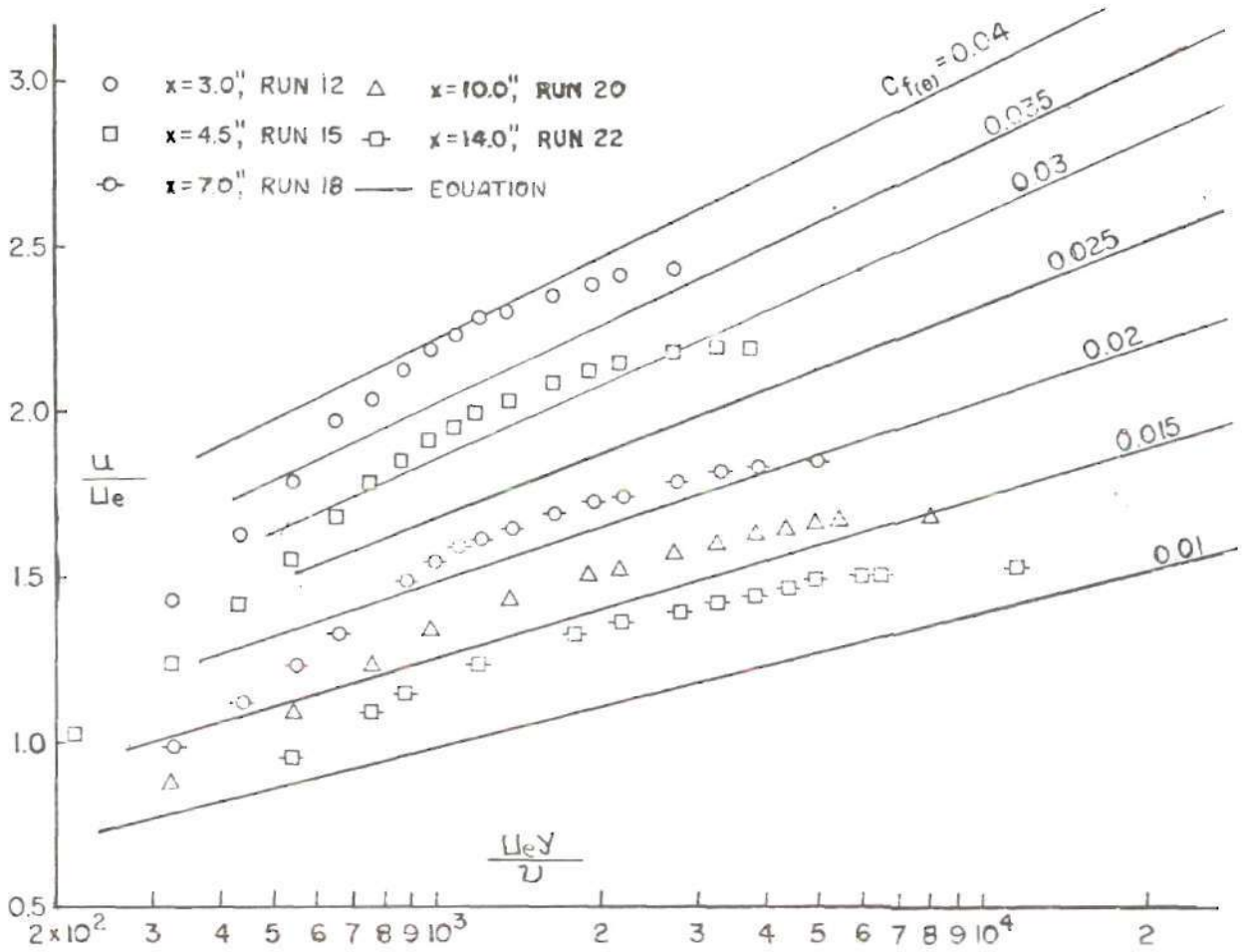

Figure 29. Clauser Chart Representation of Velocity Ratio $\frac{u}{U_e}$ in Wall-Layer for Initial Velocity Ratio of 3.2

circumstances it would be quite desirable to non-dimensionalize the wall layer velocity and wall shear with respect to the velocity U_m. This is done in Figure (30) for $\frac{U_{c(o)}}{U_{e(o)}} = 1.58$. In constructing Figure (30) use was made of the peak velocity decay curve shown in Figure (31). Figure (31) shows the decay of velocity U_m with distance X from slot exit for two velocity ratios $\frac{U_{c(o)}}{U_{e(o)}} = 1.58$ and $\frac{U_{c(o)}}{U_{e(o)}} = 3.2$. Thus when the mean velocity profiles in the wall layer are represented on Clauser charts and mean velocity and wall shear are non-dimensionalized with respect to U_m, the present study indicates values of $A_2 = 2.68$ and $B_2 = 2.04$ in equation (119).

Figure (32) shows comparisons of wall skin friction at various distances from slot exit by the various methods for a value of velocity ratio at slot exit, $\frac{U_{c(o)}}{}$, of approximately 1.58 and zero pressure gradient. In this figure the local skin friction is given from Bradshaw's (5) skin friction formula, Sigalla's (37) skin friction formula, values obtained from Clauser's chart. Figure (29), and from the present indirect numerical method. Bradshaw and Sigalla measured the local skin friction by means of a Preston tube in a wall jet flow without external stream at large distances from slot exit and recommended the following expressions:

Bradshaw's skin friction formula:

$$\frac{\tau_w}{\frac{1}{2}\rho U_m^2} = 0.0315 \left[\frac{U_m \delta_5}{\nu} \right]^{-0.182} \qquad (121)$$

and

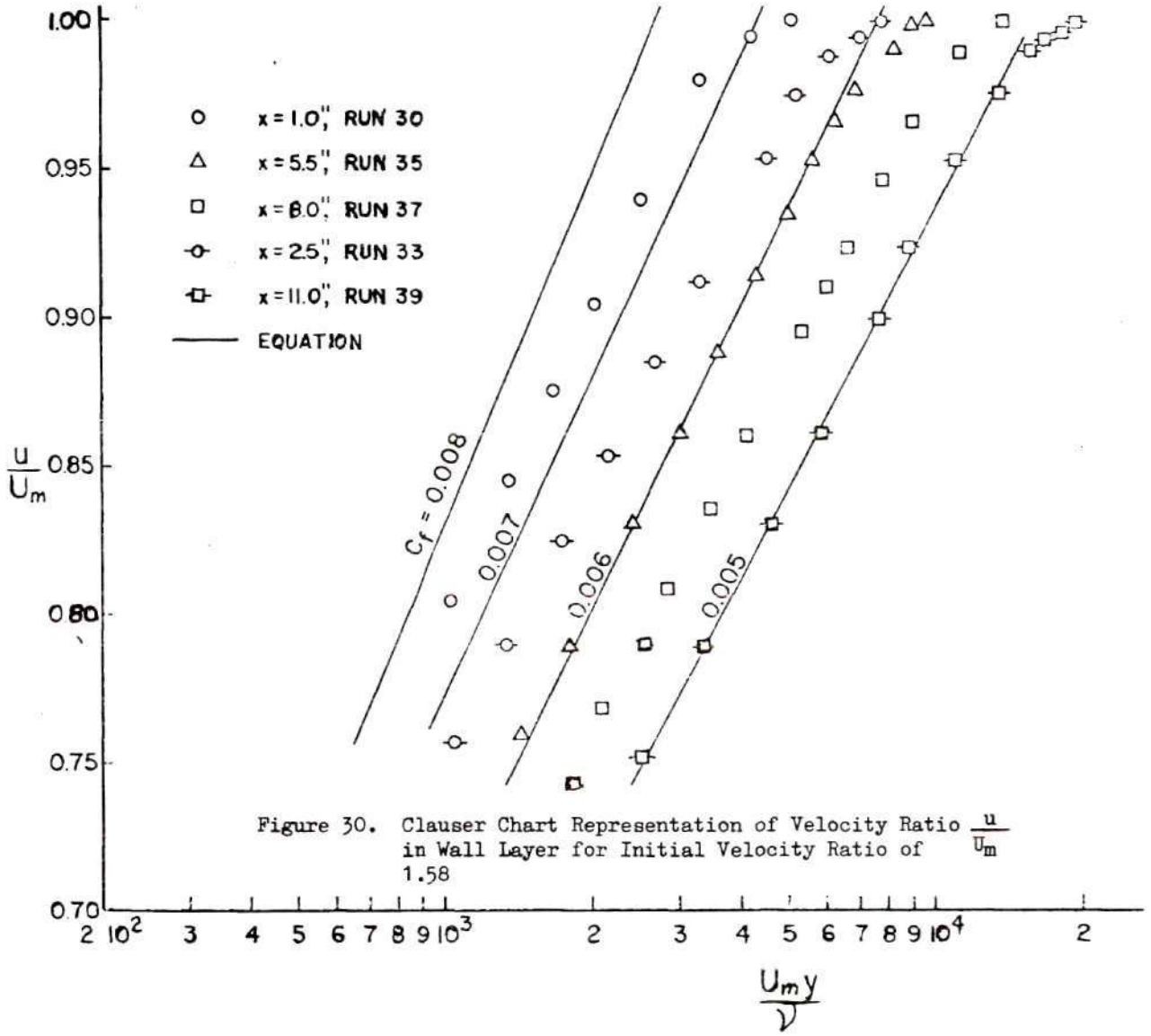

Figure 30. Clauser Chart Representation of Velocity Ratio $\frac{u}{U_m}$ in Wall Layer for Initial Velocity Ratio of 1.58

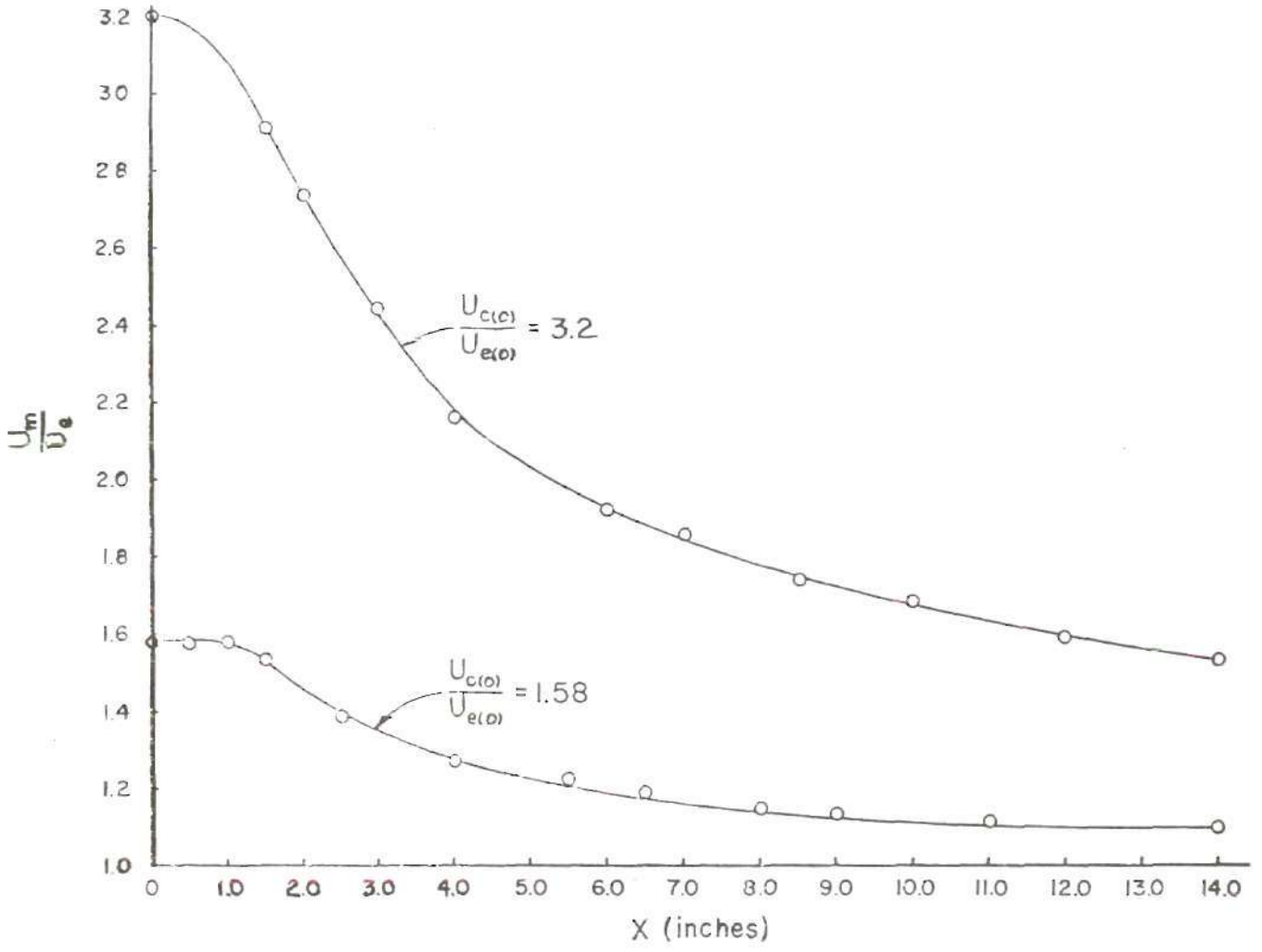

Figure 31. Decay of Peak Velocity in Wall Jet Boundary Layer in Absence of Pressure Gradient

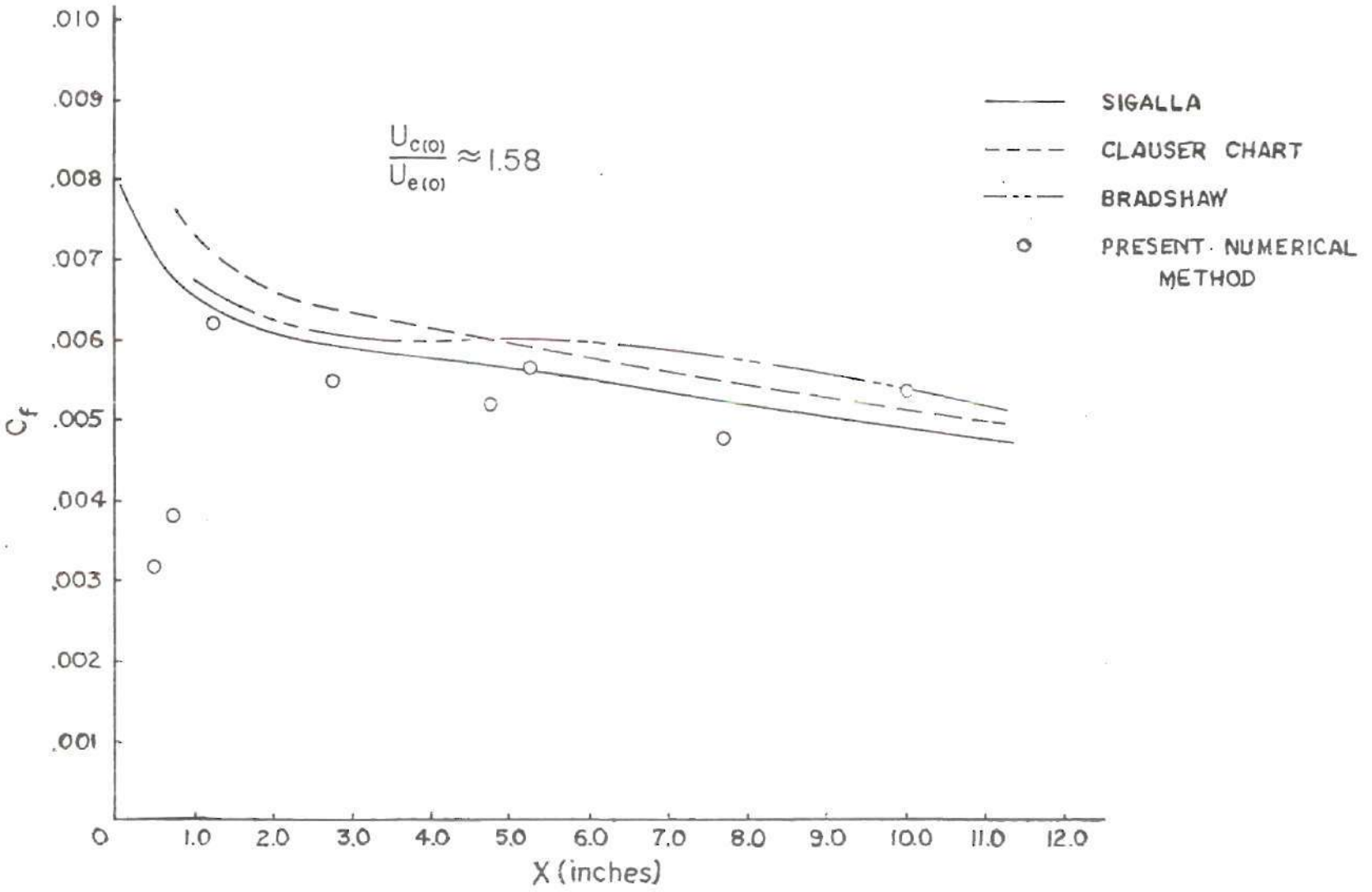

Figure 32. Comparison of Skin Friction Coefficient

Sigalla's skin friction formula:

$$\frac{\tau_w}{\frac{1}{2}\rho U_m^2} = 0.0565\left[\frac{U_m \delta_s}{\nu}\right]^{-0.25} \qquad (122)$$

where

δ_s = thickness of wall layer.

It can be seen from the results shown in Figure (32) that all four methods are in relatively good agreement, with maximum variations of approximately $\pm$ 6% from average values. Near the slot exit, however, the present numerical method deviates from the other methods. In this connection it can be pointed out that expression for skin friction derived by Bradshaw and Sigalla are based on measurements at large distances from slot exit and thus in this area the present indirect skin friction calculations may be more reliable.

Shear Integral for the Confluent Boundary Layer with Zero Pressure Gradient

For the case of zero pressure gradient and for slot exit velocity ratio, $1.50 \leq \frac{U_{c(o)}}{U_{e(o)}} \leq 3.2$, the length of the initial region is less than 10 slot heights and the wake layer occurs for less than 7 slot heights. Moreover, even for distances from slot exit of less than 7 slot heights, the shear dissipation under the above conditions is small for the wake layer as compared to the wall and jet layers. For these reasons, the shear integral for the jet and wall layers only are considered in the following discussions.

Shear work at any point in the viscous layer is equal to $(\tau \frac{\partial u}{\partial y})\, dy$ and the integral of this quantity, across an individual layer or the entire viscous layer, represents shear work for the considered layer or the shear work for the entire viscous layer, respectively. Thus $\int_0^{\delta_2} \tau \frac{\partial u}{\partial y} dy$ represents shear work for the wall layer, $\int_{\delta_3}^{\delta_4} \tau \frac{\partial u}{\partial y} dy$ represents the shear work for the jet layer and $\int_0^{\delta_4} \tau \frac{\partial u}{\partial y} dy$ represents the shear work for the entire viscous layer. These integrals occur in the dissipation energy integral equations. For example, the shear work integral, $\int_0^{\delta_5} \frac{\tau}{\rho U_m^2} \frac{\partial}{\partial y}(\frac{u}{U_m}) dy$, occurs in the dissipation energy integral equation for the wall layer.

For the case of zero pressure gradient, it is of interest to find suitable non-dimensionalizing parameters for shearing stress τ and velocity u. Figures (33A), (33B) and (33C) show the wall layer shear work integral plotted versus distance from the slot exit. The distance from slot exit is non-dimensionalized with respect to slot height. Values of wall layer shear integral shown in these figures are for two values of slot exit velocity ratios, namely, for $\frac{U_{c(o)}}{U_{e(o)}}$ equal to 1.58 and 3.2. Values of the shear work were obtained from indirect shear calculations from measures velocity profiles. In Figure (33A), shear stress τ is non-dimensionalized with respect to free stream dynamic head ρU_e^2 and velocity u is non-dimensionalized with respect to free stream velocity U_e. In Figure (33B), shear stress τ is non-dimensionalized with respect to dynamic head based on local peak velocity, ρU_m^2, and velocity is non-dimensionalized with respect to U_m. In Figure (33C), shear stress τ is non-dimensionalized with respect to local value of wall shear, τ_w, and velocity u is non-dimensionalized

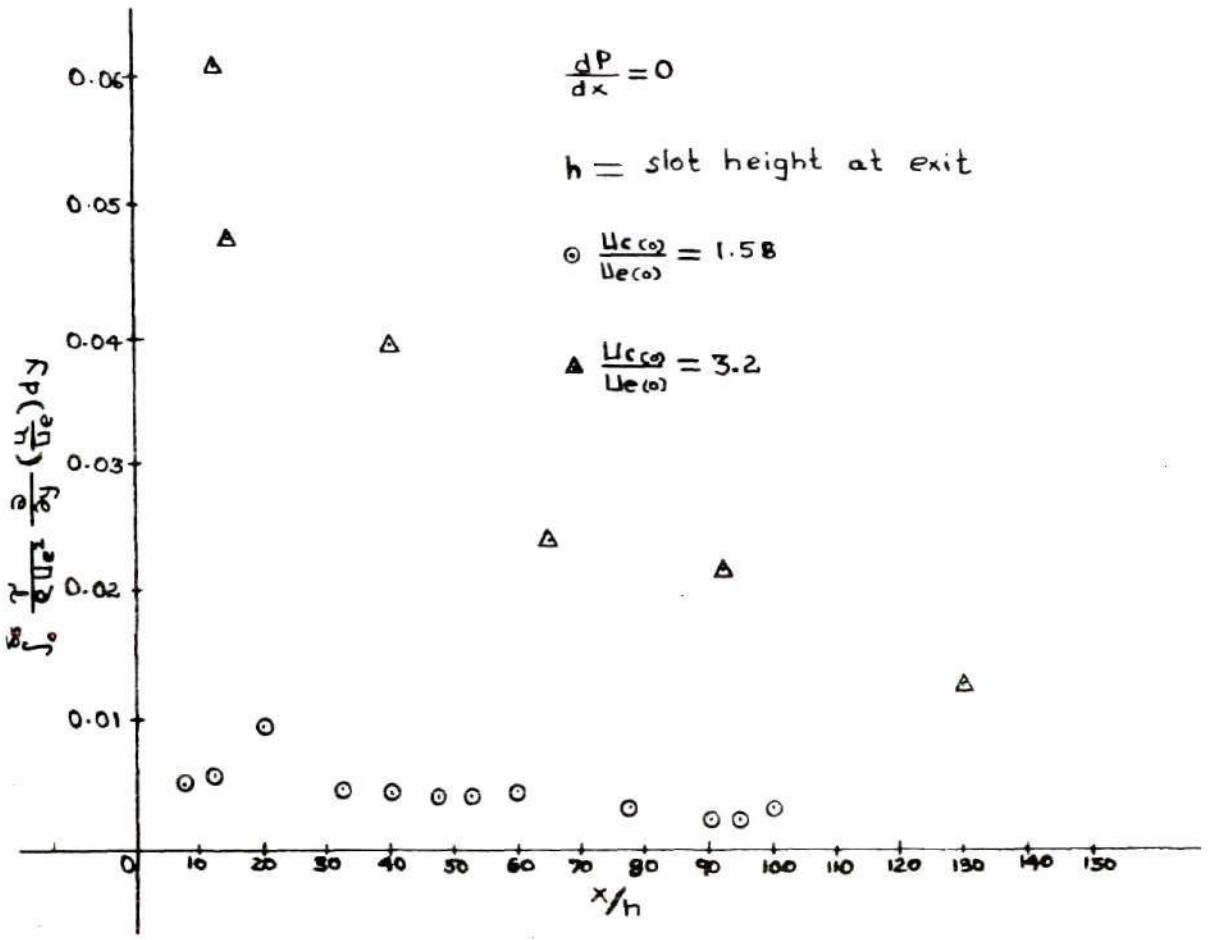

Figure 33A. Wall Layer Shear Work Integral Non-Dimensionalized with Respect to Free Stream Velocity

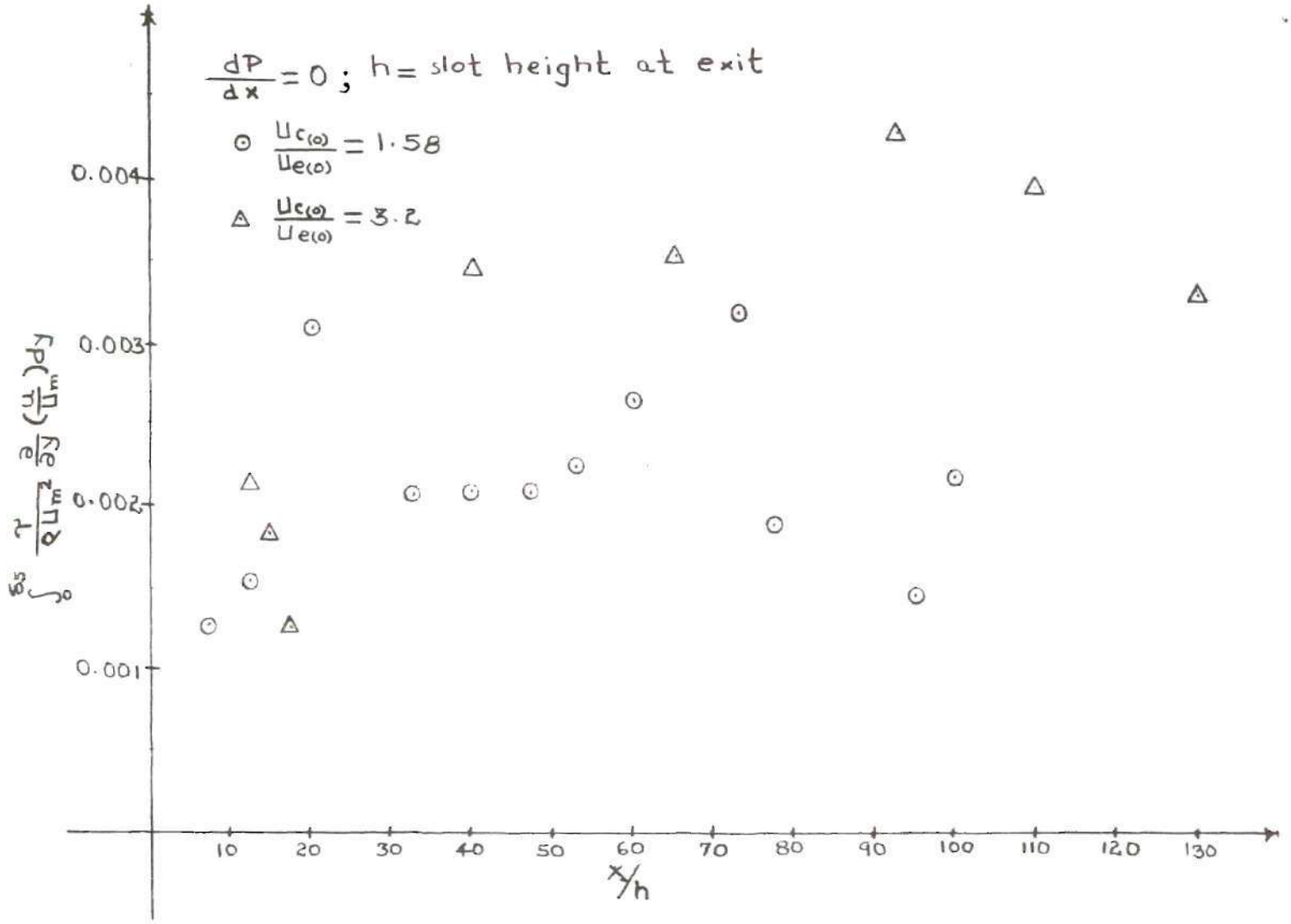

Figure 33B. Wall Layer Shear Work Integral Non-Dimensionalized with Respect to Peak Velocity U_m

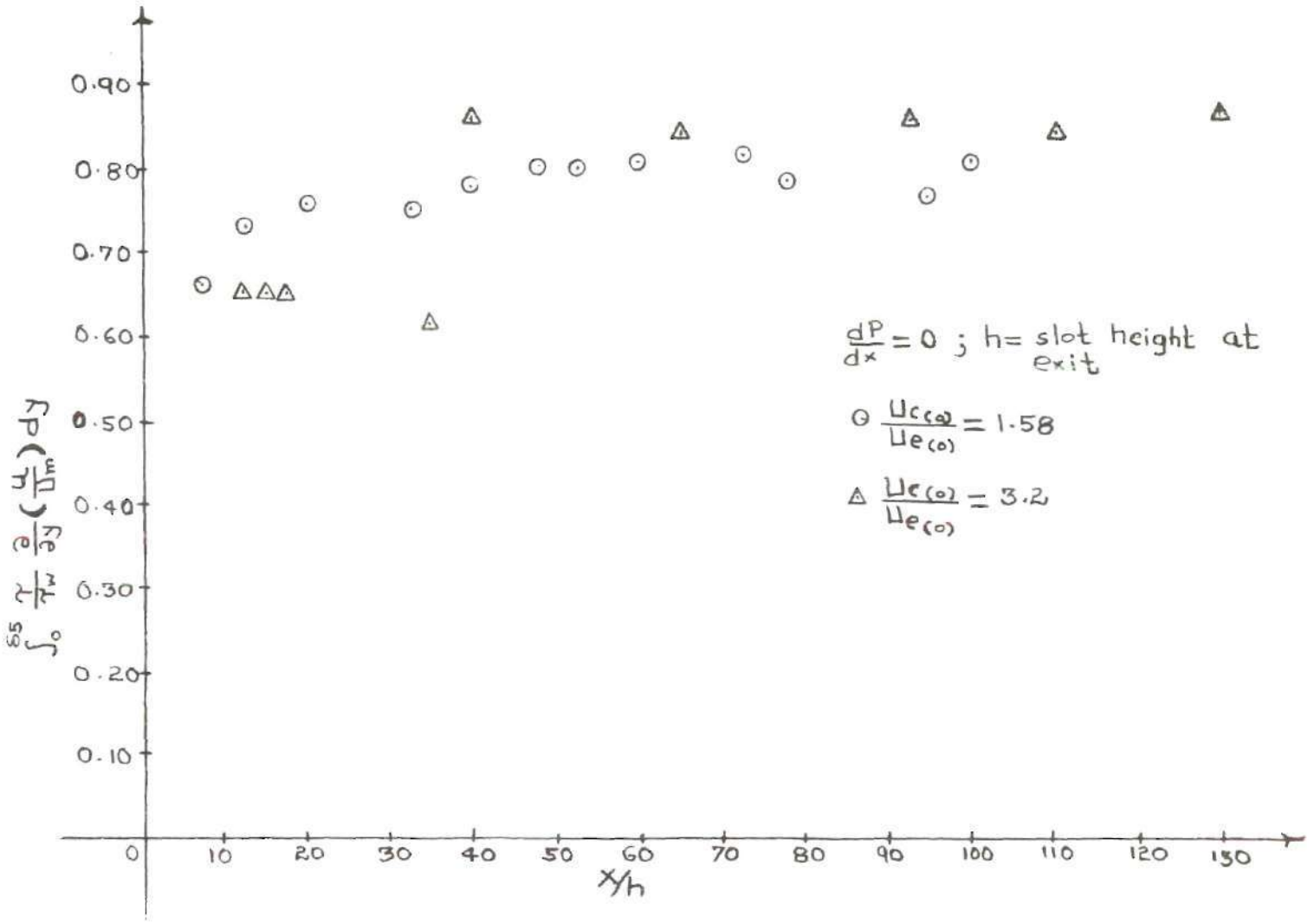

Figure 33C. Wall Layer Shear Work Integral Non-Dimensionalized with Respect to Wall Shear and Peak Velocity U_m

with respect to U_m. In Figure (33C), the points for wall shear integral, for both velocity ratios at slot exit fall on a single curve. This is not the case in Figure (33A) and (33B) where other non-dimensionalizing parameters are used.

Figures (34A), (34B), (34C) and (34D) show the shear work integral for the jet layer plotted versus distance from slot exit. Different non-dimensionalizing parameters, for shear stress τ and velocity u, are used in each of these figures. Values of the jet layer shear work integral, obtained by indirect shear calculations from measured velocity profiles, are shown plotted for two values of slot exit velocity ratios of 1.58 and 3.2. It is seen from Figure (34D) that when the shear stress τ at different points in the jet layer is non-dimensionalized with respect to local wall-shear τ_w and velocity u in the jet layer is non-dimensionalized with respect to the difference in peak and free stream velocity, i.e. $(U_m - U_e)$, the values for two slot exit velocity ratios fall nicely on the single curve. However, as seen from Figures (34A), (34B) and (34C), the above interesting result is not achieved when other non-dimensionalizing parameters are used for shear stress and local velocity in the jet layer.

Figures (35A) and (35B) show plots of total shear work integral and wall layer shear work integral plotted versus non-dimensional distance X/h from slot exit. Figure (35A) is for a slot exit velocity ratio of 3.2 whereas shear work integral for the slot exit velocity ratio of 1.58 is shown in Figure (35B). The cross-hetched areas in each figure represents the shear dissipation in the jet layer. It can be seen from these two figures, (35A) and (35B), that the non-dimensional

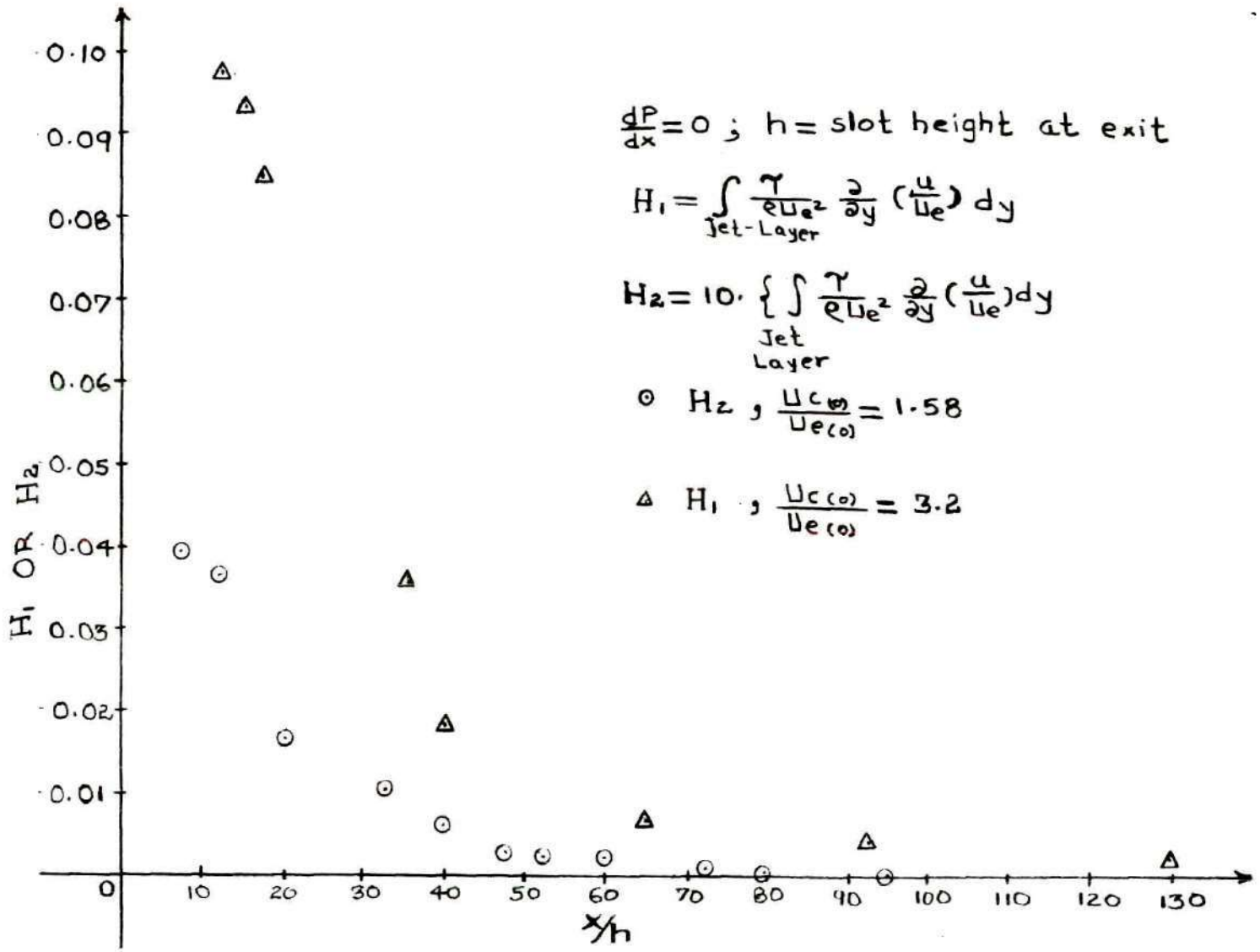

Figure 34A. Jet Layer Shear Work Integral Non-Dimensionalized with Respect to Free Stream Velocity

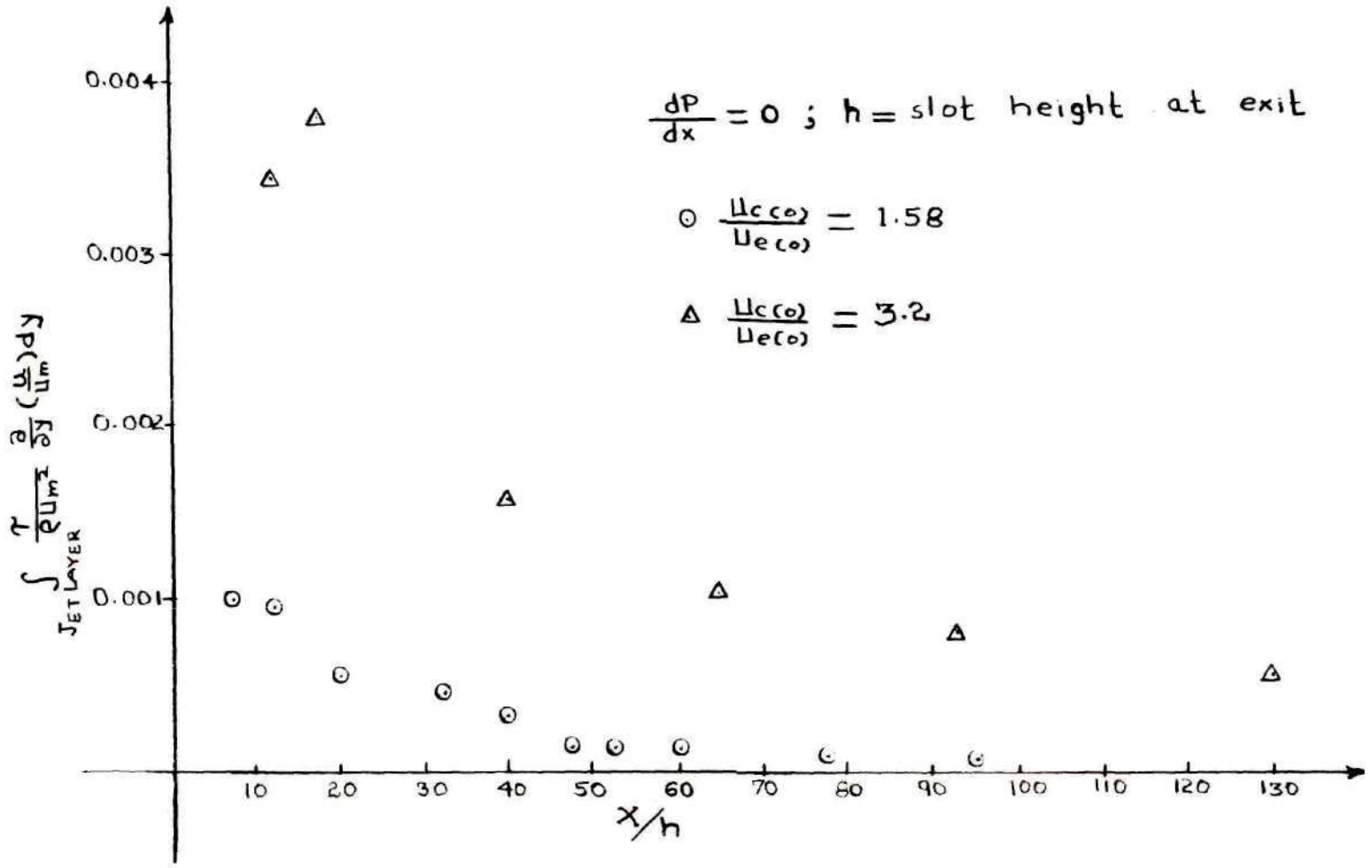

Figure 34B. Jet Layer Shear Work Integral Non-Dimensionalized with Respect to Peak Velocity U_m

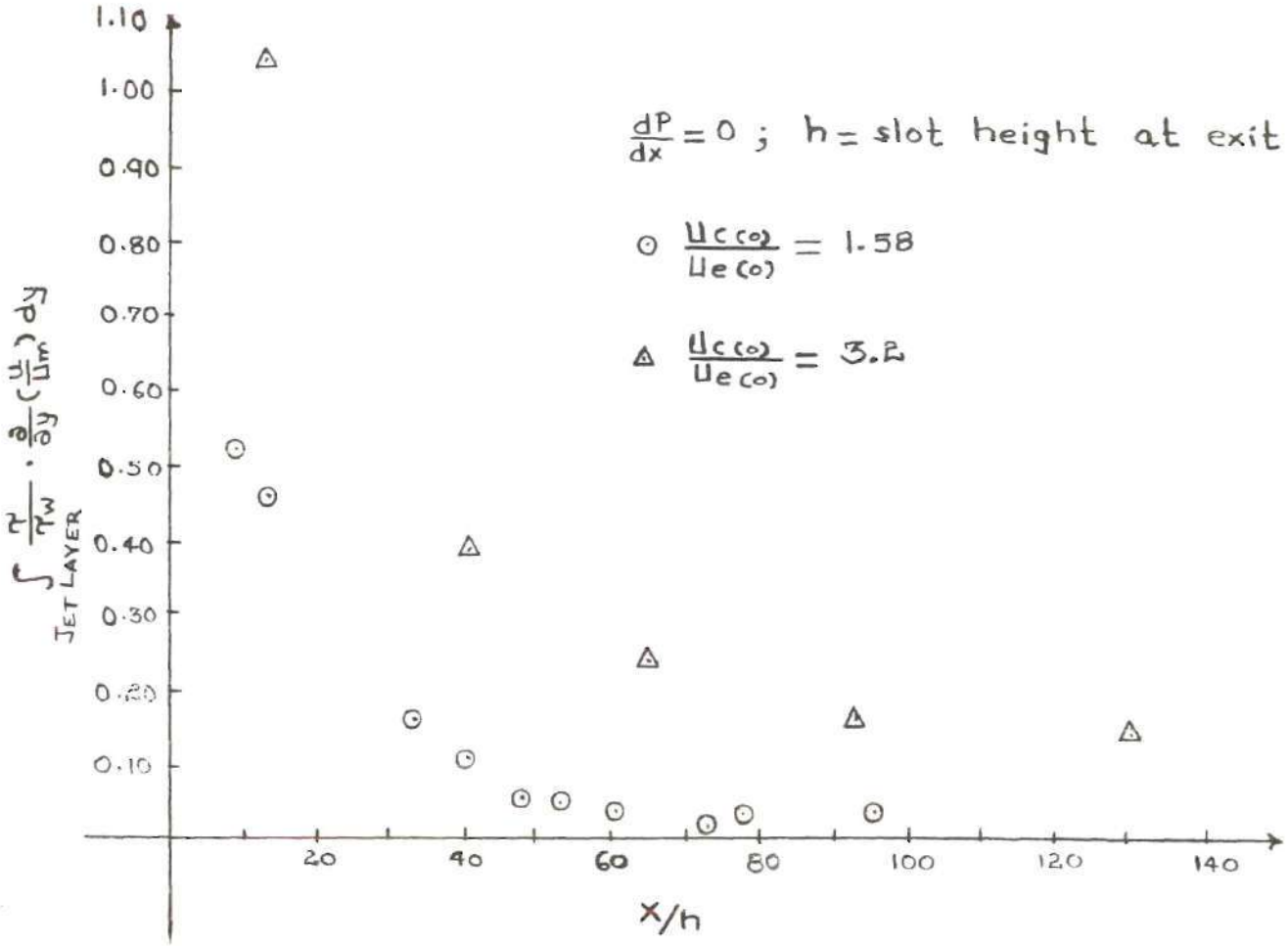

Figure 34C. Jet Layer Shear Work Integral Non-Dimensionalized with Respect to Wall Shear and Peak Velocity U_m

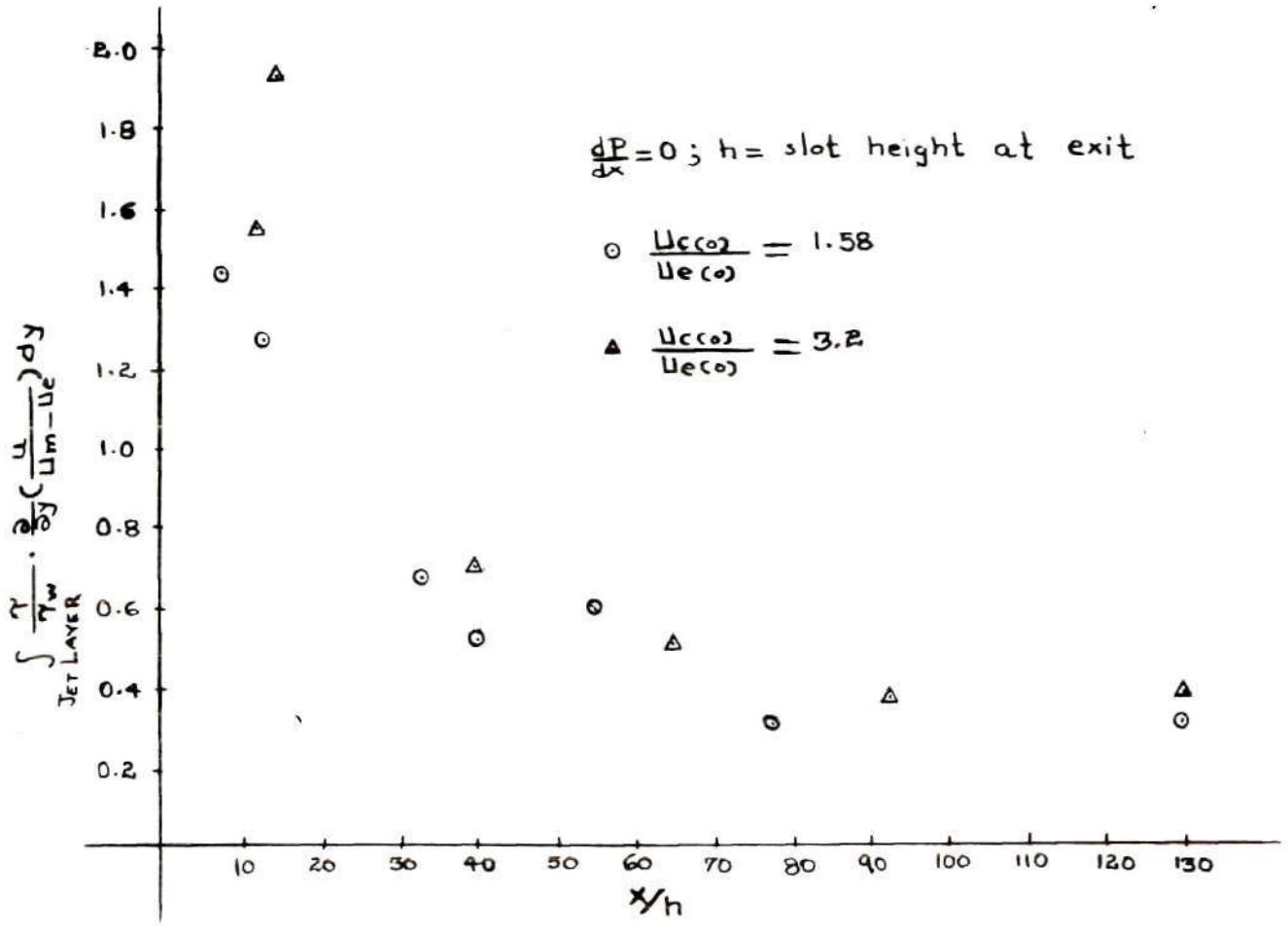

Figure 34D. Jet Layer Shear Work Integral Non-Dimensionalized with Respect to Wall Shear and Difference in Peak Velocity U_m and Free Stream Velocity

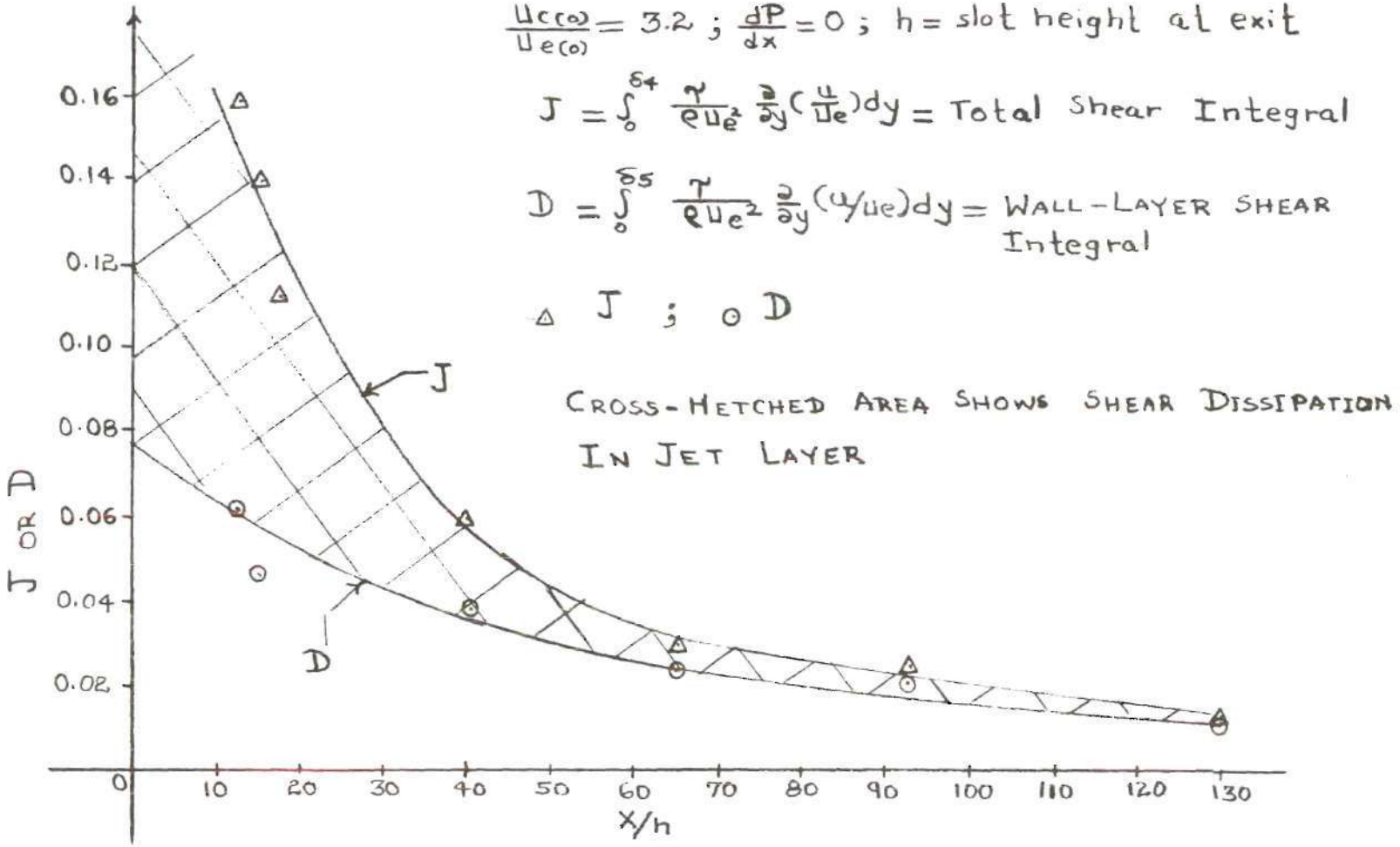

Figure 35A. Shear Work Integral Variation in Flow Direction for $\frac{U_{c(o)}}{U_{e(o)}} = 3.2$ and Zero Pressure Gradient

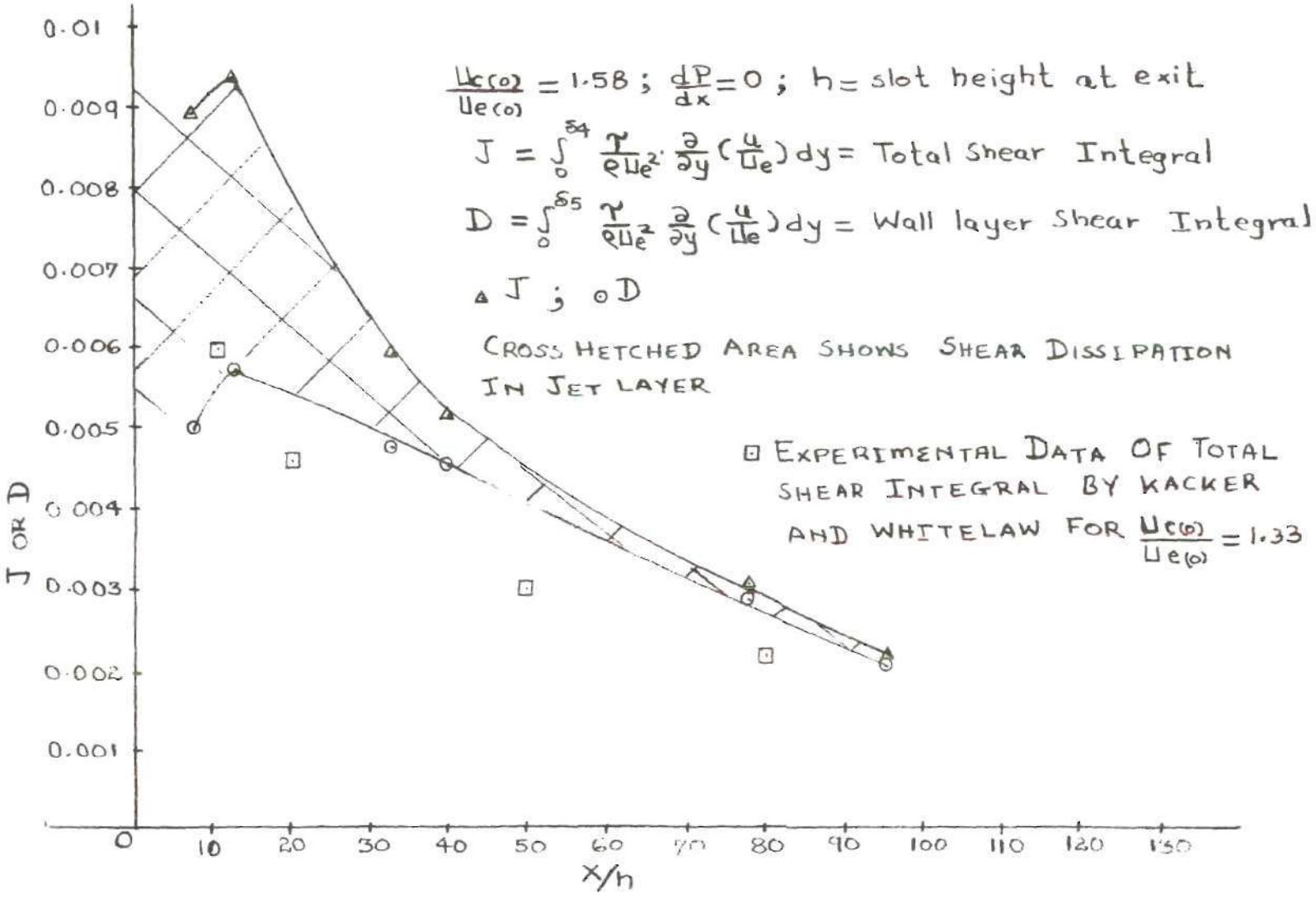

Figure 35B. Shear Work Integral Variation in Flow Direction for $\frac{U_{c(o)}}{U_{e(o)}} = 1.58$ and Zero Pressure Gradient

shear work integral is considerably larger for a slot exit velocity ratio of 3.2 than for a slot exit velocity ratio of 1.58. It is also seen from these figures that the jet layer shear work integral becomes essentially equal to zero beyond a distance of approximately 60 slot heights for both values of slot exit velocity ratio. Near slot exit, however, the shear work integral for the jet layer is approximately of the same order of magnitude as the shear work integral for the wall layer. Figure (35B) also shows plotted the values of total shear work integral measured by Kracker and Whitelaw [4] for a slot exit velocity ratio of 1.33. It can be observed that results of the present indirect shear integral calculation compare favorably, both in magnitude and trend, with the direct shear work integral measurements of Kracker and Whitelaw [4].

In the above paragraphs, the discussion of shear work integral was limited to confluent boundary layer flow with zero pressure gradient. Under these conditions, it is possible to relate the shear integral for different slot exit velocity ratios to the independent variable X or X/h. However, when the confluent boundary layer is subjected to an arbitrary pressure distribution in the flow direction, the shear work integral can no longer be represented as a function of the independent variable X/h. In the case where pressure gradient is to be considered, the shear integral must be represented as a function of non-dimensional quantities composed of dependent variables. This was done previously for the wall layer shear integral.

Correlation with Experimental Data

Theoretical equations for the different regions of the flow field in confluent boundary layer flow were derived in Chapter III. In these equations certain unknown parameters, for example, wall shear, wall layer shear work integral, shear at the points of maximum and minimum velocites, jet and wake layer similarity functions, etc., appeared. These parameters were represented as a function of groups of non-dimensional quantities composed of dependent variables for the solution of the confluent boundary layer equation. Auxiliary equations for the functional relationship of these parameters were derived in the section of Results and Discussion. The numerical form of these equations which was used for programming on digital computers was illustrated in the section on "Discussion of Numerical Solution." These sets of coupled differential equations in the various regions were solved numerically on a digital computer by a modified Euler method.

The correlation phase of the study is presented in two parts. In part (A) comparison is made of the results of calculations with present boundary layer measurements. For part (B), the effect of viscosity, due to the confluent boundary layer, in reducing the potential lift of multi-component airfoils is illustrated. A comparison with experiments of a computed boundary layer on an airfoil and a calculated pressure distribution including viscous effect is shown. The part (B) correlation is discussed in Chapter VI.

In the case of part (A), the author developed various subroutines on an IBM 360 remote controlled computer terminal at Lockheed-Georgia Company. These subroutines consisted of a computer program for the

solution of equations in different regions for the confluent boundary layer. The reason for doing this was to check out the numerical method, locate and eliminate various types of errors, and to compare computed results with the present boundary layer measurements. At the same time the validity of the functional representations for the various parameters, which were encountered in the theoretical equations, could be checked out by comparison with experimental data for different slot exit velocity ratios and pressure distributions.

Figures (36) through (43) show the correlations found in part (A). These correlations are obtained with the present experimental data. Computational results shown were obtained from the output of the confluent boundary layer subroutines which were developed by the author on the IBM 360 remote terminals at Lockheed-Georgia Company. Figures (36) through (40) show agreement between computation and experimental data in the initial region for a slot exit velocity ratio $\frac{U_{c(o)}}{U_{e(o)}}$ of approximately 1.12. Eight initial conditions, which are required for the solution of equations in the initial region, were input from measured quantities at slot exit. Referring to Figure (1), these initial conditions can be enumerated as (i) boundary layer thickness, δ_F, on the upper surface of the fore component at trailing edge, (ii) momentum thickness, θ_F, on the upper surface of fore component at the trailing edge, (iii) boundary layer thickness, δ_{s_1}, on the lower surface at the trailing edge of the fore component, (iv) momentum thickness, θ_{s_1}, on the lower surface of the fore component at trailing edge, (v) velocity, $U_{c(o)}$, and slot height, h, at the exit of the slot, (vi) velocity ratio, $\frac{U_{c(o)}}{U_{e(o)}}$, at slot exit, (vii) momentum thickness, θ_{s_2}, on the flap

upper surface at the slot exit, and (viii) form factor, H_{S2}, at the slot exit on flap upper surface. Streamwise pressure distribution, which constitutes the required boundary condition, is also required input; this measured pressure distribution is shown in Figure (4). Figure (36) shows a comparison of the calculated locus of the edges of the various layers in the initial region with experimental data; thus, line $y = \delta_{1(x)}$ is the locus of the edge of wall layer; $y = \delta_{2(x)}$ is the locus for the edge of core; $y = \delta_{3(x)}$ is the locus of the junction of the jet and the wake layer; and the line shown as $y = \delta_{4(x)}$ is the outer edge of wake layer. The line $y = \delta_{4(x)}$ corresponds to the assumption of zero shear stress in the development of the theoretical equations. In this figure, experimental data are shown as points. Experimental data for the outer edge of the wake layer at particular X locations are shown as two points; the smaller y value corresponds to the point where the measured ratio of velocity, $\frac{u}{U_e}$, is equal to 0.99 and the larger y value corresponds to the point where measured velocity ratio, $\frac{u}{U_e}$, becomes approximately equal to one. Figure (37) shows a plot of calculated values of the displacement thickness for wall layer, jet layer, and wake layer and Figure (38) shows a plot of the wall layer momentum thickness. In both of these figures the experimental data, obtained for velocity profile measurements by integration, are indicated by various symbols. Figure (39) shows a plot of calculated values of velocity ratio, $\frac{U_w}{U_e}$, at the junction of the jet and wake layer; the value of $\frac{U_w}{U_e}$ at X = 0 is obtained from a momentum balance at the trailing edge of the fore component.

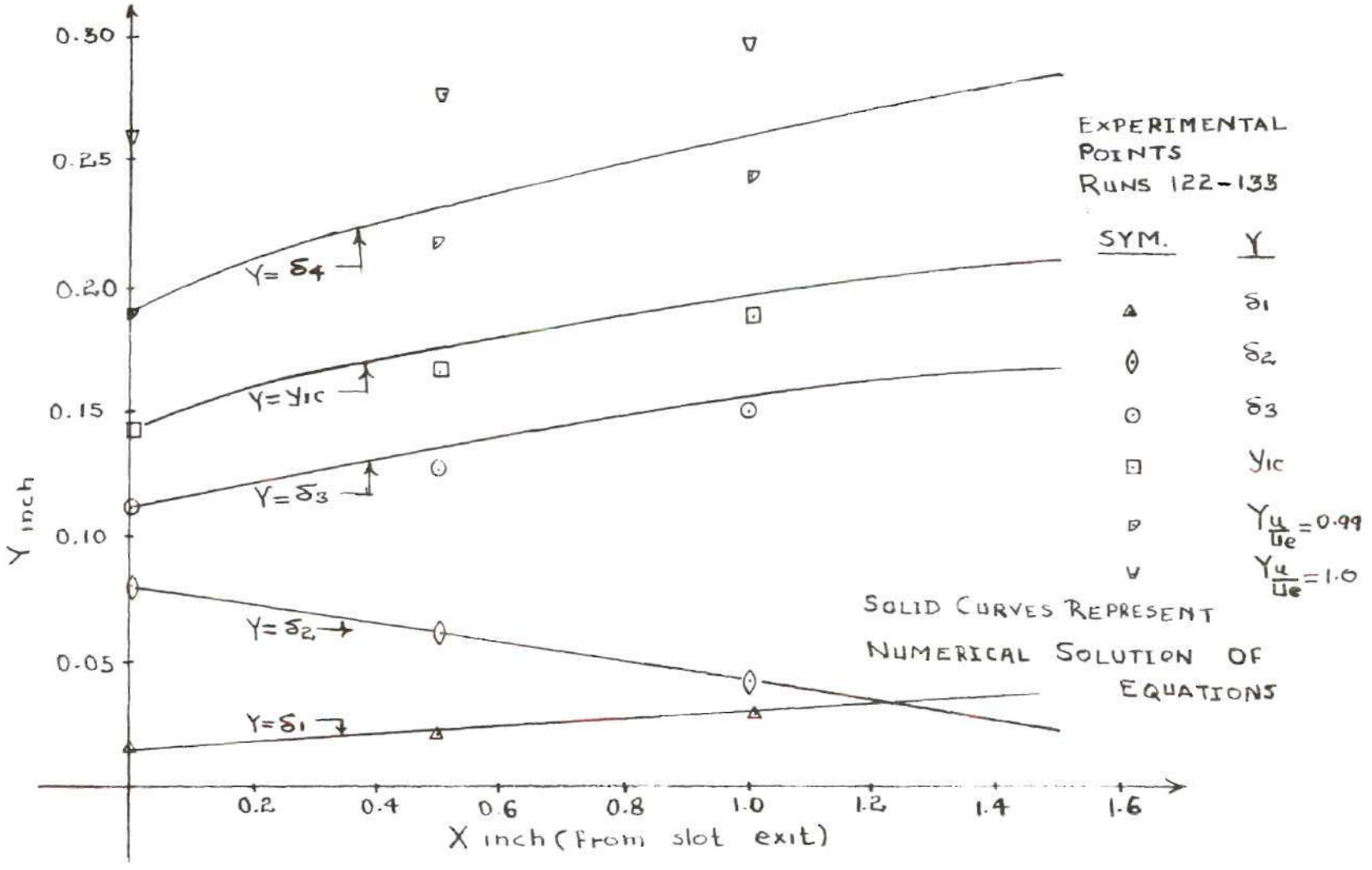

Figure 36. Comparison of Predicted and Experimental Locus of the Edges of Various Layers in the Core Region of Present Experiments

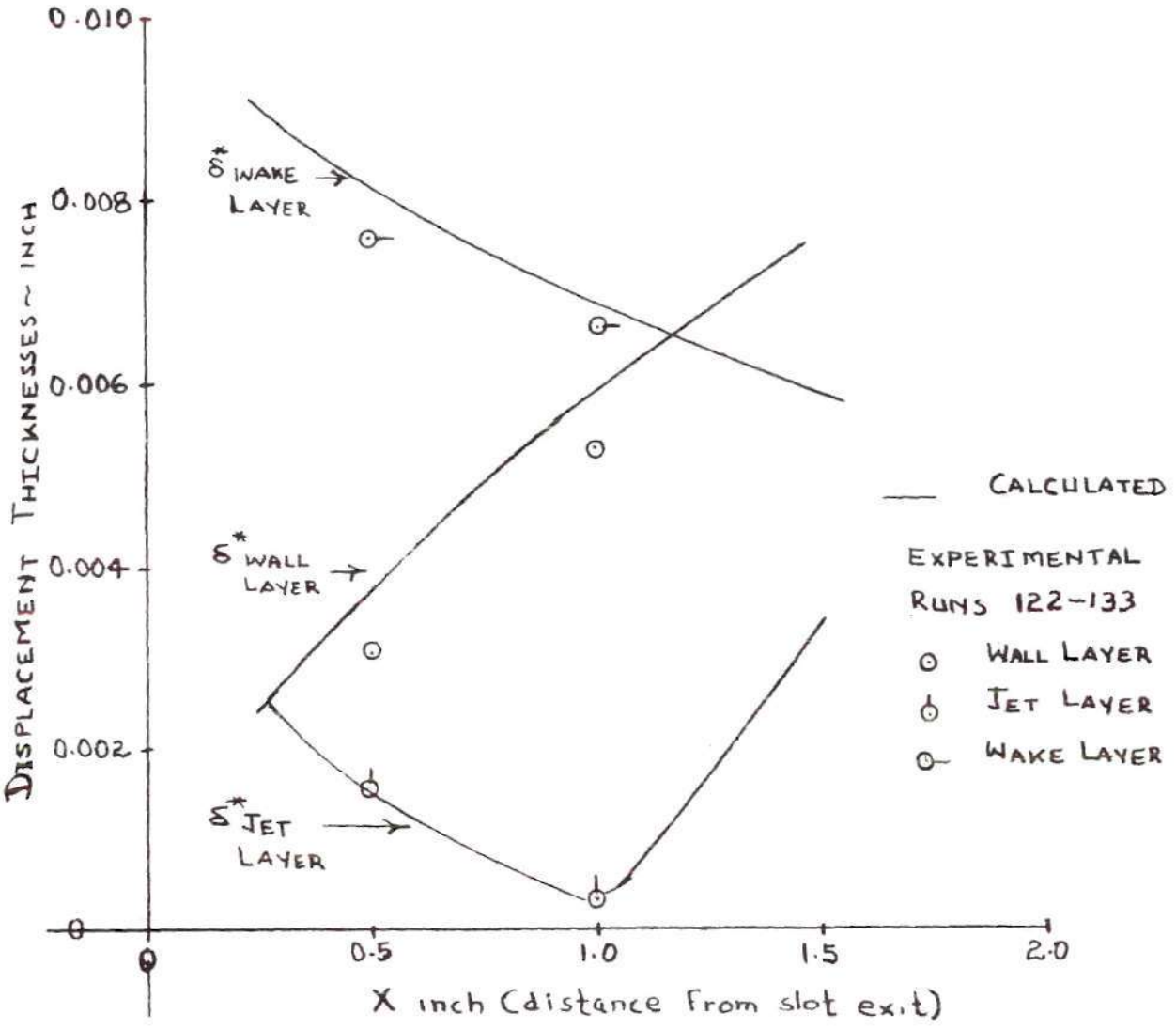

Figure 37. Comparison of Predicted and Measured Displacement Thickness of Various Layers in the Core Region of Present Experiments

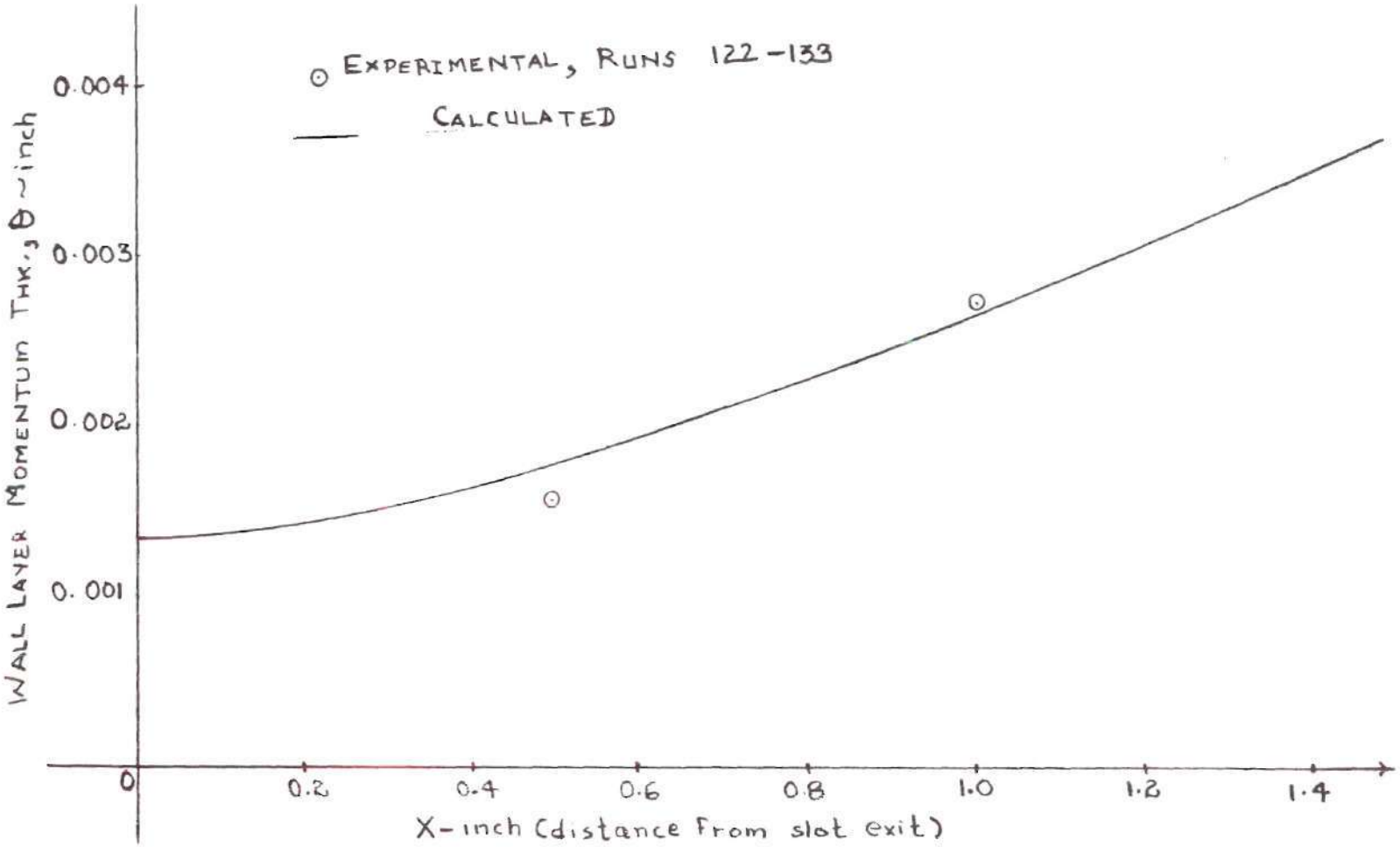

Figure 38. Comparison of Predicted and Measured Momentum Thickness of Wall Layer in the Core Region of Present Experiments

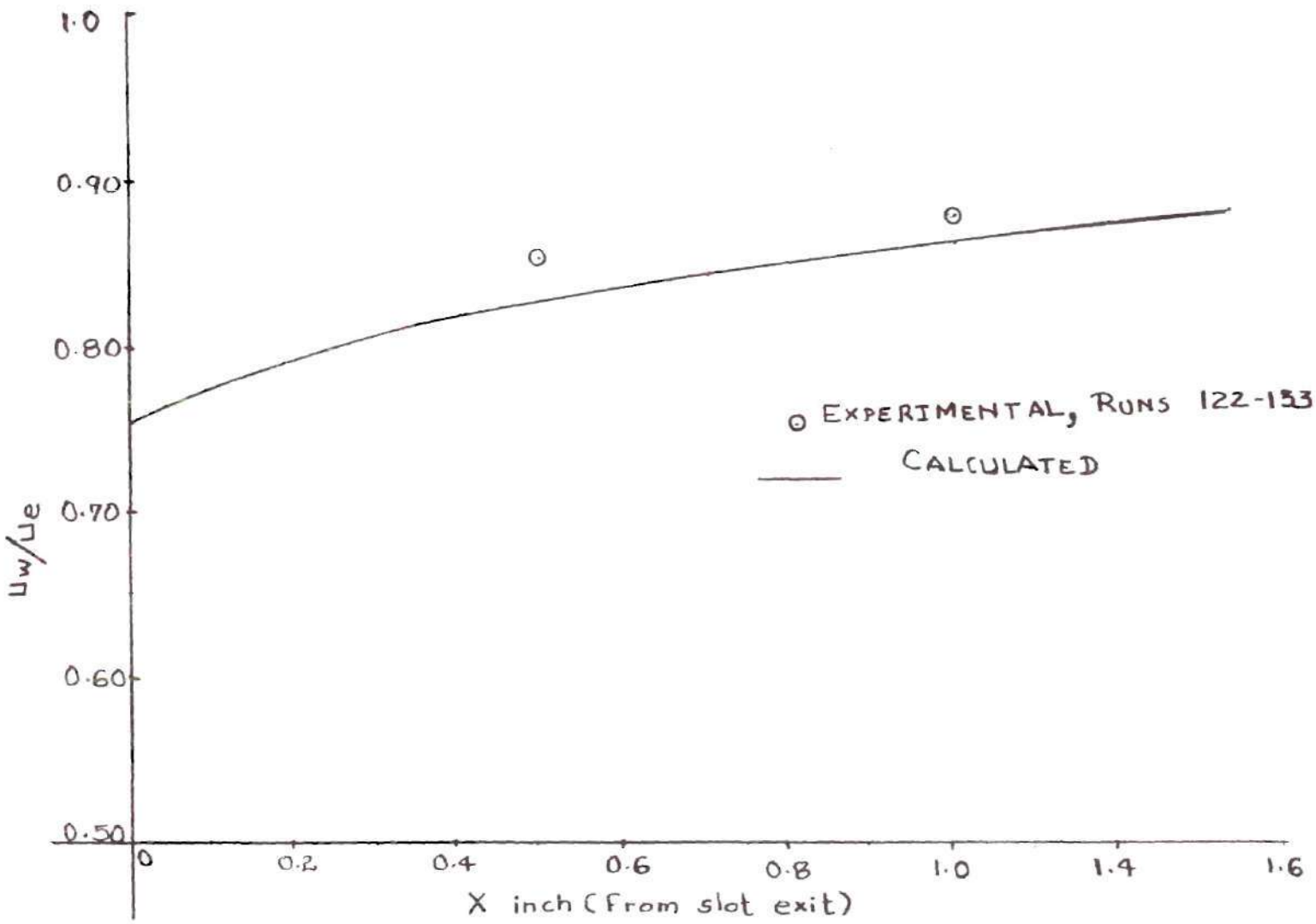

Figure 39. Comparison of Predicted and Measured Velocity at the Junction of Jet and Wake Layers of Present Experiments

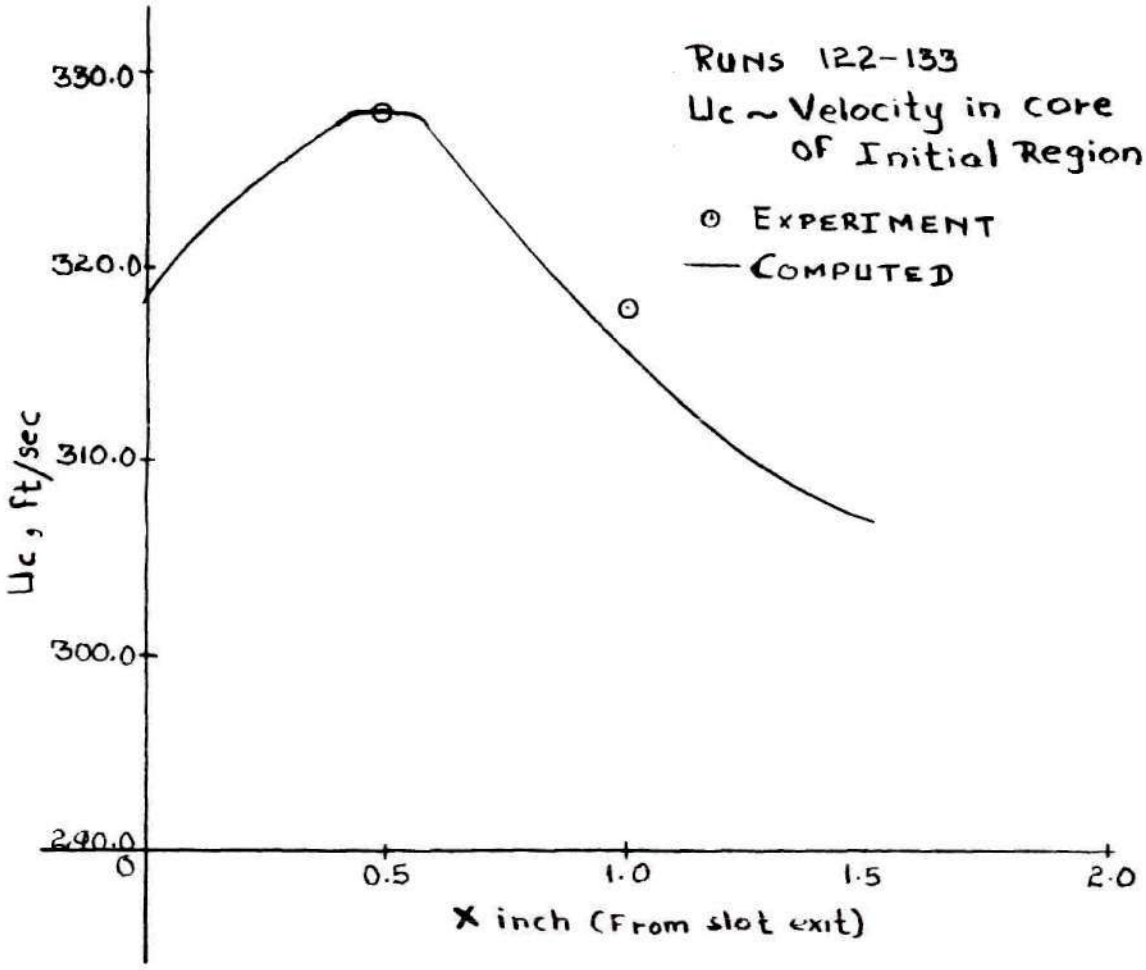

Figure 40. Comparison of Predicted and Measured Core Velocity of Present Experiments

Figure (40) shows a plot of velocity $U_{c(x)}$ in the core of the initial region. The solution for the velocity $U_{c(x)}$ is obtained from a knowledge of the external edge or potential velocity distributions, initial velocity at the slot exit and the assumption of constancy of pressure in the y direction; equations (1) and (2) are used to calculate velocity $U_{c(x)}$ in the core. Results of experimental measurements are indicated by various symbols.

Figures (41) through (43) show also part (A) type correlation with the experimental data in main region II. The experimental data corresponds to an initial slot exit velocity ratio of $\frac{U_{c(o)}}{U_{e(o)}} = 1.67$. The measured pressure distribution, which constitutes a boundary condition is shown in Figure (8). Main region II for this case starts at X = 4" from slot exit. The initial conditions at X = 4", which constitute input requirements are (i) wall layer momentum thickness, θ_5 , (ii) wall layer form factor, H_5 , (iii) ratio, $\frac{U_m}{U_e}$, and U_m in ft/sec. at X = 4", and (iv) jet layer thickness, $\delta_4 - \delta_5$. The above initial conditions were obtained from experimentally measured values at X = 4". Figure (41) shows a plot of calculated loci of the edges of the wall layer and the external edge of the jet layer. The calculated loci of the external edge of the jet layer, i.e. the line $y = \delta_{4(x)}$ corresponds to the assumption of zero shear in the theoretical equations. At a particular X location, two experimental points, for $\frac{u}{U_e} = 1.01$ and $\frac{u}{U_e} = 1.0$, are shown plotted as characterizing the edge of the jet layer. Figure (42) shows a plot of calculated values of wall layer momentum thickness, displacement thickness, dissipation energy thickness, form factor, $H = \frac{\delta^*}{\theta}$, for the wall layer and the ratio, $\frac{\delta^{**}}{\theta}$, for the

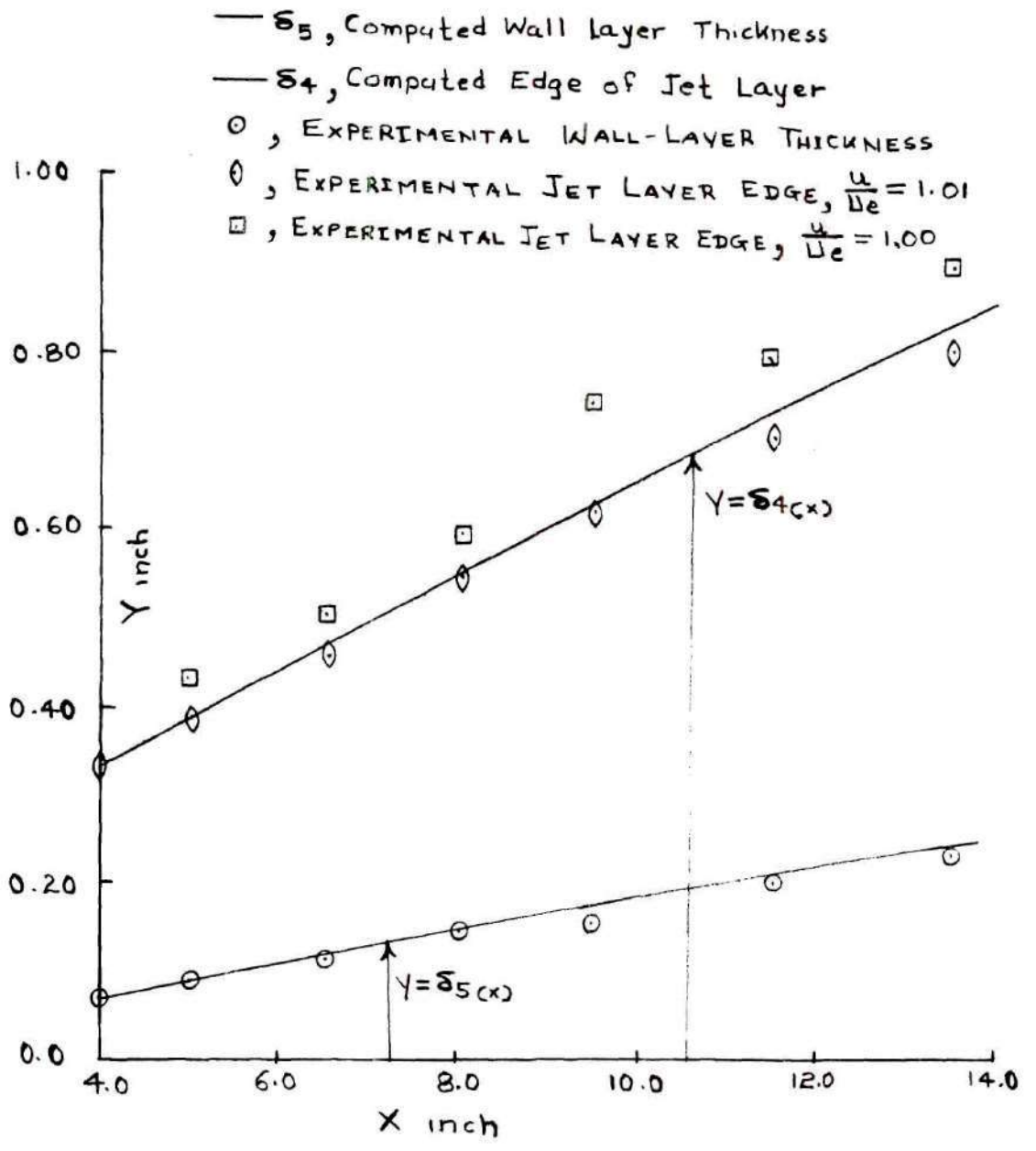

Figure 41. Comparison of Predicted and Experimental LOCI of Wall and Jet Layers in Main Region

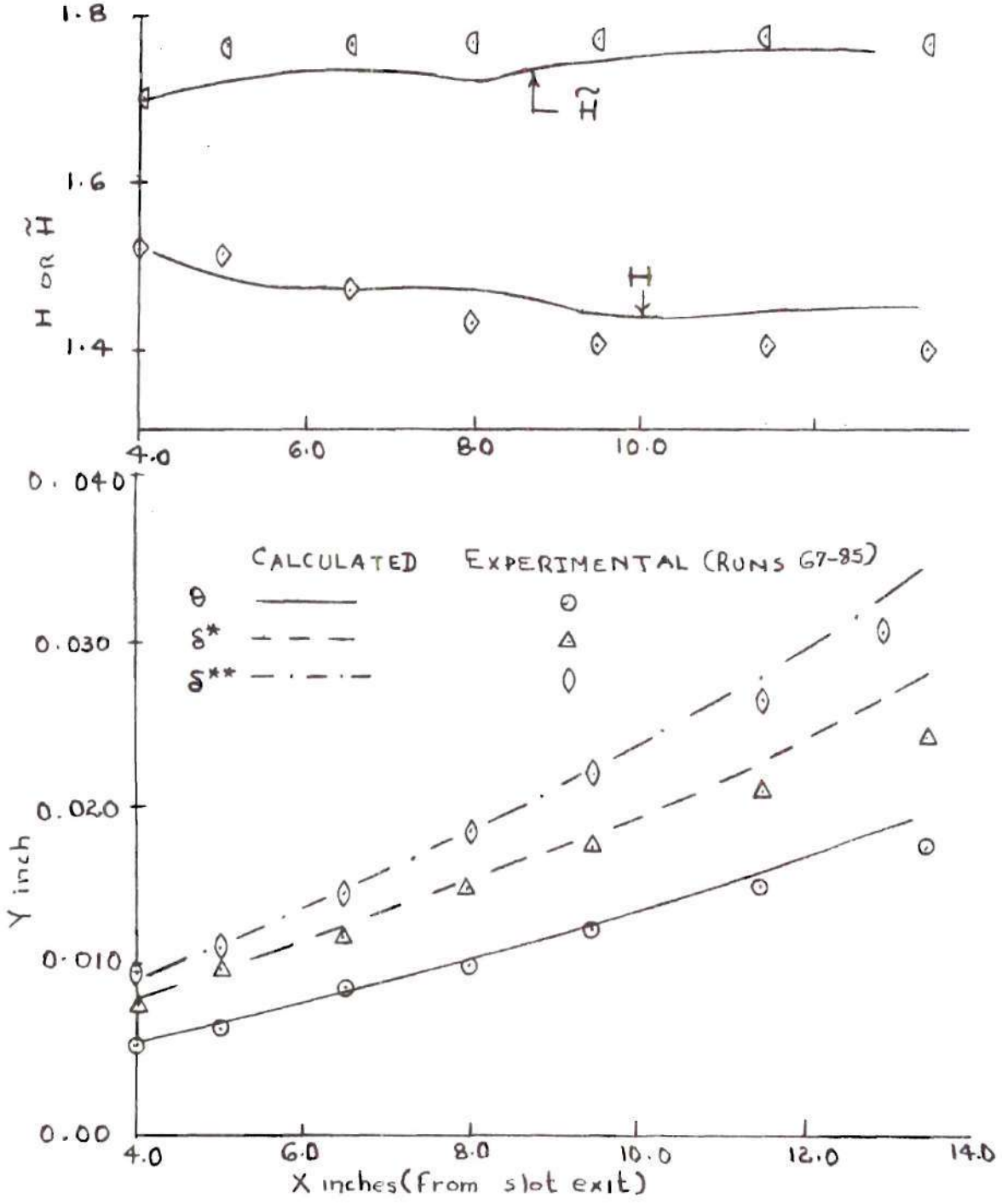

Figure 42. Comparison of Predicted and Experimental Displacement and Momentum Thicknesses and Shape Factors for Wall Layer in Main Region

wall layer. Experimental data shown plotted in this figure are obtained by integrating measured velocity profiles. Figure (43) shows results of computer program output for the velocity ratio, $\frac{u_m}{u_e}$, at the junction of the wall and jet layers and also a plot of calculated values of wall layer momentum thickness Reynolds number; experimentally determined quantities are indicated by various symbols in this figure. It should be noted at this point that a solution for $\frac{u_m}{u_e}$ is obtained by simultaneous solution of equations in the main region in contrast to the simple solution for $u_{c(x)}$ in the core region.

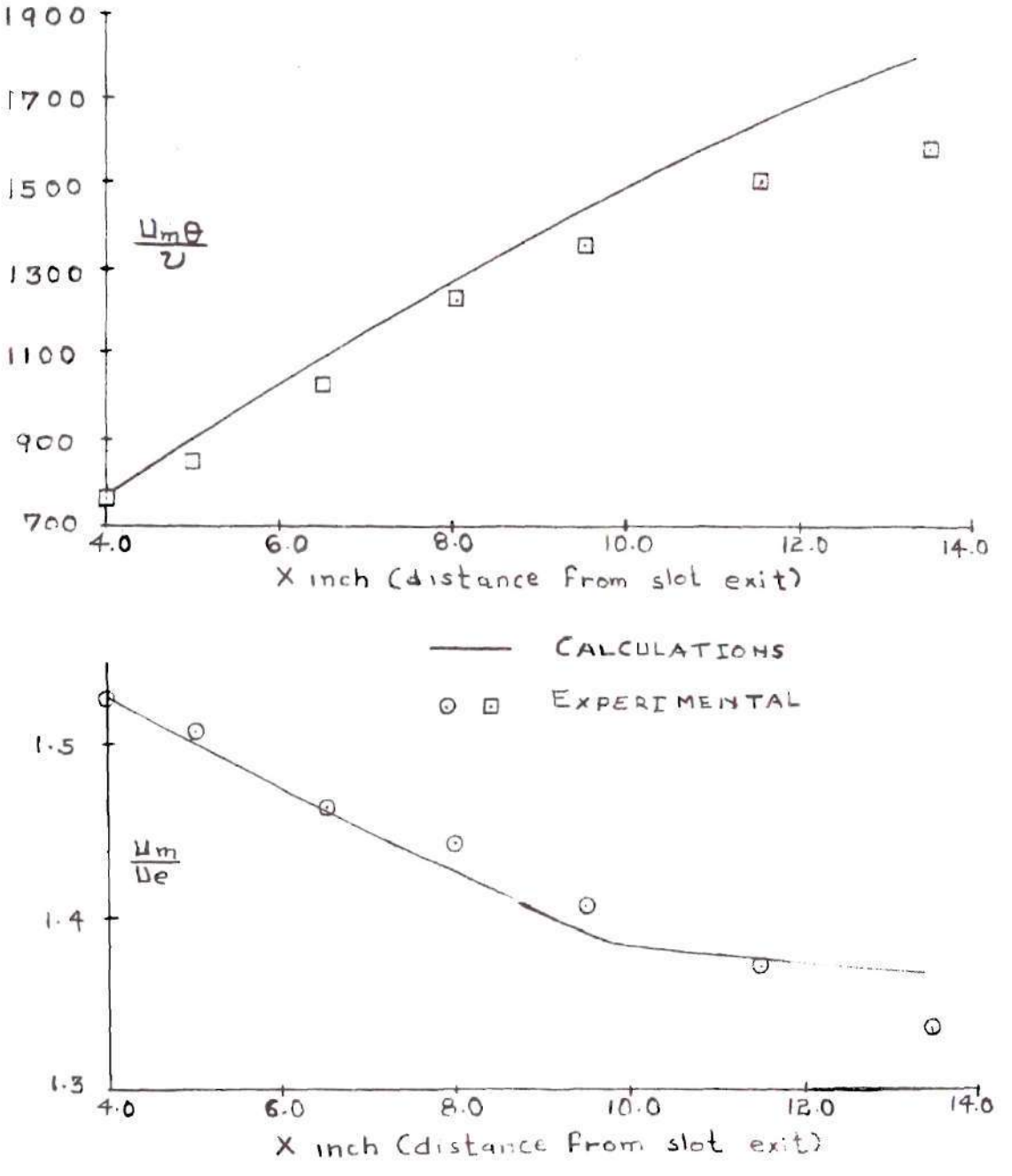

Figure 43. Comparison of Predicted and Measured Values for the Decay of the Velocity at the Junction of Wall Layer in the Main Region

CHAPTER VI

APPLICATION OF CONFLUENT BOUNDARY LAYER CALCULATIONS TO MULTI-COMPONENT AIRFOILS

In the previous chapter part (A) of the correlation was discussed where the comparison of the confluent boundary layer calculations were made with present boundary layer measurements. In this chapter, part (B) of the correlation phase will be discussed. For part (B), the effect of viscosity, due to confluent boundary layer in reducing the potential lift of multi-component airfoils is illustrated. Comparisons with experiments of a computed boundary layer on airfoils and calculated pressure distributions including viscous effects are shown.

For part (B) of the correlation, various individuals of the Aerodynamics Technology Department of Lockheed-Georgia Company, including the author, were involved. This consisted of formulation of theoretical methods for different component parts of the flow field other than the confluent boundary layer and putting together component parts in the framework of a total computer program for predictions of performance of multi-component airfoils in low-subsonic viscous flow. The various theoretical methods which are incorporated in the above computer programs can be listed as (i) Prediction of potential flow pressure distribution on the surface of multi-component airfoil [55], (ii) Laminar boundary layer calculations [56], (iii) Transition prediction method [56], (iv) Ordinary turbulent boundary layer calculation [57], (v) Confluent boundary layer calculations on the upper surfaces of all but the most

forward element of multi-component airfoils. Calculations for the performance of a given airfoil section are done with an iteration procedure, i.e. for a given geometry of airfoil section the pressure distribution is computed for zeroth iteration - the boundary layer is computed for the zeroth iteration pressure distribution - the shape of the airfoil is then altered to take into account boundary layer development - the pressure distribution is computed for this modified airfoil due to the viscous effect and so forth. This process is continued until convergence in lift coefficient is obtained. It has been found that potential flow lift, for instance, for a two-component airfoil, is reduced by as much as 25 to 30 percent due to the viscous effects. The majority of the viscous effect is, however, caused by the presence of the confluent boundary layer. This is due to the fact that it is much thicker than the ordinary turbulent boundary layer.

Figures (44) through (46) are representative of part (B) type correlation. This part (B) type correlation is presented here in order to illustrate the application of the confluent boundary layer for multi-component airfoil and the important role it plays in determining multi-component airfoil performance. In part (B) correlation, the input consists of specification of the airfoil ordinates, angle of attack, free stream Mach number, and airfoil chord. The converged solution for pressure, boundary layer quantities and lift coefficient is obtained by iteration procedure with multi-component airfoil program which has been mentioned previously. Figures (44A), (44B) and (44C) show the results of calculations for NACA 4418 (Modified) airfoil. Experimental data shown in the figures for this airfoil were taken by Seebohm (45).

Figure (44A) shows a computed plot of lift coefficient, C_L. Iteration zero corresponds to calculation of pressure distribution and lift coefficient for the hard geometry of the airfoil and does not include boundary layer effects on the airfoil, whereas for succeeding iterations, the calculated boundary layer is used to modify the airfoil surface; pressure distribution and lift coefficient are then computed during successive iterations for this boundary layer modified airfoil surface. Two important conclusions can be drawn from Figure (44A), namely, (i) approximately a 24 percent reduction in lift coefficient is caused by the presence of the boundary layer on the two-piece single slotted airfoil, mainly by the presence of the very thick confluent boundary layer on flap upper surface, and (ii) convergence in pressure distribution, boundary layer development and lift coefficient is obtained essentially within 3 - 4 iterations. Figure (44B) shows a plot of pressure distribution calculated for the fourth iteration. The experimentally determined pressure distribution as indicated by symbols agrees well with computed results. Figure (44C) shows a plot of calculated confluent boundary layer quantities on the upper surface of the flap for this airfoil. Computed results shown by the solid line are for the results of the fourth iteration. Experimental data, obtained by Seebohm (45) at two stations on the flap upper surface are shown with symbols. Figure (45) shows correlation of the confluent boundary layer on Foster's (49) airfoil. The experimental data were taken by D. N. Foster (49) of RAE in England. The procedure used for correlation in Figure (45) is the same as discussed for Figures (44A), (44B), and (44C).

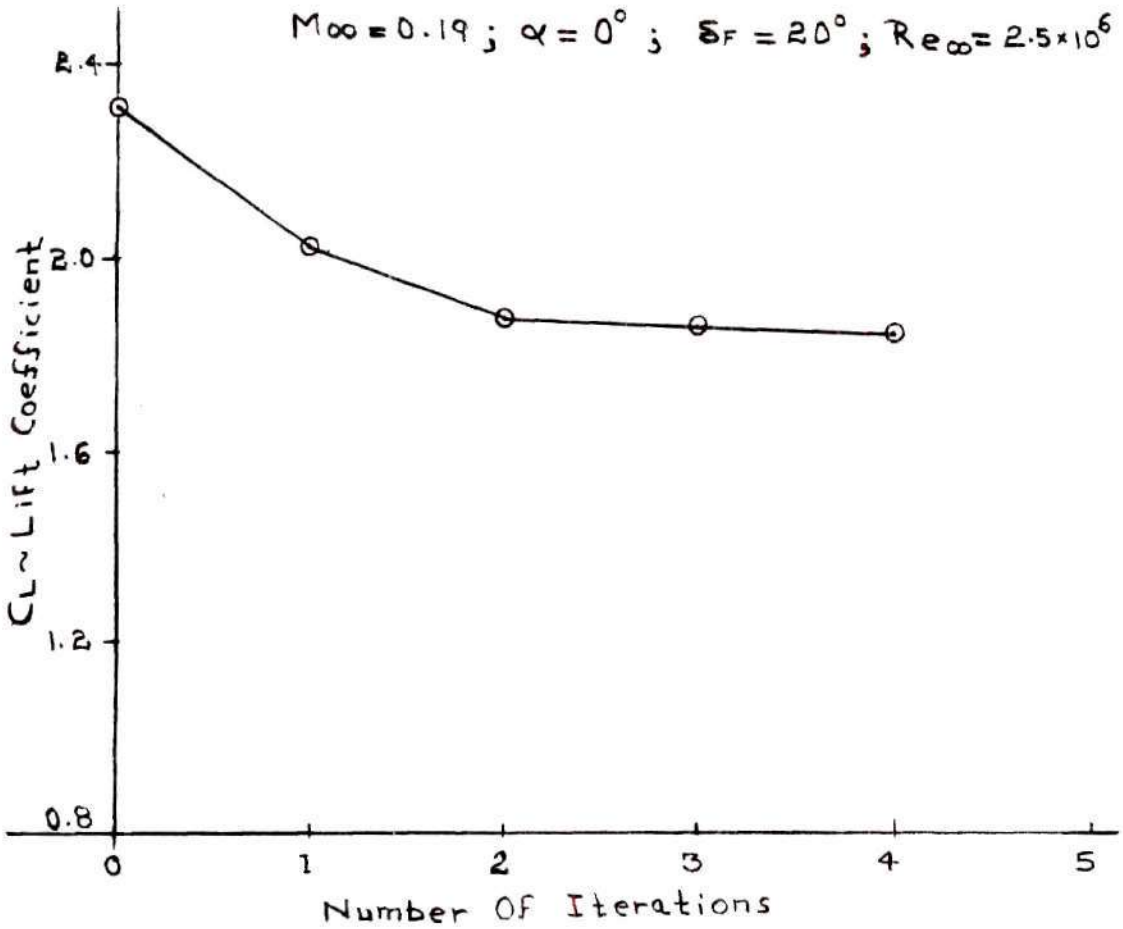

Figure 44A. Variation of Lift Coefficient with Iterations for NACA 4418 (MOD) Single Slotted Airfoil

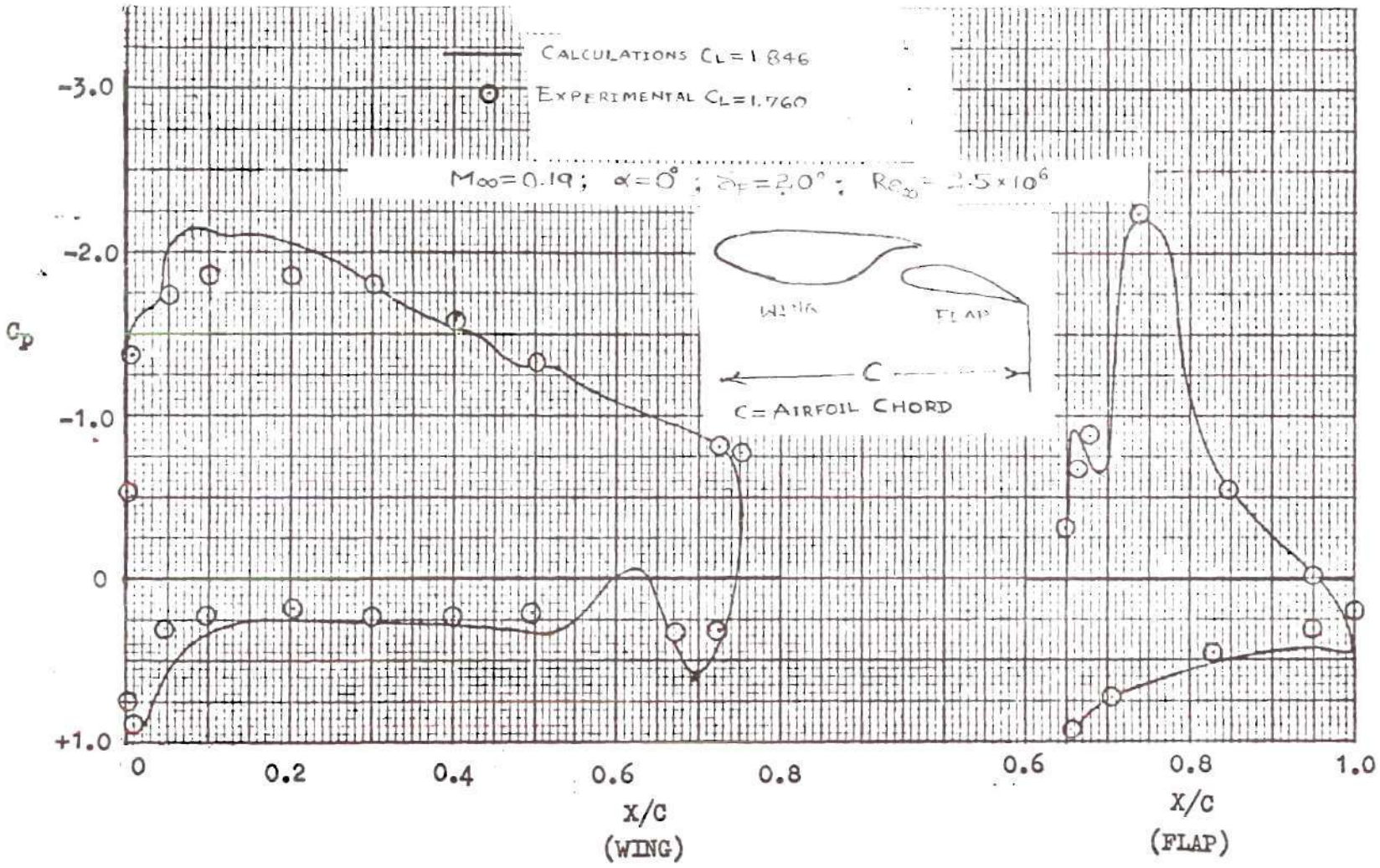

Figure 44B. Comparison of Experimental and Predicted Pressure Distributions for NACA 4418 (MOD). Single Slotted Airfoil

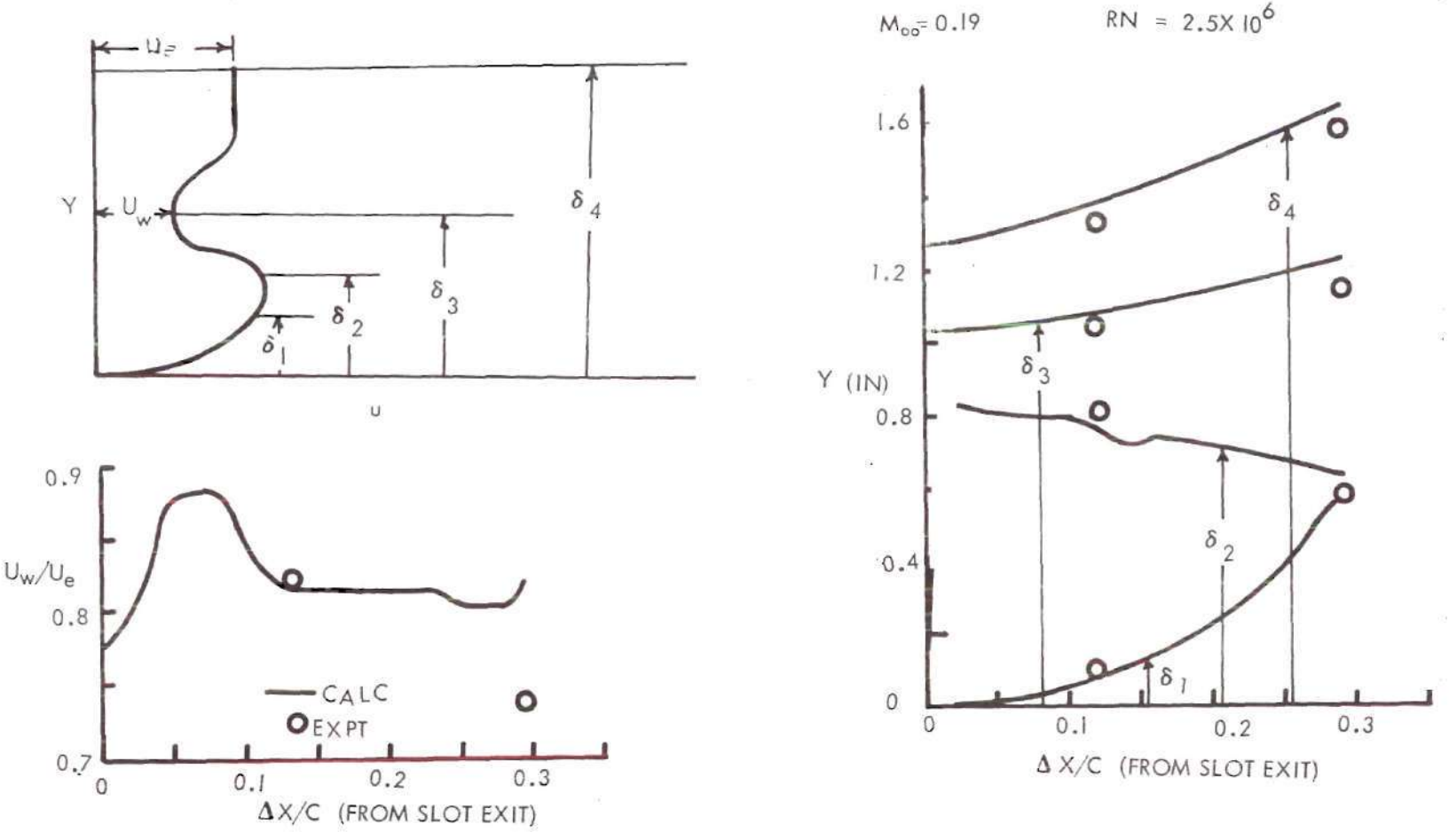

Figure 44C. Comparison of Confluent Boundary Layer Parameters for NACA 4418 (MOD). Single Slotted Airfoil

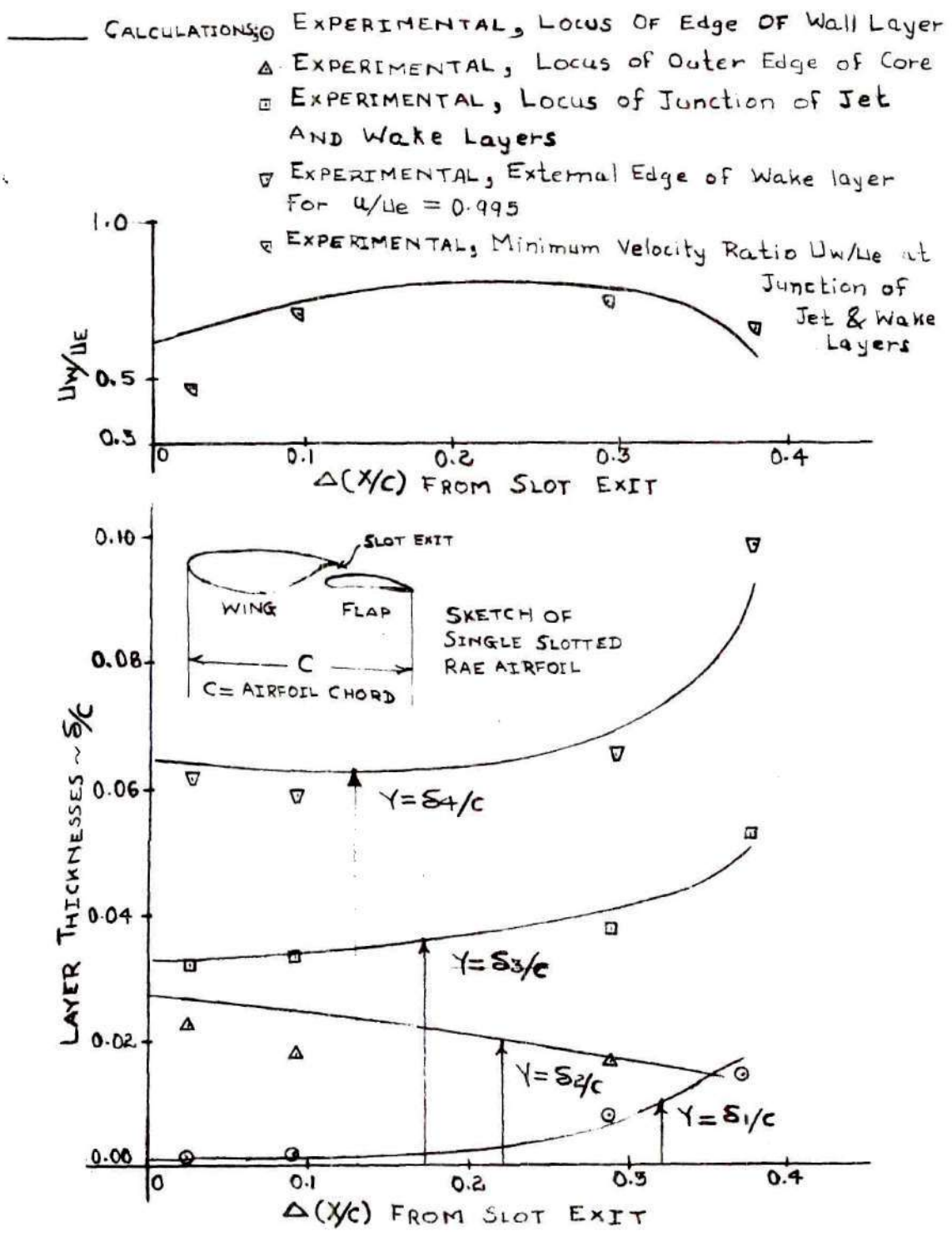

Figure 45. Comparison of Confluent Boundary Layer Parameters for Single Slotted RAE Airfoil

Figures (46A) and (46B) show calculation results for part (B) type correlation, together with experimental data (46) for NACA 23012-25% chord flap single slotted airfoil. Figure (46A) shows a comparison of pressure distribution at an angle of attack of $\alpha = 8.0°$ and flap deflection of $\delta_F = 20°$. As seen from this figure, fair agreement is obtained between calculations and experimental data. Figure (46B) shows a plot of lift coefficient versus angle of attack, α, for flap deflection, $\delta_F = 20°$; both experimental data and calculations are shown. On the same figure the calculated values of wall layer form factor on the upper surface of the flap trailing edge is plotted versus angle of attack. An experimental value of maximum lift coefficient of approximately 2.2 occurs at an angle of attack of $\alpha = 12°$, as seen in the figure; also, as seen in the lower part of the figure, values of wall layer form factor remain approximately constant at a value of 1.65 for $\alpha = 0$, 4 and 8 degrees. At an angle of attack of 12 degrees, however, calculated values of wall layer form factor at the trailing edge rises abruptly to the value of 2.25; at the same angle of attack of 12 degrees, experiment indicates that lift coefficients on this airfoil have reached maximum values. Experimental data for boundary layer measurement on this airfoil is not available. However, the phenomena illustrated in Figure (46B), namely the abrupt increase in the confluent boundary layer's wall layer form factor to the value of $H_{WALL_{T.E.\ FLAP}} = 2.25$, indicates possible criteria for determining $C_{L_{MAX}}$ for a single slotted two piece airfoil.

Figure (47) shows an important application of the confluent boundary layer calculation method in optimizing the flap gap for a given

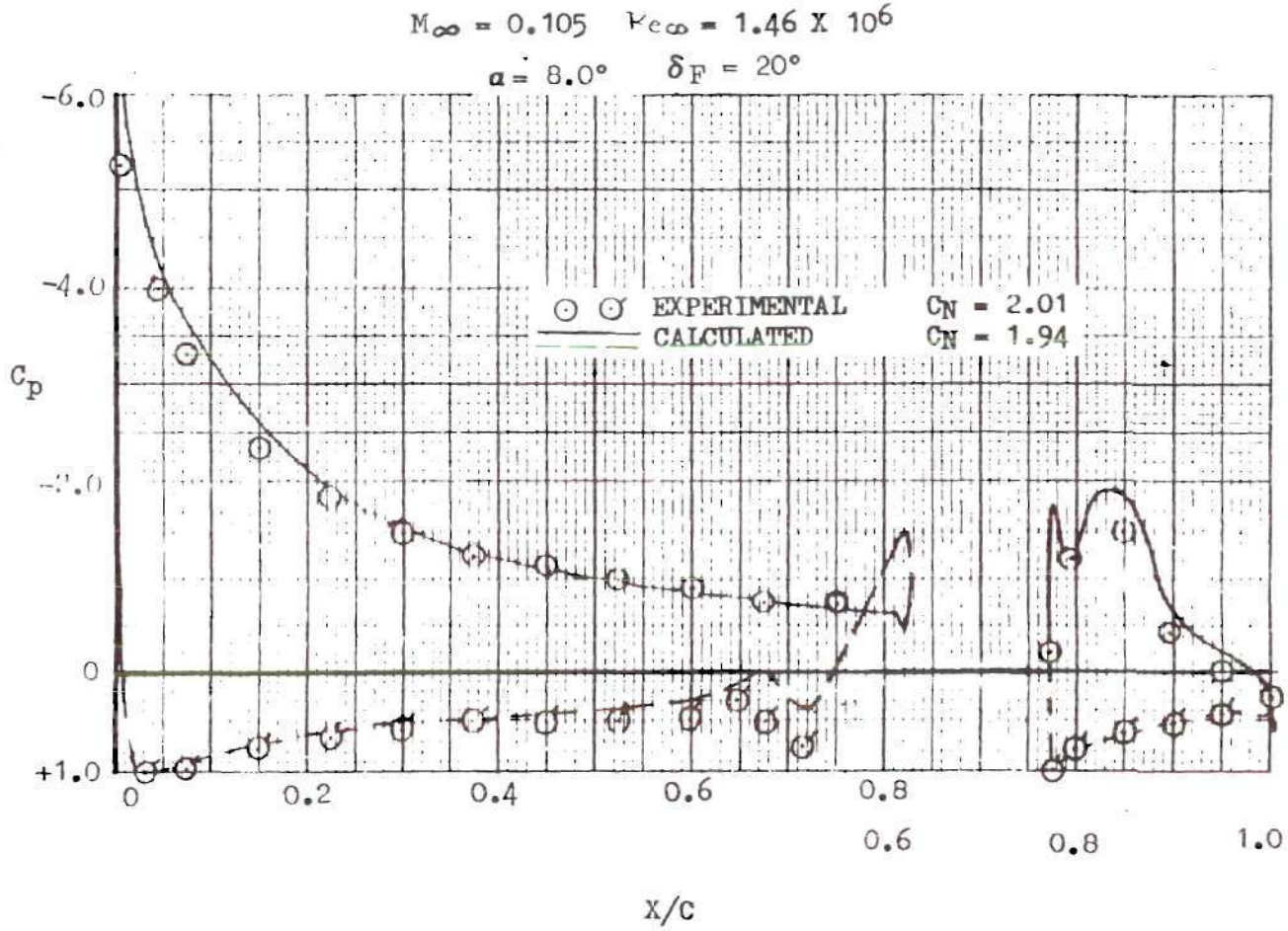

Figure 46A. Comparison of Experimental and Predicted Pressure Distributions for NACA 23012 Single Slotted Airfoil

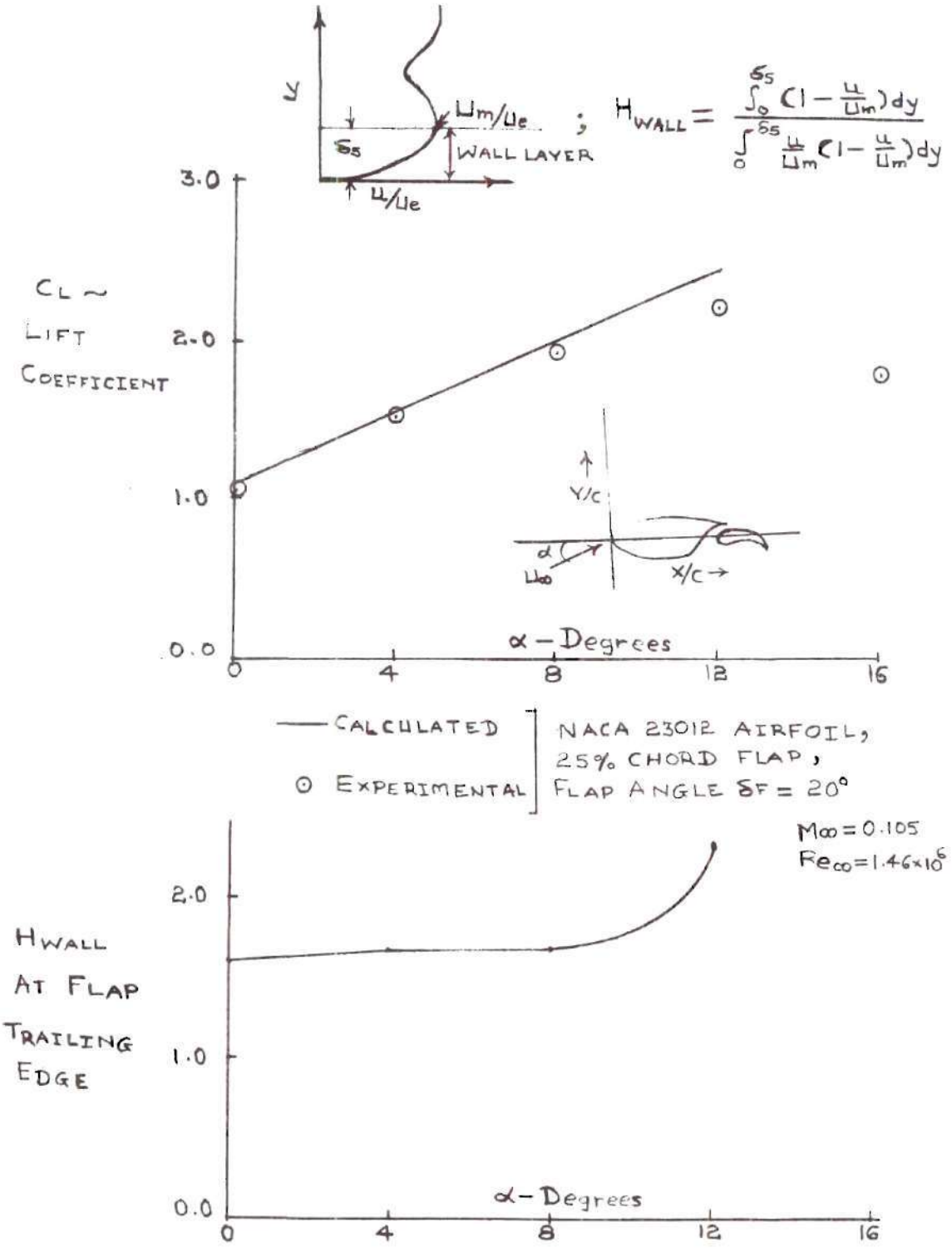

Figure 46B. Suggested $C_{L_{MAX}}$ Criteria and Correlation with NACA 23012 Single Slotted Airfoil

single slotted two piece airfoil configuration. Computed results shown in this figure are of part (B) type. This figure illustrates effectively the usefulness of confluent boundary layer calculations in conjunction with a multiple airfoil program in minimizing many times laborious and expensive wind tunnel tests for the purpose of optimizing a given airfoil configuration. The airfoil geometry and experimental data used in this correlation are from Reference (49). The airfoil consists of two components, namely, wing or main component and flap. The calculations and experimental data are for configuration (B) of Reference (49) at a constant angle of attack of zero degrees. Some interesting observations can be made from this figure, namely, (i) the zeroth iteration or potential flow lift on the flap increases with increase in the gap size, whereas the potential or inviscid lift on the wing or main component decreases as flap gap increases, and (ii) total inviscid lift, i.e. the sum of lift due to the main component and the flap, however, decreases as flap gap is increased. Experimental data for the total lift at zero angle of attack, however, shows a clear maximum at 2 percent flap gap; the maximum for the calculated viscous lift coefficient is also shown to occur at 2% flap gap. This figure illustrates that although there is some difference between the calculated and experimental value of maximum C_L the calculation results show the trends of variation of lift coefficient with gap size very well.

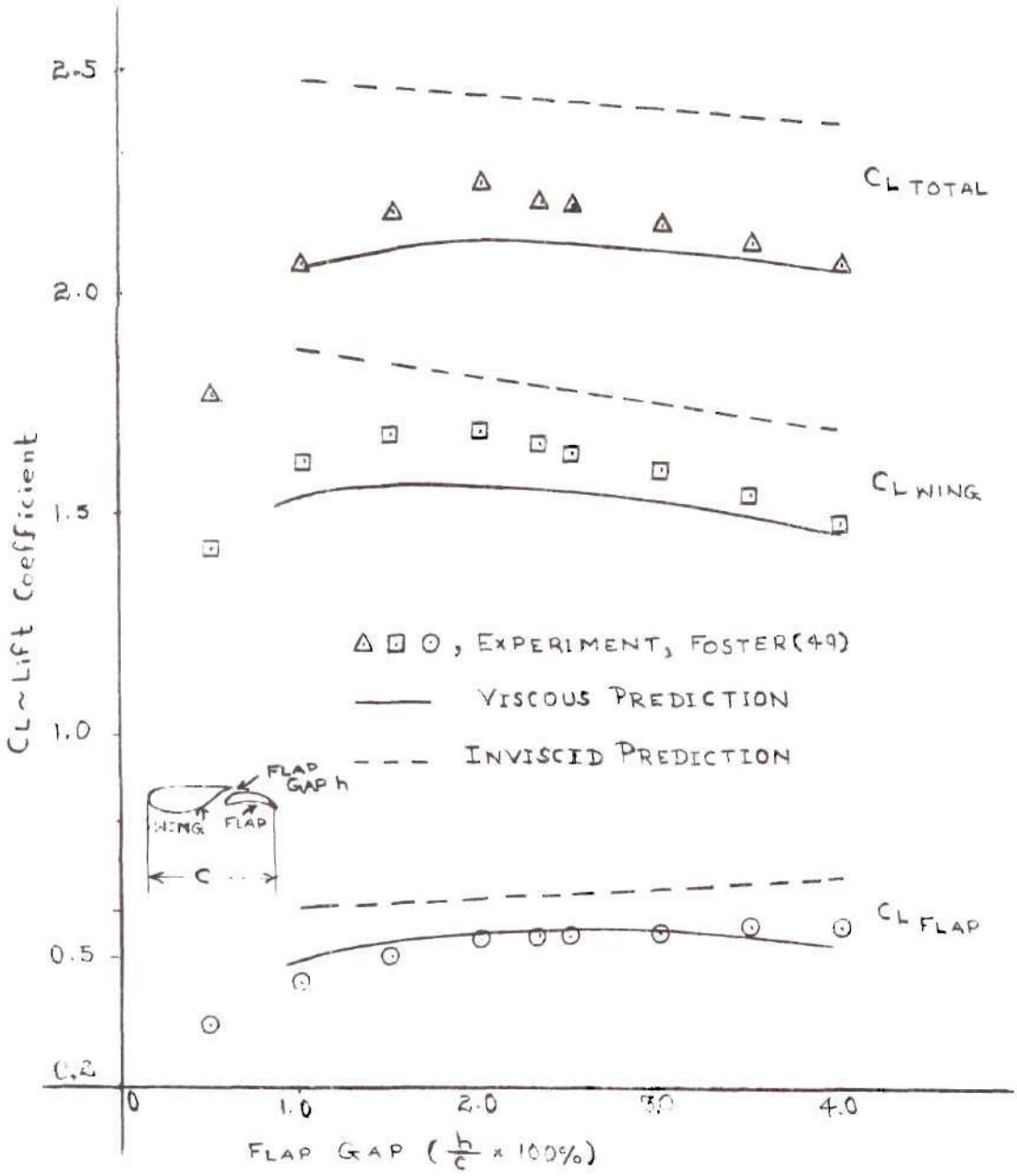

Figure 47. Comparison Between Predicted and Experimental Effect of Flap Gap on Lift Coefficient

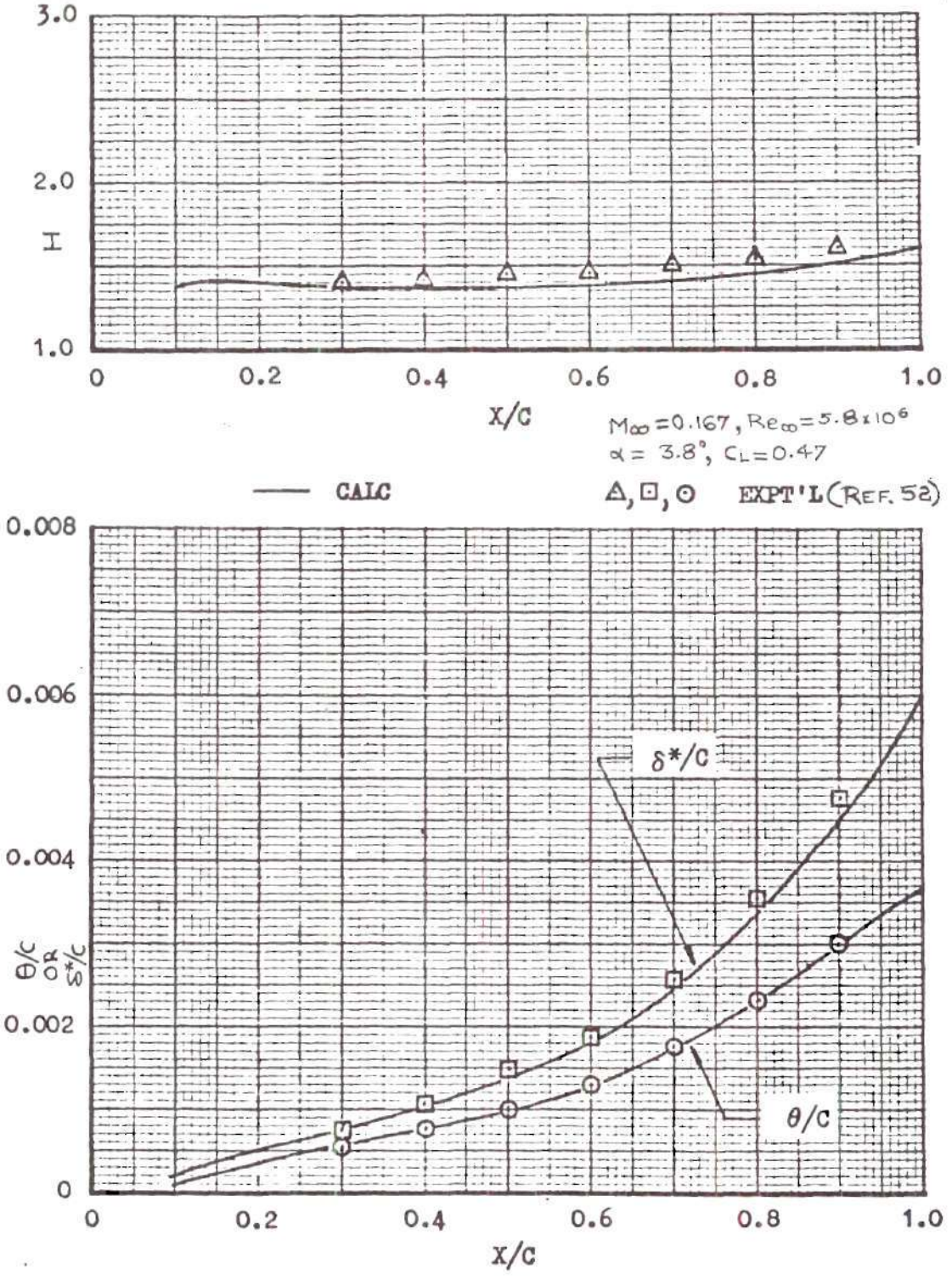

Figure 48A. Comparison of Predicted and Experimental Ordinary Turbulent Boundary Layer Parameters for NACA 63_1-012 Single Component Airfoil

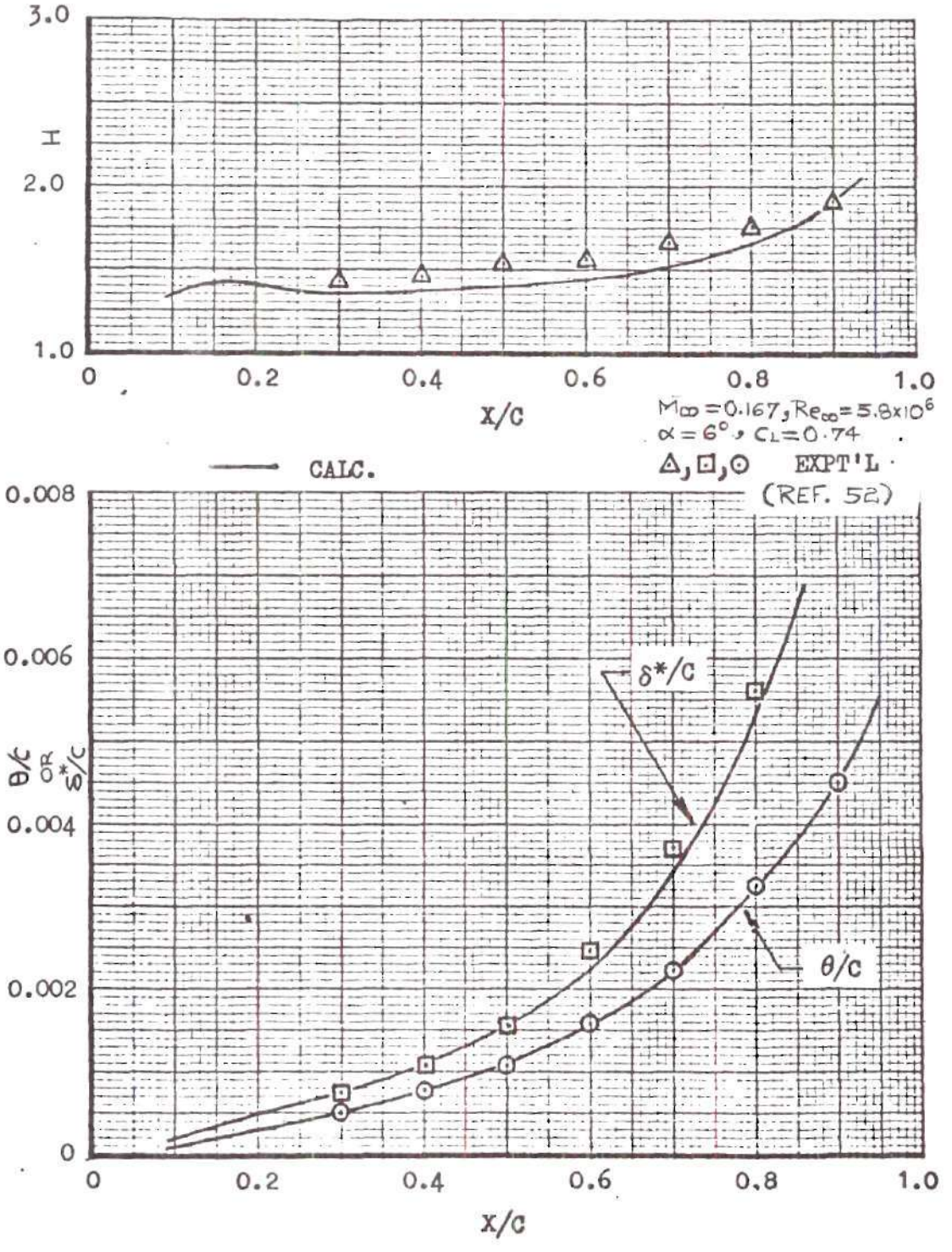

Figure 48B. Comparison of Predicted and Experimental Ordinary Turbulent Boundary Layer Parameters for NACA 63_3-018 Single Component Airfoil

CHAPTER VII

CONCLUSIONS AND RECOMMENDATIONS

Conclusions resulting from the research presented in this thesis, and recommendations for future extensions of both the theoretical and experimental results, as as follows.

Conclusions

1. Similarity of velocity profiles in the jet and wake layer is observed based on certain similarity parameters and variables. This holds true even in the presence of different pressure gradients. It is also observed, from the comparison of experimental data, that the similarity curves for free jet and free wake flow are not significantly different from those of jet and wake layer of the confluent boundary layer. The above observation facilitates derivation of an expression for calculating the profile drag of a multi-component airfoil from the confluent boundary layer quantities evaluated (or measured experimentally) at the trailing edge of a flap.

2. Wall layer velocity profiles can be represented as a one parameter family as in the case of ordinary turbulent boundary layers. However, the relation between H and $\widetilde{H}$ for the wall layer of confluent boundary layer, as observed experimentally in the initial and main regions, differs from theoretical relation derived from the assumption of power law velocity profiles. In the ordinary turbulent boundary layer region, however, the present experimental data show good comparison

with theoretical relation for H and $\bar{H}$.

3. Based on the principle of local dynamic similarity, it was possible to represent wall shear stress, wall layer shear integral and shear stress at the edge of wall layer as functions of local wall layer momentum thickness Reynold's number and local wall layer form factor for considering effects of pressure gradients. Functional relationships for skin friction coefficients, $\frac{\tau_w}{1/2\,\rho U_m^2}$, wall layer shear integral, $\int_0^{\delta_s} \frac{\tau}{\rho U_m^2} \frac{\partial}{\partial y}\left(\frac{u}{U_m}\right) dy$ and difference of wall shear at the peak velocity, $\frac{\tau_w - \tau_{(s)}}{1/2\,\rho U_m^2}$, were derived from indirect shear measurements method. Reasonable agreement is obtained for the values of these parameters computed in this study by numerical technique and direct shear measurements of other investigators. A peculiar characteristic of skin friction, and wall layer shear integral, is observed for confluent boundary layer in that it increases with local wall layer momentum thickness Reynolds number for constant value of wall layer form factor up to the point where peak velocity disappears. i.e.. up to the end of main region II. Downstream of the end of main region II, i.e., in the ordinary turbulent boundary layer region. the wall friction coefficient decreases with increasing local momentum thickness Reynolds number for constant value of form factor.

4. Generalized parameters were found for the functional representation for the shear stress at the minimum velocity point with the help of Prandtl's new shear hypothesis for free turbulent flow. These parameters consist of the product of local values of non-dimensional jet layer thickness, non-dimensional wake layer thickness, difference in velocity at the edge of wall layer and jet layer and difference in

velocity at two edges of wake layer. Functional relationship for the ratio of shear at minimum velocity point to the wall shear and the above parameters consisting of dependent variables was established from present experiments from the indirect shear measurement.

5. Shear stress profiles, calculated by numerical methods, are similar in shape and characteristics to those measured experimentally by various investigators. The value of shear stress changes sign in the neighborhood of the edge of the wall layer. The maximum value of negative shear stress which is reached in the neighborhood of wall layer depends greatly upon X location from slot exit. Value of negative shear is maximum in initial region and progressively decreases in downstream direction. Value of shear stress in the core of the initial region remains constant at near a value of zero. The magnitude of shear at the minimum velocity point may vary from a large positive value near slot exit to slight negative value farther away from slot exit when depression in velocity profile is small.

6. An analytical expression for eddy viscosity distribution was derived for ordinary turbulent boundary layer with zero pressure gradient. Eddy viscosity distribution calculated from this expression compares reasonably well with the measurements of other investigators. However, for the complex viscous confluent boundary layer flow with arbitrary initial and boundary conditions, any attempt to derive analytical expression for eddy viscosity distribution is meaningless. Hence for few conditions of Table I, eddy viscosity distributions were computed by numerical methods. Numerical computations reveal that the maximum value of the ratio of eddy viscosity, $\frac{\epsilon}{\upsilon}$, varies from a value of 100 to

approximately 350, depending upon X location, slot exit velocity ratio and pressure distribution. These large values of the ratio indicate that diffusion of mass and momentum due to turbulent fluctuations is much larger than that caused by molecular action.

7. For confluent boundary layer with zero pressure gradient, wall shear stress can be computed by making use of Clauser's chart. Wall shear stress computed in this manner compares reasonably well with present indirect shear stress computation method, as well as with the expression for wall shear given by Bradshaw [5] and Sigalla [37].

8. For confluent boundary layer with zero pressure gradient, values of shear work integrals for wall layer and jet layer for different velocity ratio $\frac{U_{c(o)}}{U_{e(o)}}$ at slot exit fall on the same curve when shear integral is non-dimensionalized in certain manner. Proper nondimensionalizing parameters for wall layer shear integral were found to be wall shear stress, τ_w, and the velocity, U_m, at the edge of wall layer. Proper non-dimensionalizing parameters for jet layer shear integrals were found to be local wall shear, τ_w, and difference in peak and free stream velocity, $(U_m - U_e)$.

9. Results of computation of the multi-layer integral method, presented in this research for the prediction of confluent boundary layer flow with arbitrary initial conditions and pressure distribution, compare reasonably with experimental measurements. Results of computations of the present method are compared with both the present experiments and also with the confluent boundary layer experimental data on the upper surface of flap of two component airfoils.

10. Computations as well as experimental data show that the

confluent boundary layer which develops on the upper surface of the flap is very thick as compared to the ordinary turbulent boundary layer which develops on the forward component of two component airfoil. As a result large viscous correction of 20 to 30 percent in lift coefficient is encountered on two component airfoils.

11. It is shown that with the incorporation of confluent boundary layer method in multiple airfoil computer program, realistic pressure distribution and lift coefficient is predicted. It is also shown possible to perform gap-optimization for the computation of most desirable gap size at the slot exit for a given two component airfoil configuration; that is, desirable in order to eliminate or minimize expensive wind tunnel testing to arrive at proper airfoil configuration.

Recommendations

1. The analytical model developed here is valid only in the speed range where the flow can be considered incompressible. This model, which can be used for application to boundary layer control range of internally or externally blown systems of STOL aircraft configuration, needs to be extended to take into account effects of compressibility for application to supercirculation range of STOL aircraft configuration as well as for transonic maneuvering.

2. Research, both experimental and analytical, is needed for more complex confluent boundary layer which develops on three component airfoil or four component airfoil with short chord vane. In this case more than three layers, i.e., wall layer, jet layer and wake layer, are present.

3. In the case of externally blown flap high lift system with hot gases entering the slot from engine exhaust, the effects of high temperature may become important in affecting flow and separation phenomena. Thus both experimental and analytical efforts should be expended to study effect of high temperature on skin friction, separation and other related characteristics of confluent boundary layer with arbitrary pressure distributions.

APPENDIX

DETAILED DERIVATION OF EQUATIONS IN MAIN REGION I BETWEEN STATIONS 1 AND 2

A summary of assumptions, boundary conditions, brief derivations and resulting equations was given in Chapter III in order to present the important points of the theory for calculating relevant physical quantities for the confluent boundary layer flow shown schematically in Figure (1). In this section a detailed derivation of the equations for main region I will be presented. This procedure is typical for the derivation of the resulting equations in the other regions.

Wall-Layer

A one parameter family of velocity profiles is assumed for the wall layer. With this assumption the effect of pressure gradient on the wall-layer is taken into account. This is not the case with the assumption of similar velocity profiles for the wall layer. In particular assume profiles of the form,

$$\frac{u}{U_m} = \left(\frac{y}{\delta_5}\right)^{1/n_2} = \left(\frac{y}{\delta_5}\right)^{2/(H-1)} \tag{123}$$

The following relations can be derived from the definitions and by the use of equation (123),

$$\delta_5^* = \int_0^{\delta_5} \left(1 - \frac{u}{U_m}\right) dy \quad ; \quad \theta_5 = \int_0^{\delta_5} \frac{u}{U_m}\left(1 - \frac{u}{U_m}\right) dy \qquad (124)$$

$$H_5 = \delta^*/\theta_5 \quad ; \quad \delta_5^{**} = \int_0^{\delta_5} \frac{u}{U_m}\left\{1 - \left(\frac{u}{U_m}\right)^2\right\} dy \quad ; \quad \tilde{H}_5 = \frac{\delta_5^{**}}{\theta_5}$$

$$\frac{u}{U_m} = \left(\frac{y}{\delta_5}\right)^{\frac{1}{n_2}} \quad ; \quad \frac{\theta_5}{\delta_5} = \frac{(H_5 - 1)}{H_5 (H_5 + 1)} = \frac{n_2}{(n_2+1)(n_2+2)}$$

$$\tilde{H}_5 = \frac{4 - H_5}{(3H_5 - 1)} \quad ; \quad n_2 = \frac{2}{(H_5 - 1)} \quad ; \quad \frac{n_2}{n_2+1} = \frac{2}{(H_5+1)}$$

$$\delta_5 \cdot \frac{n_2}{(n_2+1)} = 2\theta_5 \frac{H_5}{H_5 - 1}$$

Integrate equation (4) from y = 0 to y = δ_5 and substitute equation (10) to obtain the following equation,

$$\int_0^{\delta_5} u \frac{\partial u}{\partial x} dy - \left\{ \int_0^{\delta_5} \frac{\partial u}{\partial x} \left(\int_0^{\delta_5} \frac{\partial u}{\partial x} dy \right) dy \right\} = \int_0^{\delta_5} - \frac{1}{\rho} \frac{dP}{dx} dy + \int_0^{\delta_5} \frac{1}{\rho} \frac{\partial \tau}{\partial y} dy \qquad (125)$$

The applicable boundary conditions for equation (125) are,

$$\text{at } y = 0 : \quad u = 0 \; , \; v = 0 \; , \; \tau = \tau_w \qquad (126)$$

$$\text{at } y = \delta_5 : \quad u = U_m \; , \; \tau = \tau_{(\delta_5)} \; .$$

Replace the pressure terms in equation (3) by the Euler equation,

$$- \frac{1}{\rho} \frac{dP}{dx} = U_e \frac{dU_e}{dx} \qquad (127)$$

Simplify each term of equation (125) by making use of equation (123) as follows,

$$\int_{s_0}^{s_1} \frac{\partial N_e}{\partial n} \left\{ N_e \frac{\partial x_e}{\partial n} \right\} dn \qquad (128)$$

$$= -\left[\int_{s_0}^{s_1} \frac{\partial x_e}{\partial n} \cdot n \, N_e - \int_{s_0}^{s_1} N_e \frac{\partial x_e}{\partial n} \, dn \right] =$$

$$= -\left[n \int_{s_0}^{s_1} N_e \frac{\partial x_e}{\partial n} - \int_{s_0}^{s_1} \left(\int \frac{\partial x_e}{\partial n} \, dn \right) \frac{\partial N_e}{\partial n} \, dn \right] =$$

$$= -n \int_{s_0}^{s_1} N_e \frac{\partial x_e}{\partial n} + \int_{s_0}^{s_1} \left(\int \frac{\partial x_e}{\partial n} \, dn \right) \frac{\partial N_e}{\partial n} \, dn$$

and

$$\int_{s_0}^{s_1} N_e \frac{\partial x_p}{\partial t} \, dx = n_e \cdot \frac{dn_p}{dx} \cdot \delta_s \qquad (129)$$

$$\int_{s_0}^{s_1} N_e \frac{\partial}{\partial t} \left(\frac{1}{L_e} \right) = \frac{\partial}{\partial t} \left\{ \frac{1}{L_{(s_2)} - L_{(s_1)}} \right\} \qquad (130)$$

Substituting equations (128), (129) and (130) into (125) and rearranging,

$$- \frac{\partial}{\partial t} \left\{ \frac{1}{L_{(s_2)} - L_{(s_1)}} \right\} \qquad (131)$$

$$= \int_{s_0}^{s_1} \rho \, n \cdot \frac{\partial x_e}{\partial t} \, dx - n_e \cdot \frac{dn_p}{dx} \cdot \delta_s$$

$$= \left\{ \int_{s_0}^{s_1} \rho \frac{\partial u_n}{\partial t} \, n \, dx \right\} + \left\{ \rho (u_n n) \frac{\partial x_e}{\partial t} \right\}_{s_0}^{s_1} - \left\{ \rho (n^2) \frac{\partial x_e}{\partial t} \right\}_{s_0}^{s_1}$$

$$- n_e \cdot \frac{dn_p}{dx} \delta_s \Big\}$$

$$= \left[\int_0^{\delta_5} \frac{\partial}{\partial x}\{u(u-U_m)\}dy\right] + \left[\{\int_0^{\delta_5} u\frac{\partial U_m}{\partial x}dy\}\right.$$

$$\left. - U_e\frac{dU_e}{dx}\right]$$

$$= \left[\int_0^{\delta_5} \frac{\partial}{\partial x}\{u(u-U_m)\}\right] - \left(\frac{d\delta_5}{dx}\right)\{u(u-U_m)\}\Big|_{y=\delta_5}$$

$$+ \left[\{\int_0^{\delta_5} u.\frac{dU_m}{dx}dy\} - U_e\frac{dU_e}{dx}\delta_5\right]$$

$$= \left[-\frac{d}{dx}\{U_m^2\int_0^{\delta_5}\frac{u}{U_m}(1-\frac{u}{U_m})dy\} + \{\int_0^{\delta_5} u\frac{dU_m}{dx}dy - U_e\frac{dU_e}{dx}\delta_5\right]$$

$$= \left[-\frac{d}{dx}\{U_m^2\theta_5\} + \{U_m\frac{dU_m}{dx}\int_0^{\delta_5}\frac{u}{U_m}dy\} - \{U_e\frac{dU_e}{dx}\delta_5\}\right]$$

$$= \left[-U_m^2\frac{d\theta_5}{dx} - 2\theta_5 U_m\frac{dU_m}{dx} + \frac{\delta_5 U_m}{(\frac{n_{z+1}}{n_z})}\frac{dU_m}{dx}\left\{\left(\frac{y}{\delta_5}\right)^{\frac{n_{z+1}}{n_z}}\right\}_0^1\right.$$

$$\left. - U_e\frac{dU_e}{dx}\delta_5\right] .$$

or

$$\frac{\tau_w}{\rho U_m^2}\left\{1 - \frac{\tau_{(\delta_5)}}{\tau_w}\right\} \qquad (131A)$$

$$= \left[\frac{d\theta_5}{dx} + 2\theta_5\cdot\frac{1}{U_m}\frac{dU_m}{dx} - \delta_5\cdot\frac{n_z}{n_{z+1}}\cdot\frac{1}{U_m}\cdot\frac{dU_m}{dx}\right.$$

$$\left. + \frac{U_e}{U_m^2}\cdot\frac{dU_e}{dx}\cdot\delta_5\right]$$

$$= \left[\frac{d\theta_5}{dx} - 2\frac{\theta_5}{(H_5-1)}\cdot\frac{1}{U_m}\cdot\frac{dU_m}{dx} + \{\frac{U_e}{U_m^2}\cdot\frac{dU_e}{dx}\cdot\theta_5\right.$$

$$\left.\cdot\frac{(H_5)(H_5+1)}{(H_5-1)}\}\right]$$

Equation (131A) is the integral momentum equation for the wall layer in the main region I.

Form factor equation for the wall-layer in main region I.

Multiplying both sides of equation (4) by u and integrating from $y = 0$ to $y = \delta_5$ and then substituting into equation (10) results in the following equation:

$$\int_0^{\delta_5} \frac{\partial}{\partial x}\left(\rho u^2 \frac{\lambda_e}{\lambda_p}\right) dy + \int_0^{\delta_5} \rho v \frac{\lambda_e}{\lambda_p} \frac{\partial u}{\partial \eta} d\eta = \int_0^{\delta_5} \rho \frac{\partial}{\partial x}\left(\frac{\lambda_e}{\lambda_p} \int_0^{\eta} u \, d\eta\right) d\eta - \int_0^{\delta_5} \rho \frac{\partial u}{\partial x} d\eta \tag{132}$$

Perform the following operations on each term of equation (132) as follows:

$$\int_0^{\delta_5} \rho u^2 \frac{\partial}{\partial x}\left(\frac{\lambda_e}{\lambda_p}\right) dy = \int_0^{\delta_5} \rho u^2 \frac{\partial}{\partial x}\left(\frac{\lambda_e}{\lambda_p} \int_0^{\eta} d\eta\right) dy \tag{133}$$

$$= \int_0^{\delta_5} \rho u^2 \frac{\partial}{\partial x}\left(\frac{\lambda_e}{\lambda_p} \eta_{\delta_5}\right) dy$$

$$= \int_0^{\delta_5} \rho u^2 \frac{\partial}{\partial x}\left(\frac{\lambda_e}{\lambda_p}\right) \eta_{\delta_5} dy + \int_0^{\delta_5} \rho u^2 \frac{\lambda_e}{\lambda_p} \frac{\partial \eta_{\delta_5}}{\partial x} dy$$

and

$$\int_0^{\delta_5} \rho v \frac{\lambda_e}{\lambda_p} \frac{\partial u}{\partial \eta} d\eta \tag{134}$$

$$= \left[\rho v \frac{\lambda_e}{\lambda_p} u\right]_0^{\delta_5} - \int_0^{\delta_5} \rho u \frac{\partial}{\partial \eta}\left(\frac{\lambda_e}{\lambda_p} v\right) d\eta$$

$$= \left[\rho v \frac{\lambda_e}{\lambda_p} u\right]_0^{\delta_5} - \int_0^{\delta_5} \rho u \frac{\partial}{\partial \eta}\left(\frac{\lambda_e}{\lambda_p} v\right) d\eta$$

$$= \left[\rho v \frac{\lambda_e}{\lambda_p} u\right]_0^{\delta_5} - \int_0^{\delta_5} \rho u \frac{\partial}{\partial \eta}\left(\frac{\lambda_e}{\lambda_p} v\right) d\eta$$

Substituting equation (133) and (134) in (132) and simplifying,

$$\frac{\partial}{\partial x}\int_0^{\delta_5} u^2\,dy - \frac{U_m^2}{2}\int_0^{\delta_5}\frac{\partial u}{\partial x}\,dy - U_e\frac{dU_e}{dx}\int_0^{\delta_5} u\,dy = \frac{1}{\rho}\tau_{(\delta_5)} - \frac{1}{\rho}\int_0^{\delta_5}\frac{\partial \tau}{\partial y}\,dy \qquad (135)$$

Rearrange the terms in equation (135) and simplify as follows:

$$\frac{1}{\rho}\tau_{(\delta_5)} - \frac{1}{\rho}\int_0^{\delta_5}\frac{\partial \tau}{\partial y}\,dy \qquad (136)$$

$$= \left[\frac{1}{2}\int_0^{\delta_5}\frac{\partial}{\partial x}(u^2)\,dy - \frac{1}{2}\int_0^{\delta_5}\frac{\partial}{\partial x}(uU_m)\,dy\right.$$

$$\left. + \int_0^{\delta_5}\frac{\partial p}{\partial x}\,dy - \int_0^{\delta_5}\frac{dU_e}{dx}\,dy\right]$$

$$= \left[\frac{1}{2}\int_0^{\delta_5}\frac{\partial}{\partial x}(u(u^2-uU_m))\,dy + \left\{\int_0^{\delta_5}\frac{\partial p}{\partial x}\,dy\right\}\right.$$

$$\left. U_m\frac{dU_m}{dx} - U_e\frac{dU_e}{dx}\right]$$

$$= \left[\frac{1}{2}\frac{d}{dx}\left\{U_m^3\int_0^{\delta_5}\frac{u}{U_m}\left(\frac{u^2}{U_m^2}-1\right)dy\right\} + U_m\left\{\int_0^{\delta_5}\right.\right.$$

$$\left.\left.\int_0^1 \frac{u}{U_m}\,d\left(\frac{y}{\delta_5}\right)\right\}\cdot\left\{U_m\frac{dU_m}{dx} - U_e\frac{dU_e}{dx}\right\}\right]$$

$$= \left[-\frac{1}{2}\frac{d}{dx}\left\{U_m^3\delta_5^{**}\right\} + U_m\delta_5\left\{\int_0^1\left(\frac{y}{\delta_5}\right)^{\frac{1}{n}}d\left(\frac{y}{\delta_5}\right)\right\}\right.$$

$$\left.\cdot\left\{U_m\frac{dU_m}{dx} - U_e\frac{dU_e}{dx}\right\}\right]$$

$$= \left[-\frac{1}{2}U_m^3\frac{d\delta_5^{**}}{dx} - \frac{1}{2}\delta_5^{**}3U_m^2\frac{dU_m}{dx}\right.$$

$$\left. + U_m\delta_5\left(\frac{n}{n+1}\right)\left\{U_m\frac{dU_m}{dx} - U_e\frac{dU_e}{dx}\right\}\right]$$

$$= \left[-\frac{1}{2}U_m^3\frac{d}{dx}(\tilde{H}_5\theta_5) - \frac{3}{2}\tilde{H}_5\theta_5U_m^2\frac{dU_m}{dx}\right.$$

$$\left. + 2\theta_5\frac{H_5}{(H_5-1)}U_m\left\{U_m\frac{dU_m}{dx} - U_e\frac{dU_e}{dx}\right\}\right]$$

$$= \left[-\frac{1}{2} U_m^3 \theta_5 \frac{d(\tilde{H}_5)}{dx} - \frac{2}{5} U_m^3 \frac{H_5}{(3H_5-1)} \frac{d\theta_5}{dx} \right.$$

$$+ 2\theta_5 \frac{H_5}{(H_5-1)} U_m^2 \frac{dU_m}{dx} - 6 \frac{H_5}{(3H_5-1)} \cdot \theta_5 U_m^2 \frac{dU_m}{dx}$$

$$\left. - 2\theta_5 \frac{H_5}{(H_5-1)} U_m U_e \frac{dU_e}{dx} \right]$$

$$= \left[2U_m^3 \theta_5 \frac{1}{(3H_5-1)^2} \frac{dH_5}{dx} - \frac{1}{2} U_m^3 \frac{4H_5}{(3H_5-1)} \frac{d\theta_5}{dx} \right.$$

$$- \frac{6H_5}{3H_5-1} \theta_5 U_m^2 \frac{dU_m}{dx} + 2\theta_5 \frac{H_5}{(H_5-1)} U_m^2 \frac{dU_m}{dx}$$

$$\left. - 2\theta_5 \frac{H_5}{(H_5-1)} U_m U_e \frac{dU_e}{dx} \right] .$$

Thus,

$$\frac{dH_5}{dx} - (H_5)(3H_5-1) \frac{1}{\theta_5} \frac{d\theta_5}{dx} - 3(H_5)(3H_5-1) \frac{1}{U_m} \cdot \frac{dU_m}{dx} \qquad (137)$$

$$+ (3H_5-1)^2 \left(\frac{H_5}{H_5-1} \right) \frac{1}{U_m} \frac{dU_m}{dx} - (3H_5-1)^2 \left(\frac{H_5}{H_5-1} \right) \frac{1}{U_m^2} U_e \frac{dU_e}{dx}$$

$$= \left[\frac{(3H_5-1)^2}{\rho U_m^2} \cdot \frac{1}{2\theta_5} \cdot \tau_w \frac{\tau_{(\delta_5)}}{\tau_w} - \frac{1}{\rho U_m^2} \cdot \left\{ \frac{1}{2\theta_5} \cdot (3H_5-1)^2 \right. \right.$$

$$\left. \left. \cdot \tau_w \int_0^{\delta_5} \frac{\tau}{\tau_w} \frac{\partial}{\partial y} \left(\frac{u}{U_m} \right) dy \right\} \right] .$$

After simplification of the above equation,

$$\frac{dH_5}{dx} = \left[\frac{H_5}{\theta_5} (3H_5-1) \left(\frac{\tau_w}{\rho U_m^2} \right) + \left(\frac{H_5-1}{2\theta_5} \right) (3H_5-1) \left(\frac{\tau_w}{\rho U_m^2} \right) \left(\frac{\tau_{(\delta_5)}}{\tau_w} \right) \right. \qquad (138)$$

$$- \frac{U_e}{U_m^2} \cdot \frac{dU_e}{dx} \cdot (H_5)(3H_5-1)(H_5-1) - \left\{ \frac{(3H_5-1)^2}{2\theta_5} \right.$$

$$\left. \left. \cdot \left\{ \int_0^{\delta_5} \frac{\tau}{\rho U_m^2} \cdot \frac{\partial}{\partial y} \left(\frac{u}{U_m} \right) dy \right. \right. \right. .$$

Thus equation (16) is the form factor equation for the wall-layer in main region I.

Derivation of equations for jet-layer in the main region I.

Let $U_{w(x)}$ = velocity at $y = \delta_3$ as shown in Figure(1).

Assume "similar velocity profiles" in the jet layer as follows:

$$\eta_3 = \frac{\delta_3 - y}{\delta_3 - \delta_5} \quad ; \quad f(\eta_3) = \frac{U_m - u}{U_m - U_w} \tag{139}$$

$$y = \delta_3 - (\delta_3 - \delta_5)\eta_3 \quad ; \quad dy = -(\delta_3 - \delta_5)d\eta_3$$

$$u = U_m - (U_m - U_w) f(\eta_3)$$

$$\frac{u - U_w}{U_m - U_w} = 1 - f(\eta_3) \quad .$$

Applicable boundary conditions for the jet layer in main region I are:

$$y = \delta_5 : \quad u = U_m, \ \eta_3 = 1.0 \ ; \ f(\eta_3) = 0.0 \tag{140}$$

$$y = \delta_3 : \quad u = U_w, \ \eta_3 = 0.0 \ ; \ f(\eta_3) = 1.0 \quad .$$

Integrating equation (4) from $y = \delta_5$ to $y = \delta_3$ and using equations (8) and (10) one obtains the following:

$$\int_{\delta_5}^{\delta_3} u \frac{\partial \rho u}{\partial x} dy - \int_{\delta_5}^{\delta_3} \left\{ \frac{\partial \rho v}{\partial y} \left(\int_0^y \frac{\partial \rho u}{\partial x} dy \right) \right\} dy = \int_{\delta_5}^{\delta_3} U_e \frac{dU_e \rho}{dx} dy + \frac{1}{e} \int_{\delta_5}^{\delta_3} \frac{\partial \tau}{\partial y} dy \tag{141}$$

The second term on the left hand side of equation (140) can be simplified as follows:

Substitute equation (20) into (12) and rearrange to get,

(143)

Perform the following operations on the terms of equation (143):

(144)

$$= \left[\frac{\partial}{\partial x}\left\{\int_{\delta_s}^{\delta_3} u(u-U_w)dy\right\} + \frac{dU_w}{dx}\int_{\delta_s}^{\delta_3} u\,dy\right.$$

$$\left. - \left\{u(u-U_w)\Big|_{y=\delta_3} + \left(\frac{d\delta_3}{dx}\right)\left\{u(u-U_w)\Big|_{y=\delta_s}\right\}\left(\frac{dp}{dx}\right)\right\}\right]$$

$$= \frac{\partial}{\partial x}\int_{\delta_s}^{\delta_3} u(u-U_w)dy + \left(\frac{d\delta_3}{dx}\right)(U_m)(U_m-U_w)$$

$$+ \frac{dU_w}{dx}\int_{\delta_s}^{\delta_3} u\,dy \,.$$

and

$$\frac{\partial}{\partial x}\left\{\int_{\delta_s}^{\delta_3} u(u-U_w)dy\right\} \qquad (145)$$

$$= \frac{\partial}{\partial x}\left[\int_0^1 \{U_m - (U_m-U_w)f(\eta_3)\}\{(U_m-U_w)\cdot(1-\right.$$

$$\left. f(\eta_3)\}\{-(\delta_3-\delta_s)\}\cdot\{(\varepsilon\eta_3)f\right]$$

$$= \frac{\partial}{\partial x}\left[(U_m-U_w)(\delta_3-\delta_s)\int_0^1 \{U_m(1-f(\eta_3)) -\right.$$

$$\left. (\varepsilon\eta_3 f - 1)U_w\}(U_m-U_w)f(\eta_3) + (U_m-U_w)f(\eta_3)\right]$$

$$= \left\{\int_0^1 (1-f(\eta_3))d\eta_3\right\}\cdot\left[\frac{dp}{dx}\left\{U_m(U_m-U_w)(\delta_3-\delta_s)\right\}\right]\cdot\{\varepsilon\eta_3 p(\varepsilon\eta_3)f -$$

$$\left. - \left\{\int_0^1 f(\eta_3)d\eta_3\right\}\left[\frac{dp}{dx}\left\{(U_m-U_w)^2(\delta_3-\delta_s)\right\}\right]\{\varepsilon\eta_3 p(\varepsilon\eta_3)f -\right.$$

$$\left. + \left\{\int_0^1 f^2(\eta_3)d\eta_3\right\}\left[\frac{dp}{dx}\left\{(U_m-U_w)^2(\delta_3-\delta_s)\right\}\right]\{\varepsilon\eta_3 p(\varepsilon\eta_3)f\right] \,.$$

and

$$\left\{\frac{dU_w}{dx}\int_{\varepsilon_p}^{\delta_p} u\,dy\right\} \tag{146}$$

$$= \frac{dU_w}{dx}\int_0^1 \{U_m - (U_m - U_w)f(\eta_3)\}\cdot\{-(\delta_p-\varepsilon_p)\}\,d\eta_3$$

$$= \left[\varepsilon_{up}\{(\varepsilon_{up})f(M_\eta - w_\eta)\}\cdot\int_0^1\right]\cdot(\delta_p-\varepsilon_p)\left(\frac{x_p}{M_\eta p}\right) =$$

$$= \left(\frac{x_p}{M_\eta p}\right)(w_\eta)(\delta_p-\varepsilon_p) - \left\{\left(\frac{x_p}{M_\eta p}\right)(\delta_p-\varepsilon_p)\right.$$

$$\left.\varepsilon_{up}(\varepsilon_{up})f\cdot(M_\eta - w_\eta)\cdot\int_0^1\right.$$

Now,

$$\left\{(U_m - U_w)\int_{\varepsilon_p}^{\delta_p}\frac{x_p}{M_\eta p}dy\right\} \tag{147}$$

$$= (U_m - U_w)\left[\frac{x_p}{M_\eta p}\left\{\int_0^{\delta_p} u\,dy\right\}\right](M_\eta - w_\eta) - \left[w_\eta\left(\frac{x_p}{\delta_p p}\right)\right.$$

$$= (U_m - U_w)\left[\frac{x_p}{M_\eta p}\left\{U_m\cdot\int_0^{\frac{\delta_p}{\delta_p}}\left(\frac{w_\eta}{U_m}\right)dy\right\}\right](M_\eta - w_\eta) =$$

$$\left[\frac{x_p}{\delta_p p}w_\eta - \left\{\frac{1+u}{u}\delta_p w_\eta\right\}\right]$$

$$= \left[(U_m - U_w)\left\{\delta_p\frac{1+u}{u}\cdot\frac{dU_m}{dx}p + U_m\left(\frac{1+u}{u}\right)\cdot\frac{x_p}{\delta_p p}\right\}(M_\eta - w_\eta)\right] =$$

$$\left[\left\{\frac{x_p}{\delta_p p}\cdot w_\eta - \left(\frac{1+u}{u}\right)\frac{x_p}{p}\delta_p w_\eta + U_m\cdot\frac{\delta_p p}{x_p}\right\}\right.$$

$$= \left[(U_m - U_w)\left\{2\frac{\theta_5 H_5}{(H_5-1)}\frac{dU_m}{dx}p + \frac{U_m}{2}\frac{(1+5H)}{w_\eta}\right\}(M_\eta - w_\eta)\right] =$$

$$\left[\left\{\frac{x_p}{\delta_p p}w_\eta - \left(\frac{1+5H}{2}\right)\frac{x_p}{p}\delta_p w_\eta + U_m\delta_p\frac{x_p}{\delta_p p}\right.\right.$$

$$= \left[(U_m - U_w)\left\{2\frac{\theta_5 H_5}{(H_5-1)}\cdot\left(\frac{x_p}{w_\eta p}\right) + U_m\left(\frac{x_p}{\delta_p p}\right)\left(\frac{1+5H}{5H-1}\right)\right.\right.$$

$$\left.\left.+2U_m\delta_5\frac{1}{(H_5+1)^2}\cdot\left(-\frac{\delta H_5}{p}\right)\right\}\right] .$$

Substituting in equation (147), the previously derived relations for δ_5 in terms of θ_5 and H_5 one obtains,

$$\therefore \{(U_m - U_w) \cdot \int_0^{\delta_5} \frac{\partial u}{\partial x} dy\} \qquad (148)$$

$$= -(U_m - U_w)\left[2\theta_5 \frac{H_5}{(H_5-1)} \frac{dU_m}{dx} - U_m \frac{(H_5-1)}{(H_5+1)}\right.$$

$$\left. \cdot \frac{d}{dx}\left\{\theta_5 \frac{(H_5^2+H_5)}{(H_5-1)}\right\} + 2U_m\delta_5 \frac{1}{(H_5+1)^2}\left(-\frac{dH_5}{dx}\right)\right]$$

$$= -(U_m - U_w)\left[2\theta_5 \frac{H_5}{(H_5-1)} \cdot \frac{dU_m}{dx} - U_m H_5 \frac{d\theta_5}{dx}\right.$$

$$- (U_m)\left(\frac{H_5-1}{H_5+1}\right)\theta_5 \frac{d}{dx}\left(\frac{H_5^2+H_5}{(H_5-1)}\right) - 2\left\{U_m \theta_5 (H_5^2+H_5)\right\}$$

$$\left. \cdot \left\{\frac{1}{(H_5+1)^2} \cdot \frac{dH_5}{dx}\right\}\right]$$

$$= 2(U_m - U_w)\theta_5 \frac{H_5}{H_5-1} \frac{dU_m}{dx} - U_m(U_m - U_w)H_5 \frac{d\theta_5}{dx}$$

$$- U_m(U_m - U_w)\theta_5 \frac{dH_5}{dx} \frac{1}{(H_5^2-1)} \left\{H_5^2 - 2H_5 - 1 + 2H_5\right\}$$

$$= 2(U_m - U_w)\theta_5 \frac{H_5}{H_5-1} \frac{dU_m}{dx} - U_m(U_m - U_w)H_5 \frac{d\theta_5}{dx}$$

$$- U_m(U_m - U_w)\theta_5 \frac{dH_5}{dx} .$$

Further simplifying the terms in above equation,

$$\therefore \left\{(U_m-U_w)\int_0^{\delta_5}\frac{\partial y}{\partial x}\,dy\right\} \qquad (149)$$

$$= 2(U_m-U_w)\theta_5\frac{H_5}{H_5-1}\frac{dU_m}{dx} - U_m(U_m-U_w)H_5\frac{\tau_w}{\rho U_m^2} + \{U_m$$

$$\cdot(U_m-U_w)\cdot H_5\frac{\tau_w}{\rho U_m^2}\left(\frac{\tau_{(\delta_5)}}{\tau_w}\right)\} + \{U_m(U_m-U_w)(H_5)^2\frac{(H_5+1)}{(H_5-1)}$$

$$\cdot\,\theta_5\frac{U_e}{U_m^2}\frac{dU_e}{dx}\} - \{2U_m(U_m-U_w)H_5\frac{\theta_5}{(H_5-1)}\frac{1}{U_m}\cdot\frac{dU_m}{dx}\}$$

$$-\{U_m(U_m-U_w)\theta_5\frac{H_5}{\theta_5}(3H_5-1)\left(\frac{\tau_w}{\rho U_m^2}\right)\} - \{U_m(U_m-U_w)\theta_5$$

$$\cdot\frac{(H_5-1)}{2\theta_5}(3H_5-1)\left(\frac{\tau_w}{\rho U_m^2}\right)\left(\frac{\tau_{(\delta_5)}}{\tau_w}\right)\} + \{U_m(U_m-U_w)\theta_5\frac{U_e}{U_m^2}\frac{dU_e}{dx}$$

$$\cdot\,(H_5)(3H_5-1)(H_5-1)\} + \{U_m(U_m-U_w)\theta_5\frac{(3H_5-1)^2}{2\theta_5}\int_0^{\delta_5}\frac{\tau_w}{\rho U_m^2}\frac{\partial}{\partial y}\left(\frac{u}{U_m}\right)dy\}$$

$$= \frac{U_e}{U_m}\frac{dU_e}{dx}(U_m-U_w)\frac{H_5\theta_5}{(H_5-1)}\{3H_5^3-6H_5^2+6H_5-1\} - \{U_m\cdot$$

$$(U_m-U_w)3H_5^2\left(\frac{\tau_w}{\rho U_m^2}\right)\} - \{\frac{U_m}{2}(U_m-U_w)\left(\frac{\tau_w}{\rho U_m^2}\right)\cdot\left(\frac{\tau_{(\delta_5)}}{\tau_w}\right)$$

$$\cdot(3H_5^2-6H_5+1)\} + \{\frac{U_m}{2}(U_m-U_w)\cdot(3H_5-1)^2\cdot$$

$$\left(\int_0^{\delta_5}\frac{\tau}{\rho U_m^2}\frac{\partial}{\partial y}\left(\frac{u}{U_m}\right)dy\right)\}$$

Substitute equations (145) and (146) into (144) and also equation (147) into (144). The following resulting equation is then the momentum integral equation for the jet layer, $\delta_5 \to \delta_3$, in main region I.

$$\therefore \frac{\tau_w}{\rho}\cdot\frac{\tau_{(\delta_3\delta_2)}}{\tau_w}-\frac{\tau_{(\delta\delta_5)}}{\tau_w}\cdot\frac{\tau_w}{\rho} \tag{150}$$

$$= \left\{\int_0^1 (1-f(\eta_3))d\eta_3\right\}\cdot\left[\frac{d}{dx}\{(U_m)(U_m-U_w)(\delta_3-\delta_5)\}\right]$$

$$-\left\{\int_0^1 f(\eta_3)d\eta_3\right\}\cdot\left[\frac{d}{dx}\{(U_m-U_w)^2(\delta_3-\delta_5)\}\right]+$$

$$\left\{\int_0^1 f^2(\eta_3)d\eta_3\right\}\cdot\left[\frac{d}{dx}\cdot\{(U_m-U_w)^2(\delta_3-\delta_5)\}\right]+$$

$$(U_m)(\delta_3-\delta_5)\left(\frac{dU_m}{dx}\right)-\left\{\left(\frac{dU_w}{dx}\right)(\delta_3-\delta_5)(U_m-U_w)\right.$$

$$\left.\cdot\left(\int_0^1 f(\eta_3)d\eta_3\right)\right\}+\left\{2(U_m-U_w)\theta_5\frac{H_5(H_5+1)}{(H_5-1)^2}\frac{dU_m}{dx}\right.$$

$$-\left\{4U_m(U_m-U_w)\frac{H_5^2}{(H_5-1)^2}\left(\frac{\tau_w}{\rho U_m^2}\right)\right\}-\left\{U_m(U_m-U_w)\right.$$

$$\left.\cdot\left(\frac{\tau_w}{\rho U_m^2}\right)\left(\frac{\tau_{(\delta\delta_2)}}{\tau_w}\right)\frac{(5H_5-1)}{(H_5-1)}\right\}+\left\{2(U_m-U_w)\frac{H_5\theta_5}{(H_5-1)^2}\right.$$

$$\left.\cdot(2H_5^2-5H_5+1)\frac{U_e}{U_m}\frac{dU_e}{dx}\right\}+\left\{U_m(U_m-U_w)\right.$$

$$\left.\cdot\frac{(3H_5-1)}{(H_5-1)^2}\left(\int_0^{\delta_5}\frac{\tau}{\rho U_m^2}\frac{\partial}{\partial y}\left(\frac{u}{U_m}\right)dy\right)\right\}-\left\{U_e\frac{dU_e}{dx}\cdot\right.$$

$$\left.(\delta_3-\delta_5)\right\}.$$

The rate of growth of the jet layer in main region I is expressed by the following equation:

$$\frac{d}{dx}(\delta_3 - \delta_5) = C_3 \frac{U_m - U_w}{U_m + U_w} \qquad (151)$$

where C_3 is an empirical constant.

Derivation of the equations for the wake layer in main region I:

Let $U_{w(x)}$ = velocity at $y = \delta_3$ in main region I

and $U_{e(x)}$ = velocity at the edge of viscous layer $y = \delta_4$.

Assume "similar velocity" profiles in the region between as follows:

$$\eta_4 = \frac{y - \delta_3}{y_{2c} - \delta_3} \quad ; \quad f(\eta_4) = \frac{U_e - u}{U_e - U_w} \quad . \qquad (152)$$

where, (See Figure 1 between stations 1 and 2)

u = velocity at any distance y above the wall in the wake layer,

U_e = velocity at $y = \delta_4$ where the flow can be considered inviscid, and

y_{2c} = distance y above wall where $u = \frac{U_e + U_w}{2}$

The function, $f(\eta_4)$, representing similarity of velocity profiles in the wake layer for main region I is approximated by a least square 4th order polynomial fit.

$$f(\eta_4) = B_1 + B_2(\eta_4) + B_3(\eta_4)^2 + B_4(\eta_4)^3 + B_5(\eta_4)^4 \qquad (153)$$

where B_1, B_2, B_3, B_4 and B_5 are the coefficients of the least square polynomial.

From equations (152) and (153) we have the following relations,

$$y = \delta_3 + (y_{2c} - \delta_3)\,\eta_4 \qquad (154)$$

$$dy = (y_{2c} - \delta_3)\,d\eta_4$$

at $y = \delta_3$: $\eta_4 = 0.0$, $f(\eta_4) = 1.0$

at $y = y_{2c}$: $\eta_4 = 1.0$, $f(\eta_4) = 0.5$, $u = \frac{U_e + U_w}{2}$

at $y = \delta_4$: $f(\eta_4) = 0$, $u = U_e$

η_4 at $y = \delta_4$ found from eqn. (153)

Let K_2 = value of η_4 at $y = \delta_4$.

In a manner similar to the derivation of equation (143), the following equation can be derived for the wake layer:

$$\underset{(A_4)}{2\int_{\delta_3}^{\delta_4} u\frac{\partial u}{\partial x}\,dy} \;-\; \underset{(B_4)}{(U_e - U_w)\int_{0}^{\delta_5}\frac{\partial u}{\partial x}\,dy} \;-\; \underset{(C_4)}{(U_e - U_w)\int_{\delta_5}^{\delta_3}\frac{\partial u}{\partial x}\,dy} \qquad (155)$$

$$\underset{(D_4)}{-U_e\int_{\delta_3}^{\delta_4}\frac{\partial u}{\partial x}\,dy} \;-\; \underset{(E_4)}{\int_{\delta_3}^{\delta_4} U_e\frac{dU_e}{dx}\,dy} \;=\; \underset{(F_4)}{\frac{\tau_{c(\delta_4)}}{\rho}} \;-\; \underset{(G_4)}{\frac{\tau_{c(\delta_3)}}{\rho}} \;.$$

In order to take advantage of the one parameter family of velocity profiles for the wall-layer and similarity of velocity profiles in the jet and wake layers, the following operations are performed on the terms of equation (155),

$$(A_4) + (D_4) + (E_4) \text{ of eqn. (155)} \tag{156}$$

$$= 2\int_{\delta_3}^{\delta_4} u \frac{\partial u}{\partial x} dy - U_e \int_{\delta_3}^{\delta_4} \frac{\partial u}{\partial x} dy - \int_{\delta_3}^{\delta_4} U_e \frac{dU_e}{dx} dy$$

$$= \int_{\delta_3}^{\delta_4} \frac{\partial}{\partial x}(u^2) dy - \int_{\delta_3}^{\delta_4} U_e \frac{\partial u}{\partial x} dy - \int_{\delta_3}^{\delta_4} u \frac{dU_e}{dx} dy - \int_{\delta_3}^{\delta_4} u \frac{dU_e}{dx} dy$$

$$- \int_{\delta_3}^{\delta_4} U_e \frac{dU_e}{dx} dy$$

$$= -\frac{\partial}{\partial x} \int_{\delta_3}^{\delta_4} u(U_e - u) dy - U_w (U_e - U_w) \cdot \frac{d\delta_3}{dx}$$

$$- \frac{dU_e}{dx} \cdot \int_{\delta_3}^{\delta_4} (U_e - u) dy$$

The terms of equation (156) are further simplified as follows:

$$-\left(\frac{dU_e}{dx}\right) \int_{\delta_3}^{\delta_4} (U_e - u) dy \tag{157}$$

$$= -\left(\frac{dU_e}{dx}\right) \int_0^{K_2} (U_e - U_w) f(\eta_4) (y_{2c} - \delta_3) d\eta_4$$

$$= -\left(\frac{dU_e}{dx}\right) \cdot (U_e - U_w)(y_{2c} - \delta_3) \int_0^{K_2} f(\eta_4) d\eta_4 .$$

and

$$-\frac{\partial}{\partial x}\left\{\int_{\delta_3}^{\delta_4} u(U_e-u)dy\right\} \tag{158}$$

$$= -\frac{\partial}{\partial x}\left[\int_0^{K_2}\{U_e-(U_e-U_w)f(\eta_4)\}\cdot\{(U_e-U_w)f(\eta_4)(y_{2c}-\delta_3)\}d\eta_4\right]$$

$$= -\frac{d}{dx}\left[U_e(U_e-U_w)(y_{2c}-\delta_3)\right]\cdot\left\{\int_0^{K_2} f(\eta_4)d\eta_4\right\} +$$

$$\frac{d}{dx}\left[(y_{2c}-\delta_3)(U_e-U_w)^2\right]\cdot\left\{\int_0^{K_2} f^2(\eta_4)d\eta_4\right\} .$$

and thus following equation is obtained,

$$\rho\int_{\delta_3}^{\delta_4} u\frac{\partial u}{\partial x}dy - U_e\int_{\delta_3}^{\delta_4}\frac{\partial u}{\partial x}dy - \int_{\delta_3}^{\delta_4} U_e\frac{dU_e}{dx}dy \tag{159}$$

$$= -\left\{\int_0^{K_2} f(\eta_4)d\eta_4\right\}\cdot\left[\frac{d}{dx}\left\{U_e(U_e-U_w)(y_{2c}-\delta_3)\right\}\right]$$

$$+\left\{\int_0^{K_2} f^2(\eta_4)d\eta_4\right\}\cdot\left[\frac{d}{dx}\left\{(U_e-U_w)^2(y_{2c}-\delta_3)\right\}\right] - (U_w)(U_e-U_w)\left(\frac{\partial\delta_1^*}{\partial p}\right)$$

$$-\left(\frac{dU_e}{dx}\right)(U_e-U_w)\cdot(y_{2c}-\delta_3)\left\{\int_0^{K_2} f(\eta_4)d\eta_4\right\} .$$

and

$$-(U_e-U_w)\left\{\int_{\delta_5}^{\delta_3}\frac{\partial u}{\partial x}dy\right\} \tag{160}$$

$$= -(U_e-U_w)\left[\frac{\partial}{\partial x}\left\{\int_{\delta_5}^{\delta_3} u\,dy\right\} - \left(\frac{\partial\delta_1^*}{\partial x}\right)\cdot(U_w) + U_m\left(\frac{\partial\delta_5^*}{\partial x}\right)\right]$$

$$= -(U_e-U_w)\frac{d}{dx}\left\{U_m(\delta_3-\delta_5)\right\} + (U_e-U_w)\cdot\frac{d}{dx}\left\{(U_m-U_w)\right.$$

$$\left.\cdot(\delta_3-\delta_5)\right\}\cdot\left\{\int_0^1 f(\eta_3)d\eta_3\right\} + (U_e-U_w)U_w\frac{\partial\delta_3^*}{\partial x} - U_m(U_e-U_w)\frac{\partial\delta_5^*}{\partial x} .$$

and

$$-(U_e-U_w)\left\{\int_0^{\delta_5}\frac{\partial u}{\partial x}dy\right. \tag{161}$$

$$= -(U_e - U_w)\left[\frac{\partial}{\partial x}\int_0^{\delta_5} u\,dy - U_m \frac{d\delta_5}{dx}\right]$$

$$= -(U_e - U_w)\left[\frac{d}{dx}\left\{U_m \delta_5 \frac{n}{n+1}\right\}\right] + U_m(U_e - U_w)\frac{d\delta_5}{dx}$$

$$= -(U_e - U_w)\left[\frac{d}{dx}\left\{U_m 2\theta_5 \frac{H_5}{(H_5-1)}\right\}\right] + U_m(U_e - U_w)\frac{d\delta_5}{dx}$$

$$= -2(U_e - U_w)\frac{\theta_5 H_5}{(H_5-1)} \cdot \frac{dU_m}{dx} - 2(U_e - U_w)\frac{U_m H_5}{(H_5-1)}\frac{d\theta_5}{dx}$$

$$+ 2U_m(U_e - U_w)\theta_5 \cdot \frac{1}{(H_5-1)^2}\frac{dH_5}{dx} + U_m(U_e - U_w)\frac{d\delta_5}{dx} \cdot$$

Substitute equations (159), (160), (161), (138) and (131A) into equation (155) to obtain the following momentum integral equation for the wake layer in main region I:

$$\therefore -\frac{\tau(\delta_3)}{\rho} \tag{162}$$

$$= -\left\{\int_0^{K_2} f(\eta_4)\,d\eta_4\right\}\cdot\left[\frac{d}{dx}\left\{U_e(U_e - U_w)\cdot(y_{2c} - \delta_3)\right\}\right]$$

$$+ \left\{\int_0^{K_2} f^2(\eta_4)\,d\eta_4\right\}\cdot\left[\frac{d}{dx}\left\{(U_e - U_w)^2\cdot(y_{2c} - \delta_3)\right\}\right]$$

$$- \left\{\int_0^{K_2} f(\eta_4)\,d\eta_4\right\}\cdot\left[\left(\frac{dU_e}{dx}\right)\cdot(U_e - U_w)\cdot(y_{2c} - \delta_3)\right]$$

$$- (U_e - U_w)\cdot(U_m)\cdot\frac{d}{dx}\{\delta_3 - \delta_5\} - \left[(U_e - U_w)\cdot\frac{dU_m}{dx}\right.$$

$$\left.\cdot(\delta_3 - \delta_5)\right] + \left\{\int_0^{1} f(\eta_3)\,d\eta_3\right\}\cdot\left[(U_e - U_w)\frac{d}{dx}\{(U_m - U_w)\right.$$

$$\left.\cdot(\delta_3 - \delta_5)\}\right] - 2\cdot(U_e - U_w)\cdot\theta_5\frac{H_5(H_5+1)}{(H_5-1)^2}\cdot\left(\frac{dU_m}{dx}\right)$$

$$+ 4\cdot(U_m)\cdot(U_e-U_w)\cdot\left(\frac{\tau_w}{\rho U_m^2}\right)\cdot\left\{\frac{H_5^2}{(H_5-1)^2}\right\}$$

$$+ (U_m)\cdot(U_e-U_w)\cdot\left(\frac{5H_5-1}{H_5-1}\right)\cdot\left(\frac{\tau_w}{\rho U_m^2}\right)\cdot\left(\frac{\tau_{(\delta_5)}}{\tau_w}\right)$$

$$+ 2\cdot(U_e-U_w)\cdot\left(\frac{U_e}{U_m}\right)\cdot\left(\frac{dU_e}{dx}\right)\cdot\theta_5\,\frac{H_5}{(H_5-1)^2}\cdot(2H_5^2-5H_5+1)$$

$$- (U_m)\cdot(U_e-U_w)\cdot\left[\left\{(3H_5-1)^2\cdot\frac{1}{(H_5-1)^2}\right\}\right.$$

$$\left.\cdot\left\{\int_0^{\delta_5}\frac{\tau}{\rho U_m^2}\frac{\partial}{\partial y}\left(\frac{u}{U_m}\right)dy\right\}\right] .$$

The growth rate equation for the wake-layer in main region I is expressed as,

$$\frac{d}{dx}(y_{2c}-\delta_3) = c_4\,\frac{U_e-U_w}{U_e+U_w} \qquad (163)$$

where c_4 is an empirical constant.

REFERENCES

1. Glauert, M. B., "The Wall Jet", Journal of Fluid Mechanics, Volume 1, 1956.

2. Myers, G. E., Schauer, J. J., and Eustis, R. H., "Plane Turbulent Wall Jet Flow Development and Friction Factor", Journal of Basic Engineering, Volume 85, Pages 47-54, March 1963.

3. Kruka, V. and Eskinati, S., "The Wall Jet in a Moving Stream", Journal of Fluid Mechanics, Volume 20, Part 4, 1964.

4. Kacker, S. C. and Whitelaw, J. H., "Some Properties of the Two Dimensional Turbulent Wall Jet in a Moving Stream", Journal of Applied Mechanics, Volume 35, Pages 641-651, December 1968.

5. Bradshaw, P., and Gee, M. T., "Turbulent Wall Jets with and without an External Stream", A.R.C. 22, 008 June 1960.

6. Harris, G. L., "The Turbulent Wall Jet in a Moving Stream", Proceeding of Specialists Meeting sponsored by AGARD Fluid Dynamics Panel, May 1965.

7. Escudier, M. P. and Whitelaw, J. H., "The Influence of Strong Adverse Pressure Gradients on the Effectiveness of Film Cooling", International Journal of Heat and Mass Transfer, Volume 11, Pages 1289-1292, August 1968.

8. Nicoll, W. B. and Whitelaw, J. H., "The Effectiveness of the Uniform Density, Two Dimensional Wall Jet", International Journal of Heat and Mass Transfer", Volume 10, Pages 623-639, 1967.

9. Kind, R. J., "A Calculation Method for Circulation Control by Tangential Blowing Around a Bluff Trailing Edge", The Aeronautical Quarterly, Volume XIX, Part 3, August 1968.

10. Gartshore, I. S., Newman, B. G., "The Turbulent Wall Jet in an Arbitrary Pressure Gradient", The Aeronautical Quarterly, Volume XX, Part I, February 1969.

11. Bangert, L. H., "The Turbulent Wall Jet with an Initial Boundary Layer." AIAA Paper presented at 4th Fluid and Plasma Dynamics Conference, Palo Alto, California, June 21-23, 1971.

12. Hartnett, J. P., Biokebak, R. C., and Eckert, E. R. G., "Velocity Distributions, Temperature Distributions, Effectiveness and Heat Transfer for Air Injected through a Tangential Slot into a Turbulent Boundary Layer", Journal of Heat Transfer, Volume 83, Pages 293-306, August 1961.

13. Sebun, R. A., Back, L. H., "Effectiveness and Heat Transfer for a Turbulent Boundary Layer with Tangential Injection and Variable Free-stream Velocity", Journal of Heat Transfer, February 1962, Volume 84, Pages 235-244, August 1962.

14. Albertson, M. L., Dai,Y. B., Jensen, R. A., and Rouse, H., "Diffusion of Submerged Jets", Proc. Am.Soc. Civil Engrs., 74, 1751, (1948).

15. Schlichting, H., Boundary Layer Theory, McGraw-Hill Book Company, Inc., New York, (1962).

16. Rotta, J., "Schubspannungs verteilung und Energie dissipation Bei Turbulenten Grenzschichten", Ing. Arch., Volume 20, Pages 195-207, 1952.

17. Prundtl, L., Tietjens, O., Fundamentals of Hyro- and Aero Mechanics, New York, (1934).

18. Boussinesg, J., Theory de l'ecoulement tourbillant. Mem. Pre. par. div. suv. XXIII, Paris (1877).

19. Reichardt, H., Messungen turbulenter Schwankunger. Naturwiss-enschal'ten 404 (1938); see also ZAMM 13, 177 (1933) and ZAMM 18, 358 (1938).

20. von Karman, Th., Mechanische Ähnlichveit und Turbulenz. Nach Ges. Wiss. Göttingen, Math. Phys. Klasse. 58 (1930) and Proc. 3rd Intern. Congress Appl. Mech., Stockholm, Pt. I, 85 (1930), NACA TM G11 (1931).

21. Nikuradse. J., Gesetzmässigkeit der turbulenten strömung in glatten Rohren. Forschungsheft 356 (1932).

22. Klebanoff, P. S., 'Characteristics of Turbulence in a Boundary Layer with Zero Pressure Gradient", NACA Tech. Notes 3178, 1954.

23. Townsend, A. A., Proc. Cambridge Phil. Soc., Volume 47, p. 375, 1951.

24. Hama, F. R., Advances in Applied Mechanics, Vol. 4, p. 28, New York, 1956.

25. Rubesin, M. W., "A Modified Reynolds Analog for the Turbulent Boundary Layer on Flat Plate", NACA TN 2917 (1953).

26. Ludwieg, H., and Tillman, W., Untersuchangen über die Wandschubspunning in turbulenten Reibungsschichten. Ing.-Arch. 17, 288-299 (1949). English translation in NACS TN 1285 (1950).

27. Schubauer, G. B., and Ulebunoff, P. S., "Investigation of the Turbulent Boundary Layer", NACA Rep. 1030 (1951).

28. Ulebanoff, P. S. and Diehl, Z. W., "Some Features of Artificially Thickened Fully Developed Turbulent Boundary Layer with Zero Pressure Gradient", NACA Rep. No. 1110 (1952).

29. Schulz-Grunow, F., Neues Widerstundgesetz für glatte platten. Luft Fahrt Forschung 17, 239 (1940), also NACA TM No. 986 (1941).

30. Allan, J. F., and Cutland, R. S., Trans. North East Coast Inst. Engrs. and Shipbuilders, 69, 245 (1953).

31. Clauser, F. H., "Turbulent Boundary Layers in Adverse Pressure Gradients", Journal of Aerospace Sciences, Vol. 21, (1954).

32. Clauser, F. H., "The Turbulent Boundary Layer", Advances in Applied Mechanics, Vol. IV, Academic Press, New York, 1954.

33. Townsend, A. A., "The Structure of Turbulent Shear Flow", Cambridge University Press, New York, 1956.

34. Rotta, J., Das in Wandnähe gultige Geschwindigkeitsgesetz turbulenter Strömungen. Ing.-Arch. 18, 277-280 (1950).

35. Nikuradse, J., Strömungs gesetze in rauhen Rohren. For schungsheft 361 (1933).

36. Patel, V. C., "Calibration of the Preston Tube and Limitations on Its Use in Pressure Gradients", Journal of Fluid Mechanics, Vol. 23, 1965, p. 185.

37. Sigalla, A., "Measurements of Skin Friction in a Plane Turbulent Wall Jet", Journal of Royal Aeronautical Society, Volume 62, Pages 873-877, December 1958.

38. MacMillan, F. A., "Experiments on Pitot-Tubes in Shear Flow", A.R.C. Technical Report, RSM No. 3028, 1957.

39. Abramovich, G. N., "The Theory of Turbulent Jets", The M.I.T. Press Cambridge. 1963.

40. Escudier, M. P. and Nicoll, W. B., "The Entrainment Function in Turbulent Boundary-Layer and Wall Jet Calculations", Journal of Fluid Mechanics, Vol. 25, Part 2, page 337.

41. Schwart, W. R. and Cosart, W. P., "The Two Dimensional Turbulent Wall Jet," Journal of Fluid Mechanics, Vol. 10, Part 4, June 1961.

42. Myers, G. E., Schauer, J.J. and Eustis, R. H., "Heat Transfer to Plane Turbulent Wall Jets", Journal of Heat Transfer, August 1963.

43. Parajpe, S. C. and Sridhar, K., "Effects of Initial Gap on the Turbulent Jet Flow Over Curved Wall", The Aeronautical Journal of the Royal Aeronautical Society, Vol. 72, January 1968.

44. Mallonee, R. C. and Jacoby, S. L., "Plane Turbulent Compressible Wall Jet with and without Parallel Free Stream", ASME Paper No. 68-FE-40.

45. Seebohm, T.,"Boundary Layer, Transition and Wake Measurements at Low Mach Number for an Airfoil with Single Slotted Flap," Report 69-1, Mechanical Engineering Research Laboratories, McGill University.

46. Wenzinger, C. J. and Delano, J. B., "Pressure Distribution over an NACA 23012 Airfoil with Slotted and Plain Flap", NACA TR 633.

47. Harris, T. A. and Lowry. J. G., "Pressure Distribution Over an NACA 23012 Airfoil with a Fixed Slot and a Slotted Flap, NACA TR 732, 1942.

48. Wenzinger, C. J., "Pressure Distribution Over an NACA 23012 Airfoil with an NACA 23012 External-Airfoil Flap", NACA TR 614, 1937.

49. Foster, D. N., "The Flow Around Wing Sections with High Lift Devices," AIAA Paper 71-96 presented January 1971 meeting at New York.

50. Lawford, J. A. and Foster, D. N., "Low Speed Wind-Tunnel Tests on a Wing Section with Plain Leading and Trailing Edge Flaps Having Boundary-Layer Control by Blowing", ARC-R/M 3639.

51. Nash, J. F., "A Practical Calculation Method for Compressible Turbulent Boundary Layers in Two Dimensional and Axisymmetric Flows", Lockheed-Georgia Research Memo-ER-9428, August 1967.

52. Goult, Donalt E., "Boundary Layer and Stalling Characteristics of the NACA 63009 Airfoil Section", NACA TN 1894.

53. Scarborough, J. B., Numerical Mathematical Analysis, The John Hopkins Press, Sixth Edition, 1960.

54. Neale, O. D., Experimental Study of Two-Dimensional Turbulent Wall Jet Development With and Without Longitudinal Free Stream Pressure Gradient. Ph.D. Thesis, Georgia Institute of Technology, 1971.

55. Martin, G. W., "Calculation of the Potential Pressure Distribution Over Multiple Interacting, Two-Dimensional Airfoils in Incompressible Inviscid Flow," Lockheed-Georgia Company, ER-9439, 1967.

56. Goradia, S. H., Bennett, J. A., "Method of Analysis of Two-Dimensional Airfoils With Subsonic and Transonic Applications," Lockheed-Georgia ER-8591, 1966.

57. Stevens, W. A., Goradia, S. H., Braden, J. A., "Mathematical Model for Two-Dimensional Multi Component Airfoils in Viscous Flow," Lockheed-Georgia ER-10896, March 1971.

VITA

Suresh Harkisondas Goradia was born on November 12, 1937 in Bombay, India. He completed his high school education in June of 1953 and passed secondary school certificate examination with first class honours. He joined University of Bombay where he studied physics, chemistry and mathematics for two years and passed his Inter-Science examination with first class. He joined School of Mechanical Engineering of the Gujarat University and obtained B.S. in Mechanical Engineering in 1959 securing first class honours and standing fourth in order of merit in University. He came to U.S.A. in 1960 to pursue graduate studies in the School of Mechanical Engineering at the University of Michigan where he received his M.S. in Mechanical Engineering in 1961 with highest honours. He joined Georgia Tech for his Ph.D. program in 1964 where he continued his graduate studies in Mechanical Engineering while working full time at Lockheed-Georgia Company. He completed his Doctorate program at Georgia Tech in August of 1971.

His twelve years of experience in industry consists mainly of applied research in the field of fluid flow, heat transfer and thermodynamics. At the present time he is a Senior Aerodynamics Engineer at Lockheed-Georgia Company.